RESEARCH

REPORT

INVESTIGATION OF SURFACE FLUCTUATING PRESSURES
ON A ¼-SCALE YC-14 UPPER SURFACE BLOWN
FLAP MODEL

By
Richard S. Pappa

Prepared for:

NASA

NATIONAL AERONAUTICS AND SPACE ADMINISTRATION
LANGLEY RESEARCH CENTER
HAMPTON, VIRGINIA 23665

CONTRACT NUMBER NAS1-14740

WYLE LABORATORIES REPORT NUMBER 50900

JANUARY 1979

WYLE LABORATORIES
SCIENTIFIC SERVICES & SYSTEMS GROUP
3200 MAGRUDER BLVD., HAMPTON, VIRGINIA

TABLE OF CONTENTS

TABLE OF CONTENTS (continued)

TABLE OF CONTENTS (continued)

v

TABLE OF CONTENTS (continued)

INVESTIGATION OF SURFACE FLUCTUATING PRESSURES
ON A 1/4-SCALE YC-14 UPPER SURFACE BLOWN FLAP MODEL

By Richard S. Pappa

Wyle Laboratories
Hampton, Virginia 23666

SUMMARY

Fluctuating pressures were measured at 30 positions on the surfaces of a 1/4-scale YC-14 wing and fuselage model during an outdoor static testing program at the Langley Research Center. These data were obtained as part of a NASA program to study the fluctuating loads imposed on STOL aircraft configurations and to further the understanding of the scaling laws of unsteady surface pressure fields.

Fluctuating pressure data were recorded at several discrete engine thrust settings for each of 16 configurations of the model. These data were reduced using the techniques of random data analysis to obtain auto- and cross-spectral density functions and coherence functions for frequencies from 0 to 10 kHz, and cross-correlation functions for time delays from 0 to 10.24 ms.

Effort was made to select formats for data presentation consistent with those of previous investigators of surface fluctuating pressures, and several normalizations by flow parameters are included to compare the results of this program with those of other tests. In addition to contributing to the data base of fluctuating pressure measurements on actual STOL vehicle designs, results of this program provide the following items of particular interest:

- Good collapse of normalized PSD functions on the USB flap was found using a technique applied by Lilley and Hodgson to data from a laboratory wall-jet apparatus.

- Results indicate that the fluctuating pressure loading on surfaces washed by the jet exhaust flow was dominated by hydrodynamic pressure variations, loading on surfaces well outside the flow region dominated by acoustic pressure variations, and loading near the flow boundaries from a mixture of the two.

● Narrow-band convection velocity functions measured on the model differed somewhat in shape from those generally reported by other investigators for surface pressures under developed turbulent boundary layers. These differences were correlated with differences in the mean flow conditions over the model.

INTRODUCTION

The National Aeronautics and Space Administration (NASA) is currently involved in a research program to study the fluctuating loads imposed on the surfaces of short-takeoff-and-landing (STOL) aircraft. Both upper surface blown (USB) flap and externally blown flap (EBF) concepts are being studied. The overall program objective is to advance methods for predicting the fluctuating loads of various STOL configurations, either by simplified analytical techniques or by scaling experimental test data obtained from small-scale model tests, and to use these data in estimating both the sonic fatigue life of critical aircraft components and the levels of radiated interior cabin noise. Highlights of investigations conducted by NASA on STOL fluctuating loads in the past six years are contained in References 1 through 5. Several of these investigations contain data obtained during actual aerodynamic testing of a STOL configuration. Development and testing of STOL concepts has been the subject of extensive work by NASA and industry for over two decades (see References 6 through 9).

Under contract to NASA, Wyle Laboratories conducted an investigation of the unsteady pressures at 30 positions in the vicinity of the jet exhaust on the surfaces of a 1/4-scale YC-14 boiler plate wing and fuselage section. The YC-14 transport, the Boeing Co.'s entry in the USAF advanced medium STOL (AMST) competition, uses upper surface blowing technology to achieve STOL performance. Measurements of surface fluctuating pressures were obtained in conjunction with simultaneous measurements of the static aerodynamic performance of the 1/4-scale model by NASA. Sensor positions for

the fluctuating pressure measurements were chosen to correspond geometrically with those selected by Boeing for a ground test of a full-scale YC-14 model; thus, in addition to providing basic USB research information, the results of this test program provide a direct opportunity for further investigation of the scaling laws of unsteady surface pressure fields and their application to the design of STOL vehicles. Preliminary interpretations of fluctuating pressure measurements obtained on the Boeing full-scale model were published in References 10 and 11.

The goals of this report, presented in their order of importance, are:

1. To provide statistical descriptions of the surface fluctuating pressure field measured on a 1/4-scale aircraft section to allow future comparisons with similarly measured data on the full-scale aircraft. A comparison of these data would help advance the understanding of the scaling relationships of surface fluctuating pressures, allowing better use of models to estimate the fluctuating loads on full-scale vehicles. With the anticipation of large fluctuating pressure loading on some STOL structural components, the ability to accurately predict the characteristics of the surface fluctuating pressure field from results of scale-model tests may likely impact on the design process of future configurations.

    Effort will be made to provide these scale-model data in forms which could be similarly selected for use with the full-scale data, and used in combination with a knowledge of the structural design and vibration characteristics of the full-scale vehicle, to estimate both the sonic fatigue potential present and the levels of radiated interior cabin noise. This will allow an assessment of the accuracy of scaling techniques to directly predict these important characteristics of the full-scale aircraft from pressure data measured on the 1/4-scale model. An increase in the reliability of fluctuating pressure scaling techniques may well increase the use of scale models to obtain these data.

3

2. To contribute information to the data base of surface fluctuating pressure measurements on actual aircraft configurations.

3. To normalize these data for comparisons with similar results reported by other investigators, and to discuss possible causes of deviations in the comparisons.

4. To use these data to gain additional insight into the sources and generating mechanisms of surface fluctuating pressures, and to compare these findings with those reported for other tests and from theoretical investigations.

APPARATUS AND TECHNIQUE

Model

A photograph of the model located at an outdoor testing site at the Langley Research Center (LaRC) is shown in figure 1. Tests were conducted from November 1975 through August 1976. The test apparatus is a 1/4-scale model of a full-scale YC-14 section from the left side of the aircraft near the jet exhaust which was tested by Boeing at their Tulalip facility in December 1975.

By the Coanda effect, the exhaust flow of an engine mounted along the upper surface of the wing attaches itself to the surface of a curved retractable trailing edge flap. As the flap is extended, the attached flow is deflected downward, and the resulting change in flow momentum, along with supercirculation induced by the jet flap effect, results in high lift. Additionally, the YC-14 design employs wing-mounted flow deflectors, termed 'vortex generators,' to further augment powered life. A photograph of the model taken during a flow-visualization test with the vortex generators in a raised position is presented in figure 2. The engine exhaust flow is clearly seen deflecting downward along the blackened fuselage sidewall as it passes over the upper surface of the curved flap, shown in its fully extended position. (Note that the top of the fuselage is located at the same height as the top of the

wing, and that a blackened screen is positioned behind the fuselage section to aid in the flow visualization.)

The major components and fundamental dimensions of the model are designated in figure 3. The model consisted of a JT15D-1 turbofan engine exhausting through a D-shaped nozzle onto the upper surface of a boiler plate 1/4-scale YC-14 wing and fuselage section model. The JT15D engine had a rated thrust of 8.9 kN (2000 lb), a bypass ratio of 3.3, and was operated over a fan-pressure-ratio range of 1.1 to 1.4. The entire model was mounted on a floating test rig instrumented with force gauges to obtain data on the static flow-turning and thrust-recovery performance of the configuration. Test variables consisted of engine thrust settings from idle to full power, raised and retracted positions of wing-mounted vortex generators, three deployment angles of the USB flap, two heights of the model above ground, and the installation or removal of a rubber seal at the junction of the USB flap and fairing.

All external surface features of the exhaust nozzle, wing, flaps, fuselage, and vortex generators of the model were scaled from the YC-14. The internal geometry of the nozzle, however, was modified slightly from that selected by Boeing for use with a 222-kN (50000-lb.) thrust CF6-50D turbofan engine in the full-scale model test. The modified nozzle design provided calculated agreement of fan- and core-flow velocities of the 1/4-scale and full-scale models within 10% at operating fan pressure ratios of 1.4. Except for a large difference in thrust, the JT15D and the CF6-50D engines have similar operating characteristics, as discussed in Reference 12.

An exhaust nozzle side door on the model was fixed in the "open" position for all tests, corresponding to the configuration of the YC-14 during low-speed operation. The side door was designed to increase the nozzle cutback which helps force the exhaust stream to spread outboard, reducing the thickness of the jet. This thinning of the jet results in better attachment of the flow to the wing and flap surfaces, delaying the onset of flow separation. More complete details of the nozzle and propulsion system characteristics of the

YC-14 are contained in References 13 and 14.

Four wing-mounted, rectangular-blade vortex generators were mounted in either an "up" or a "down" position. In addition to the basic vortex generator geometry selected by Boeing, fluctuating pressure data were also obtained for one run sequence with an additional set of vortex generators having a double span and a 10° increased angle of attack on the two outside plates. This modification was an attempt to further energize the boundary layer to improve flow attachment.

Changes in flap angle were accomplished using three bolt-on boiler plate units modeling the geometries of fully retracted, intermediate, and fully extended flap settings. These flap settings corresponded to angles of 16°, 70°, and 86.5° between the upper surface of the flap trailing edge and the horizontal. The two-segment YC-14 flap arrangement was modeled as a single unit designed with appropriately contoured main-flap and aft-flap regions.

Two model heights were used for testing to investigate changes in aerodynamic data with ground proximity. The two selected heights corresponded to the YC-14 airplane at wheel-contact height (taxi condition) and at an airborne upper-surface wing height of 9.16 m (30 ft). These conditions were modeled by upper-surface wing heights of 1.45 m (4.75 ft) and 2.29 m (7.5 ft), respectively.

A minor test parameter, selected during the program in an attempt to obtain better correlation between the NASA 1/4-scale and the Boeing full-scale aerodynamic data, was the sealing of a gap approximately 1 cm wide located between the inboard edge of the USB flap and the fairing structure. The presence or removal of the seal, however, was found to have only a minimal effect on the measurements of surface fluctuating pressures.

Instrumentation

Surface fluctuating pressure data were obtained at 30 positions on the model. These positions are shown in figure 4. The measurement positions on each of the three flap units modeled those of the Boeing sensors after both main and aft flaps are moved into their appropriate positions. Accordingly, no measurement positions were used on the 16° flap, while sensor positions on the 70° and 86.5° flaps were determine by holding the main flap trailing edge-to-sensor and aft flap trailing edge-to-sensor distances constant.

Three types of pressure transducers were used. Those selected for positions on the wing and USB flap were miniature, strain gage units (Kulite XCEH-1-125-5D) designed to withstand temperatures up to 260° C (500° F). These sensors performed satisfactorily throughout the program, with maximum temperatures of approximately 215° C (420° F) being measured near the two flap locations along the engine centerline. The less severe temperature environment on the surfaces of the fuselage and fairing permitted the use of a lower temperature-rated, piezoelectric transudcer (PCB 112A21). These transducers also performed satisfactorily, where measured temperatures never exceeded 60° C (140° F). A third type of pressure transducer (Kulite CQH-125-5D), a low temperature strain gage unit, was added after results of the first two test configurations revealed vibration-induced contamination of the pressure data obtained from the piezoelectric sensors used in the fuselage area. Three of these low temperature units were installed adjacent to existing sensor position numbers 3, 9, and 12 and designated positions 103, 109, and 112, respectively. After test configuration 2, increased vibration isolation of the piezoelectric transducers in the fuselage area was obtained for frequencies above 60 Hz by remounting them in steel sleeve adapters which supported the transducers by thin rubber diaphragms. Photographs of the Kulite and PCB pressure sensors are provided in figure 5.

In addition, eleven accelerometers, mounted on the inner surfaces of

the model adjacent to fluctuating pressure transducers, were used to verify the integrity of data obtained from the pressure sensors. These accelerometer data were used to relate spectral peaks of the pressure data, whose frequencies did not change with engine power settings, to structural resonance responses of the model. Additional information on the acceleration sensitivity of the pressure sensors in their installed positions was obtained by analyzing the output signals of the pressure transducers during vibration tests of the model conducted with the engine off. During the testing program, high levels of broadband fluctuating pressures were found to obscure the vibration-induced effects at most measurement positions and test configurations.

Coordinates of the fluctuating pressure sensor positions are given in figure 6. Note that the sensor at position 23, located in the inboard nozzle wall near the exit plane, measured the pressure on the inner surface of the nozzle.

Test Procedure

Fluctuating pressure data were obtained for 16 configurations of the model. A complete listing of these test configurations is provided in Table I. Note that two preliminary configurations were tested using a "straight-plug" primary nozzle. Following testing of configuration 2, a "skewed-plug" primary nozzle constructed to closely model the full-scale YC-14 nozzle geometry was installed. The geometries of the two nozzle designs are shown in figure 7. At each test configuration, data were recorded on analog magnetic tape for several fixed, engine power levels. Thrust settings of 25%, 50%, 75%, and 100% of full power were selected for run sequences 1 through 12. A maximum thrust of 75% of full power was maintained throughout the remainder of the program following an engine bearing failure after testing of configuration 12. For several configurations, data were also obtained continuously while the engine thrust was gradually increased from idle to maximum thrust.

At each test condition, complete static-turning performance data and surface static-pressure and temperature distributions were also obtained. A summary of the static aerodynamic characteristics of the model is contained in Reference 12.

Flow Measurements

To aid in the interpretation of surface fluctuating pressure data, information on the flow pattern over the model obtained from reference 12 and some additional unpublished NASA data are included here.

Velocity profiles. - Flow surveys of total pressures, static pressures and total temperatures normal to the surface of the model were made using a 48-cm-high rake, and these data were used to calculate the steady flow velocity profiles at various positions on the model. Rake data were obtained at the exit plane of the nozzle, above the USB flap pressure transducers, and at the trailing edge of the flap, for a range of engine power settings.

Measured flow velocities normal to the surface of the model along the engine centerline are shown in figure 8(a). These profiles are consistent with the classical structure of a wall jet, a sketch of which is shown in Figure 8(b) (from Reference 15). At each downstream station, the behavior of the flow field below the velocity maximum approximates that of a boundary layer flow while the behavior above approximates that of a free jet flow. With increased distance downstream of the nozzle, the maximum velocity, U_{max}, tends to decrease, the height of U_{max} above the surface tends to increase, and the profile above U_{max} tends to approach U_{max}.

Flow velocity data obtained at the exit of the nozzle with the skewed-plug primary nozzle installed are presented in figure 9. A bulging of the central region of the profile near the centerline at maximum thrust setting, shown in figure 9(a), indicates an increase in the contribution of the inner core flow to the combined core and secondary flow field exiting the nozzle. The vertical

location of the velocity maximum remains near the center of the profile, however, unaffected by the thrust setting.

Figure 9(b) shows constant velocity contours measured at the nozzle-exit plane, and illustrates the nonsymmetric nature of the flow. The velocity maximum is shown to occur at a higher distance above the wing at locations slightly inboard from the nozzle centerline than at locations slightly outboard from the centerline.

Velocity profiles measured above the pressure sensor positions on the main USB flap are provided in figure 10. As shown in figure 10(a) for data obtained above position 39, increases in engine thrust setting resulted in increases in both the magnitude of the velocity maximum and in its height above the model. Figure 10(b) presents velocity profiles obtained at 100% thrust setting above the other three sensors on the main flap, and shows a continuous decrease in maximum velocity with a slight decrease in its height with distance outboard from the nozzle centerline. Velocity profiles similarly obtained above the four sensors on the aft USB flap are provided in figure 11.

Note that for all data presented in figures 10 and 11, the flow-survey probes were fixed in a vertical plane parallel to the nozzle centerline, thus measuring only a component of the velocity when this direction was not along the local streamline. All velocity profile data above the USB flaps were obtained with the vortex generators up and with the 86.5° flap and skewed-plug primary nozzle installed.

Considerable information is available in the literature on the aerodynamic characteristics of wall jets, both in still air and below moving streams. The primary analytical work available is that of Glauert (Ref. 16). He obtained a theoretical description of the turbulent wall jet by a near-similar solution, assuming the variation of shear stress with mean velocity below the velocity peak the same as in turbulent pipe flow and that the eddy viscosity was constant above the velocity peak. Experiments have verified the basic validity of the Glauert model, and additionally, provided extensive

10

measurements over a large variety of flow conditions (see References 17 through 20).

For a wall jet above a flat surface in still air, Myers, et al, (Ref. 15) report near logarithmic changes in both the peak velocity, U_{max}, and in the height of the peak velocity above the surface with increased downstream distance. Effects of Reynolds number were negligible for both magnitude and location of U_{max}. An additional observation related to the present study, reported by Bradshaw and Gee (Reference 17), was that a wall jet on a curved surface tends to grow more quickly than one on a flat surface.

Some indication of the flow pattern over the fuselage and fairing surfaces of the 1/4-scale YC-14 model with the 86.5° flap installed was achieved through photographs of a field of tufts. Figure 12 presents a comparison of flow patterns obtained at 25% and 100% engine thrust settings. Three basic situations are displayed: turbulent flow is indicated in those areas where the tufts are moving randomly; more steady flow is indicated in those areas on the fuselage near the bottom of the model where the tufts tend to point in a particular direction; and no flow is indicated in areas high on the fuselage where the tufts are motionless. By a comparison of the two photographs, the extent of flow activity up the fuselage is also seen to increase slightly with increased jet flow velocity. These general indications of flow patterns help in the interpretation of surface fluctuating pressure data obtained at positions on the fuselage of the model.

Surface static pressures and temperatures. - Figure 13 presents static pressure isobars obtained from an extensive array of static pressure taps over the surfaces of the wing and flaps, and shows the effect of deployment of the vortex generators on the shape of these contours. The increase in flow turning achieved with the vortex generators raised is seen by the increased spread of suction pressures downstream along the USB flaps. A small increase in lateral flow spreading also occurs when the vortex generators are raised. Note that these data were obtained at a full thrust setting with the straight-plug

primary nozzle installed.

Surface static pressure and temperature isobars at a full thrust engine setting with the skewed-plug primary nozzle installed are presented in figure 14. Note that the point of maximum suction pressure does not correspond to the point of maximum surface temperature. Although not shown, a significant decrease in surface temperature resulted when the straight-plug primary nozzle was replaced by the skewed-plug configuration. This skewed-plug design was selected to direct the hot core flow gases upward before leaving the outer exhaust nozzle as a method of reducing the surface temperature environment of the USB flaps with minimal effect on the STOL performance characteristics.

BACKGROUND DISCUSSION

The characteristics of surface fluctuating pressures and their effects on aerospace vehicles have been studied for over 20 years. To date, however, most experimental work has dealt with the conditions associated with high-speed missiles and launch vehicles, with commercial aircraft during cruise, with high-performance aircraft during maneuvering conditions, or with simple wind tunnel models (usually flat plates). Little experimental data exists describing the surface fluctuating pressure environment and associated loads on STOL vehicles, particularly during the severe conditions of powered-lift operation. Based upon the consistency of results presented by previous investigators, however, the basic features of the fluctuating pressure field on the 1/4-scale YC-14 model may be estimated.

Two types of pressure variations having distinctly different properties must be considered. The fluctuating pressures may result either from the local balancing of momentum fluctuations in turbulent flow or they may be acoustic pressure waves. For the first type, commonly termed the turbulent (boundary layer) pressure field, the compressibility of the flow is not important and the pressure fluctuation levels are of order ρu^2, where ρ is the mean fluid density and u is the local velocity fluctuation level.

12

To emphasize the independence of compressibility, the turbulent pressure field is occasionally referred to as the hydrodynamic pressure field (see Reference 21, e.g.) For the second type, the acoustic field, the compressibility is a significant factor in determining both the speed and the strength of the pressure disturbances, with the pressure fluctuation levels being of order $\rho u c$, where ρ and u are defined above and c is the local sonic velocity. Acoustic pressures may either be of a discrete frequency nature or may be distributed over a broad, continuous frequency spectrum.

The discrete frequency, or "pure-tone", acoustic pressures are likely to be either engine tones, produced at multiples and combinations of the compressor- and turbine-blade-passing frequencies, or the result of regular fluid oscillations (vortex shedding) occurring at edges, protuberances or discontinuities of appropriate geometry. The sources of broadband acoustic pressures, on the other hand, are generally more difficult to diagnose--being by-products of the turbulent flow and fluid-mixing processes and existing in spatial "source regions" generally having no well defined boundaries. Separation of the effects of individual broadband acoustic pressure sources is difficult, although considerable information is available associating various types of "source mechanisms" with their measurable statistical properties.

At measurement positions under the exhaust flow and near its boundaries, the surface fluctuating pressure field generally consists of a mixture of hydrodynamic and acoustic pressures. The hydrodynamic pressure field is a direct result of the existence of a fluctuating velocity field, being related in incompressible flow by a Poisson's equation. The velocity field, in turn, may be thought of as driven by a vorticity field and related by the Biot-Savart law. Thus, the hydrodynamic pressure field may be thought of as the combined result of the effects of vorticity distributed throughout the turbulent fluid motion.

The hydrodynamic pressure field, a random function of both space and time, may be regarded as a continuous distribution of harmonic pressure

components of various amplitudes, frequencies, and wavelengths. Accordingly, all statistical properties are uniquely defined mathematically by the wave number frequency spectrum of the pressure field, or alternatively by its Fourier transform, the space-time correlation function. For a stationary homogenous field, the space-time correlation is only a function of space and time separation and is independent of the actual measurement time or position in the field. Although stationarity is reasonable to assume for tests conducted at a constant engine thrust setting, homogeneity may only be assumed over spatial regions within which changes in the mean flow characteristics are small.

A basic model of the hydrodynamic pressure field measured at a surface beneath a turbulent boundary layer regards the field as a decaying, convecting pressure pattern consisting of a combination of wave number components, each of which is associated with a reasonably small range of convection speeds. High-frequency pressure components are associated with small turbulent eddies located near the surface, and convect downstream at 0.5 - 0.7 times the free stream flow velocity. The low-frequency components, on the other hand, are associated with vorticity in the outer regions of the boundary layer or with larger size eddies, and convect downstream at 0.8 - 0.9 times the free stream velocity. These pressure components tend to remain coherent in the direction of flow for a time proportional to the time to be convected their wavelength, and to remain coherent over lateral distances proportional to their wavelengths. Further discussion of several fluctuating-pressure-field models of varying complexities is contained in Reference 22.

Attempts by previous investigators at obtaining nondimensional collapse of hydrodynamic pressure data have consisted of efforts to select a set of flow parameters which can be related to the distribution of turbulent levels and scales, and which can be obtained with a reasonable number of measurements. Good nondimensional collapse of data, for various flow conditions, has been widely reported by using the following flow descriptions: a) a typical length

scale of the flow such as the local boundary layer height, b) a typical velocity scale of the flow such as the free stream flow velocity, and c) a measure of the relative level of fluctuating velocity such as the free stream dynamic pressure.

Using forms consistent with those selected by previous investigators, surface fluctuating pressure data obtained on the 1/4-scale YC-14 model will now be presented and analyzed.

RESULTS

A Hewlett-Packard 5451B Fourier analyzer system was used for processing the fluctuating pressure data recorded on analog magnetic tape. For each of 16 test configurations, 96 pairs of data were processed to obtain the following functions: a) the root-mean-square (rms) value of each input channel, b) the power spectral density (PSD) of each channel, c) the probability density function of each channel, d) the coherence function between channels, e) the cross-correlation function between channels, and f) the cross spectral function between channels. The cross spectral function was obtained in both magnitude/phase and co/quad (normalized to ± 1) forms. Data were simultaneously digitized on both input channels at 50 000 samples per second, with antialiasing low-pass analog filters (48 dB/octave) set to 12 500 Hz. These settings ensured alias-free digital data at frequencies up to 10 000 Hz. All functions were calculated by ensemble averaging of 350 records of 1024 time samples each.

Spectra of Surface Pressures

Engine tones. - Figure 15 shows a sample method of quickly examining the variation of surface pressure spectra at a fixed measurement position with thrust setting. These data were obtained during run up of the engine from idle

15

condition to nearly 100% thrust while the pressure signal was recorded. Each line represents a 40-Hz-resolution, pressure spectrum over frequencies from 0 to 14 kHz. Although the spectral magnitude information is unscaled, increased ease in interpreting frequency information is provided by this technique. As shown in this data obtained at wing position 32 (for test configuration 10), several discrete-frequency engine tones which increase in regular order with increased thrust setting are present. Each of these peaks are directly related to multiples of the compressor- and turbine-blade-passing frequencies, and Table II provides this information for each test run. Another important feature to note in figure 15 is the steadily increasing magnitude of low-frequency energy at frequencies below 4 kHz with increasing thrust.

Variation of spectra with thrust setting. - More quantitative measurements of pressure spectra were obtained by analyzing steady-state rather than data obtained during run up of the engine. Power spectral density plots obtained at 25%, 50%, 75%, and 100% engine thrust settings during test configuration 6 are shown in figures 16 through 22. These data are arranged in seven geometric groups of four measurement positions each. Generally, fluctuating pressures increased in both level and in frequency with increasing flow velocity.

The following observations are noted in these data:

- Spectra obtained at most measurement positions were dominated by a single low-frequency peak, and were generally broadband random signals.

- The spectra at nozzle position 23 show no appreciable falloff up to 10 kHz.

- The high-frequency falloff rate was virtually independent of engine thrust setting.

- Discrete-frequency engine tones appear in most measurements, but dominate only in those spectra measured at nozzle position 23.

- Vibration contamination, characterized by spectral components

16

which do not change frequency with a change in thrust setting, was significantly present at flap measurement positions 36 and 40 for this test configuration and present to a small degree at most fuselage measurement positions.

● The frequency resolution of 48.8 Hz used to obtain these spectra was too large to resolve a low-frequency peak at measurement positions on the lower fuselage.

● Two distinct broadband peaks are evident in the spectra measured at the three wing positions, with the high-frequency peak occurring at approximately five times the frequency of the low-frequency peak. Considering the sketch shown in figure 8(b), note that the velocity profile near the nozzle exit $(0 < x < x_o)$ for this configuration differs from the shape of a developed wall jet $(x > x_o)$ by the presence of a central core region (II).

Note also the following:

1. The low-frequency spectral peak is present at nozzle position 23 whereas the higher frequency peak is not (see figure 16).

2. The low-frequency peak corresponds to the single peak appearing at positions on the USB flap, and the high-frequency peak has vanished (compare figures 6, 7, and 8).

3. Reference 23 suggests that the dominant contribution to the surface fluctuating pressure field under a developed wall jet arises from the region near and above the velocity maximum.

4. The velocity profile at position 39 (first sensor on flap downstream of position 43) does not show a plateau region of nearly uniform velocity corresponding to region II (see figure 10 (a)).

Based upon these observations, it is believed that the presence of two distinct spectral peaks at measurement positions on the wing is related to the existence of the core region (II) in the velocity profiles at these positions and further, that the low-frequency peak results from sources in the core region and above whereas the high-frequency peak results from sources in the inner or wall layer (I). (If the frequency scale is contracted by a factor of four, the characteristic spectral shape measured at wing position 43 on the 1/4-scale model agrees quite closely with results of the Boeing full-scale test, presented in Reference 11.)

Variation with test configuration. - Figures 23 through 29 present spectra obtained at 75% engine thrust settings for all 16 test configurations arranged in seven geometric groups of four measurement positions each. Table III provides a listing of the test configurations plotted at each measurement position.

The following observation are noted in these data:

●   The effects of deployment of the vortex generators were predominant at most measurement positions over the effects of changes in any other test parameter at fixed thrust setting.

●   Deployment of the vortex generators consistently increased or maintained the spectral levels with the exception of small frequency regions in the data obtained at measurement positions 41 and 43.

●   A consistent shift of affected spectral region upward in frequency when the vortex generators were raised occurred with an increased distance from the nozzle exit. Examination of figures 23, 24, and 25 shows the affected region limited to midfrequencies at wing position 32, spreading out to frequencies above 10 000 Hz

18

at position 43, shifting to still higher frequencies at position 39, and collapsing below 1000 Hz at position 41.

- Spectra at the two outboard flap measurement positions showed no change with test configuration.

- Deployment of the vortex generators affected the surface pressure PSDs at both upstream and downstream measurement positions, including position 23 located in the side wall of the exhaust nozzle.

- Small increases in the PSD functions occurred at several measurement positions when the standard set of vortex generators was replaced by the modified set. Specifically, the affected positions were numbers 32, 34, and 41 on the wing and USB flaps, and position numbers 1, 6, 7, 20, 109, and 112 on the fuselage and fairing.

Additional, more specific observations noted in these data are included on each of figures 23 through 29.

Spatial variation along wing and flap. - The spatial variation of pressure spectra on the wing and USB flap along the engine centerline is presented in figure 30. Note that these data are arbitrarily aligned vertically to illustrate the change in shape between measurements, and in fact, that overall level of the pressure disturbances increased at successively greater distances downstream. These data of both figures 30 (a) and 30 (b) show a gradual change of spectral shape from near the engine exhaust nozzle to near the trailing edge of the flap. To assume knowledge of the pressure spectral shapes at all locations between measurement positions 32 and 41 due to the continuously varying character of these spectra appears reasonable. A number of small spectral peaks, particularly in the data measured at wing positions 32 and 33, appear to be vibration-induced components by their consistent frequency from one measurement to the next.

At least two spectral regions show a consistent decrease in frequency

with increased distance downstream from the nozzle. These regular decreases in peak frequency imply Strouhal relationships where the product of frequency and a characteristic length, divided by a characteristic velocity, remains constant. Accordingly, an increase in length scale and/or a decrease in velocity scale of the predominate, unsteady pressure disturbances has apparently occurred with downstream flow distance. This observation emphasizes that the predominant sources of unsteady pressure measured on the wing and flap of the model are likely to be local in nature and that better normalization of these data should occur by using local rather than global (such as the flow conditions at the exit of the nozzle) flow parameters.

Normalization by flow parameters. - Similar measurements of the PSD of pressure fluctuations beneath a turbulent wall jet were reported by Lilley and Hodgson (Reference 23). Although their data were obtained under laboratory conditions and at a lower flow velocity (maximum of 32 m/sec (105 fps)), the flow conditions were quite similar to those over the USB flap of the model. Using the technique of Reference 23, spectral data from this test were normalized using the following flow parameters to nondimensionalize both the magnitude and frequency scales of the PSD function:

U_m, the maximum local flow velocity immediately above the measurement position

Z_m, the height above the surface at which U_m occurs;

$Z_{1/2}$, the height (in the outer region, above Z_m) where the flow velocity is $1/2 U_m$;

ρ, the fluid density.

Data selected for use were obtained on the main and aft USB flaps of the 1/4-scale YC-14 model at a 100% thrust setting (Run 284). Local velocity data were extracted from the velocity profiles presented in figures 10 and 11. These normalized data are presented in figure 31 (b) and the comparison with the measurements of Reference 23, included in figure 31(a), is seen to be very good. (Note that in the low-speed experiment of Lilley and Hodgson, the fluid

20

density ρ was constant, whereas for the current normalization, the density selected was that occurring at Z_m and was calculated from the measured pressure and temperature by the ideal gas law.) Based on these results, the simple normalization approach presented here should be considered for use in estimating surface pressure PSD functions of other wall jet configurations using the local mean velocity profiles.

Similar normalizations were done using data at USB flap positions 39 and 41 for the four thrust settings of runs 284 through 287. As shown in figures 32(a) and 32(b), these spectra also demonstrate good collapse for three thrust settings of four at each position and show reasonable agreement at all four thrust settings with the data of Reference 23. Table IV includes a tabulation of the flow parameters used to obtain the data shown in figures 31(b) and 32.

Overall Fluctuating Pressure Levels

<u>Variation with test configuration.</u> - The overall fluctuating pressure level (OAFPL) of each measurement is provided in Table V. (Data are in dB referenced to 2×10^{-5} Pa.) A cursory examination shows that OAFPLs generally increased with an increase in thrust setting. Note also that not only do the levels vary among measurement positions, but that the increase in dB with thrust setting does not remain constant from one position to the next.

A convenient method to examine the changes in OAFPLs with test configuration is obtained by plotting all data obtained at a fixed engine thrust setting. Plots of OAFPL data obtained at each of the 16 tests at a 75% thrust setting are provided in figures 33(a) through 33(g).

The following observations are noted in these data:

- The highest OAFPL for all test configurations did not occur along the nozzle centerline, but at position 34 on the main USB flap located 24.5 cm outboard from the centerline.

- The lowest OAFPL consistently occurred at measurement position

112 located at the downstream, inboard corner of the upper fuse-lage.

- The OAFPLs of data obtained at wing position 43 for all configurations with the vortex generators up were consistently higher than those data obtained with the vortex generators down.

- A significantly higher OAFPL occurred at main flap position 34 with the modified set of vortex generators in a raised position (configuration 16) than with the basic set of vortex generators raised (configuration 15).

- Comparison of data between configurations 4 and 5 and between 8 and 9 revealed insignificant change in OAFPLs with the installation or removal of the flap/fuselage seal except at positions in the lower fuselage region, where levels were from 1.6 to 7.4 dB higher when the seal was installed.

- The spread in OAFPLs among the four measurement positions of each geometric group was significantly greater in the upper fuselage and lower fuselage regions than in the other five groups.

- Effect of changes in model height were small.

Spatial variation on surface of model. - To aid in visualizing the distribution of OAFPL values over the surface of the model, sketches of the model were made with a bar shown at each of the measurement positions whose height is proportional to the calculated mean-square value of fluctuating pressure. Figure 34 presents data using this technique and shows the effect of deployment of the vortex generators. These sketches illustrate that the highest overall pressure levels generally occurred at positions on the USB flaps followed by positions on the fairing side. Also note than an increase in OAFPL occurs from flap position 39 to position 41 (along the nozzle centerline) whereas the OAFPL decreases when progressing from the main flap sensor to the aft flap sensor at any of the other three flap stations.

Additional data of this form are presented in figure 35 which shows the

22

changes in OAFPL with a decrease in engine thrust setting (for test configuration 6). These figures reveal a decrease at all measurement positions with a decreased thrust setting; although, the rates of decrease are difficult to compare from data in this form.

Variation with jet flow velocity. - A logical method to investigate the rates of change of OAFPL with thrust setting is to plot the OAFPL versus some measure of the jet-flow velocity. The flow velocity parameter selected for these plots was the maximum nozzle centerline exit velocity. These velocity data were obtained at 25%, 50%, 75%, and 100% engine thrust settings by extracting the peak velocity values from the four curves shown in figure 9(a).

Plots of OAFPL versus flow velocity are presented in figures 36 through 42 using data obtained from test configurations 9 and 10. These data are arranged to additionally show the effects of deployment of the vortex generators. The values for "slope" shown in these figures is the corresponding power law exponent of the velocity at which the mean square fluctuating pressure changed. That is, a slope of 2.0 signifies an increase of 6 dB/doubling of velocity while a slope of 4.0 is an increase of 12 dB/doubling.

The following observations are noted in these data:

- Excellent straight-line correlation is obtained for most measurements when presented in this format.

- The slopes of best-fit lines through the four data points varied both within each geometric group and with deployment of the vortex generators.

- The largest change in slope with deployment of the vortex generators was an increase of 0.98 at position 43, located on the wing in the midst of the vortex generators.

- Slopes at measurement positions in the upper fuselage region were significantly higher than those at positions in the other geometric regions.

- The largest deviation from straight-line variation occurred at

those measurement positions in the lower fuselage region.

Table VI provides a complete set of best-fit exponents calculated in this manner. The linear correlation coefficient of OAFPL with maximum nozzle centerline exit velocity (on a logarithmic basis) was found to be greater than 0.99 for nearly all measurement positions and test configurations.

To investigate these "exponent" or "slope" data further, the information in Table VI is plotted by geometric groups in figures 43(a) through 43(g). Several interesting features of the data appear from inspection of these figures. First, note the large variation in the data, both with test configuration and with location on the model. Exponents ranging from less than 2.0 to about 6.0 were measured. This wide data spread suggests substantial differences between the characteristics of source mechanisms contributing to the fluctuating pressure sensed at each position.

A comparison of figures 43(c) and 43(d) shows that although the calculated exponents at both aft flap and at upper fuselage positions were nearly independent of test configuration (with the 86.5° flap installed), the rates of increase of OAFPL with flow velocity were considerably different for the two locations. While overall pressure levels at the flap positions increased at approximately the 3.5 power of the nozzle flow velocity, the levels at upper fuselage positions increased at approximately the 5th power of the flow velocity. Intermediate between these two rates of increase, the data at fairing top measurement positions appear to cluster around the value of 4.0, as shown in figure 43(e).

As illustrated previously in the tuft photographs of figure 12, virtually no flow extended onto the upper fuselage region of the model. In contrast, from interpretation of the surface static pressure contour plots provided in figures 13 and 14, and from flow-survey data obtained above the positions of the flap pressure sensors, the surfaces of the USB flaps lie largely under the direct path of the jet exhaust flow. Relating these characteristics to the data in figures 43(c) and 43(d) suggests the dominance of higher exponent,

24

acoustic pressure sources at locations outside the flow, and of lower exponent, hydrodynamic pressure sources within it, plus a mixture of these two influences near the flow boundaries. Further examples of this relationship are noted on figures 43(b), 43(d) and 43(g) by circled regions whose data follow these trends.

A somewhat different effect is noted in the data of wing position 43, located in the midst of the vortex generators. As highlighted in figure 43(a), calculated exponents at this position fell into two consistent bands: exponents for all test configurations with the vortex generators down fell in the range of 3.5 to 4.0, while exponents for all configurations with the vortex generators up ranged from approximately 4.5 to 5.0. Since hydrodynamic pressure variations are undoubtedly dominant over acoustic variations at this wing position under the main jet-flow path for all test configurations, this change in exponent must be related to changes in the turbulent pressure field. It is not surprising that the rate at which the fluctuating velocity increased (which controls the rate at which hydrodynamic pressures increased) relative to the mean-flow velocity was greater with the vortex generators up since the design of the vortex generators, in fact, is aimed at increasing the levels of vorticity present.

These findings of various rates of increase of fluctuating pressures with flow velocity are in general agreement with previous investigations. In particular, there exists theoretical and experimental evidence of aeroacoustic source mechanisms whose strengths increase as fourth or sixth powers of flow velocity. These results correspond with the range of exponents displayed by the upper fuselage data presented in figure 43(d). Additional agreement may be found with data results of a previous USB model test, presented in Reference 3, of similarly defined Mach number exponents whose values averaged 3.8 at surface measurement positions in regions beneath the jet flow.

Correlation of Surface Pressures

Correlation characteristics of the unsteady surface pressure field were investigated by interpretation of cross-correlation functions obtained between selected pairs of surface pressure measurements. All data presented are derived from cross-correlation functions computed for 1024 lag values, for time delays from 0.0 to 10.24 milliseconds.

A knowledge of the space-time correlation of the surface pressure is necessary to assess the dynamic loads applied to the structure. Pressures correlated over distances comparable to the bending wavelength of the (skin) structure at a particular frequency are more efficiently coupled to the structure than those correlated over larger or smaller distances. High values of correlation, existing in combination with the appropriate length scales, increase the potential for structural fatigue failures. In addition, a knowledge of the pressure correlation characteristics is useful in studying the generating mechanisms and relative importance of the fluctuating pressure sources which exist.

Correlation function on wing and flap along nozzle centerline. - Typical cross-correlation functions obtained between measurement positions on the wing and flap along the nozzle centerline are presented in figures 44 and 45. In figure 44, cross-correlation functions between the pressure measured at the first wing position downstream from the nozzle, number 32, and each of the other four positions along the nozzle centerline are shown for both vortex generators up and down conditions. The functions presented in figures 44(a) and 44(b) were computed from data obtained during runs at 100% thrust setting in test configurations 7 and 8, respectively.

The pattern of data presented in figure 44(b) for a test with the vortex generators down is typical of measurements obtained beneath "clean" turbulent boundary layer flows and implies the existence of a decaying, convecting pressure pattern by the uniformly decreasing values of peak correlation at

26

increasing time delays. The data presented in figure 44(a), for a test with the vortex generators up, also show decaying values of peak correlation at successively increasing time delays; however, the rate of decay of the correlation peak does not appear uniform. This is indicative of the nonuniform flow pattern established as the presence of the vortex generators causes additional fluid to be entrained downward and to the sides by pressure gradients along the span of the plate surfaces. As shown later, the presence of the vortex generators systematically reduced the value of peak correlation between those positions on the model where the flow field was affected.

Figure 45 presents additional cross-correlation functions obtained between measurement positions on the wing and shows the effect of changes in engine thrust setting. Cross-correlation functions between wing positions 32 and 33 with the vortex generators up and then down are shown in figures 45(a) and 45(b), respectively. Cross-correlation functions for the same tests between wing positions 32 and 43 are shown in figures 45(c) and 45(d). Note that the values of peak correlation decrease and the corresponding time delays increase as the separation distance between measurement positions increases for all four engine thrust settings. Notice in addition, however, that the effects of changes in thrust setting from one measurement pair to the other is not uniform, but that the peak value of correlation extends over a 2-to-1 range in figure 45(a), but only over a 1.15-to-1 range in figure 45(c). This implies a change in the character of the fluctuating pressure disturbances on the wing as a function of the flow velocity with the vortex generators in the up position. On the other hand, the peak value of correlation is seen to decrease more uniformly with the vortex generators in the down position, by a comparison of figures 45(b) and 45(d). Note also that generally the peak values of correlation neither increase nor decrease monotonically as a function of engine power setting.

Spatial correlation. - To provide information on the spatial correlation characteristics of the fluctuating pressures on the surfaces of the model, the

correlation coefficient between pairs of measurement positions at a time delay of zero are compared. These data for all 64 tests and the selected analysis pairs are provided in Table VII. To allow easier investigation of trends in these data as a function of test configuration, all values obtained during runs at a 75% engine thrust setting are plotted in figures 46(a) through 46(i).

Examining these figures, the following observations are noted:

- Spatial correlation is less than 0.2 for the majority of measurement pairs selected for analysis.

- The effects of the raising or lowering of the vortex generators on the spatial correlation between wing positions 32 and 33 and between positions 33 and 43 were found to be dominant over the effects of changes in the flap angle, changes in the height of the model, or the presence of the flap/fuselage seal.

- The value of correlation between wing measurement positions 32 and 33 (with the vortex generators down) changed from approximately -0.1 for all test configurations with the skewed-plug primary nozzle installed to approximately +0.05 with the straight-plug nozzle (see figure 46(f)). Changes in spatial correlation were also observed with changes in nozzle shape between USB flap positions 39 and 34 and between positions 34 and 38.

- Larger variations generally exist between the various measurement pairs than between configurations for a selected measurement pair.

- No consistent trends were noted in these data with changes in either the model height above ground or with the installation of the seal at the flap/fuselage function.

To estimate the area over which the surface pressures are correlated on the wing and flaps, the correlation coefficient at zero time delay can be plotted as a function of sensor separation distance in both a longitudinal line down the nozzle centerline and along either of two lateral lines across the

flaps. The "correlation length" of the pressures is then classically taken as either the integral of this function or as the distance to the first zero crossing, and the correlation area is calculated by the product of the longitudinal correlation length and the lateral correlation length.

Longitudinal and lateral space correlation functions over the wing and flap surfaces of the model are presented in figures 47(a) through 47(d) for longitudinal separation down the nozzle centerline from position 32, and in figures 48(a) through 48(d) for lateral separation across the main USB flap from position 39. As suggested by the curves sketched through the available data points, the longitudinal correlation function first crosses zero at a separation distance of less than 10 cm and tends to oscillate about the zero line. On the other hand, the lateral correlation appears to decay more slowly and approaches zero at higher separation distances. Similar results have been almost universally measured by other investigators. Results obtained by Bull (Reference 24) are included in figure 49 where the abscissa is the separation distance, ξ, divided by the boundary layer displacement thickness, δ^*. (Note the discrepancy of data in figure 48(a) obtained for configurations 1 and 2 with the straight-plug primary nozzle. This may be attributed to the difference in the flow field over the USB flap between the straight-plug and skewed-plug configurations.)

Although spatial correlation functions are shown for the pressure field on the surfaces of the wing and flaps, some indication of the spatial correlation characteristics on the surface of the fuselage is also available. Specifically, data shown in figure 46(b) illustrate that the spatial correlation between measurement positions 6 and 4 (separation distance = 14 cm) in the lower fuselage region remained approximately +0.5 for all test configurations. Comparing this value with the space correlation functions at wing position 32 shown in figure 47 (separation distance from 32 to 33 = 12.5 cm) implies a larger pressure correlation length on the lower fuselage surface than on the wing surface.

This observation is consistent with the results of previous investigators who report the measurement of longitudinal pressure correlation lengths nearly proportional to the convection velocity of the pressure disturbances. Although the flow-velocity profile was not measured adjacent to the lower fuselage surface, the average velocity is undoubtedly lower in this region than above the surface of the wing near the nozzle exit.

Peak correlation coefficients. - The coupling between surface fluctuating pressures and the vibration of a structure is dependent upon the spatial correlation lengths of the pressures and also upon the strength of the correlation as a function of time delay. The degree of correlation between the pressures sensed at two measurement positions on the model at a time delay of strongest correlation is designated as the value of "peak correlation coefficient". Table VIII provides a compilation of peak correlation coefficient data for all 64 tests and the selected analysis pairs. These data were obtained for each pair by extracting the maximum value that the cross-correlation function obtained for time delays of the pressure sensed at the first measurement position from 0.0 to 10.24 ms. Again, to allow investigation of trends in these data, all values obtained during runs at a 75% thrust setting are plotted as a function of test configuration number in figures 50(a) through 50(i).

Several of the trends noted previously to occur in plots of correlation coefficient at zero time delay versus configuration number (presented in figures 46(a) through 46(i)) also appear in these plots of peak correlation coefficient versus configuration. Specifically, the following observations are noted in these data:

- Correlation between measurement positions 3 and 103, located on the fairing sidewall and separated by 2.5 cm, was greater than 0.8.
- Peak correlation coefficients with the 86.5° flap installed were consistently higher between fuselage measurement positions 6 and 4 with the flap/fuselage junction gap open than with the gap sealed.

Increases in peak correlation from 0.50 to 0.60 and from 0.38 to 0.55 between test configurations 4 and 5 and between 9 and 8, respectively, were noted with the removal of the flap/fuselage seal (see figure 50(b)).

- Larger values of peak correlation were observed between measurements at side fairing positions 7 and 3 and between lower fuselage positions 6 and 15 with the 16° USB flap installed than with either the 70° or 86.5° flap.

- Trends showing an increase in correlation with lowering of the vortex generators were noted in data obtained between measurement positions 32 and 33, 33 and 43, and 39 and 34. Also noted in the data obtained between positions 32 and 33 was a significantly smaller correlation with the straight-plug primary nozzle installed than with the skewed-plug primary nozzle.

- Correlation between upper fuselage measurement positions 109 and 112 was consistently lower with the 16° flap installed than with either the 86.5° or 70° flaps installed.

Broadband convection velocities. - Additional information characterizing the surface pressure field which may be extracted from the cross-correlation functions is the time delay at which the correlation function obtains its peak value. This time delay may be considered the average time required for the pressure disturbances (in general, a combination of small, large, slow, and fast turbulent sources and acoustic sources) to travel from the first measurement position to the second.

Table IX provides velocities calculated by dividing these time delay data into the corresponding physical separation distances between measurement positions, for all 16 test configurations and the selected analysis pairs. Data from measurement pairs oriented along directions significantly different from the estimated direction of travel of the pressure disturbances are not included. The data are designated "broadband convection velocities" to denote

that they are average values over frequency and that a convective pressure process is likely to dominate over most surfaces of the model.

Examination of these data indeed show the classical characteristics of a convecting pressure field at most measurement positions, with the velocities measured along the nozzle centerline on the order of 0.6 to 0.8 times the flow velocity at the peak of the velocity profile. Data obtained between upper fuselage measurement positions 109 and 112, on the other hand, show values remaining near 350 m/sec for all thrust settings, indicating the dominance of acoustic pressure disturbances in this region. Small changes in velocity which do occur in these data obtained between positions 109 and 112 are attributed to changes in the sonic velocity with changes in the local fluid temperature.

To investigate changes in these broadband convection velocity data as a function of test configuration, all data obtained for runs at 75% engine thrust setting are plotted in figures 51(a) through 51(h). The "sonic region" designated in these figures marks the upper and lower velocities of the speed of sound in still air at 230° C (440° F) and 0° C (32° F), respectively. The following observations are noted on examination of these data:

- A significant decrease in convection velocity between lower fuselage measurement positions 4 and 15 with the 16° flap occurs when the vortex generators are lowered. This implies a change in the basic characteristics of the pressure field in this region from a domination of acoustic disturbances when the vortex generators are up to a lower speed convective process when the vortex generators are down.

- Broadband convection velocities calculated between wing and main flap positions 32 and 29 were significantly higher for test configurations with the straight-plug primary nozzle installed and with the modified vortex generators in the raised position than for test configurations 5 through 10 (skewed-plug primary nozzle and

32

runs with standard vortex generators both up and down).

- The variation in calculated broadband convection velocity with test configuration between wing positions 32 and 33 was small for the 12 configurations for which data were available, ranging from 248 to 270 m/sec.

- Contrasting effects were noted between data from positions 34 and 35 and from positions 39 and 41 when the vortex generators were raised. An increase in broadband convection velocity was noted from flap positions 39 to 41, located along the nozzle centerline, while a decrease was noted from flap positions 34 to 35, located along a parallel line 24.5 cm outboard from the nozzle centerline. This is indicative of a flow acceleration from 39 to 41 and a flow deceleration from 34 to 35 with deployment of the vortex generators.

- Data measured between upper fuselage positions 109 and 112 consistently fell in the "sonic region" for all test configurations for which data were available.

Narrowband convection velocities. - The phase angle portion of a cross-spectral function obtained between two fluctuating pressure signals is the average phase difference occurring between the two signals at each frequency. For the situation of a pressure disturbance traveling from one measurement position to another, the calculated phase angle at each frequency can be associated with the time required by a vector revolving at that frequency to rotate through the corresponding phase angle. By dividing this time into the distance between the measurement positions, a measure of the "narrowband" velocity can be obtained. For those regions of the model where a convective process dominates, this plot of velocity versus frequency may be appropriately termed a "narrowband convection velocity" plot.

Cross-spectral phase data obtained between three pairs of adjacent positions on the wing and flap along the nozzle centerline for four engine thrust

settings with the vortex generators down are presented in figure 52, and similar data with the vortex generators up are presented in figure 53. These data all start at zero phase angle at zero frequency and typically proceed as a series of sloping lines of decreasing values of phase angle at increasing values of frequency. These phase angle data were obtained by computing the arctangent of the imaginary (quad) and real (co) portions of the cross-spectral functions. Cross-spectral functions in co- and quad-spectral forms corresponding to those phase data of figures 52 and 53 are included in figures 54 and 55, respectively. Note that although these data are generally quite small at high frequencies, their ratio is often still deterministic, as indicated by definable visual trends in most of the phase angle plots up to 10 000 Hz. The anomalous behavior above 5000 Hz of the co/quad-spectral functions calculated between measurement positions 43 and 39 at 50% engine thrust setting is not understood, but is believed to be a spurious effect introduced by the data-reduction process.

Because of the random character of portions of the phase angle data presented in figures 52 and 53, difficulty would arise in using these functions to calculate the corresponding narrowband convection velocities. To obtain a more useful phase data for this intended purpose, the cross-spectral functions between wing measurement positions 32 and 33 for configuration 9 were recomputed using a 97.6-Hz frequency resolution and 1200 ensemble time averages, rather than a 48.8-Hz resolution and 350 averages. (These two values were used for the complete bulk data reduction program including the data presented in figures 52 and 53.) By decreasing the resolution and increasing the statistical confidence with which the cross-spectral functions were calculated, the data presented in the first column of figure 52 were found to form considerably smoother varying functions of frequency, with better defined breakpoint frequencies and irregular jumps in phase angle only at those points corresponding to discrete frequency acoustic tones.

Narrowband convection velocities between measurement positions 32 and 33 using these recomputed phase angle data were obtained for configuration 9

tests at 25%, 50%, 75%, and 100% engine thrust settings and are provided in the left-hand plot of figure 56. Of particular interest to note in this plot is the significant change in these functions at frequencies ranging from 2400 Hz at a 25% engine thrust setting to 3800 Hz at a 100% engine thrust setting. Below these frequencies, the narrowband velocity plots indicate relatively constant velocity as a function of frequency.

Data in these low-frequency regions are indicative of pressure convective processes by magnitudes approximately 0.8 times the maximum of the local velocity profile above the measurement positions. Also note that the broadband convection velocities calculated from the delay times of maximum correlation (designated V_{BB} in figure 56) correspond to the narrowband convection velocities in these low-frequency regions. (The large peaks at approximately 200 Hz in the narrowband velocity data of figure 56 are believed to be vibration-induced components.)

The monotonically increasing trend of all four functions presented in figure 56 at high frequencies is difficult to understand. This behavior may be related to increased contributions of acoustic pressure disturbances (which travel in the range of 325 to 375 m/sec near these measurement positions) to the high-frequency portion of the fluctuating pressure field at these positions. The average velocity of the pressure disturbances at each frequency may be considered to be the weighted average of the hydrodynamic pressures moving at their convection velocity and of the acoustic pressures moving at the sonic velocity. Note that although the perturbations on the data of figure 56 may likely be random irregularities, the trends indicated, i.e., a plateau region, a sharp drop and then a steadily increasing function, are the result of definitive cross-spectral phase angle data over these frequencies.

It is worth reemphasizing at this point that the cross-spectral function of a turbulent pressure field is a function of both frequency and wave number. This contrasts with the simpler form of the cross-spectral function for longitudinal acoustic pressure waves, where the spectrum contains energy only at a

particular wave number for each frequency. Each component of the wave number frequency spectrum of a turbulent pressure field is associated with a ratio of the speed of a turbulent eddy divided by the size of the eddy, i.e., large eddies moving quickly contribute energy to the spectrum at the same frequency as small eddies moving slowly.

Complete wave number frequency spectra are formidable to obtain experimentally because of the requirement for an extensive array of measurement positions. An assumption usually made by previous experimenters was that the complete spectrum (or equivalently the space-time correlation function) could be estimated from a combination of measurements made in both longitudinal and in lateral directions to the flow.

Estimation of wave number spectra on the wing and flaps could be obtained by Fourier transformation of the space correlation functions presented in figures 47 and 48. Obviously, the accuracy of the results depends upon the accuracy with which these space correlation functions are known. This was rather poor for this test as only five sensors were used in the longitudinal direction and four in the lateral direction. In addition, it is reasonable to expect spatial nonhomogeneities in the fluctuating pressure field over these distances because of the significant changes noted in the velocity profiles both down the engine centerline and along the USB flaps.

A method which may be used to provide some information on the wave number (or wavelength) distribution of fluctuating pressures is to plot measurements of narrowband convection velocity versus the angular frequency divided by the narrowband convection velocity (equal to wave number for a pure convective process). This method was used on those narrowband convection velocity data of figure 56, measured between wing positions 32 and 33 for test configuration 9. Following the method used by Bull (Reference 25), convection velocity and wave number are both made nondimensional by dividing by the free stream velocity U_o, and by multiplying by the boundary layer displacement thickness, δ^*, respectively. Values selected for U_o and δ^* to perform

36

these normalizations were estimated from the velocity profiles measured at the exit plane of the nozzle and at main flap position 39 located along the nozzle centerline (because no velocity measurements were made above the wing sensor positions). The velocity at the peak of the local vertical profile was considered for this wall jet flow configuration to be analogous to the free stream velocity for the normal boundary layer flow configuration. The displacement thickness was then estimated as 0.35 times the height of the local velocity maximum.

These plots of nondimensional narrowband convection velocity versus nondimensional wave number are shown in figure 57(a). The previous results of Bull, calculated from data under a conventional turbulent boundary layer, are included in figure 57(b). Consistent with Bull's data, and those of other investigators, these data measured on the 1/4-scale YC-14 model wing fell in the range 0.6-0.85. However, a significant difference noted between the data of figures 57(a) and 57(b) is that while Bull's data appear as concave-up curves, the present data collapse as a concave-down trend.

Bull noted that his data suggest that the larger eddies (i.e., low wave number components) tend to move at 0.8 times the free stream velocity and all move at nearly the same speed, while the smaller eddies move at approximately 0.6 times the free stream velocity and display a wider spread in average velocity (depending upon the sensor separation distance). Most investigators believe that pressure disturbances displaying a particular convection velocity are related to sources in that portion of the boundary layer of equal flow velocity. By this assumption, the peak in the data of figure 57(a) may well be related to sources located near the peak in the characteristic wall jet velocity profile measured above the wing and flaps.

In the region from the surface of the model to the velocity peak, the velocity profile of a wall jet flow may be readily compared with a conventional boundary layer profile. Accordingly, it is reasonable to also assume that the high wave number components of figure 57(a) are associated with the flow

region below the velocity maximum (following Bull's interpretation of figure 57(b)). A further assumption would be an association of the low wave number components of figure 57(a) with sources in the flow region above the velocity maximum. Although not supported by measurements on this model, this third assumption would be consistent if the scale of the turbulence was significantly larger above the velocity maximum than below, such that if an increasing scale of turbulence existed with increasing distance above the wing surface. This characteristic has, in fact, been measured experimentally by Kacker and Whitelaw on a wall jet under a moving stream (Reference 19, figure 9), in their investigation of the effectiveness of wall jets for film cooling.

Phase angle data from three additional pairs of measurement positions which displayed interesting trends are presented in figure 58. Measurement positions 1, 8, and 2 are located in a row along the top of the fuselage fairing and positions 9 and 112 are located in the upper fuselage region. Data for each of the three measurement pairs are shown for four engine thrust settings of configuration 9.

Data presented in figures 58(a) and 58(b) for measurement positions 1-8 and 8-2, respectively, are similar, and show an interesting behavior with changes in engine thrust setting. Systematic decreases in phase angle with increasing frequency from 0 to 10 kHz are seen to be most predominant at a 75% thrust setting, particularly in figure 58(a). On the other hand, data at 50% and 25% engine thrust settings show a phase angle of approximately zero at most frequencies. This implies the presence of a pressure disturbance traveling at nearly 90° to the direction of the line passing between the measurement positions.

As shown previously in figure 12, the photographs of tufts attached to the fuselage and fairing indicated that the flow boundary extended progressively farther up the fuselage with increases in engine thrust setting. From the data of figure 58, the flow boundary appears to be located slightly outboard of measurement positions 1, 8, and 2 during the 50% and 25% thrust settings of

test configuration 9, and that the high-frequency portions of the bottom two phase angle plots of both figures 58(a) and 58(b) are the result of a broadband acoustic pressure disturbance propagating from a downstream station located in the vicinity of the flap trailing edge. (See figure 6 for locations of positions 1, 8, and 2.) In fact, the slight positive increase in phase angle measured with increasing frequency implies that the disturbance traveled in a slightly upstream direction. The sharp change in phase angle at approximately 400 Hz in all four plots of figure 58(a) is believed to be a vibration-induced component.

Examination of phase angle data presented in figure 58(c), calculated between upper fuselage positions 109 and 112, shows a strikingly constant character both with frequency and with thrust setting. These data indicate unequivocally the domination of a fluctuating pressure disturbance propagating between these sensors, with the negative slope implying that the disturbance was sensed at upstream position 109 first. The narrowband convection velocities which may be calculated from these data are found to be independent of frequency and are equal to those broadband velocities calculated from the time delays of maximum correlation.

A small change in convection velocity noted with changes in thrust setting in the data of figure 58(c) may be related to either a change in fluid temperature or to a small change in the effective source location. Fluid temperatures approximately ambient near these measurement positions in combination with calculated "convection" velocities from 325 to 365 m/sec for these tests imply that an acoustic disturbance traveled in a direction nearly along the line connecting positions 109 and 112. Figure 6 shows this line points very closely to the center of the nozzle-exit plane.

Coherence of Surface Pressures

The coherence function calculated between two fluctuating pressure signals provides a measure of the similarity of the pressure components measured at one position with those measured at the other as a function of frequency. It is defined as the magnitude of the cross-spectral density function squared, divided by the product of the autospectral densities of the individual signals, and will always fall in the range of 0.0 to 1.0.

Coherence functions for the same data whose phase angle functions were shown in figure 58 are provided in figure 59. Generally, an increase in coherence is noted with a decrease in engine thrust setting except between the 100% and 75% thrust setting data of columns (a) and (b), where a slight decrease is noted. Of particular interest to note in these data are: 1) the appearance of two large dips in the data of column (a) at 25% thrust, 2) the fact that coherence was significantly more constant versus thrust setting in column (c) than in either column (a) or (b), and 3) that coherence at 25% thrust was significantly higher than at 75% or 100% thrust between positions 1 and 8 and positions 8 and 2.

Spatial variation along wing and flap. - To provide additional information on the coherence of the surface fluctuating pressure field, figures 60 through 63 provide coherence functions calculated from measurements taken on the wing and USB flaps along the nozzle centerline. Examining figures 60 and 61 first, the changes in the coherence function with both the raising of the vortex generators and with changes in sensor separation distance are seen. Figure 60 provides the effect of increase in separation from wing position 32 while figure 61 presents data from adjacent pairs of sensors along the centerline.

Examination of these data provides the following observations:

- The coherence function for measurements with the vortex generators down displayed two broad frequency regions whereas those with the vortex generators up consistently showed more and nar-

rower frequency peaks.

●　Coherence of the fluctuating pressure field between measurement pairs along the nozzle centerline at 100% thrust setting was insignificant above 3000 Hz except at discrete frequencies corresponding to those of known acoustic engine tones. This characteristic is particularly interesting to note in combination with the phase angle data and the high-frequency, narrowband convection velocity data shown in figure 56 -- the coherence of the pressure disturbances sensed at positions 32 and 33 (with the vortex generators down) is seen to drop to values < 0.05 above frequencies corresponding to the "break points" of the velocity data in figure 56.

Variation with thrust level and deployment of vortex generators. - Figures 62 and 63 show changes of the coherence function with both the raising of the vortex generators and with changes in engine thrust setting. Figure 62 provides data obtained between measurement positions 32 and 33 while figure 63 provides data between positions 32 and 43.

Examination of these data provides the following observations:

●　Raising of the vortex generators affected the coherence function calculated between measurement positions 32 and 33, both located upstream from the vortex generators. This impact was not as significant, however, as that on the coherence between measurement positions 32 and 43 (position 43 is located on the wing among the vortex generators).

●　The significant drop in coherence noted between two broad frequency peaks with the vortex generators down became significantly smaller at lower thrust settings between measurement positions 32 and 33 but remained approximately constant between positions 32 and 43.

●　Coherence of the pressure field for these measurement positions was generally greater at low thrust settings than at high thrust

settings.

- The high-frequency point above which the coherence was insignificantly small generally decreases in frequency with a decrease in engine thrust setting. In fact, distinguishably similar regions of the coherence function generally decreased in frequency with a decrease in engine thrust setting.

Maximum values of coherence functions. - The maximum value of the coherence function for each analysis pair for all 16 test configurations are provided in Table X. Although the entire coherence function is needed for a knowledge of the distribution of coherence with frequency, these data do provide an indication of the maximum coherence attained at any frequency (from 0 to 10 kHz) for each measurement pair and configuration tested. Thus, they are particularly useful to indicate those analysis pairs where the coherence was small; for those pairs of high maximum coherence a more detailed description of the function may be desired.

To examine changes in the maximum value of the coherence function with changes in test configuration, the data in Table X obtained for runs at 75% thrust setting are plotted versus test configuration number in figures 64(a) through 64(i). The following observations are noted in these data:

- The maximum coherence along the nozzle centerline between measurement position 32 and between successive positions 33, 43, 39, and 41 was approximately 0.8, 0.55, 0.25, and 0.05, respectively. These values varied little as a function of test configuration.

- Trends of a decrease in maximum coherence with raising of the vortex generators were observed in the data obtained between measurement pairs 39 and 34 and between 43 and 39, all located in the immediate vicinity of the vortex generators. No trends were noted between other analysis pairs when the vortex generators were raised.

● A wide data spread is noted for most analysis pairs with changes in test configuration.

Cross-Spectral Magnitude Functions

For a stationary, homogeneous pressure field, the properties of the field are completely defined by the space-time, cross-correlation function $R(\vec{\xi}, \tau)$, where $\vec{\xi}$ is the separation in space and τ is the separation in time.

By taking Fourier transforms of $R(\vec{\xi}, \tau)$ with respect to $\vec{\xi}$ or τ and holding the other variable constant, one obtains either the frequency spectrum, defined by

$$S(\vec{\xi}, f) = \int_{-\infty}^{\infty} R(\vec{\xi}, \tau) e^{-j2\pi f\tau} d\tau \qquad (1)$$

or the wave number spectrum, defined by

$$S(\vec{k}, \tau) = \int_{-\infty}^{\infty} R(\vec{\xi}, \tau) e^{-j2\pi \vec{k} \cdot \vec{\xi}} d\vec{\xi} \qquad (2)$$

A third form, the combined wave number frequency spectrum, may be obtained by taking either the wave number Fourier transform of $S(\vec{\xi}, f)$ or the frequency Fourier transform of $S(\vec{k}, \tau)$. Alternately, the wave number frequency spectrum, $S(\vec{k}, f)$, may be obtained by

$$S(\vec{k}, f) = \int_{-\infty}^{\infty} \int_{-\infty}^{\infty} R(\vec{\xi}, \tau) e^{-j2\pi(\vec{k} \cdot \vec{\xi} + f\tau)} d\vec{\xi} \, d\tau \qquad (3)$$

Note that the space-time correlation function and the three forms of the spectrum function presented in Equations (1) through (3) all contain the same information viewed in different ways, and that the particular form selected for use depends upon the requirements of the desired application.

To examine the properties of the fluctuating pressure field over the

43

surfaces of the 1/4-scale YC-14 model, data have thus far been presented in the forms of space-time correlation functions (at discrete separation distances and at time separations up to 10.24 ms), frequency spectra at zero space separation (PSD functions), and frequency spectra at discrete space separations in co/quad and phase forms (cross spectra). To complement these data, a few plots of the magnitude of the frequency spectrum (cross spectral) functions are included here. These plots represent the final form in which data for this test are provided.

Figures 65 through 67 provide plots of the magnitude of the frequency spectrum for data obtained on the wing and USB flap along the nozzle centerline during test configuration 8. Figure 65 illustrates the change as a function of longitudinal separation distance at a fixed engine thrust setting, and figures 66 and 67 show the effect of engine thrust setting between positions 32 and 33 and positions 32 and 43, respectively. Note that the magnitude portion of the cross spectral function is of the same form as the autospectrum (PSD) function, except that it is calculated from pressure signals obtained at two different positions rather than from two copies of the same signal. Accordingly, because of the smoothly varying nature of the PSD functions over most surfaces of the model (shown in figures 16 through 30), the cross spectral magnitude functions may be estimated quite closely as the smoothed average of PSD functions obtained at the two individual measurement positions.

CONCLUDING REMARKS

Fluctuating pressures on the surfaces of a 1/4-scale YC-14 ground-test model were investigated. This project is one phase of an ongoing NASA program to further the understanding of the characteristics of the surface fluctuating pressure fields existing on powered-lift STOL aircraft configurations and to increase the accuracy of techniques used to predict the resulting dynamic loading environments. Results of this test provide the following items

44

of interest towards the objectives of this program:

- Overall fluctuating pressure levels on the order of 160 dB at most positions on the 1/4-scale YC-14 model imply that significant structural dynamic loading is likely to exist on USB configurations in the vicinity of the jet exhaust. These high levels of loading will exist not only on the primary wing and flap structures, but also on adjacent regions of the fuselage sidewall. Thus, in addition to creating the need for special structural design considerations for the wing and flap components, the proximity of the engine exhaust to the fuselage of the aircraft in this USB concept demands that attention also be given to techniques for isolating the high exterior sound levels from the interior compartment areas. The sonic fatigue and interior cabin noise problems are both further amplified by the dominance of low-frequency energy in the fluctuating pressures. (Spectral peaks below 200 Hz were measured at most positions on this 1/4-scale model.)

- Power spectral densities of the fluctuating pressure signals measured at positions on the USB flaps were found to collapse in non-dimensional form quite well upon previous data presented by Lilley and Hodgson from a laboratory wall jet apparatus. The flow parameters selected for these normalizations were:

  1) The maximum flow velocity existing in the profile normal to the surface at the measurement position (U_m).

  2) The flow dynamic pressure at the vertical location of the velocity maximum ($1/2 \, \rho \, U_m^2$); and

  3) The vertical distance from the point of maximum velocity above the measurement position to a point further away from the surface where the velocity fell to one-half of the maximum value ($Z_{1/2} - Z_m$).

Use of these parameters to normalize surface pressures under a

45

wall jet flow is quite analogous to the nearly universal use of free stream velocity, full stream dynamic pressure and boundary layer height to obtain good collapse of pressure data under developed turbulent boundary layer flows. Although good agreement of non-dimensionalized spectra from measurements on the USB flap of the 1/4-scale YC-14 model was found with the data of Lilley and Hodgson, additional work is needed to make this a viable prediction technique for STOL pressure spectra using a knowledge of the local mean velocity profiles. In particular, the effects of changes in the shape of the local velocity profile (holding U_m, ρ, $Z_{1/2}$ and Z_m constant) on the corresponding surface PSD must be investigated.

- Excellent straight-line correlation was found to exist between overall fluctuating pressure levels in the region washed by the jet exhaust flow and a single value of flow velocity (plotted on a logarithmic basis) which was measured at the peak of the velocity profile in the center of the nozzle exit plane. The rate of increase of OAFPL with the velocity, however, varied substantially both with measurement position and with model configuration. In particular, significantly lower rates of increase were noted in regions known to be dominated by hydrodynamic pressures than in regions dominated by acoustic pressures. A more thorough understanding of the wide spread found in these data is needed before this information may be used to predict the changes in surface OAFPLs on STOL configurations using a knowledge of the mean flow boundaries.

- It should be emphasized, in closing, that although the characteristics of the surface fluctuating pressures measured on the 1/4-scale YC-14 model were related throughout the report to the characteristics of the mean flow field, the fluctuating properties of the

46

flow undoubtedly bear a more intimate relationship to the resulting pressures. However, because the mean flow properties are generally more easy to obtain, their use in investigating the fluctuating pressures are nearly universally reported by investigators in this field. The relationship of the mean flow conditions to the distribution of the fluctuating fluid properties deserves additional attention at this point in the study of USB dynamic loads, particularly for the configuration of a wall jet flow over a curved surface, with arbitrary pressure gradient.

REFERENCES

1. Lansing, D. L.; Mixson, J. S.; Brown, T. J.; and Drischler, J. A.: Externally Blown Flap Dynamic Loads. NASA SP-320, Oct. 1972, pp. 131-142.

2. Lansing, D. L.; Drischler, J. A.; Brown, T. J.; and Mixson, J. S.: Dynamic Loading of Aircraft Surfaces Due to Jet Exhaust Impingement. AGARD CP-113, May 1973. Paper No. 3.

3. Mixson, J. S.; Schoenster, J. A.; and Willis, C. M.: Fluctuating Pressures on Aircraft Wing and Flap Surfaces Associated with Powered-Lift Systems. AIAA paper 75-472, March 1975.

4. Schoenster, J. A.; Willis, C. M.; Schroeder, J. C.; and Mixson, J. S.: Acoustic-Loads Research for Powered-Lift Configurations. NASA SP-406, May 1976, pp. 429-443.

5. Willis, C. M.; Schoenster, J. A.; and Mixson, J. S.: Acoustic Loads on Upper-Surface-Blown Powered-Lift Systems. AIAA paper 77-1363, Oct. 1977.

6. Wick, B. H.; and Kuhn, R. E.: Turbofan STOL Research at NASA. Astronautics and Aeronautics, Vol. 9, May 1971, pp. 32-50.

7. Conference: STOL Technology. NASA SP-320, October 1972.

8. Conference: Powered-Lift Aerodynamics and Acoustics. NASA SP-406, May 1976.

9. AIAA/NASA Ames V/STOL Conference. June 1977, (AIAA papers 77-565 through 77-618).

10. Harkonen, D. L.; and Reed, J. B.: YC-14 Ground and Flight Experiments for NASA, Ground Test Final Report. Boeing Co. Report D748-10113-1, April 1976.

11. Sussman, M. B.; Harkonen, D. L.; and Reed, J. B.: USB Measurements Based on Full-Scale Static Engine Ground Tests. AIAA paper 76-624, July 1976.

12. Hassell, J. L.: Results of Static Tests of a 1/4-Scale Model of the Boeing YC-14 Powered-Lift System. NASA SP-406, May 1976, pp. 45-62.

13. Skavdahl, H.; Wang, T.; and Hirt, W.J.: Nozzle Development for the Upper Surface-Blown Jet Flap on the YC-14 Airplane. SAE paper 740469, April 1974.

14. Grotz, A.: Development of the YC-14 Propulsion System. AIAA paper 75-1314, September 1975.

15. Myers, G.F.; Schaver, J.J.; and Eustis, R.H.: Plane Turbulent Wall Jet Flow Development and Friction Factor. J. Basic Eng., Vol. 85, March 1963, pp. 47-54.

16. Glauert, M.B.: The Wall Jet. J. Fluid Mech., Vol. 1, 1956, pp. 625-643.

17. Bradshaw, P.; and Gee, M.T.: Turbulent Wall Jets with and without an External Stream. British Aeronautical Research Council, R & M Report 3252, June 1960.

18. Seban, R.A.; and Back L.H.: Velocity and Temperature Profiles in a Wall Jet. Inter. J. Heat and Mass Transfer, Vol. 3, 1961, pp. 255-265.

19. Kacker, S.C.; and Whitelaw, J.H.: Some Properties of the Two-Dimensional Turbulent Wall Jet in a Moving Stream. J. Appl. Mech., Vol. 35, Dec. 1968, pp. 641-651.

20. Goradia, S.H.; and Colwell, G.T.: Parametric Study of a Two-Dimensional Turbulent Wall Jet in a Moving Stream with Arbitrary Pressure Gradient. AIAA Journal, Vol. 9, Nov. 1971, pp. 2156-2165.

21. Ffowcs-Williams, J.E.: Hydrodynamic Noise. Annual Review of Fluid Mechanics, Vol. 1, 1969, pp. 197-222.

22. Chandiramani, K.L.: Interpretation of Wall Pressure Measurements Under a Turbulent Boundary Layer. BBN Report 1310, 1965.

23. Lilley, G.M.; and Hodgson, T.H.: On Surface Pressure Fluctuations in Turbulent Boundary Layers. College of Aeronautics (Crandall) Note 101, 1960.

24. Bull, M.K.: Wall-Pressure Fluctuations Associated with Subsonic Turbulent Boundary Layer Flow. J. Fluid Mech., Vol. 28, 1967, pp. 719-754.

25. Bull, M. K.: Properties of the Fluctuating Wall-Pressure Field of a Turbulent Boundary Layer. AGARD Report 455, 1963.

STRAIGHT PLUG PRIMARY NOZZLE

CONFIG.	RUN	THRUST, %	VORTEX GENERATORS	FLAP DEFLECTION, DEGREES	MODEL HEIGHT, METERS	FLAP/FUSELAGE JUNCTION
1	133	100	UP	86.5	1.45	SEALED
	134	75				
	135	50				
	136	25				
2	142	100	DOWN	86.5	1.45	SEALED
	143	75				
	144	50				
	145	25				

SKEWED PLUG PRIMARY NOZZLE

CONFIG.	RUN	THRUST, %	VORTEX GENERATORS	FLAP DEFLECTION, DEGREES	MODEL HEIGHT, METERS	FLAP/FUSELAGE JUNCTION
3	270	100	DOWN	86.5	1.45	SEALED
	271	75				
	272	50				
	273	25				
4	275	100	UP	86.5	1.45	SEALED *
	276	75				
	281	50				
	282	25				
5	284	100	UP	86.5	1.45	OPEN
	285	75				
	286	50				
	287	25				
6	289	100	DOWN	86.5	1.45	OPEN *
	290	75				
	291	50				
	292	25				
7	301	100	UP	86.5	2.29	OPEN *
	302	75				
	303	50				
	304	25				
8	306	100	DOWN	86.5	2.29	OPEN *
	307	75				
	308	50				
	309	25				
9	326	100	DOWN	86.5	2.29	SEALED
	327	75				
	328	50				
	329	25				
10	331	100	UP	86.5	2.29	SEALED
	332	75				
	333	50				
	334	25				
11	491	100	UP	16.0	2.29	OPEN
	492	75				
	493	50				
	494	25				
12	499	100	UP	16.0	1.45	OPEN
	500	75				
	501	50				
	502	25				
13	556	IDLE	DOWN	16.0	1.45	OPEN
	558	25				
	560	50				
	562	75				
14	567	IDLE	DOWN	70.0	1.45	SEALED
	569	25				
	571	50				
	573	75				
15	574	IDLE	UP	70.0	1.45	SEALED
	575	25				
	576	50				
	577	75				
16	578	IDLE	UP: MODIFIED	70.0	1.45	SEALED
	579	25				
	580	50				
	581	75				

*Signifies data also recorded during run up of engine

TABLE II
RUN-BY-RUN TABULATION OF PRINCIPAL
ENGINE PURE-TONE FREQUENCIES (HZ)

RUN	FAN RPM N1	COMPRESSOR RPM N2	SRF** 1	SRF 2	① FAN (28B)	② COMP (16B)	③ LOW TURBINE (55B)	④ LOW TURBINE (61B)	⑤ FAN + COMP	⑥ COMP (32B)
133	15087	31044	251	517	7041	8278	13830	15338	15319	16557
134	13064	28700	218	478	6097	7653	11975	13282	13750	15307
135	10780	26372	180	440	5031	7033	9882	10960	12063	14065
136	8191	23183	137	386	3822	6182	7508	8328	10005	12364
142	15102	30000*	252	500	7048	8000	13844	15354	15048	16000
143	13143	27800*	219	463	6133	7413	12048	13362	13547	14827
144	10931	26400*	182	440	5101	7040	10020	11113	12141	14080
145	8056	22350*	134	373	3759	5960	7385	8190	9719	11920
270	14126	29983	235	500	6592	7995	12949	14361	14588	15991
271	12649	28051	211	468	5903	7480	11595	12860	13383	14961
272	10644	25870	177	431	4967	6899	9757	10821	11866	13797
273	7857	21747	131	362	3667	5799	7202	7988	9466	11598
275	14165	30043	236	501	6610	8011	12985	14401	14622	16023
276	12859	28360	214	473	6001	7563	11787	13073	13564	15125
281	10802	26232	180	437	5041	6995	9902	10982	12036	13990
282	8364	22695	139	378	3903	6052	7667	8503	9955	12104
284	13991	29944	233	499	6529	7985	12825	14224	14514	15970
285	12794	28393	213	473	5971	7571	11728	13007	13542	15143
286	10922	26357	182	439	5097	7029	10012	11104	12125	14057
287	8273	22597	138	377	3861	6026	7584	8411	9887	12052
289	13982	29905	233	498	6525	7975	12817	14215	14500	15949
290	12684	28222	211	470	5919	7526	11627	12895	13445	15052
291	10805	26181	180	436	5042	6982	9905	10985	12024	13963
292	8396	22769	140	379	3918	6072	7696	8536	9990	12143
301	13782	29592	230	493	6432	7891	12634	14012	14323	15782
302	12298	27690	205	462	5739	7384	11273	12503	13123	14768
303	10441	25705	174	428	4872	6855	9571	10615	11727	13709
304	8002	22168	133	369	3734	5911	7335	8135	9646	11823
306	13761	29545	229	492	6422	7879	12614	13990	14300	15757
307	12350	27677	206	461	5763	7381	11321	12556	13144	14761
308	10445	25634	174	427	4874	6836	9575	10619	11710	13671
309	7934	21975	132	366	3703	5860	7273	8066	9563	11720
326	13753	29537	229	492	6418	7877	12607	13982	14295	15753
327	12246	27568	204	459	5715	7351	11226	12450	13066	14703
328	10407	25592	173	427	4857	6825	9540	10580	11681	13649
329	7913	21946	132	366	3693	5852	7254	8045	9545	11705
331	13793	29593	230	493	6437	7891	12644	14023	14328	15783
332	12271	27625	205	460	5726	7367	11248	12476	13093	14733
333	10480	25706	175	428	4891	6855	9607	10655	11746	13710
334	7932	21998	132	367	3702	5866	7271	8064	9568	11732
491	14058	29829	234	497	6560	7954	12887	14292	14515	15909
492	12495	27805	208	463	5831	7415	11454	12703	13246	14829
493	10780	25930	180	432	5031	6915	9882	10960	11945	13829
494	8220	22410	137	374	3836	5976	7535	8357	9812	11952
499	14045	29915	234	499	6554	7977	12875	14279	14532	15955
500	12538	27993	209	467	5851	7465	11493	12747	13316	14930
501	10728	26029	179	434	5006	6941	9834	10907	11947	13882
502	8058	22269	134	371	3760	5938	7387	8192	9699	11877

* RPM estimated from spectral peaks. (N2 tachometer malfunction)
** Shaft rotation frequency
Data not available for runs 556 - 581

TABLE III

Test configurations plotted in figures 23 - 29

CONFIGURATION NO.

POS. NO.	1	2	3	4	5	6	7	8	9	10	11	12	13	14	15	16
20			X	X			X	X	X	X	X	X	X		X	X
30	X	X	X	X	X	X	X	X	X	X	X	X	X		X	X
30		X	X	X	X	X	X	X	X	X	X	X	X		X	X
43	X		X	X	X	X	X	X	X	X	X	X		X		
36	X	X	X	X	X	X		X	X	X				X	X	X
38	X	X	X	X	X	X	X	X	X	X				X	X	X
34	X	X	X	X	X	X	X	X	X	X				X	X	X
39	X	X			X	X	X	X	X	X				X	X	X
37	X	X	X	X		X	X	X	X	X				X	X	
40	X	X	X	X	X	X	X	X	X	X				X		
35	X	X	X	X	X	X	X	X	X	X						
41					X	X	X	X	X							
9			X	X	X	X	X	X	X	X	X	X	X		X	X
109				X	X	X	X	X	X		X	X	X		X	X
112					X	X	X	X	X		X	X	X		X	X
20					X	X	X	X	X		X	X	X		X	X
10				X	X	X	X	X	X	X	X	X	X		X	
11					X	X	X	X	X		X	X	X		X	X
02						X		X	X	X						
7					X	X	X	X	X	X	X	X	X	X	X	
3			X	X	X	X	X	X	X	X	X	X	X	X	X	X
03					X	X	X	X	X		X	X	X	X	X	
11					X	X	X	X	X		X	X	X	X	X	X
6				X	X	X	X	X	X	X	X	X	X		X	X
4				X	X	X	X	X	X	X	X	X	X		X	
45				X	X	X	X	X	X	X	X	X	X		X	X
15				X	X	X	X	X	X	X	X	X	X		X	

53

TABLE IV

Data used for spectral normalizations shown in figures 31 and 32

	Position number	U_m (m/s)	At U_m P(Pa)	$T(°C)$	$Z_{1/2}$ (cm)	Z_m (cm)	Approx. degrees from flow direction
Main flap	36	192	3110	35	12.7	1.52	45
	38	204	3590	38	47.0	1.78	30
	34	252	5740	135	15.0	1.78	15
	39	383	6940	338	24.0	4.57	0
Aft flap	37	152	3590	40	21.0	1.52	40
	40	156	3830	60	14.5	1.52	25
	35	220	6940	121	21.0	1.78	10
	41	319	5020	266	46.0	5.84	0
39							
Run 284 (100% thrust)	383	6940	338	24.0	4.57	0
Run 285 (75% thrust)	343	5740	335	24.0	4.06	0
Run 286 (50% thrust)	295	4780	332	22.0	2.79	0
Run 287 (25% thrust)	219	2630	313	21.0	1.78	0
41							
Run 284 (100% thrust)	319	5020	266	46.0	5.84	0
Run 285 (75% thrust)	293	5020	260	43.0	5.33	0
Run 286 (50% thrust)	252	4300	257	37.0	4.32	0
Run 287 (25% thrust)	179	2150	235	37.0	2.54	0

TABLE V

OVERALL FLUCTUATING PRESSURE LEVELS

1/4-SCALE YC-14 TEST

POSITION NOS.	133	134	135	136	142	143	144	145	270	271	272	273	275	276	281	282
1	152.0*	149.1*	144.9*	138.9*	151.1*	148.4*	144.1*	137.7*	138.3*	138.1*	138.3*	135.3*	156.1*	151.8*	148.9	144.8
2	154.4*	151.7*	146.9*	140.8*	154.5*	151.1*	146.1*	137.6*	137.5*	134.6*	134.0*	129.1*	.0+	.0+	.0+	.0+
3	163.9*	160.0*	155.4*	149.2*	169.1*	165.8*	160.2*	152.8*	137.4*	135.0*	133.5*	129.5*	159.9	157.8	154.0	151.0
4	155.9*	153.8*	150.5*	146.2*	158.3*	156.2*	152.3*	147.3*	159.3*	157.9*	154.8*	149.4*	156.0	154.9	152.4	148.1
6	153.0*	151.1*	147.9*	143.9*	153.1*	151.2*	147.6*	143.0*	156.8*	155.1*	152.5*	147.8*	153.8	153.2	151.9	149.0
7	157.0*	155.1*	152.6*	148.7*	158.4*	156.0*	153.5*	147.8*	136.4*	134.4*	133.8*	128.9*	159.2	157.7	155.8	153.8
8	152.3*	152.7*	147.6*	139.5*	157.9*	154.9*	143.9*	137.6*	136.8*	135.4*	134.6*	129.6*	159.7*	157.2*	152.8*	145.9
9	162.3*	158.4*	152.6*	145.0*	161.6*	157.6*	150.3*	140.3*	142.7*	139.3*	136.4	128.5	143.9	141.6	136.0	129.5
10	152.5*	149.1*	144.1*	139.0*	151.0*	147.9*	143.5*	137.0*	137.0*	135.7*	136.8*	135.1*	151.7	149.4	140.1	144.0*
11	.0+	.0+	.0+	.0+	.0+	.0+	.0+	.0+	.0+	.0+	.0+	.0+	.0+	.0+	.0+	.0+
12	140.2*	136.1*	130.4*	128.4*	139.5*	136.1*	130.7*	125.3*	.0+	.0+	.0+	.0+	144.7*	142.3*	.0+	.0+
13	161.2*	158.2*	154.6*	149.5*	162.6*	160.5*	156.8*	150.3*	138.3*	135.4*	131.4*	125.0*	158.6	157.0	.0+	156.7
14	159.4*	155.5*	150.1*	145.0*	161.4*	158.3*	153.7*	147.1*	158.2*	155.3*	152.0*	147.3*	157.3	155.2	.0+	147.2
15	160.2*	156.6*	152.2*	148.0*	160.7*	157.1*	151.7*	144.9*	155.0*	153.4*	150.3*	145.1*	152.3	151.3	.0+	147.4
20	146.0*	103.4*	105.8*	129.3*	126.4*	100.4*	93.0*	129.7*	.0+	.0+	.0+	.0+	151.7	148.4	144.4	139.7
23	156.6*	152.8*	149.0*	146.3*	156.6*	153.3*	149.4*	146.2*	153.1	149.3	145.6	140.3	153.5	150.5	130.4*	124.8*
32	154.8	150.9	145.6	140.5	153.4	150.2	145.9	139.7	152.8	149.5	145.8	140.3	154.4	151.7	150.4*	141.8
33	139.2*	119.2*	143.9	138.6	152.3	148.6	143.9	137.8	153.4	150.4	146.3	140.2	155.5	151.7	148.6*	141.9
34	164.4	162.1	158.8	154.0	164.0	162.0	159.3	153.8	163.0	161.4	158.6	153.6	164.7	163.1	160.1	155.6
35	142.4*	159.6	155.6	150.4	162.4	160.2	156.3	150.3	160.9	158.2	154.8	149.1	161.8	160.1	157.2	152.3
36	159.8	156.8	152.7	147.7	159.3	157.0	153.0	147.1	161.9	159.0	154.4	147.2	162.5	160.3	156.8	150.5
37	160.2*	157.3*	153.0*	147.6*	159.9*	157.6*	153.1*	146.8*	157.3	155.1	151.5	145.9	157.6	155.5	154.6	147.8
38	161.1	158.4	155.0	150.0	161.5	159.1	155.5	150.0	161.8	159.8	156.1	150.8	161.7	159.7	156.9	152.2
39	160.5	158.7	155.0	150.9	159.6	157.6	154.3	149.3	159.8*	157.8*	155.2*	151.5*	164.6*	160.7*	170.7*	166.4*
40	159.7	157.1	153.1	148.1	160.6	158.0	154.3	147.9	158.5	156.3	153.2	147.2	161.0	159.1	155.4	151.6
41	161.2	159.1	155.1	150.3	162.1	159.6	156.4	150.0	160.2	157.8	154.5	149.0	161.7	159.7	155.7	151.8
43	.0+	.0+	189.9*	.0+	.0+	.0+	.0+	.0+	154.4	151.6	148.6	142.8	158.0	155.3	151.2	145.1
103	.0+	.0+	.0+	.0+	.0+	.0+	.0+	.0+	162.0	160.3	157.4	151.6	160.1	158.1	155.4	150.6
109	.0+	.0+	.0+	.0+	.0+	.0+	.0+	.0+	143.6	139.7	134.5	127.4	145.5	142.2	137.3	130.5
112	.0+	.0+	.0+	.0+	.0+	.0+	.0+	.0+	138.3	134.3	128.8	122.9	139.1	135.7	130.8	124.7

(+ DESIGNATES DATA WAS NOT OBTAINED; * DESIGNATES QUESTIONABLE DATA)

OVERALL FLUCTUATING PRESSURE LEVELS

1/4-SCALE YC-14 TEST

POSITION NOS.	284	285	286	287	289	290	291	292	301	302	303	304	306	307	308	309
1	152.1	151.1	147.8	142.5	152.6	150.0	147.4	142.3	153.3	150.4	148.0	142.7	152.6	149.7	146.5	141.6
2	155.5	153.1	148.9	143.5	155.1	152.6	148.7	142.8	155.4	152.6	148.8	143.2	154.6	151.9	147.7	141.9
3	159.6	158.0	154.9	149.6	161.6	160.2	158.0	153.2	.0+	.0+	.0+	.0+	.0+	.0+	.0+	.0+
4	154.4	153.3	151.5	147.3	153.6	151.1	148.3	143.5	154.5	152.7	150.8	147.1	151.8	149.9	149.3	142.6
6	152.6	151.3	150.5	147.7	149.5	147.0	144.2	138.9	152.2	151.3	149.7	147.0	149.0	146.8	140.6	138.7
7	158.5	157.2	155.4	151.7	160.6	138.0*	155.5	151.1	157.8	156.2	154.5	151.2	159.1	156.8	154.6	149.8
8	161.4*	157.4*	150.5	144.1	158.6	153.0	149.4	144.0	155.9	152.9	149.7	144.1	154.8	152.5	148.5	142.8
9	143.9	142.1	135.5	128.8	141.3	138.1	133.6	127.2	143.8	140.0	135.2	128.4	141.7	137.8	139.9	126.5
10	.0+	.0+	.0+	.0+	.0+	.0+	.0+	.0+	.0+	.0+	.0+	.0+	.0+	.0+	.0+	.0+
11	.0+	.0+	.0+	.0+	.0+	.0+	.0+	.0+	.0+	.0+	.0+	.0+	.0+	.0+	.0+	.0+
12	.0+	.0+	.0+	.0+	.0+	.0+	.0+	.0+	.0+	.0+	.0+	.0+	.0+	.0+	.0+	.0+
13	157.9	156.8	154.1	149.2	.0+	.0+	.0+	.0+	.0+	.0+	.0+	.0+	.0+	.0+	.0+	.0+
14	155.3	153.6	151.3	148.0	157.9	155.7	153.1	148.9	155.9	153.2	151.1	147.1	156.6	154.6	151.6	148.2
15	150.8	149.2	146.9	143.6	147.6	145.7	144.6	140.1	151.6	149.9	147.9	144.4	146.7	144.1	141.7	140.2
20	150.9	148.7	144.5	138.1	150.5	147.9	143.8	136.6	151.4	149.9	143.0	137.3	150.5	147.2	143.0	137.2
23	156.0*	153.1*	147.3	140.6	156.5*	149.5*	145.8	140.5	152.5	149.9	146.2	141.7	151.5	149.0	142.1*	141.6
32	154.5	152.0	147.9	141.3	152.8	150.4	147.1	141.7	155.1	152.0	147.3	141.3	153.0	150.2	146.4	140.8
33	154.8	151.5	147.6	141.3	152.6	148.0	145.2	141.3	155.3	151.4	147.1	141.5	152.9	150.2	146.5	141.1
34	164.1	162.9	160.4	155.4	162.0	161.3	158.9	154.4	164.6	162.6	159.8	155.1	162.6	160.9	158.6	153.9
35	161.5	160.1	157.4	151.7	160.4	158.1	155.1	150.1	161.7	159.7	156.7	151.8	159.9	157.8	154.7	149.7
36	162.3	160.4	156.2	150.4	162.0	159.6	155.6	149.3	160.7*	158.0*	154.3*	149.6*	160.8	157.1	153.5	147.8
37	157.3	155.7	152.9	147.0	157.0	155.1	152.0	147.1	.0+	.0+	.0+	.0+	.0+	.0+	.0+	.0+
38	161.5	159.6	156.6	151.5	161.3	159.4	156.4	151.9	162.1	159.5	156.5	151.7	161.7	159.8	156.4	151.5
39	160.4	158.7	155.8	151.0	158.6	156.8	153.9	149.2	160.9	158.7	155.7	151.1	158.6	156.5	153.5	149.0
40	160.7	144.8*	155.8	150.9	159.3	156.5	154.3	149.1	161.2	158.9	155.7	151.2	159.5	157.2	154.7	149.1
41	161.6	159.6	156.8	151.7	161.6	159.6	156.7	152.1	161.8	159.2	156.0	151.0	162.1	159.9	156.7	151.4
43	157.5	155.0	151.2	144.8	153.8	151.4	148.7	143.7	158.0	155.0	150.7	144.6	153.7	151.4	148.4	143.3
103	159.4	158.1	155.1	149.6	161.0	159.6	157.2	152.5	159.6	157.4	154.5	149.8	161.0	159.3	156.6	151.7
109	144.8	141.6	137.1	130.1	143.0	139.7	135.2	129.2	145.2	141.4	136.5	130.3	143.0	139.3	134.8	128.7
112	138.3	135.2	130.6	124.1	137.2	133.9	129.2	123.6	138.6	134.7	129.7	124.0	137.4	133.5	128.3	122.8

(+ DESIGNATES DATA WAS NOT OBTAINED; * DESIGNATES QUESTIONABLE DATA)

TABLE V (concluded)

OVERALL FLUCTUATING PRESSURE LEVELS

1/4-SCALE YC-14 TEST

POSITION NOS.	326	327	328	329	331	332	333	334	491	492	493	494	499	500	501	502
								RUN NUMBER								
1	152.9	149.5	146.7	141.6	153.2	150.4	147.5	143.3	153.8	150.5	147.5	142.7	153.1	150.3	147.5	142.4
2	155.0	152.1	147.2	141.2	155.4	153.0	149.5	143.9	155.1	152.5	149.3	144.6	.0+	182.0*	184.3*	151.7*
3	.0+	.0+	.0+	.0+	.0+	.0+	.0+	.0+	156.9	155.4	153.4	149.8	156.7	155.1	153.5*	148.6
4	158.1	155.3	154.6	150.1	154.9	154.1	152.3	148.4	148.5	144.8	141.1	134.9	147.7	144.4	140.4	134.3
6	155.2	152.0	151.8	148.3	152.7*	152.7*	152.9*	149.9*	146.7	142.9	138.9	132.1	146.3	142.7	138.2	132.2
7	156.1	155.1	156.7*	152.3	159.1	157.3	155.2	151.6	151.9	149.4	146.8	142.3	151.8	149.5	146.7	141.3
8	155.7	152.6	149.0	143.0	155.7	152.8	149.7	144.3	155.2	152.5	149.3	144.3	154.9	152.2	149.0	143.8
9	141.9	138.0	133.8	127.1	143.9	140.1	135.7	128.5	143.9	139.7	135.2	128.1	143.0	139.2	134.5	128.5
10	.0+	.0+	.0+	.0+	153.2*	150.6*	147.2*	142.6*	146.0*	145.7*	144.5*	143.0*	154.2	152.2	148.8	142.8
11	.0+	.0+	.0+	.0+	.0+	.0+	.0+	.0+	.0+	.0+	.0+	.0+	.0+	.0+	.0+	.0+
12	.0+	.0+	.0+	.0+	.0+	.0+	.0+	.0+	141.8	138.9	136.4	133.0	140.4	136.8	133.2	127.1
13	.0+	.0+	.0+	.0+	159.6	157.3	154.5	149.6	169.0*	163.6*	154.8	150.6	166.7*	164.2*	154.5*	149.3
14	159.7	157.1	154.2	150.4	157.7	155.3	152.7	149.1	150.0	147.6	146.5	141.7	149.5	147.0	144.7	140.3
15	154.0	151.5	151.1	147.0	153.1	152.2	151.0	146.8	143.0	138.5	133.7	126.1	143.0	138.8	133.8	126.5
20	149.8	146.4	140.6	133.5	.0+	.0+	.0+	.0+	152.8	150.5	146.9	141.8	152.3	149.8	146.8	140.7
23	151.6	148.6	145.4	141.7	152.8	149.9	146.6	141.9	154.4	151.0	147.7	142.1	152.8	150.4	147.0	142.0
32	153.2	150.1	146.7	141.0	154.7	151.6	147.4	141.2	154.6	151.7	147.6	141.5	154.5	151.8	147.1	140.7
33	153.2	149.9	146.4	141.0	155.1	151.3	147.3	141.2	155.8	151.9	148.0	142.1	155.2	151.7	147.4	141.3
34	162.7	161.1	158.7	154.1	164.6	162.7	160.1	155.3	.0+	.0+	.0+	.0+	.0+	.0+	.0+	.0+
35	160.6	158.5	155.5	150.0	161.5	159.9	157.3	152.0	.0+	.0+	.0+	.0+	.0+	.0+	.0+	.0+
36	160.3	157.4	153.9	148.3	160.6	158.2	154.6	149.8	.0+	.0+	.0+	.0+	.0+	.0+	.0+	.0+
37	.0+	.0+	.0+	.0+	.0+	.0+	.0+	.0+	.0+	.0+	.0+	.0+	.0+	.0+	.0+	.0+
38	161.9	159.6	156.7	151.6	161.8	159.5	156.7	151.6	.0+	.0+	.0+	.0+	.0+	.0+	.0+	.0+
39	159.2	156.6	154.3	149.3	161.0	158.7	156.0	151.1	.0+	.0+	.0+	.0+	.0+	.0+	.0+	.0+
40	159.4	157.1	154.9	149.3	161.4	159.0	155.8	151.4	.0+	.0+	.0+	.0+	.0+	.0+	.0+	.0+
41	160.7	158.7	155.2	150.2	162.0	159.4	156.8	152.1	.0+	.0+	.0+	.0+	.0+	.0+	.0+	.0+
43	153.9	151.3	148.4	143.4	158.0	154.9	151.0	144.7	158.2	154.9	151.2	145.3	157.6	154.5	150.6	144.4
103	161.8	159.9	157.6	153.2	.0+	.0+	.0+	.0+	157.1	156.0	154.1	149.4	157.2	155.3	153.5	149.3
109	143.5	139.5	135.0	128.5	145.2	141.4	136.8	129.7	144.8	140.7	136.2	129.9	144.3	140.5	135.8	129.2
112	137.9	133.6	128.8	122.7	139.4	134.8	130.2	124.0	138.4	133.9	129.2	123.7	137.3	133.4	128.6	122.9

(+ DESIGNATES DATA WAS NOT OBTAINED; * DESIGNATES QUESTIONABLE DATA)

OVERALL FLUCTUATING PRESSURE LEVELS

1/4-SCALE YC-14 TEST

POSITION NOS.	556	558	560	562	567	569	571	573	574	575	576	577	578	579	580	581
								RUN NUMBER								
1	137.2	141.5	145.8	148.7	137.4*	145.9*	146.0*	148.6*	137.2	142.8	147.1	150.1	136.3	142.7	147.5	151.1
2	135.7	142.2	147.6	151.0	134.6	139.2	144.9	149.6	136.1	141.5	147.1	150.6	134.3	141.4	146.7	150.3
3	140.2*	146.4*	151.8*	157.1*	145.2*	151.6*	157.8*	161.7*	142.9*	148.9*	155.5*	160.1*	147.7*	150.7*	156.8*	160.8*
4	130.6	134.9	140.4	143.8	137.0*	148.5*	152.6*	154.0*	146.4	150.3	153.8	154.8	146.4	149.6	153.6	164.7*
6	130.2	133.5	138.3	142.2	139.5	143.6	147.4	148.0	143.1	147.2	149.5	151.3	146.6	150.5	154.7	157.2
7	132.2	138.5	143.6	146.8	143.4	150.2	155.2	157.4	146.4	151.4	154.5	156.3	148.9	153.2	157.5	160.2
8	136.4*	150.8*	167.2*	171.4*	141.8*	146.1*	163.4*	167.5*	139.1*	155.1*	175.8*	178.5*	135.7*	163.5*	179.5*	181.3*
9	105.6*	85.5*	85.6*	.0+	.0+	.0+	.0+	.0+	.0+	.0+	.0+	.0+	.0+	.0+	.0+	.0+
10	151.4*	169.0*	184.0*	184.7*	.0+	.0+	.0+	.0+	.0+	.0+	.0+	.0+	.0+	.0+	.0+	.0+
11	.0+	.0+	.0+	174.4*	.0+	.0+	.0+	.0+	.0+	.0+	.0+	.0+	.0+	.0+	.0+	.0+
12	132.4*	131.0*	132.5*	.0+	.0+	.0+	.0+	.0+	.0+	.0+	.0+	.0+	.0+	.0+	.0+	.0+
13	143.4*	149.1	154.0	156.5	143.5	150.1	155.4	158.2	142.4	148.9	154.3	157.1	141.9	147.7	153.1	156.5
14	121.6*	126.2*	133.7*	132.9*	126.1*	132.6*	138.1*	138.1*	124.3*	125.2*	127.6*	133.9*	127.0*	127.5*	122.7*	134.7*
15	131.8	133.3	135.8	139.7	140.2*	144.2*	147.4*	147.8*	145.2	148.5	151.1	153.0	143.8	147.4	152.0	155.0*
20	134.5	140.4	145.5	149.0	132.5*	150.9*	149.1*	159.4*	134.7	137.1	141.7	145.9	149.3*	136.1	142.0	146.2
23	144.7*	148.7*	151.6*	155.9*	143.6*	133.1*	136.8*	142.4*	144.5*	148.7*	152.7*	157.2*	125.7*	149.1*	153.1*	157.7*
32	134.2	140.4	146.2	150.1	143.2	154.6*	160.3*	164.2*	134.3	140.8	147.2	151.8	140.8	140.8	147.5	152.4
33	133.3	140.1	146.2	150.2	133.5	154.4*	160.4*	164.2*	133.5	140.7	147.0	151.8	145.7*	140.8	147.5	152.3
34	.0+	.0+	.0+	.0+	145.8*	144.0	152.8	159.0	147.6	154.6	156.5	161.6	151.1	158.6	163.7	166.6
35	.0+	.0+	.0+	.0+	144.8	151.9	157.3	160.3	145.3	152.4	157.8	160.4	143.9	151.8	156.3	159.2
36	.0+	.0+	.0+	.0+	141.0	148.1	153.5	156.8	140.9	148.0	153.4	156.9	141.1	148.0	153.4	156.7
37	.0+	.0+	.0+	.0+	103.6*	103.4*	103.6*	103.7*	103.5*	103.5*	103.5*	103.7*	103.2*	103.2*	103.3*	103.6*
38	.0+	.0+	.0+	.0+	144.4	151.7	156.4	159.8	144.3	151.0	156.4	159.3	143.1	150.0	155.4	158.4
39	.0+	.0+	.0+	.0+	139.9	146.6	151.6	154.3	141.2	148.5	154.1	158.1	142.2	149.2	155.0	158.4
40	.0+	.0+	.0+	.0+	144.3	150.9	156.1	159.1	146.7	152.3	157.3	160.8	149.9	153.9	157.7	100.5
41	.0+	.0+	.0+	.0+	155.6*	157.4*	160.6*	163.7*	157.2*	159.1*	160.4*	162.5*	157.2	159.6	121.6*	163.3
43	135.3	142.3	147.8	151.4	135.9	142.7	148.2	151.2	135.6	143.4	150.6	155.1	142.8	143.9	150.7	155.2
103	.0+	.0+	.0+	.0+	.0+	.0+	.0+	.0+	.0+	.0+	.0+	.0+	.0+	.0+	.0+	.0+
109	120.6	127.0	133.6	138.3	120.8	156.2*	160.9*	167.5*	121.9	129.3	136.7	141.4	155.8*	129.9	138.1	143.2
112	114.7	119.3	126.6	131.9	115.1	135.4*	136.8*	134.1*	115.7	122.6	130.4	135.6	135.9*	123.4	132.0	137.3

(+ DESIGNATES DATA WAS NOT OBTAINED; * DESIGNATES QUESTIONABLE DATA)

TABLE VI

Best-fit exponent N, where $\overline{P^2} = CV^n$

1/4-SCALE YC-14 TEST

CONFIGURATION NO.

POSITION NO.	1	2	3	4	5	6	7	8	9	10	11	12	13	14	15	16
1	3.46*	3.56*	1.01*	3.70*	3.40	3.48	3.55	3.72	3.77	3.34	3.72	3.61	3.15	1.07*	3.19	3.65
2	3.62*	4.48*	2.70*	.00+	4.16	4.24	4.18	4.38	4.77	3.95	3.58	.00+	3.86	4.51	3.99	3.89
3	3.82*	4.33*	2.61*	3.05	3.48	2.90	.00+	.00+	.00+	.00+	2.43	2.75	4.60	4.42	4.89	4.42
4	2.57*	2.94*	3.46*	2.76	2.45	3.43	2.51	2.93	2.57	2.27	4.58	4.56	3.90	2.46*	2.02	6.24*
6	2.42*	2.70*	3.10	1.67	1.63	3.60	1.53	3.68	2.14	.96*	4.93	4.80	3.77	2.01	1.78	2.94
7	2.18*	2.77*	2.46*	1.84	2.33	.60*	2.23	3.14	1.15*	2.55	3.24	3.58	3.64	3.20	2.15	3.07
8	3.67*	5.58*	2.41*	4.78*	5.99*	4.77	3.99	4.16	4.31	3.86	3.71	3.77	9.29*	9.67*	10.71*	8.36*
9	4.56*	5.69*	4.78*	5.07	5.40	4.83	5.25	4.84	5.01	5.23	5.34	4.93	.00+	.00+	.00+	.00+
10	3.54*	3.69*	.50*	2.54*	.00+	.00+	.00+	.00+	.00+	3.62*	1.07*	3.95	7.26*	.00+	.00+	.00+
11	.00+	.00+	.00+	.00+	.00+	.00+	.00+	.00+	.00+	.00+	.00+	.00+	.00+	.00+	.00+	.00+
12	3.03*	3.74*	.00+	.00+	.00+	.00+	.00+	.00+	.00+	.00+	2.93*	4.48	.00+	.00+	.00+	.00+
13	3.05*	3.29*	4.56*	.00+	3.05	.00+	.00+	.00+	.00+	3.41	6.35*	6.29*	3.27*	3.57	3.62	3.86
14	3.76*	3.78*	3.69	.00+	2.50	3.06	2.93	2.89	3.15	2.91	2.73	3.09	3.18*	2.56*	3.60*	2.49*
15	3.16*	4.17*	3.44*	.00+	2.47	2.49	2.45	2.15	2.24	2.16	5.71	5.57	2.70	1.65*	1.96	3.33
20	1.03*	-2.89*	.00+	4.08	4.45	4.80	4.83	4.54	5.64	.00+	3.79	3.95	3.75	3.22*	3.80	4.40*
23	2.60*	2.67*	4.30	10.66*	5.37*	5.14*	3.70	3.56*	3.34	3.69	4.14	3.70	3.05*	3.93*	3.64*	3.68*
32	3.73	3.60	4.23	4.20*	4.56	3.80	4.75	4.18	4.13	4.62	4.49	4.78	4.24	4.19*	4.79	5.05
33	-2.02*	3.79	4.52	4.54*	4.59	3.67	4.66	4.04	4.12	4.69	4.61	4.73	4.42	4.29*	4.83	5.01*
34	2.74	2.70	3.26	3.16	3.83	2.90	3.26	2.98	2.96	3.19	.00+	.00+	.00+	6.54*	2.89	3.52
35	-.70*	3.23	4.03	3.29	3.41	3.52	3.41	3.51	3.64	3.28	.00+	.00+	.00+	3.70	3.54	3.61
36	3.17	3.25	5.07	4.18	4.17	4.39	3.80*	4.16	4.08	3.71	.00+	.00+	.00+	3.82	3.90	3.82
37	3.32	3.51	3.94	3.26	3.57	3.42	.00+	.00+	.00+	.00+	.00+	.00+	.00+	.13*	.08*	.17*
38	2.91	3.04	3.82	3.26	3.45	3.24	3.53	3.54	3.52	3.47	.00+	.00+	.00+	3.53	3.66	3.70
39	2.57	2.74	2.83*	-1.43*	3.25	3.25	3.36	3.29	3.32	3.37	.00+	.00+	.00+	3.39	4.19	4.04
40	3.06	3.36	3.88	3.28	1.56*	3.41	3.43	3.53	3.41	3.42	.00+	.00+	.00+	3.60	3.71	2.87
41	2.91	3.19	3.84	3.46	3.40	3.26	3.68	3.68	3.64	3.34	.00+	.00+	.00+	2.71	1.43*	-1.26*
43	.00+	.00+	3.93	4.44	4.37	3.43	4.60	3.55	3.56	4.54	4.37	4.50	3.98	3.74	5.13	4.94
103	.00+	.00+	3.60	3.25	3.43	2.94	3.35	3.21	2.93	.00+	2.67	2.73	.00+	.00+	.00+	.00+
109	.00+	.00+	5.54	5.16	5.04	4.72	5.08	4.86	5.08	5.28	5.04	5.14	4.93	4.79*	5.30	5.83*
112	.00+	.00+	5.27	4.94	4.88	4.66	4.98	4.99	5.14	5.18	4.95	4.90	5.49	-.41*	5.68	6.09*

where $\overline{P^2}$ = mean-square pressure, C = constant, V = maximum nozzle centerline exit velocity

(+ DESIGNATES DATA WAS NOT OBTAINED; * DESIGNATES QUESTIONABLE DATA)

TABLE VII

CORRELATION COEFFICIENT AT ZERO TIME DELAY

1/4-SCALE YC-14 TEST

POSITION NOS.	133	134	135	136	142	143	144	145	270	271	272	273	275	276	281	282
1- 8	.05*	.01*	.00*	-.02*	.03*	.03*	.09*	.09*	.30*	.04*	-.19*	-.45*	-.08*	-.10*	-.07*	-.03
3- 6	.00+	.00+	.00+	.00+	.00+	.00+	.00+	.00+	.00+	.00+	.00+	.00+	.26	.25	.20	.11
6- 4	.48*	.47*	.47*	.43*	.29*	.26*	.32*	.29*	.31*	.26*	.22*	.21*	.48	.44	.43	.33
7- 3	-.12*	-.11*	-.13*	-.22*	-.14*	-.16*	-.25*	-.33*	.34*	.29*	.25*	.17*	-.12	-.11	-.11	-.06
8- 2	.02*	.05*	.02*	.03*	.01*	.04*	.12*	.16*	.77*	.83*	1.02*	.47*	.00+	.00+	.00+	.00+
9- 2	.01*	.01*	-.02*	.07*	.02*	.03*	.02*	.00*	.00+	.00+	.00+	.00+	.00+	.00+	.00+	.00+
9- 3	.00+	.00+	.00+	.00+	.00+	.00+	.00+	.00+	-.06*	-.05*	-.08*	-.11*	-.05	-.07	-.08	-.11
10- 1	-.11*	-.15*	-.17*	-.32*	-.09*	-.15*	-.15*	-.18*	.85*	.66*	.86*	.20*	-.07*	-.08*	-.11	-.06*
10- 2	-.03*	-.03*	.03*	.12*	-.06*	-.06*	-.07*	-.09*	.04*	-.14*	.15*	-.10*	.00+	.00+	.00+	.00+
10- 8	-.16*	-.13*	-.17*	-.19*	-.12*	-.10*	-.14*	-.19*	.21*	-.08*	-.10*	-.11*	-.10*	-.12*	-.11*	-.22*
13- 14	.08*	.07*	.08*	.00+	.03*	.02*	-.03*	-.06*	-.02*	.02*	.05*	.07*	.13	.04	.00+	-.11
13- 20	-.06*	.00+	.01*	-.15*	-.05*	-.05*	.02*	.04*	.00+	.00+	.00+	.00+	.00+	.00+	.00+	.00+
14- 13	.00+	.00+	.00+	.01*	.00+	.00+	.00+	.00+	.00+	.00+	.00+	.00+	.00+	.00+	.00+	.00+
14- 15	.00*	.02*	.01*	.06*	-.02*	-.02*	-.03*	-.04*	-.07*	-.02*	.06*	.01*	.07	-.03	.00+	-.12
20- 12	.06*	.04*	.04*	-.02*	-.03*	.05*	.04*	.12*	.00+	.00+	.00+	.00+	.01*	.02*	.00+	.00+
32- 33	-.04*	.02*	.03	.03	.04	.05	.06	.05	-.18	-.13	-.09	-.06	-.21	-.19	-.11*	-.07
32- 37	.00+	.00+	.00+	.00+	.00+	.00+	.00+	.00+	-.02	.00	.00	.01	.00	.00	-.11*	-.03
32- 39	.01	-.03	-.05	-.06	-.03	-.04	-.05	-.02	-.03*	-.04*	-.05*	-.02*	-.02*	.02*	-.11*	.02*
32- 41	-.02	.00	-.02	.00	-.02	-.02	-.02	.01	.00	.00	-.02	.01	.00	.01	-.11*	.00
32- 43	.00+	.00+	.00*	.00+	.00+	.00+	.00+	.00+	.00+	.00+	.00+	.00+	.00+	.00+	.00+	.00+
34- 35	-.10*	-.09	-.07	-.09	-.10	-.12	-.11	-.14	-.10	-.14	-.12	-.15	-.06	-.06	.00+	-.05
34- 38	.05	.12	.12	.18	.14	.19	.18	.18	.01	.06	.05	.06	-.02	-.02	.00+	.01
35- 40	.11*	.09	.12	.14	.03	.04	.06	.06	-.10	-.05	-.08	-.05	-.15	-.11	-.08	-.09
36- 37	-.08*	-.12*	-.07*	-.07*	-.08*	-.11*	-.06*	-.07*	.00+	.00+	.00+	.00+	.00+	.00+	.00+	.00+
38- 36	.00+	.00+	.00+	.00+	.00+	.00+	.00+	.00+	.02	-.05	-.04	-.10	-.02	-.02	-.05	-.10
38- 40	.00	-.02	-.05	-.02	-.07	-.05	-.06	-.04	.00+	.00+	.00+	.00+	.00+	.00+	.00+	.00+
39- 34	-.12	-.15	-.21	-.22	-.33	-.35	-.43	-.41	-.26*	-.29*	-.30*	-.17*	-.02*	.00+	.06*	.10*
39- 41	-.02	.02	.05	.05	.04	.06	.06	.01	.02*	.01*	.00*	.01*	.00*	.01*	-.11*	.04*
40- 37	-.15*	-.13*	-.19*	-.17*	-.15*	-.16*	-.16*	-.15*	.00+	.00+	.00+	.00+	.00+	.00+	.00+	.00+
43- 35	.00+	.00+	.00+	.00+	.00+	.00+	.00+	.00+	-.02	-.03	-.03	.00	.00	-.03	-.04	-.02
109-112	.00+	.00+	.00+	.00+	.00+	.00+	.00+	.00+	.03	.08	.19	.35	.03	.06	.20	.26

(+ DESIGNATES DATA WAS NOT OBTAINED; * DESIGNATES QUESTIONABLE DATA)

CORRELATION COEFFICIENT AT ZERO TIME DELAY

1/4-SCALE YC-14 TEST

POSITION NOS.	284	285	286	287	289	290	291	292	301	302	303	304	306	307	308	309
1- 2	.00+	.00+	.00+	.00+	.00+	.00+	.00+	.00+	-.19	-.23	-.20	-.14	-.18	-.19	-.24	-.17
1- 7	.00+	.00+	.00+	.00+	.00+	.00+	.00+	.00+	-.19	-.23	-.20	-.21	-.16	-.22	-.20	-.24
1- 8	-.02*	-.10*	-.10	-.04	-.10	-.10	-.06	-.09	-.12	-.07	-.08	.00	-.09	-.08	-.06	-.07
6- 4	.62	.56	.42	.36	.59	.61	.59	.76	.63	.63	.49	.48	.61	.52	.63	.76
7- 3	.02	-.03	-.03	.11	.00	-.02*	-.11	-.05	.00+	.00+	.00+	.00+	.00+	.00+	.00+	.00+
8- 2	-.08*	-.09*	-.05	-.05	-.06	-.09	-.04	-.04	-.08	-.05	-.03	.05	-.04	-.11	.01	.02
9- 2	.08	.09	.11	.08	.14	.17	.22	.19	.13	.12	.13	.09	.15	.16	.00	.10
13- 14	.13	.11	.10	.03	.00+	.00+	.00+	.00+	.00+	.00+	.00+	.00+	.00+	.00+	.00+	.00+
13- 20	.13	.09	.08	.04	.00+	.00+	.00+	.00+	.00+	.00+	.00+	.00+	.00+	.00+	.00+	.00+
14- 15	.07	.01	.01	-.12	-.02	.10	-.05	-.07	.14	.11	.02	-.28	.16	.07	.10	.09
20- 15	-.07	-.09	-.10	-.09	-.09	.00	-.02	-.16	-.05	-.07	-.07	-.04	-.06	-.08	-.06	-.08
32- 33	-.19	-.19	-.11	-.08	-.12	-.09	-.07	-.05	-.17	-.20	-.10	-.06	-.11	-.09	-.06	-.06
32- 37	.00	.00	.00	-.02	.00	-.02	.00	-.02	.00+	.00+	.00+	.00+	.00+	.00+	.00+	.00+
32- 39	.00	.01	.03	.03	.01	.03	.02	.02	-.03	.01	.02	.02	.02	.02	.02	.02
32- 41	.01	.00	.00	-.02	-.02	.00	.01	.02	.01	-.02	-.02	.00	.00	.00	.00	-.02
32- 43	.00+	.00+	.00+	.00+	.00+	.00+	.00+	.00+	.01	-.05	-.02	-.05	-.02	-.05	-.05	-.08
33- 37	.00	.01	-.02	.02	.00	.01	-.02	-.04	.00+	.00+	.00+	.00+	.00+	.00+	.00+	.00+
33- 43	.00+	.00+	.00+	.00+	.00+	.00+	.00+	.00+	.00	.01	-.04	-.05	-.07	-.08	-.10	-.13
34- 35	-.03	-.06	-.07	-.09	-.10	-.12	-.09	-.12	-.07	-.07	-.05	-.06	-.10	-.10	-.11	-.09
34- 38	-.02	.03	.00	.03	.05	.04	.05	.05	.00	.00	.02	.03	.03	.05	.04	.07
35- 40	-.11	-.11*	-.10	-.16	-.08	-.09	-.04	-.04	-.11	-.11	-.09	-.11	-.06	-.07	.00	-.02
38- 36	-.02	-.02	-.04	-.08	.01	.02	.00	-.03	-.04*	-.06*	-.11*	-.09*	-.06	-.05	-.08	-.11
38- 40	.06	.07*	.08	.04	.05	.04	.07	.04	.08	.05	.04	.03	.06	.06	.03	.02
39- 34	.00+	.00+	.00+	.00+	.00+	.00+	.00+	.00+	.16	.18	.20	.20	.33	.34	.42	.45
39- 41	.02	.04	.02	.04	.08	.06	.07	.04	-.02	.03	.03	.05	.07	.09	.07	.09
43- 35	.00+	.00+	.00+	.00+	-.03	.00	-.03	-.04	.00+	.00+	.00+	.00+	.00+	.00+	.00+	.00+
43- 39	.00+	.00+	.00+	.00+	.00+	.00+	.00+	.00+	.06	.01	-.06	-.14	-.22	-.27	-.32	-.32
43- 40	.00+	.00+	.00+	.00+	.01	.01	-.02	.01	.00+	.00+	.00+	.00+	.00+	.00+	.00+	.00+
43- 41	-.02	-.02	.01	-.03	-.02	.01	.00	.00	.00+	.00+	.00+	.00+	.00+	.00+	.00+	.00+
109-112	.02	.10	.17	.39	.04	.11	.23	.44	.04	.07	.17	.39	.07	.12	.21	.47

(+ DESIGNATES DATA WAS NOT OBTAINED; * DESIGNATES QUESTIONABLE DATA)

TABLE VII (concluded)

CORRELATION COEFFICIENT AT ZERO TIME DELAY

1/4-SCALE YC-14 TEST

POSITION NOS.	326	327	328	329	331	332	333	334	491	492	493	494	499	500	501	502
1- 2	-.14	-.16	-.11	-.08	-.20	-.26	-.22	-.20	-.27	-.26	-.26	-.25	.00+	.00+	.00+	.00+
1- 7	-.17	-.20	-.26*	-.23	-.17	-.23	-.28	-.27	.00+	.00+	.00+	.00+	.00+	.00+	.00+	.00+
1- 8	-.09	-.08	.03	.09	-.10	-.10	-.09	-.02	-.12	-.15	-.16	-.14	-.13	-.16	-.15	-.13
1- 20	.00+	.00+	.00+	.00+	.00+	.00+	.00+	.00+	-.04	-.05	-.03	-.02	-.05	.01	-.03	-.06
2- 20	.00+	.00+	.00+	.00+	.00+	.00+	.00+	.00+	.02	.01	.00	-.02	.00+	.00+	.00+	.00+
3- 13	.00+	.00+	.00+	.00+	.00+	.00+	.00+	.00+	-.03*	-.09*	-.12	-.11	-.07*	-.08*	-.14*	-.18
3-103	.00+	.00+	.00+	.00+	.00+	.00+	.00+	.00+	.86	.82	.79	.79	.83	.87	.00*	.84
4- 14	.00+	.00+	.00+	.00+	.00+	.00+	.00+	.00+	.32	.31	.27	.22	.34	.34	.33	.24
4- 15	.00+	.00+	.00+	.00+	.00+	.00+	.00+	.00+	.00+	.00+	.00+	.00+	.07	.09	.10	.06
6- 4	.40	.36	.23	.20	.56*	.40*	.34*	.27*	.47	.53	.59	.62	.51	.56	.63	.56
6- 14	.00+	.00+	.00+	.00+	.00+	.00+	.00+	.00+	.06	.02	-.04	-.04	.05	.03	-.02	.02
6- 15	.00+	.00+	.00+	.00+	.00+	.00+	.00+	.00+	-.06	-.03	.05	-.06	-.05	-.05	.01	.02
7- 3	.00+	.00+	.00+	.00+	.00+	.00+	.00+	.00+	.07	.03	-.05	-.10	.10	.03	-.02*	-.06
7- 13	.00+	.00+	.00+	.00+	.00+	.00+	.00+	.00+	-.09*	-.14*	-.33	-.31	-.20*	-.13*	-.23*	-.35
7-103	.00+	.00+	.00+	.00+	.00+	.00+	.00+	.00+	.09	-.02	-.08	-.10	.05	-.02	-.06	-.11
8- 2	-.06	-.02	.02	.16	-.07	-.05	-.06	-.03	-.06	-.10	-.14	-.11	.00+	-.04*	-.05*	-.06*
8- 20	.00+	.00+	.00+	.00+	.00+	.00+	.00+	.00+	.00+	.00+	.00+	.00+	-.26	.00+	.00+	.00+
9- 2	.13	.14	.17	.11	.09	.13	.12	.08	.00+	.00+	.00+	.00+	.00+	.00+	.00+	.00+
9- 12	.00+	.00+	.00+	.00+	.00+	.00+	.00+	.00+	-.04	-.02	-.09	.00	-.03	-.04	-.09	.06
10- 1	.00+	.00+	.00+	.00+	.02*	.03*	-.06*	-.17*	.00+	.00+	.00+	.00+	-.08	-.09	-.19	-.23
10- 20	.00+	.00+	.00+	.00+	.00+	.00+	.00+	.00+	-.04*	-.03*	-.02*	-.04*	.01	.03	.00	.02
13- 15	.00+	.00+	.00+	.00+	-.05	-.04	-.07	-.03	.00+	.00+	.00+	.00+	.00+	.00+	.00+	.02+
14- 15	.08	.07	.02	.06	.10	.00	-.02	-.10	.18	.20	.22	.29	.18	-.04	.23	.24
20- 15	-.05	-.08	-.04	-.05	.00+	.00+	.00+	.00+	.00+	.00+	.00+	.00+	.00+	.00+	.00+	.00+
23- 32	.00+	.00+	.00+	.00+	.00+	.00+	.00+	.00+	.05	-.02	-.02	-.05	-.03	-.03	-.03	-.03
23- 33	.00+	.00+	.00+	.00+	.00+	.00+	.00+	.00+	.01	.00	-.02	-.07	-.05	.00	-.02	-.02
23- 43	.00+	.00+	.00+	.00+	.00+	.00+	.00+	.00+	.01	.00	.01	.02	.01	.00	.02	.03
32- 33	-.11	-.08	-.07	-.06	-.18	-.20	-.12	-.06	-.18	-.19	-.10	-.06	-.10	-.18	-.10	-.05
32- 39	.01	.03	.01	.02	-.02	.01	.04	.03	.00+	.00+	.00+	.00+	.00+	.00+	.00+	.00+
32- 41	.00	.03	.00	.01	.01	.00	-.02	.00	.00+	.00+	.00+	.00+	.00+	.00+	.00+	.00+
32- 43	-.03	-.05	-.05	-.09	.00	-.03	-.03	-.06	-.03	-.04	-.03	-.05	-.02	-.04	-.04	-.06
33- 43	-.07	-.07	-.10	-.12	-.03	.01	.01	-.05	.00	.04	.01	-.03	.01	.03	.00	-.05
34- 35	-.09	-.11	-.09	-.11	-.03	-.05	-.07	-.08	.00+	.00+	.00+	.00+	.00+	.00+	.00+	.00+
34- 38	.03	.03	.05	.10	.00	.01	.03	.04	.00+	.00+	.00+	.00+	.00+	.00+	.00+	.00+
35- 40	-.07	-.07	-.04	-.04	-.09	-.09	-.09	-.11	.00+	.00+	.00+	.00+	.00+	.00+	.00+	.00+
38- 36	-.05	-.06	-.07	-.08	-.05	-.04	-.09	-.07	.00+	.00+	.00+	.00+	.00+	.00+	.00+	.00+
38- 40	.05	.05	.05	.05	.06	.08	.01	.05	.00+	.00+	.00+	.00+	.00+	.00+	.00+	.00+
39- 34	.31	.34	.34	.39	.20	.19	.18	.18	.00+	.00+	.00+	.00+	.00+	.00+	.00+	.00+
39- 41	.06	.04	-.02	-.04	-.02	.02	.01	.02	.00+	.00+	.00+	.00+	.00+	.00+	.00+	.00+
43- 39	-.25	-.27	-.33	-.32	.07	.00	-.07	-.12	.00+	.00+	.00+	.00+	.00+	.00+	.00+	.00+
109-112	.05	.12	.19	.36	.03	.07	.14	.27	-.02	.01	.06	.20	.00	.01	.06	.22

(+ DESIGNATES DATA WAS NOT OBTAINED; * DESIGNATES QUESTIONABLE DATA)

CORRELATION COEFFICIENT AT ZERO TIME DELAY

1/4-SCALE YC-14 TEST

POSITION NOS.	556	558	560	562	567	569	571	573	574	575	576	577	578	579	580	581
1- 2	-.09	-.25	-.34	-.37	-.13*	-.09*	-.15*	-.22*	-.14	-.10	-.27	-.28	-.18	-.16	-.23	-.23
1- 8	.06*	-.06*	.10*	.03*	.09*	.03*	.00*	-.03*	.07*	-.06*	-.08*	-.07*	-.04*	-.11*	-.09*	-.07*
1- 20	-.09	-.03	-.08	-.09	.00+	.00+	.00+	.00+	.00+	.00+	.00+	.00+	.00+	.00+	.00+	.00+
2- 20	.03	.03	.04	.08	.00+	.00+	.00+	.00+	.00+	.00+	.00+	.00+	.00+	.00+	.00+	.00+
3- 13	-.21*	-.14*	-.02*	.00*	-.11*	-.12*	-.12*	-.11*	-.09*	-.16*	-.10*	-.08*	.09*	.04*	.03*	.02*
4- 14	.07*	.24*	.19*	.36*	.26*	.24*	.22*	.25*	.09*	.17*	.15*	.19*	.21*	.18*	.05*	.02*
4- 15	-.23	-.39	-.26	-.23	.00+	.00+	.00+	.00+	.00+	.00+	.00+	.00+	.00+	.00+	.00+	.00+
6- 4	-.29	.03	.17	.30	.25*	.34*	.41*	.45*	.39	.41	.41	.49	.39	.35	.29	.16*
6- 14	-.05*	-.16*	.01*	.05*	-.05*	-.07*	.00*	-.04*	-.04*	-.10*	-.14*	-.12*	-.07*	.00*	-.04*	-.05*
6- 15	.40	.30	.22	.13	-.13*	-.13*	-.09*	-.15*	-.10	-.14	-.16	-.22	.03	.06	.08	.05
7- 3	-.07*	-.03*	.10*	.21*	-.30*	-.25*	-.14*	-.04*	-.02*	-.06*	.03*	.03*	.14*	.17*	.06*	.05*
7- 13	-.24*	-.28	-.30	-.27	.03	.02	.01	-.07	.00	-.07	-.05	-.06	-.10	-.07	.01	-.03
8- 2	.10*	.00*	-.04*	.02*	.17*	.09*	-.04*	.01*	.09*	.00*	.01*	.00*	.07*	.00*	-.06*	.01*
9- 12	.05*	.04*	.03*	.00+	.00+	.00+	.00+	.00+	.00+	.00+	.00+	.00+	.00+	.00+	.00+	.00+
10- 1	.05*	-.05*	-.04*	-.05*	.00+	.00+	.00+	.00+	.00+	.00+	.00+	.00+	.00+	.00+	.00+	.00+
10- 20	.02*	.01*	.03*	.03*	.00+	.00+	.00+	.00+	.00+	.00+	.00+	.00+	.00+	.00+	.00+	.00+
11-109	.00+	.00+	.00+	-.02*	.00+	.00+	.00+	.00+	.00+	.00+	.00+	.00+	.00+	.00+	.00+	.00+
14- 15	-.03*	-.23*	-.13*	-.03*	.04*	-.03*	.02*	.06*	-.09*	.01*	.03*	.04*	.04*	-.06*	.03*	.00*
23- 32	-.06*	-.02*	-.03*	.01*	-.04*	-.06*	.02*	.01*	-.04*	-.02*	-.02*	.01*	-.05*	-.03*	.03*	.00+
23- 33	.01*	-.02*	.00*	-.03*	.00+	.00+	.00+	.00+	.00+	.00+	.00+	.00+	.00+	.00+	.00+	.00+
23- 43	.00*	.01*	.03*	-.04*	.00+	.00+	.00+	.00+	.00+	.00+	.00+	.00+	.00+	.00+	.00+	.00+
32- 33	.01	-.05	-.06	-.11	.04	-.04*	-.05*	-.10*	.01	-.06	-.09	-.10	.04*	-.04	-.12	-.18
32- 39	.00+	.00+	.00+	.00+	.02	.04*	.03*	.00*	.01	.02	.00	.00	-.02	.01	-.02	-.03
32- 41	.00+	.00+	.00+	.00+	.00*	.00*	.00*	.00*	.00*	.00*	.01*	-.02*	.00	.00	.00*	.00
32- 43	-.05	-.10	-.08	-.06	-.05	-.09*	-.09*	-.05*	-.05	-.07	-.05	-.03	-.05	-.08	-.03	-.03
33- 43	-.12	-.14	-.12	-.07	.00+	.00+	.00+	.00+	.00+	.00+	.00+	.00+	.00+	.00+	.00+	-.03
39- 34	.00+	.00+	.00+	.00+	.33*	.26	.24	.25	.15	.16	.11	.08	.05	.02	.01	-.03
39- 36	.00+	.00+	.00+	.00+	-.04	-.02	-.03	-.03	.00	-.03	-.02	.00	.00	.00	-.02	.00
39- 38	.00+	.00+	.00+	.00+	.09	.07	.03	.01	-.05	-.04	-.07	-.05	-.02	-.03	-.05	-.05
41- 35	.00+	.00+	.00+	.00+	-.03*	-.06*	-.11*	-.13*	-.05*	-.04*	-.10*	-.08*	-.07	-.07	-.06*	-.10
41- 37	.00+	.00+	.00+	.00+	.01*	-.07*	-.06*	-.02*	-.07*	-.06*	-.03*	-.03*	.03*	.01*	.02*	-.03*
41- 40	.00+	.00+	.00+	.00+	.04*	-.02*	.02*	-.02*	.02*	.03*	.00*	.01*	-.05	.01	-.05*	-.03
109- 20	.00+	.00+	.00+	.00+	.04*	.11*	.23*	.22*	.05	.11	.13	.14	.06*	.10	.13	.13
109-112	.23	.11	.05	.02	.39	.38*	.19*	.12*	.39	.27	.14	.07	.29*	.19	.11	.05

(+ DESIGNATES DATA WAS NOT OBTAINED; * DESIGNATES QUESTIONABLE DATA)

TABLE VIII

PEAK CORRELATION COEFFICIENTS

1/4-SCALE YC-14 TEST

POSITION NOS.	133	134	135	136	142	143	144	145	270	271	272	273	275	276	281	282
1- 8	.23*	.19*	.28*	.19*	.10*	.11*	.28*	.43*	.34*	.10*	.00*	.00*	.20*	.29*	.31*	.33
3- 6	.00+	.00+	.00+	.00+	.00+	.00+	.00+	.00+	.00+	.00+	.00+	.00+	.28	.26	.22	.13
6- 4	.53*	.60*	.61*	.60*	.31*	.30*	.34*	.32*	.33*	.29*	.23*	.22*	.51	.50	.5?	.47
7- 3	.20*	.21*	.23*	.14*	.10*	.11*	.09*	.05*	.37*	.34*	.31*	.23*	.24	.25	.19	.11
8- 2	.21*	.16*	.21*	.31*	.09*	.11*	.26*	.30*	.00*	.07*	1.09*	.55*	.00+	.00+	.00+	.00+
9- 2	.04*	.04*	.07*	.11*	.05*	.04*	.06*	.10*	.00+	.00+	.00+	.00+	.00+	.00+	.00+	.00+
9- 3	.00+	.00+	.00+	.00+	.00+	.00+	.00+	.00+	.05*	.05*	.03*	.00*	.08	.10	.10	.06
10- 1	.25*	.33*	.39*	.42*	.30*	.35*	.36*	.46*	.90*	.74*	.93*	.27*	.25*	.35*	.19	.30*
10- 2	.04*	.05*	.05*	.17*	.05*	.07*	.07*	.05*	.00*	.00*	.23*	.00*	.00+	.00+	.00+	.00+
10- 8	.10*	.11*	.08*	.16*	.05*	.06*	.12*	.13*	.25*	.00*	.00*	.00*	.13*	.14*	.19*	.05*
13- 14	.09*	.09*	.11*	.00+	.04*	.02*	.03*	.07*	.00*	.03*	.06*	.09*	.16	.09	.00+	.19
13- 20	.02*	.00+	.03*	.05*	.01*	.01*	.04*	.05*	.00+	.00+	.00+	.00+	.00+	.00+	.00+	.00+
14- 13	.00+	.00+	.00+	.03*	.00+	.00+	.00+	.00+	.00+	.00+	.00+	.00+	.00+	.00+	.00+	.00+
14- 15	.17*	.15*	.16*	.14*	.13*	.12*	.09*	.06*	.20*	.18*	.12*	.07*	.19	.12	.00+	.00
20- 12	.13*	.04*	.04*	.21*	.06*	.05*	.04*	.23*	.00+	.00+	.00+	.00+	.09*	.07*	.00+	.00+
32- 33	.21*	.13*	.20	.20	.41	.36	.30	.31	.51	.54	.50	.54	.32	.40	.19*	.51
32- 37	.00+	.00+	.00+	.00+	.00+	.00+	.00+	.00+	.01	.01	.01	.01	.01	.01	.19*	.02
32- 39	.06	.06	.06	.05	.05	.07	.05	.05	.08*	.07*	.06*	.03*	.05*	.06*	.19*	.03*
32- 41	.02	.01	.01	.02	.02	.02	.02	.02	.02	.02	.02	.02	.02	.01	.19*	.01
32- 43	.00+	.00+	.01*	.00+	.00+	.00+	.00+	.00+	.00+	.00+	.00+	.00+	.00+	.00+	.00+	.00+
34- 35	.14*	.15	.14	.10	.23	.23	.20	.12	.17	.15	.15	.13	.14	.12	.00+	.10
34- 38	.19	.22	.21	.25	.19	.23	.22	.20	.14	.15	.20	.17	.12	.18	.00+	.20
35- 40	.17*	.15	.17	.19	.08	.10	.11	.12	.04	.03	.03	.00	.07	.06	.03	.01
36- 37	.08*	.10*	.06*	.05*	.07*	.09*	.04*	.04*	.00+	.00+	.00+	.00+	.00+	.00+	.00+	.00+
38- 36	.00+	.00+	.00+	.00+	.00+	.00+	.00+	.00+	.03	.05	.05	.06	.02	.04	.04	.04
38- 40	.07	.06	.07	.03	.11	.07	.09	.05	.00+	.00+	.00+	.00+	.00+	.00+	.00+	.00+
39- 34	.09	.13	.12	.12	.16	.19	.23	.18	.13*	.16*	.15*	.15*	.02*	.01*	.07*	.11*
39- 41	.02	.03	.06	.06	.10	.17	.20	.15	.10*	.08*	.11*	.10*	.12*	.11*	.19*	.06*
40- 37	.03*	.02*	.04*	.04*	.01*	.02*	.01*	.05*	.00+	.00+	.00+	.00+	.00+	.00+	.00+	.00+
43- 35	.00+	.00+	.00+	.00+	.00+	.00+	.00+	.00+	.02	.02	.02	.02	.02	.02	.02	.02
109-112	.00+	.00+	.00+	.00+	.00+	.00+	.00+	.00+	.50	.48	.50	.52	.50	.53	.57	.50

(+ DESIGNATES DATA WAS NOT OBTAINED; * DESIGNATES QUESTIONABLE DATA)

PEAK CORRELATION COEFFICIENTS

1/4-SCALE YC-14 TEST

POSITION NOS.	284	285	286	287	289	290	291	292	301	302	303	304	306	307	308	309
1- 2	.00+	.00+	.00+	.00+	.00+	.00+	.00+	.00+	.15	.16	.17	.11	.14	.14	.17	.11
1- 7	.00+	.00+	.00+	.00+	.00+	.00+	.00+	.00+	.30	.29	.31	.22	.28	.31	.30	.23
1- 8	.02*	.20*	.41	.46	.31	.42	.40	.35	.42	.44	.39	.40	.44	.44	.39	.42
6- 4	.66	.60	.50	.47	.62	.64	.62	.79	.68	.67	.55	.47	.65	.55	.66	.70
7- 3	.26	.23	.23	.28	.34	.39*	.35	.36	.00+	.00+	.00+	.00+	.00+	.00+	.00+	.00+
8- 2	.21*	.20*	.37	.35	.21	.37	.35	.35	.37	.40	.35	.37	.35	.38	.38	.39
9- 2	.12	.15	.20	.22	.16	.20	.27	.29	.17	.18	.22	.28	.18	.22	.04	.30
13- 14	.18	.17	.13	.08	.00+	.00+	.00+	.00+	.00+	.00+	.00+	.00+	.00+	.00+	.00+	.00+
13- 20	.14	.09	.09	.06	.00+	.00+	.00+	.00+	.00+	.00+	.00+	.00+	.00+	.00+	.00+	.00+
14- 15	.22	.14	.11	.07	.11	.18	.11	.09	.28	.22	.14	.00	.30	.19	.19	.21
20- 15	.04	.03	.04	.05	.02	.04	.06	.00	.06	.05	.05	.05	.05	.02	.02	.03
32- 33	.31	.40	.40	.51	.49	.52	.56	.53	.27	.40	.46	.49	.46	.51	.53	.53
32- 37	.02	.01	.01	.01	.01	.01	.02	.01	.00+	.00+	.00+	.00+	.00+	.00+	.00+	.00+
32- 39	.05	.05	.06	.05	.07	.07	.06	.04	.06	.05	.06	.05	.05	.06	.05	.04
32- 41	.02	.01	.02	.02	.02	.02	.01	.02	.02	.02	.02	.01	.02	.02	.02	.01
32- 43	.00+	.00+	.00+	.00+	.00+	.00+	.00+	.00+	.21	.23	.24	.21	.24	.26	.25	.22
33- 37	.02	.03	.02	.04	.02	.02	.02	.02	.00+	.00+	.00+	.00+	.00+	.00+	.00+	.00+
33- 43	.00+	.00+	.00+	.00+	.00+	.00+	.00+	.00+	.34	.38	.42	.41	.44	.41	.42	.40
34- 35	.12	.14	.13	.09	.16	.16	.15	.10	.14	.15	.13	.14	.19	.16	.12	.14
34- 38	.14	.13	.18	.19	.16	.15	.18	.15	.13	.13	.18	.18	.15	.16	.17	.20
35- 40	.07	.06*	.05	.00	.04	.04	.03	.04	.05	.07	.00	.03	.02	.04	.03	.00
38- 36	.04	.04	.03	.04	.04	.05	.05	.06	.04*	.06*	.06*	.05*	.05	.03	.05	.09
38- 40	.09	.11*	.10	.10	.06	.05	.09	.05	.09	.09	.11	.06	.07	.07	.06	.04
39- 34	.00+	.00+	.00+	.00+	.00+	.00+	.00+	.00+	.18	.21	.24	.24	.34	.34	.43	.46
39- 41	.12	.11	.10	.10	.10	.10	.08	.06	.11	.09	.09	.07	.10	.10	.08	.10
43- 35	.00+	.00+	.00+	.00+	.02	.02	.02	.04	.00+	.00+	.00+	.00+	.00+	.00+	.00+	.00+
43- 39	.00+	.00+	.00+	.00+	.00+	.00+	.00+	.00+	.12	.15	.16	.22	.27	.33	.37	.32
43- 40	.00+	.00+	.00+	.00+	.02	.02	.02	.02	.00+	.00+	.00+	.00+	.00+	.00+	.00+	.00+
43- 41	.02	.02	.03	.01	.04	.03	.03	.03	.00+	.00+	.00+	.00+	.00+	.00+	.00+	.00+
109-112	.51	.54	.55	.55	.52	.52	.55	.59	.49	.53	.56	.60	.54	.50	.56	.52

(+ DESIGNATES DATA WAS NOT OBTAINED; * DESIGNATES QUESTIONABLE DATA)

TABLE VIII (concluded)

PEAK CORRELATION COEFFICIENTS

1/4-SCALE YC-14 TEST

POSITION NOS.	326	327	328	329	331	332	333	334	491	492	493	494	499	500	501	502
1- 2	.13	.11	.13	.07	.13	.15	.15	.08	.19	.22	.17	.17	.00+	.00+	.00+	.00+
1- 7	.30	.33	.27*	.20	.28	.37	.34	.14	.00+	.00+	.00+	.00+	.00+	.00+	.00+	.00+
1- 8	.41	.40	.33	.33	.42	.49	.42	.35	.40	.45	.43	.40	.46	.50	.42	.40
1- 20	.00+	.00+	.00+	.00+	.00+	.00+	.00+	.00+	.09	.08	.07	.05	.06	.10	.10	.04
2- 20	.00+	.00+	.00+	.00+	.00+	.00+	.00+	.00+	.36	.37	.37	.37	.00+	.00+	.00+	.00+
3- 13	.00+	.00+	.00+	.00+	.00+	.00+	.00+	.00+	.15*	.22*	.44	.38	.33*	.15*	.40*	.35
3-103	.00+	.00+	.00+	.00+	.00+	.00+	.00+	.00+	.86	.83	.79	.79	.83	.88	.81*	.84
4- 14	.00+	.00+	.00+	.00+	.00+	.00+	.00+	.00+	.47	.44	.42	.38	.48	.46	.46	.45
4- 15	.00+	.00+	.00+	.00+	.00+	.00+	.00+	.00+	.00+	.00+	.00+	.00+	.39	.37	.32	.24
6- 4	.42	.38	.25	.22	.60*	.44*	.41*	.34*	.66	.68	.69	.69	.68	.71	.72	.61
6- 14	.00+	.00+	.00+	.00+	.00+	.00+	.00+	.00+	.27	.27	.26	.21	.25	.30	.31	.27
6- 15	.00+	.00+	.00+	.00+	.00+	.00+	.00+	.00+	.36	.33	.25	.22	.30	.29	.24	.20
7- 3	.00+	.00+	.00+	.00+	.00+	.00+	.00+	.00+	.49	.50	.49	.48	.51	.56	.55*	.46
7- 13	.00+	.00+	.00+	.00+	.00+	.00+	.00+	.00+	.08*	.14*	.24	.20	.16*	.11*	.25*	.19
7-103	.00+	.00+	.00+	.00+	.00+	.00+	.00+	.00+	.49	.52	.46	.54	.49	.52	.57	.52
8- 2	.35	.32	.34	.34	.36	.42	.34	.35	.40	.41	.40	.37	.00+	.03*	.02*	.15*
8- 20	.00+	.00+	.00+	.00+	.00+	.00+	.00+	.00+	.00+	.00+	.00+	.00+	.21	.00+	.00+	.00+
9- 2	.13	.14	.18	.17	.14	.18	.19	.19	.00+	.00+	.00+	.00+	.00+	.00+	.00+	.00+
9- 12	.00+	.00+	.00+	.00+	.00+	.00+	.00+	.00+	.22	.20	.19	.06	.24	.24	.21	.18
10- 1	.00+	.00+	.00+	.00+	.26*	.32*	.36*	.35*	.00+	.00+	.00+	.00+	.33	.34	.36	.34
10- 20	.00+	.00+	.00+	.00+	.00+	.00+	.00+	.00+	.03*	.01*	.02*	.02*	.03	.04	.04	.05
13- 15	.00+	.00+	.00+	.00+	.05	.04	.00	.04	.00+	.00+	.00+	.00+	.00+	.00+	.00+	.00+
14- 15	.23	.19	.13	.10	.18	.12	.08	.00	.40	.36	.34	.35	.39	.24	.35	.24
20- 15	.03	.01	.01	.00	.00+	.00+	.00+	.00+	.00+	.00+	.00+	.00+	.00+	.00+	.00+	.00+
23- 32	.00+	.00+	.00+	.00+	.00+	.00+	.00+	.00+	.09	.04	.04	.06	.04	.04	.05	.04
23- 33	.00+	.00+	.00+	.00+	.00+	.00+	.00+	.00+	.07	.03	.03	.05	.04	.03	.04	.04
23- 43	.00+	.00+	.00+	.00+	.00+	.00+	.00+	.00+	.03	.04	.03	.03	.03	.05	.03	.03
32- 33	.46	.51	.54	.49	.27	.39	.44	.47	.31	.41	.46	.48	.38	.40	.47	.49
32- 39	.07	.07	.05	.05	.05	.05	.05	.05	.00+	.00+	.00+	.00+	.00+	.00+	.00+	.00+
32- 41	.02	.02	.02	.01	.02	.02	.02	.01	.00+	.00+	.00+	.00+	.00+	.00+	.00+	.00+
32- 43	.24	.24	.24	.20	.21	.23	.25	.21	.21	.20	.22	.20	.21	.22	.23	.21
33- 43	.42	.43	.43	.39	.32	.37	.42	.38	.30	.37	.36	.40	.33	.37	.40	.39
34- 35	.18	.15	.12	.12	.13	.12	.13	.10	.00+	.00+	.00+	.00+	.00+	.00+	.00+	.00+
34- 38	.13	.16	.18	.19	.12	.13	.17	.18	.00+	.00+	.00+	.00+	.00+	.00+	.00+	.00+
35- 40	.02	.01	.04	.01	.06	.03	.02	.03	.00+	.00+	.00+	.00+	.00+	.00+	.00+	.00+
38- 36	.04	.04	.07	.03	.04	.04	.07	.04	.00+	.00+	.00+	.00+	.00+	.00+	.00+	.00+
38- 40	.06	.07	.06	.08	.09	.11	.08	.10	.00+	.00+	.00+	.00+	.00+	.00+	.00+	.00+
39- 34	.31	.35	.35	.40	.21	.21	.22	.23	.00+	.00+	.00+	.00+	.00+	.00+	.00+	.00+
39- 41	.09	.12	.14	.13	.12	.10	.07	.05	.00+	.00+	.00+	.00+	.00+	.00+	.00+	.00+
43- 39	.30	.32	.34	.32	.12	.15	.17	.21	.00+	.00+	.00+	.00+	.00+	.00+	.00+	.00+
109-112	.50	.51	.54	.54	.47	.52	.53	.53	.43	.44	.44	.42	.42	.44	.43	.41

(+ DESIGNATES DATA WAS NOT OBTAINED; * DESIGNATES QUESTIONABLE DATA)

PEAK CORRELATION COEFFICIENTS

1/4-SCALE YC-14 TEST

POSITION NOS.	556	558	560	562	567	569	571	573	574	575	576	577	578	579	580	581
1- 2	.08	.21	.25	.29	.00*	.06*	.09*	.15*	.00	.12	.17	.21	.01	.13	.14	.14
1- 8	.26*	.04*	.11*	.05*	.17*	.10*	.07*	.08*	.26*	.14*	.06*	.06*	.35*	.11*	.07*	.03*
1- 20	.00	.02	.10	.16	.00+	.00+	.00+	.00+	.00+	.00+	.00+	.00+	.00+	.00+	.00+	.00+
2- 20	.20	.37	.43	.44	.00+	.00+	.00+	.00+	.00+	.00+	.00+	.00+	.00+	.00+	.00+	.00+
3- 13	.36*	.41*	.40*	.31*	.18*	.26*	.18*	.16*	.15*	.20*	.17*	.19*	.13*	.13*	.10*	.14*
4- 14	.16*	.35*	.27*	.47*	.32*	.34*	.36*	.40*	.15*	.31*	.32*	.39*	.24*	.21*	.18*	.05*
4- 15	.28	.04	.09	.12	.00+	.00+	.00+	.00+	.00+	.00+	.00+	.00+	.00+	.00+	.00+	.00+
6- 4	.37	.33	.20	.35	.27*	.41*	.46*	.50*	.43	.49	.53	.61	.41	.39	.38	.21*
6- 14	.00*	.15*	.19*	.29*	.09*	.15*	.23*	.25*	.10*	.19*	.19*	.23*	.02*	.02*	.00*	.04*
6- 15	.43	.39	.23	.29	.11*	.08*	.08*	.16*	.00	.00	.11	.18	.06	.08	.10	.17*
7- 3	.44*	.53*	.44*	.39*	.15*	.16*	.14*	.18*	.14*	.23*	.12*	.15*	.17*	.19*	.11*	.13*
7- 13	.11*	.22	.34	.32	.05	.03	.08	.09	.04	.07	.04	.06	.00	.02	.03	.01
8- 2	.36*	.12*	.06*	.06*	.21*	.22*	.06*	.05*	.21*	.11*	.05*	.05*	.32*	.05*	.02*	.04*
9- 12	.05*	.05*	.04*	.00+	.00+	.00+	.00+	.00+	.00+	.00+	.00+	.00+	.00+	.00+	.00+	.00+
10- 1	.10*	.03*	.03*	.04*	.00+	.00+	.00+	.00+	.00+	.00+	.00+	.00+	.00+	.00+	.09*	.00+
10- 20	.03*	.02*	.04*	.04*	.00+	.00+	.00+	.00+	.00+	.00+	.00+	.00+	.00+	.00+	.00+	.00+
11-109	.00+	.00+	.00+	.01*	.00+	.00+	.00+	.00+	.00+	.00+	.00+	.00+	.00+	.00+	.00+	.00+
14- 15	.07*	.16*	.09*	.11*	.13*	.16*	.20*	.24*	.00*	.11*	.15*	.18*	.06*	.00*	.11*	.04*
23- 32	.05*	.03*	.04*	.02*	.08*	.04*	.03*	.03*	.07*	.04*	.03*	.05*	.06*	.03*	.03*	.05*
23- 33	.04*	.04*	.04*	.04*	.00+	.00+	.00+	.00+	.00+	.00+	.00+	.00+	.00+	.00+	.00+	.00+
23- 43	.03*	.02*	.03*	.03*	.00+	.00+	.00+	.00+	.00+	.00+	.00+	.00+	.00+	.00+	.00+	.00+
32- 33	.40	.46	.45	.46	.42	.46*	.48*	.47*	.40	.43	.42	.33	.35*	.42	.37	.28
32- 39	.00+	.00+	.00+	.00+	.02	.06*	.08*	.04	.03	.05	.06	.04	.04	.06	.05	.05
32- 41	.00+	.00+	.00+	.00+	.01*	.01*	.01*	.01*	.01*	.01*	.02*	.01*	.01	.02	.01*	.01
32- 43	.16	.19	.23	.25	.16	.18*	.23*	.24*	.16	.20	.25	.22	.14	.20	.22	.20
33- 43	.36	.40	.44	.42	.00+	.00+	.00+	.00+	.00+	.00+	.00+	.00+	.00+	.00+	.00+	.00+
39- 34	.00+	.00+	.00+	.00+	.34*	.26	.24	.25	.17	.20	.12	.12	.07	.06	.06	.05
39- 36	.00+	.00+	.00+	.00+	.02	.02	.02	.03	.01	.02	.03	.02	.02	.02	.02	.01
39- 38	.00+	.00+	.00+	.00+	.14	.12	.11	.11	.06	.08	.08	.07	.06	.07	.07	.07
41- 35	.00+	.00+	.00+	.00+	.02*	.04*	.00*	.01*	.01*	.02*	.02*	.02*	.00	.02	.01*	.02
41- 37	.00+	.00+	.00+	.00+	.04*	.00*	.00*	.02*	.00*	.05*	.01*	.01*	.07*	.05*	.05*	.03*
41- 40	.00+	.00+	.00+	.00+	.06*	.01*	.04*	.04*	.04*	.05*	.04*	.03*	.00	.03	.01*	.00
109- 20	.00+	.00+	.00+	.00+	.07*	.15*	.26*	.26*	.07	.13	.15	.18	.13*	.16	.18	.20
109-112	.44	.40	.41	.42	.57	.58*	.50*	.50*	.62	.56	.54	.52	.56*	.60	.61	.57

(+ DESIGNATES DATA WAS NOT OBTAINED; * DESIGNATES QUESTIONABLE DATA)

TABLE IX

BROADBAND CONVECTION VELOCITIES, m/s

1/4-SCALE YC-14 TEST

POSITION NOS.	RUN NUMBER															
	133	134	135	136	142	143	144	145	270	271	272	273	275	276	281	282
1- 8	183*	144*	116*	116*	175*	161*	139*	88*	0>	0>	0*	0*	110*	110*	100*	86
6- 4	279*	248*	179*	131*	0>	367*	410*	199*	0>	367	0>	0>	0>	199	162	110
7- 3	107*	109*	104*	90*	99*	99*	92*	17*	0>	0>	0>	0>	94	87	87	68
8- 2	302*	302*	94*	62*	324*	324*	282*	94*	0>	0>	0>	0>	0+	0+	0+	0+
10- 1	176*	132*	125*	115*	173*	170*	138*	87*	0>	0>	0>	0>	143*	132	91	94*
32- 33	282*	296*	183	141	296	248	207	138	311	259	214	144	296	259	62*	151
32- 39	337	282	222	170	341	287	227	156	262*	230*	184*	129<	173	144	330*	97<
32- 41	0>	110<	104<	100<	164<	144<	136<	201<	164<	143<	247<	0>	199<	0>	0>	0>
32- 43	0+	0+	205<	0+	0+	0+	0+	0+	0+	0+	0+	0+	0+	0+	0+	0+
34- 35	153*	120	103	72	135	120	95	68	181	130	111	82	114	77	0+	72
38- 40	108	99	76	62<	126	95	82	68	0+	0+	0+	0+	0+	0+	0+	0+
39- 41	41<	0>	0>	0>	107	98	77	59	100*	93*	75*	59*	235	375	178*	320*
109-112	0+	0+	0+	0+	0+	0+	0+	0+	358	373	381	325	351	351	358	331

--- DATA CALCULATED BY DIVIDING TIME DELAY OF MAX. CORRELATION INTO SENSOR SEPARATION DISTANCE ---

(+ DESIGNATES DATA WAS NOT OBTAINED; * DESIGNATES QUESTIONABLE DATA; < DESIGNATES MAX. CORRELATION COEFFICIENT < 0.05)
(> DESIGNATES QUESTIONABLE DATA; CALCULATED VALUE > 500 MPS)
(- DESIGNATES CORRELATION COEFF. REMAINED <0 FOR TIME DELAYS FROM 0.0 TO 10.24 MS)

BROADBAND CONVECTION VELOCITIES, m/s

1/4-SCALE YC-14 TEST

POSITION NOS.	RUN NUMBER															
	284	285	286	287	289	290	291	292	301	302	303	304	306	307	308	309
1- 2	0+	0+	0+	0+	0+	0+	0+	0+	115	111	106	71	87	100	94	78
1- 8	40<	110*	103	85	107	110	104	77	116	110	107	86	116	105	107	77
6- 4	0>	0>	199	136	0>	0>	0>	0>	0>	0>	199	148	0>	0>	0>	0>
7- 3	116	94	90	83	104	90*	76	65	0+	0+	0+	0+	0+	0+	0+	0+
8- 2	123*	116*	105	78	120	108	99	74	123	113	105	74	108	98	99	76
32- 33	296	259	214	155	296	259	214	151	282	248	207	159	282	259	207	155
32- 39	178	147	134	98	156	137	116	92<	176	153	131	88	157	134	120	84<
32- 41	0>	0>	0>	0>	278<	230<	0>	0>	198<	165<	158<	0>	238<	194<	157<	224<
32- 43	0+	0+	0+	0+	0+	0+	0+	0+	283	252	208	153	292	255	208	151
33- 43	0+	0+	0+	0+	0+	0+	0+	0+	284	243	205	157	291	248	205	151
34- 35	111	98	92	79	176	143	118	83	107	86	82	66	178	150	103	82
38- 40	0>	375*	320	171	0>	0>	452	0>	0>	299	248	196	0>	0>	271	320<
39- 41	235	410	346	280	98	90	0>	62	215	207	289	271	96	0>	0>	0>
43- 39	0+	0+	0+	0+	0+	0+	0+	0+	137	132	113	94	169	142	126	94
109-112	351	351	358	337	351	337	373	325	351	351	358	331	351	331	331	325

--- DATA CALCULATED BY DIVIDING TIME DELAY OF MAX. CORRELATION INTO SENSOR SEPARATION DISTANCE ---

(+ DESIGNATES DATA WAS NOT OBTAINED; * DESIGNATES QUESTIONABLE DATA; < DESIGNATES MAX. CORRELATION COEFFICIENT < 0.05)
(> DESIGNATES QUESTIONABLE DATA; CALCULATED VALUE > 500 MPS)
(- DESIGNATES CORRELATION COEFF. REMAINED <0 FOR TIME DELAYS FROM 0.0 TO 10.24 MS)

TABLE IX (concluded)

BROADBAND CONVECTION VELOCITIES, m/s

1/4-SCALE YC-14 TEST

POSITION NOS.	326	327	328	329	331	332	333	334	491	492	493	494	499	500	501	502
1- 2	94	82	83	81	109	108	97	73	129	104	97	71	0+	0+	0+	0+
1- 8	110	107	101	73	116	111	105	85	114	113	98	71	114	110	100	75
1- 20	0+	0+	0+	0+	0+	0+	0+	0+	122	112	97	70	110	110	101	75<
2- 20	0+	0+	0+	0+	0+	0+	0+	0+	127	107	94	69	0+	0+	0+	0+
3- 13	0+	0+	0+	0+	0+	0+	0+	0+	108*	98	81	66	106*	94	81	60
4- 14	0+	0+	0+	0+	0+	0+	0+	0+	0>	0>	103	85	0>	0>	103	71
4- 15	0+	0+	0+	0+	0+	0+	0+	0+	0+	0+	0+	0+	369	369	369	361
6- 4	0>	0>	0>	0>	0>	199*	162*	118*	0>	0>	0>	0>	0>	0>	0>	0>
6- 14	0+	0+	0+	0+	0+	0+	0+	0+	0>	141	100	82	0>	142	108	81
6- 15	0+	0+	0+	0+	0+	0+	0+	0+	387	387	395	381	395	402	402	155
7- 3	0+	0+	0+	0+	0+	0+	0+	0+	134	115	91	66	132	109	94	69
7- 13	0+	0+	0+	0+	0+	0+	0+	0+	107*	101	87	64	107*	100	84	63
7-103	0+	0+	0+	0+	0+	0+	0+	0+	134	110	90	67	130	110	90	63
8- 2	110	110	96	64	120	103	100	73	127	116	92	72	0+	52<	40<	65*
8- 20	0+	0+	0+	0+	0+	0+	0+	0+	0+	0+	0+	0+	123	0+	0+	0+
9- 12	0+	0+	0+	0+	0+	0+	0+	0+	381	381	358	36	381	381	365	337
10- 1	0+	0+	0+	0+	152*	143*	115*	87*	0+	0+	0+	0+	134	127	106	79
10- 20	0+	0+	0+	0+	0+	0+	0+	0+	96<	102<	420<	120<	124<	0>	101<	0>
32- 33	282	248	207	155	282	248	207	151	296	259	214	172	296	259	214	155
32- 39	154	135	114	85	170	150	127	98	0+	0+	0+	0+	0+	0+	0+	0+
32- 41	113<	0>	182<	0>	178<	164<	0>	128<	0+	0+	0+	0+	0+	0+	0+	0+
32- 43	297	255	208	151	283	252	208	152	292	255	216	159	292	263	213	155
33- 43	291	248	209	151	284	243	209	159	284	248	217	161	284	254	209	159
34- 35	178	135	117	73	105	94	78	69	0+	0+	0+	0+	0+	0+	0+	0+
38- 40	0>	410	452	202	0>	0>	255	171	0+	0+	0+	0+	0+	0+	0+	0+
39- 41	106	95	78	64	223	205	410	248	0+	0+	0+	0+	0+	0+	0+	0+
43- 39	171	143	123	94	132	129	108	94	0+	0+	0+	0+	0+	0+	0+	0+
109-112	351	365	325	325	344	351	351	325	365	365	358	325	365	365	365	331

BROADBAND CONVECTION VELOCITIES, m/s

1/4-SCALE YC-14 TEST

POSITION NOS.	556	558	560	562	567	569	571	573	574	575	576	577	578	579	580	581
1- 2	54	77	104	121	0*	92*	83*	113*	0-	80	105	134	60<	71	108	127
1- 8	57*	77<	0>	175*	56*	75*	99*	77*	63*	82*	74*	53*	61*	66*	60*	56<
1- 20	0-	87<	110	127	0+	0+	0+	0+	0+	0+	0+	0+	0+	0+	0+	0+
2- 20	67	78	108	125	0+	0+	0+	0+	0+	0+	0+	0+	0+	0+	0+	0+
3- 13	39*	58	81	84	47	66	91	92	47	52	72	91	84	73	111	108
4- 14	54*	78*	127*	429*	108*	108*	120*	134*	68*	84*	91*	120*	0>	120*	106*	257*
4- 15	108	87<	41	38	0+	0+	0+	0+	0+	0+	0+	0+	0+	0+	0+	0+
6- 4	19	17	0>	0>	179*	118*	199*	179*	88	127	155	199	0>	127	127	148*
6- 14	0*	31*	144*	188*	66*	90*	126*	118*	66*	78*	95*	118*	31<	0>	31<	152<
6- 15	42	0>	0>	453	41*	51*	79*	87*	0-	0-	79	103	0>	0>	91	108
7- 3	52	72	109	221	37	60	83	125	45	57	47	221	104	146	411	45
7- 13	44*	62	90	107	0>	0>	70	85	46<	65	82<	94	0-	34<	38<	83<
8- 2	55*	63*	78*	186*	92*	66*	81*	88*	56*	58*	186*	30*	59*	105*	25<	35<
9- 12	0>	0>	0>	0+	0+	0+	0+	0+	0+	0+	0+	0+	0+	0+	0+	0+
10- 1	66*	72<	22<	18<	0+	0+	0+	0+	0+	0+	0+	0+	0+	0+	0+	0+
10- 20	0>	465<	0>	0>	0+	0+	0+	0+	0+	0+	0+	0+	0+	0+	0+	0+
32- 33	111	163	222	270	95	159*	222*	270*	95	159	222	270	95*	159	222	259
32- 39	0+	0+	0+	0+	60<	93*	122*	155*	61<	99	132	281<	65<	99	159	281
32- 41	0+	0+	0+	0+	94<	149<	0>	223<	112<	0>	0>	192<	105<	155<	237<	91<
32- 43	104	157	227	275	104	160*	224*	275*	104	163	221	267	104	156	224	267
33- 43	102	159	221	271	0+	0+	0+	0+	0+	0+	0+	0+	0+	0+	0+	0+
109-112	337	337	344	389	337	337*	397*	389*	337	344	365	365	337*	351	358	358

--- DATA CALCULATED BY DIVIDING TIME DELAY OF MAX. CORRELATION INTO SENSOR SEPARATION DISTANCE ---

(+ DESIGNATES DATA WAS NOT OBTAINED; * DESIGNATES QUESTIONABLE DATA; < DESIGNATES MAX. CORRELATION COEFFICIENT < 0.05)
(> DESIGNATES QUESTIONABLE DATA; CALCULATED VALUE > 500 MPS)
(- DESIGNATES CORRELATION COEFF. REMAINED <0 FOR TIME DELAYS FROM 0.0 TO 10.24 MS)

TABLE X

MAXIMUM VALUE OF COHERENCE FCT.
1/4-SCALE YC-14 TEST

POSITION NOS.	133	134	135	136	142	143	144	145	270	271	272	273	275	276	281	282
1- 8	.53*	.39*	.50*	.16*	.33*	.29*	.48*	.68*	.71*	.65*	.65*	.56*	.34*	.43*	.43*	.39
3- 6	.00+	.00+	.00+	.00+	.00+	.00+	.00+	.00+	.00+	.00+	.00+	.00+	.19	.18	.21	.11
6- 4	.77*	.61*	.59*	.51*	.37*	.27*	.34*	.25*	.41*	.28*	.20*	.13*	.51	.50	.46	.42
7- 3	.45*	.37*	.37*	.27*	.55*	.39*	.32*	.23*	.64*	.63*	.62*	.57*	.41	.31	.20	.16
8- 2	.49*	.43*	.48*	.45*	.56*	.66*	.74*	.81*	.89*	.86*	.82*	.72*	.00+	.00+	.00+	.00+
9- 2	.18*	.14*	.22*	.85*	.13*	.17*	.17*	.65*	.00+	.00+	.00+	.00+	.00+	.00+	.00+	.00+
9- 3	.00+	.00+	.00+	.00+	.00+	.00+	.00+	.00+	.15*	.08*	.05*	.04*	.17	.19	.16	.13
10- 1	.50*	.76*	.59*	.73*	.42*	.50*	.51*	.56*	.83*	.81*	.60*	.49*	.43*	.39*	.20	.47*
10- 2	.06*	.09*	.06*	.82*	.06*	.08*	.08*	.65*	.66*	.55*	.42*	.34*	.00+	.00+	.00+	.00+
10- 8	.14*	.15*	.18*	.46*	.08*	.19*	.14*	.73*	.71*	.64*	.14*	.03*	.13*	.14*	.20*	.19*
13- 14	.14*	.12*	.10*	.00+	.02*	.03*	.02*	.05*	.12*	.14*	.17*	.10*	.16	.05	.00+	.20
13- 20	.26*	.00+	.03*	.31*	.25*	.04*	.05*	.35*	.00+	.00+	.00+	.00+	.00+	.00+	.00+	.00+
14- 13	.00+	.00+	.00+	.30*	.00+	.00+	.00+	.00+	.00+	.00+	.00+	.00+	.00+	.00+	.00+	.00+
14- 15	.48*	.33*	.20*	.23*	.53*	.33*	.15*	.11*	.19*	.16*	.08*	.05*	.18	.18	.00+	.08
20- 12	.28*	.08*	.06*	.42*	.30*	.15*	.07*	.54*	.00+	.00+	.00+	.00+	.11*	.18*	.00+	.00+
32- 33	.62*	.67*	.80	.75	.72	.68	.73	.73	.79	.83	.84	.80	.71	.79	.20*	.82
32- 37	.00+	.00+	.00+	.00+	.00+	.00+	.00+	.00+	.02	.02	.05	.03	.01	.01	.20*	.03
32- 39	.24	.28	.20	.12	.23	.26	.25	.37	.24*	.17*	.20*	.25*	.22*	.28*	.20*	.18*
32- 41	.03	.03	.01	.03	.05	.11	.07	.09	.03	.09	.06	.13	.04	.04	.20*	.02
32- 43	.00+	.00+	.01*	.00+	.00+	.00+	.00+	.00+	.00+	.00+	.00+	.00+	.00+	.00+	.00+	.00+
34- 35	.20*	.21	.15	.08	.28	.26	.22	.13	.15	.10	.13	.11	.17	.13	.00+	.09
34- 38	.19	.23	.21	.15	.15	.18	.19	.15	.12	.74	.14	.12	.10	.17	.00+	.13
35- 40	.14*	.12	.13	.15	.05	.07	.03	.05	.03	.02	.04	.03	.08	.05	.06	.05
36- 37	.29*	.49*	.21*	.11*	.23*	.37*	.20*	.09*	.00+	.00+	.00+	.00+	.00+	.00+	.00+	.00+
38- 36	.00+	.00+	.00+	.00+	.00+	.00+	.00+	.00+	.06	.07	.08	.11	.07	.08	.10	.12
38- 40	.04	.05	.02	.04	.06	.05	.03	.02	.00+	.00+	.00+	.00+	.00+	.00+	.00+	.00+
39- 34	.09	.18	.19	.17	.25	.26	.31	.30	.20*	.29*	.31*	.26*	.01*	.01*	.12*	.14*
39- 41	.03	.08	.04	.05	.28	.26	.31	.24	.12*	.12*	.13*	.00*	.09*	.08*	.20*	.05*
40- 37	.11*	.06*	.07*	.07*	.09*	.09*	.08*	.04*	.00+	.00+	.00+	.00+	.00+	.00+	.00+	.00+
43- 35	.00+	.00+	.00+	.00+	.00+	.00+	.00+	.00+	.03	.01	.01	.06	.03	.02	.02	.01
109-112	.00+	.00+	.00+	.00+	.00+	.00+	.00+	.00+	.59	.62	.61	.67	.68	.72	.68	.68

(+ DESIGNATES DATA WAS NOT OBTAINED; * DESIGNATES QUESTIONABLE DATA)

MAXIMUM VALUE OF COHERENCE FCT.
1/4-SCALE YC-14 TEST

POSITION NOS.	284	285	286	287	289	290	291	292	301	302	303	304	306	307	308	309
1- 2	.00+	.00+	.00+	.00+	.00+	.00+	.00+	.00+	.15	.20	.37	.53	.17	.17	.12	.21
1- 7	.00+	.00+	.00+	.00+	.00+	.00+	.00+	.00+	.31	.32	.35	.44	.29	.33	.26	.23
1- 8	.06*	.42*	.43	.48	.38	.49	.42	.40	.55	.52	.44	.52	.52	.53	.45	.42
6- 4	.69	.60	.45	.43	.60	.54	.46	.40	.76	.68	.56	.42	.59	.52	.54	.37
7- 3	.35	.26	.24	.18	.46	.46*	.36	.31	.00+	.00+	.00+	.00+	.00+	.00+	.00+	.00+
8- 2	.40*	.34*	.40	.34	.35	.48	.46	.41	.40	.46	.48	.60	.47	.43	.46	.45
9- 2	.22	.28	.30	.26	.30	.24	.39	.34	.34	.32	.36	.32	.30	.34	.07	.35
13- 14	.16	.18	.08	.02	.00+	.00+	.00+	.00+	.00+	.00+	.00+	.00+	.00+	.00+	.00+	.00+
13- 20	.13	.09	.14	.11	.00+	.00+	.00+	.00+	.00+	.00+	.00+	.00+	.00+	.00+	.00+	.00+
14- 15	.27	.17	.07	.06	.21	.13	.06	.03	.39	.19	.06	.07	.29	.22	.14	.07
20- 15	.06	.04	.05	.02	.06	.07	.06	.04	.08	.09	.07	.03	.11	.11	.10	.04
32- 33	.75	.83	.84	.81	.84	.79	.83	.83	.74	.80	.79	.80	.74	.77	.83	.83
32- 37	.01	.01	.02	.02	.02	.02	.01	.05	.00+	.00+	.00+	.00+	.00+	.00+	.00+	.00+
32- 39	.29	.24	.28	.17	.18	.25	.20	.16	.28	.24	.18	.13	.15	.16	.22	.13
32- 41	.04	.04	.03	.03	.06	.02	.02	.10	.03	.07	.02	.01	.04	.02	.08	.12
32- 43	.00+	.00+	.00+	.00+	.00+	.00+	.00+	.00+	.55	.55	.57	.45	.53	.51	.50	.47
33- 37	.05	.07	.03	.03	.01	.02	.02	.02	.00+	.00+	.00+	.00+	.00+	.00+	.00+	.00+
33- 43	.00+	.00+	.00+	.00+	.00+	.00+	.00+	.00+	.70	.66	.69	.71	.66	.64	.65	.61
34- 35	.15	.18	.19	.13	.11	.15	.13	.14	.14	.16	.12	.12	.13	.17	.12	.14
34- 38	.12	.15	.15	.16	.17	.11	.11	.12	.10	.12	.11	.12	.16	.15	.18	.10
35- 40	.05	.06*	.07	.07	.04	.02	.01	.03	.06	.04	.05	.05	.03	.02	.02	.05
38- 36	.07	.09	.06	.08	.07	.12	.07	.09	.03*	.07*	.08*	.08*	.08	.05	.05	.11
38- 40	.12	.11*	.11	.07	.06	.05	.06	.04	.14	.12	.10	.05	.10	.07	.05	.07
39- 34	.00+	.00+	.00+	.00+	.00+	.00+	.00+	.00+	.22	.20	.26	.26	.30	.36	.37	.42
39- 41	.08	.06	.05	.04	.13	.09	.14	.10	.08	.09	.04	.05	.08	.11	.09	.10
43- 35	.00+	.00+	.00+	.00+	.02	.04	.01	.04	.00+	.00+	.00+	.00+	.00+	.00+	.00+	.00+
43- 39	.00+	.00+	.00+	.00+	.00+	.00+	.00+	.00+	.45	.39	.44	.36	.64	.67	.67	.57
43- 40	.00+	.00+	.00+	.00+	.04	.02	.03	.04	.00+	.00+	.00+	.00+	.00+	.00+	.00+	.00+
43- 41	.02	.03	.03	.01	.05	.06	.03	.04	.00+	.00+	.00+	.00+	.00+	.00+	.00+	.00+
109-112	.66	.69	.74	.73	.63	.68	.65	.63	.70	.67	.67	.65	.61	.61	.63	.62

(+ DESIGNATES DATA WAS NOT OBTAINED; * DESIGNATES QUESTIONABLE DATA)

TABLE X (concluded)

MAXIMUM VALUE OF COHERENCE FCT.

1/4-SCALE YC-14 TEST

POSITION NOS.	326	327	328	329	331	332	333	RUN NUMBER 334	491	492	493	494	499	500	501	502
1- 2	.15	.17	.58	.84	.17	.20	.14	.08	.25	.27	.22	.24	.00+	.00+	.00+	.00+
1- 7	.33	.33	.29*	.35	.34	.36	.37	.28	.00+	.00+	.00+	.00+	.00+	.00+	.00+	.00+
1- 8	.48	.50	.50	.84	.54	.56	.50	.41	.54	.60	.53	.54	.63	.56	.52	.72
1- 20	.00+	.00+	.00+	.00+	.00+	.00+	.00+	.00+	.10	.10	.06	.16	.09	.06	.08	.22
2- 20	.00+	.00+	.00+	.00+	.00+	.00+	.00+	.00+	.45	.47	.36	.32	.00+	.00+	.00+	.00+
3- 13	.00+	.00+	.00+	.00+	.00+	.00+	.00+	.00+	.33*	.46*	.57	.56	.64*	.35*	.95*	.54
3-103	.00+	.00+	.00+	.00+	.00+	.00+	.00+	.00+	.94	.93	.92	.88	.94	.94	.93*	.89
4- 14	.00+	.00+	.00+	.00+	.00+	.00+	.00+	.00+	.92	.87	.81	.77	.90	.87	.84	.77
4- 15	.00+	.00+	.00+	.00+	.00+	.00+	.00+	.00+	.00+	.00+	.00+	.00+	.71	.69	.62	.46
6- 4	.49	.47	.28	.13	.63*	.54*	.52*	.39*	.95	.93	.92	.87	.95	.92	.88	.81
6- 14	.00+	.00+	.00+	.00+	.00+	.00+	.00+	.00+	.71	.65	.55	.37	.71	.67	.60	.44
6- 15	.00+	.00+	.00+	.00+	.00+	.00+	.00+	.00+	.71	.68	.61	.57	.72	.69	.61	.53
7- 3	.00+	.00+	.00+	.00+	.00+	.00+	.00+	.00+	.70	.67	.69	.60	.70	.66	.69*	.58
7- 13	.00+	.00+	.00+	.00+	.00+	.00+	.00+	.00+	.20*	.21*	.35	.31	.32*	.23*	.33*	.35
7-103	.00+	.00+	.00+	.00+	.00+	.00+	.00+	.00+	.68	.69	.66	.64	.68	.66	.64	.61
8- 2	.50	.51	.60	.89	.46	.50	.42	.40	.55	.53	.42	.45	.00+	.06*	.12*	.39*
8- 20	.00+	.00+	.00+	.00+	.00+	.00+	.00+	.00+	.00+	.00+	.00+	.00+	.22	.00+	.00+	.00+
9- 2	.27	.25	.22	.16	.32	.38	.27	.17	.00+	.00+	.00+	.00+	.00+	.00+	.00+	.00+
9- 12	.00+	.00+	.00+	.00+	.00+	.00+	.00+	.00+	.43	.37	.58	.46	.45	.37	.54	.45
10- 1	.00+	.00+	.00+	.00+	.40*	.47*	.42*	.44*	.00+	.00+	.00+	.00+	.53	.55	.60	.50
10- 20	.00+	.00+	.00+	.00+	.00+	.00+	.00+	.00+	.03*	.02*	.02*	.12*	.03	.03	.05	.30
13- 15	.00+	.00+	.00+	.00+	.04	.03	.02	.05	.00+	.00+	.00+	.00+	.00+	.00+	.00+	.00+
14- 15	.22	.17	.09	.04	.23	.15	.16	.07	.71	.62	.60	.62	.65	.37	.65	.79
20- 15	.06	.02	.02	.02	.00+	.00+	.00+	.00+	.00+	.00+	.00+	.00+	.00+	.00+	.00+	.00+
23- 32	.00+	.00+	.00+	.00+	.00+	.00+	.00+	.00+	.70	.37	.34	.63	.39	.38	.32	.23
23- 33	.00+	.00+	.00+	.00+	.00+	.00+	.00+	.00+	.74	.24	.26	.70	.33	.28	.33	.55
23- 43	.00+	.00+	.00+	.00+	.00+	.00+	.00+	.00+	.28	.50	.21	.17	.30	.44	.22	.46
32- 33	.79	.78	.81	.82	.69	.77	.80	.79	.67	.78	.81	.81	.69	.80	.79	.79
32- 39	.20	.18	.24	.17	.30	.28	.30	.14	.00+	.00+	.00+	.00+	.00+	.00+	.00+	.00+
32- 41	.03	.02	.07	.08	.03	.02	.02	.02	.00+	.00+	.00+	.00+	.00+	.00+	.00+	.00+
32- 43	.50	.49	.54	.50	.56	.58	.59	.50	.51	.47	.53	.44	.54	.52	.51	.46
33- 43	.70	.67	.66	.65	.69	.72	.70	.67	.68	.64	.66	.68	.69	.66	.68	.67
34- 35	.21	.14	.17	.15	.14	.16	.14	.09	.00+	.00+	.00+	.00+	.00+	.00+	.00+	.00+
34- 38	.18	.15	.14	.13	.12	.08	.15	.16	.00+	.00+	.00+	.00+	.00+	.00+	.00+	.00+
35- 40	.04	.04	.01	.04	.05	.05	.06	.07	.00+	.00+	.00+	.00+	.00+	.00+	.00+	.00+
38- 36	.09	.08	.09	.04	.06	.09	.12	.08	.00+	.00+	.00+	.00+	.00+	.00+	.00+	.00+
38- 40	.09	.04	.04	.05	.13	.15	.07	.06	.00+	.00+	.00+	.00+	.00+	.00+	.00+	.00+
39- 34	.27	.28	.32	.34	.18	.20	.23	.18	.00+	.00+	.00+	.00+	.00+	.00+	.00+	.00+
39- 41	.18	.14	.09	.10	.07	.10	.04	.03	.00+	.00+	.00+	.00+	.00+	.00+	.00+	.00+
43- 39	.67	.66	.67	.55	.44	.42	.42	.35	.00+	.00+	.00+	.00+	.00+	.00+	.00+	.00+
109-112	.63	.69	.66	.65	.67	.67	.69	.69	.70	.71	.64	.63	.64	.66	.60	.53

(+ DESIGNATES DATA WAS NOT OBTAINED; * DESIGNATES QUESTIONABLE DATA)

MAXIMUM VALUE OF COHERENCE FCT.

1/4-SCALE YC-14 TEST

POSITION NOS.	556	558	560	562	567	569	571	RUN NUMBER 573	574	575	576	577	578	579	580	581
1- 2	.62	.18	.28	.31	.23*	.59*	.11*	.13*	.20	.33	.16	.20	.56	.28	.24	.24
1- 8	.79*	.06*	.89*	.04*	.66*	.44*	.03*	.11*	.25*	.14*	.03*	.88*	.74*	.11*	.04*	.02*
1- 20	.28	.06	.10	.14	.00+	.00+	.00+	.00+	.00+	.00+	.00+	.00+	.00+	.00+	.00+	.00+
2- 20	.65	.48	.49	.54	.00+	.00+	.00+	.00+	.00+	.00+	.00+	.00+	.00+	.00+	.00+	.00+
3- 13	.41*	.49*	.50*	.60*	.21*	.20*	.20*	.26*	.24*	.21*	.28*	.33*	.60*	.06*	.09*	.11*
4- 14	.17*	.40*	.38*	.57*	.21*	.36*	.34*	.45*	.05*	.24*	.31*	.39*	.07*	.06*	.09*	.02*
4- 15	.78	.45	.45	.45	.00+	.00+	.00+	.00+	.00+	.00+	.00+	.00+	.00+	.00+	.00+	.00+
6- 4	.84	.66	.64	.65	.29*	.47*	.57*	.50*	.29	.48	.54	.71	.18	.25	.29	.10*
6- 14	.16*	.26*	.24*	.38*	.13*	.14*	.16*	.30*	.06*	.19*	.33*	.25*	.01*	.02*	.02*	.06*
6- 15	.60	.45	.33	.35	.05*	.07*	.07*	.18*	.07	.08	.20	.32	.02	.08	.15	.90*
7- 3	.63*	.62*	.65*	.59*	.28*	.26*	.27*	.36*	.37*	.30*	.29*	.31*	.41*	.13*	.14*	.17*
7- 13	.15*	.25	.32	.39	.14	.11	.09	.09	.09	.06	.10	.08	.32	.50	.03	.03
8- 2	.75*	.07*	.10*	.02*	.35*	.23*	.04*	.06*	.17*	.12*	.03*	.04*	.74*	.06*	.03*	.02*
9- 12	.03*	.04*	.05*	.00+	.00+	.00+	.00+	.00+	.00+	.00+	.00+	.00+	.00+	.00+	.00+	.00+
10- 1	.06*	.09*	.09*	.04*	.00+	.00+	.00+	.00+	.00+	.00+	.00+	.00+	.00+	.00+	.00+	.00+
10- 20	.05*	.02*	.02*	.01*	.00+	.00+	.00+	.00+	.00+	.00+	.00+	.00+	.00+	.00+	.00+	.00+
11-109	.00+	.00+	.00+	.01*	.00+	.00+	.00+	.00+	.00+	.00+	.00+	.00+	.00+	.00+	.00+	.00+
14- 15	.24*	.21*	.24*	.55*	.05*	.14*	.09*	.16*	.03*	.14*	.20*	.16*	.01*	.02*	.07*	.09*
23- 32	.82*	.46*	.27*	.18*	.84*	.71*	.33*	.20*	.82*	.44*	.27*	.41*	.79*	.24*	.22*	.24*
23- 33	.79*	.14*	.31*	.41*	.00+	.00+	.00+	.00+	.00+	.00+	.00+	.00+	.00+	.00+	.00+	.00+
23- 43	.58*	.10*	.06*	.26*	.00+	.00+	.00+	.00+	.00+	.00+	.00+	.00+	.00+	.00+	.00+	.00+
32- 33	.89	.83	.80	.75	.90	.77*	.80*	.77*	.90	.80	.86	.79	.82*	.83	.87	.82
32- 39	.00+	.00+	.00+	.00+	.53	.52*	.23*	.22*	.46	.20	.24	.23	.57	.22	.20	.32
32- 41	.00+	.00+	.00+	.00+	.09*	.17*	.06*	.06*	.10*	.03*	.07*	.03*	.04	.02	.01*	.01
32- 43	.88	.47	.50	.53	.84	.72*	.48*	.49*	.74	.42	.60	.58	.80	.56	.53	.54
33- 43	.91	.59	.64	.67	.00+	.00+	.00+	.00+	.00+	.00+	.00+	.00+	.00+	.00+	.00+	.00+
39- 34	.00+	.00+	.00+	.00+	.33*	.32	.26	.23	.18	.20	.20	.15	.29	.04	.07	.08
39- 36	.00+	.00+	.00+	.00+	.02	.05	.02	.02	.03	.02	.02	.02	.06	.01	.02	.02
39- 38	.00+	.00+	.00+	.00+	.29	.14	.05	.05	.84	.22	.08	.02	.41	.08	.05	.02
41- 35	.00+	.00+	.00+	.00+	.14*	.03*	.09*	.17*	.02*	.02*	.06*	.10*	.04	.02	.05*	.10
41- 37	.00+	.00+	.00+	.00+	.11*	.08*	.03*	.03*	.05*	.05*	.02*	.01*	.11*	.04*	.02*	.01*
41- 40	.00+	.00+	.00+	.00+	.06*	.03*	.04*	.05*	.01*	.02*	.02*	.04*	.03	.49	.02*	.04
109- 20	.00+	.00+	.00+	.00+	.31*	.28*	.34*	.31*	.29	.27	.30	.38	.41*	.38	.39	.50
109-112	.79	.65	.63	.61	.72	.67*	.65*	.61*	.84	.73	.68	.67	.81*	.83	.75	.74

(+ DESIGNATES DATA WAS NOT OBTAINED; * DESIGNATES QUESTIONABLE DATA)

Take stick on
in the place of
page 66

... stick pro
opposite side of
page 66

Do not scatter
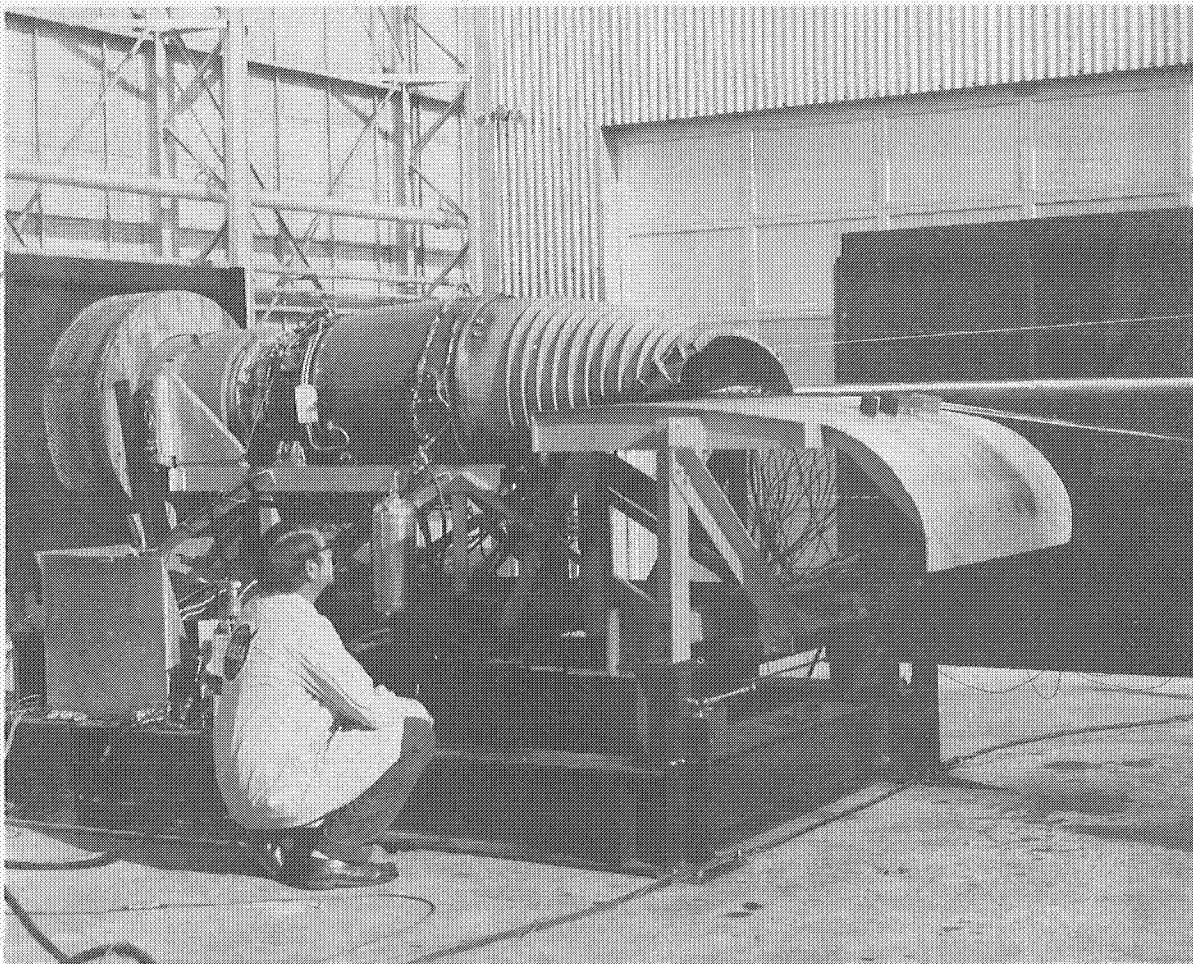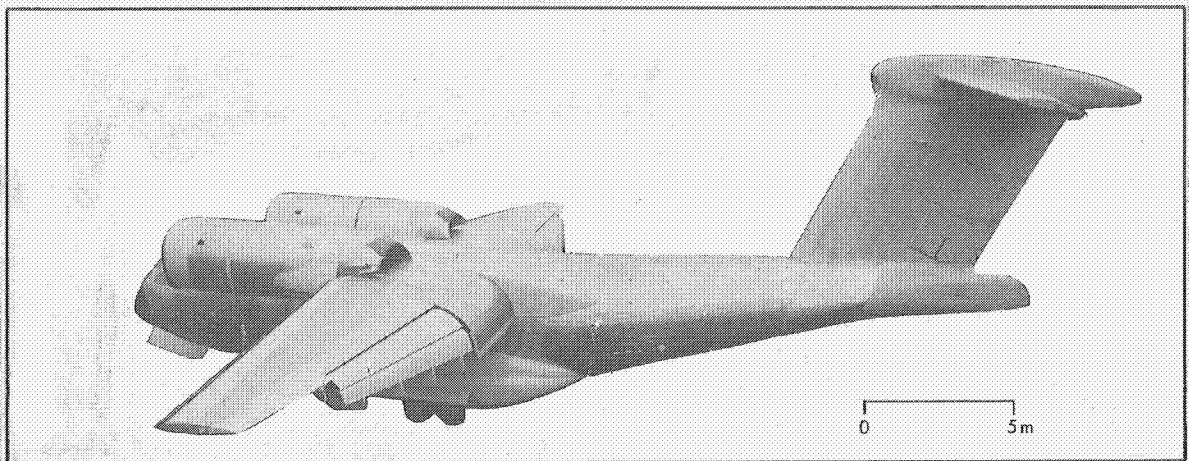
Figure 1. - Comparative views of Boeing YC-14 aircraft
and 1/4-scale YC-14 test apparatus.
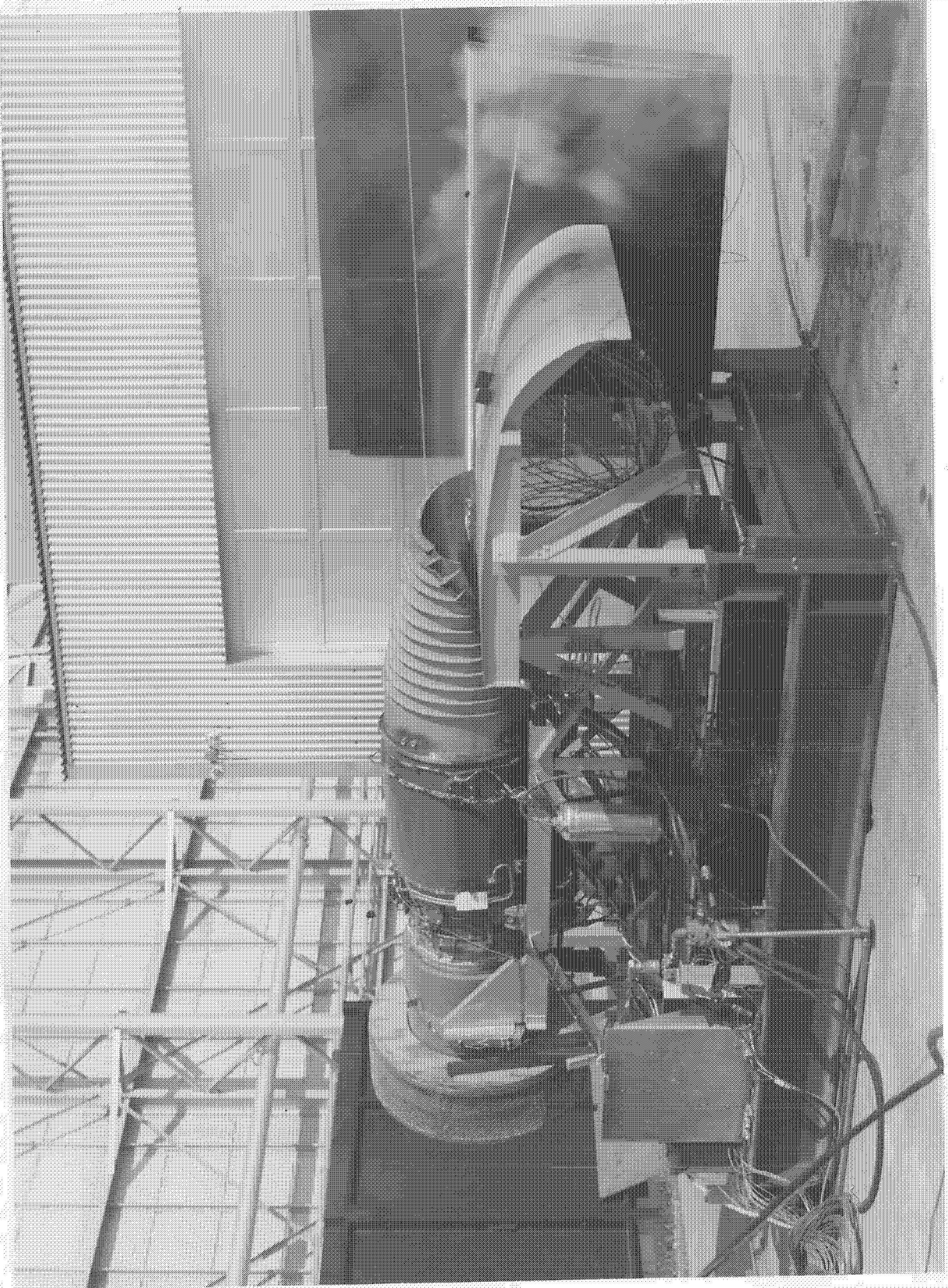
Figure 2. - Flow visualizarion.
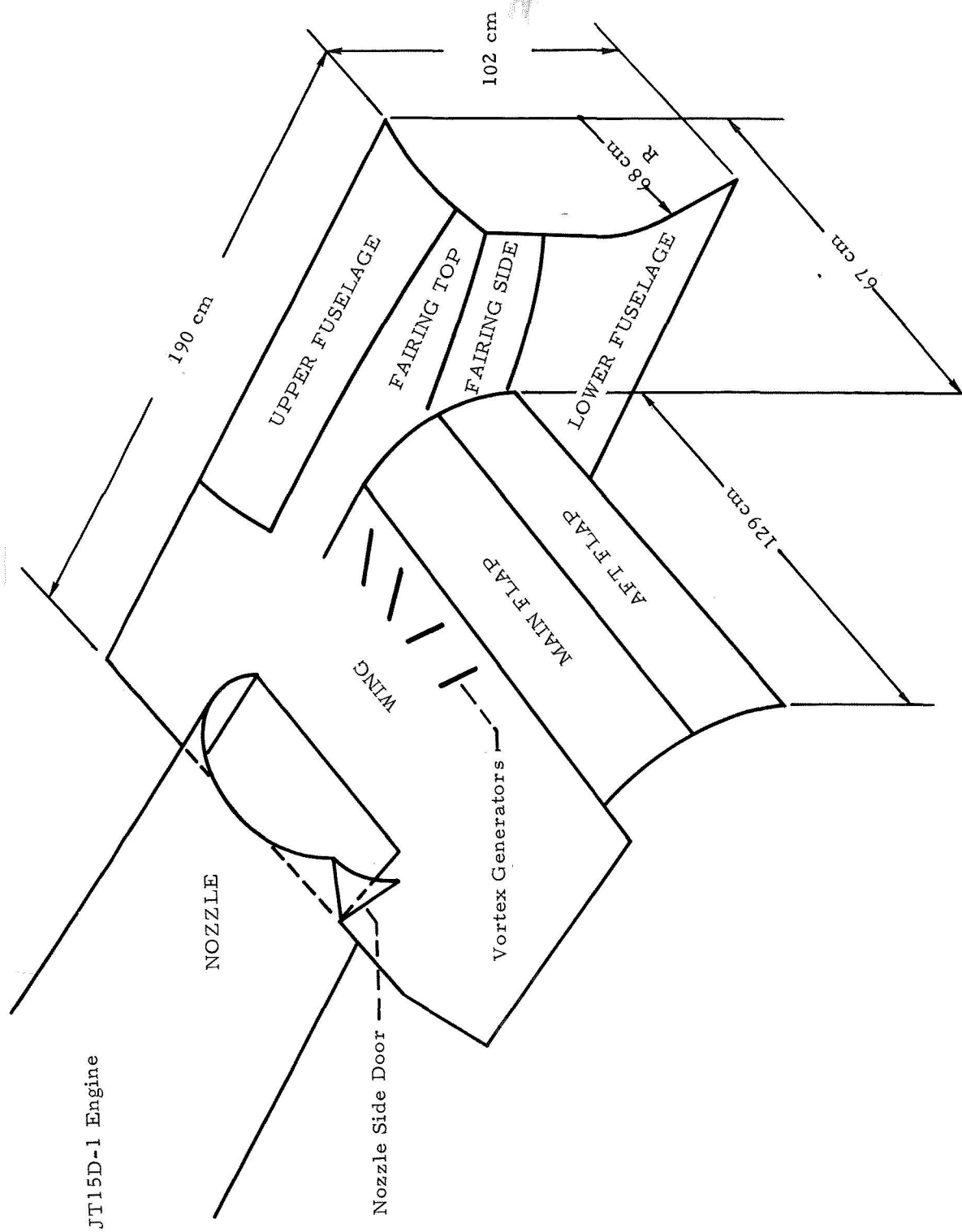
Figure 3. – Nomenclatures used in describing model
and fundamental dimensions.

69

Transducer model no.

○ Kulite XCEH-1-125-5D   (K1)
● Kulite CQH-125-5D   (K2)
□ PCB 112A21   (P)

Run Nos.	Position Numbers					
	36	37	39	40	41	
133-145	P	P	P	P	K1	K1
270-273	P	K1	K1	P	P	K1
275-334	P	K1	K1	K1	P	P
567-581	K2	P	K1	K1	P	P
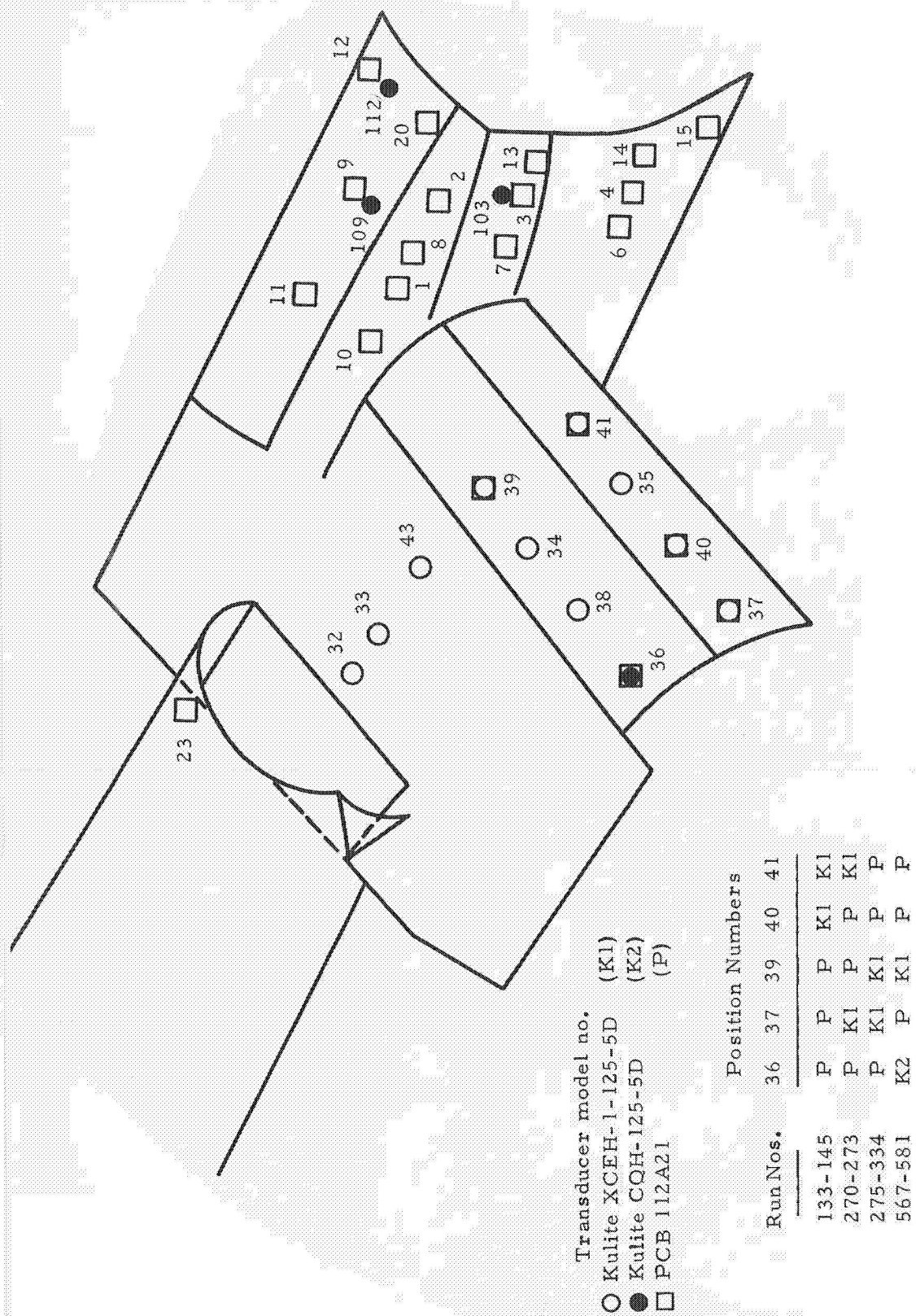
Figure 4. - Schematic of surface fluctuating pressure measurement positions and transducer assignments.
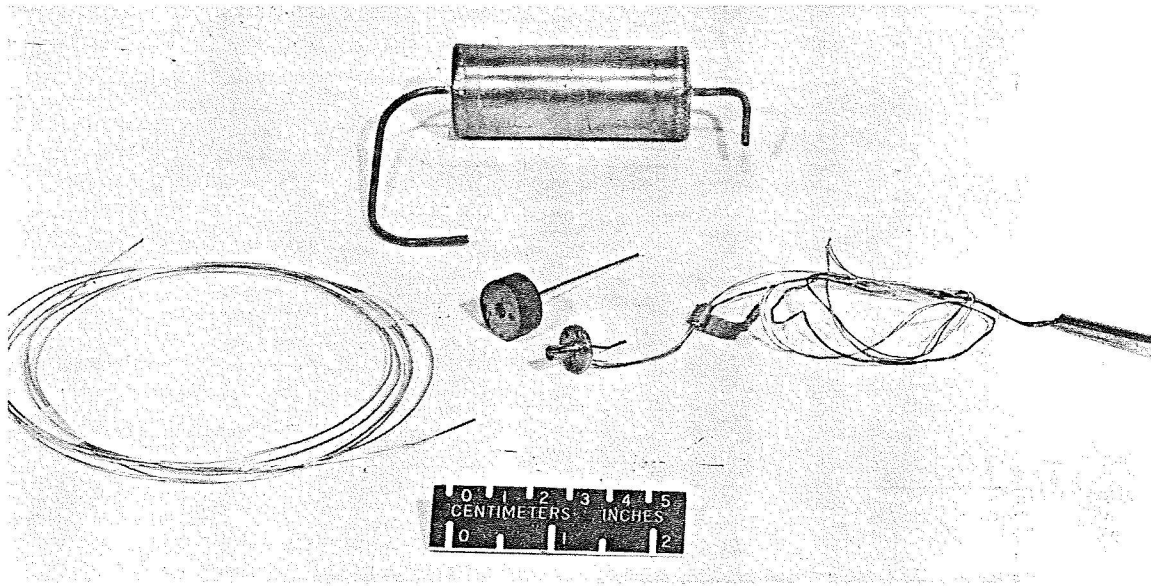
(a) Kulite sensor showing elements of low-frequency,
high-pass filtering technique.
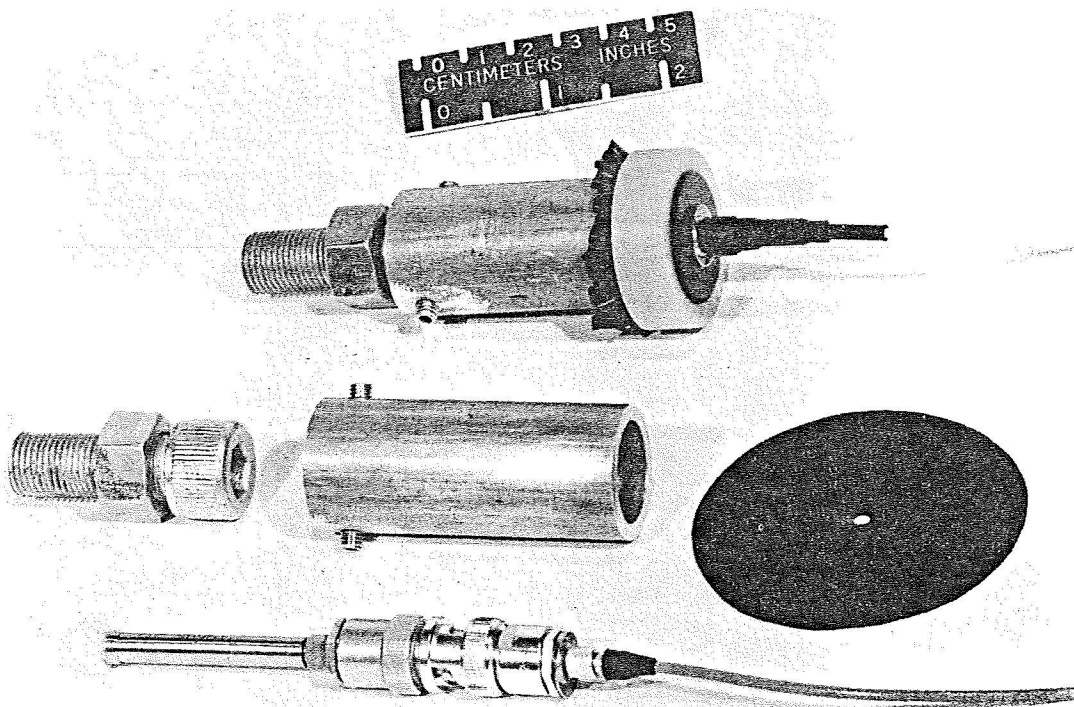
(b) PCB sensor showing elements of vibration-isolation technique.

Figure 5. - Kulite and PCB fluctuating pressure sensors.
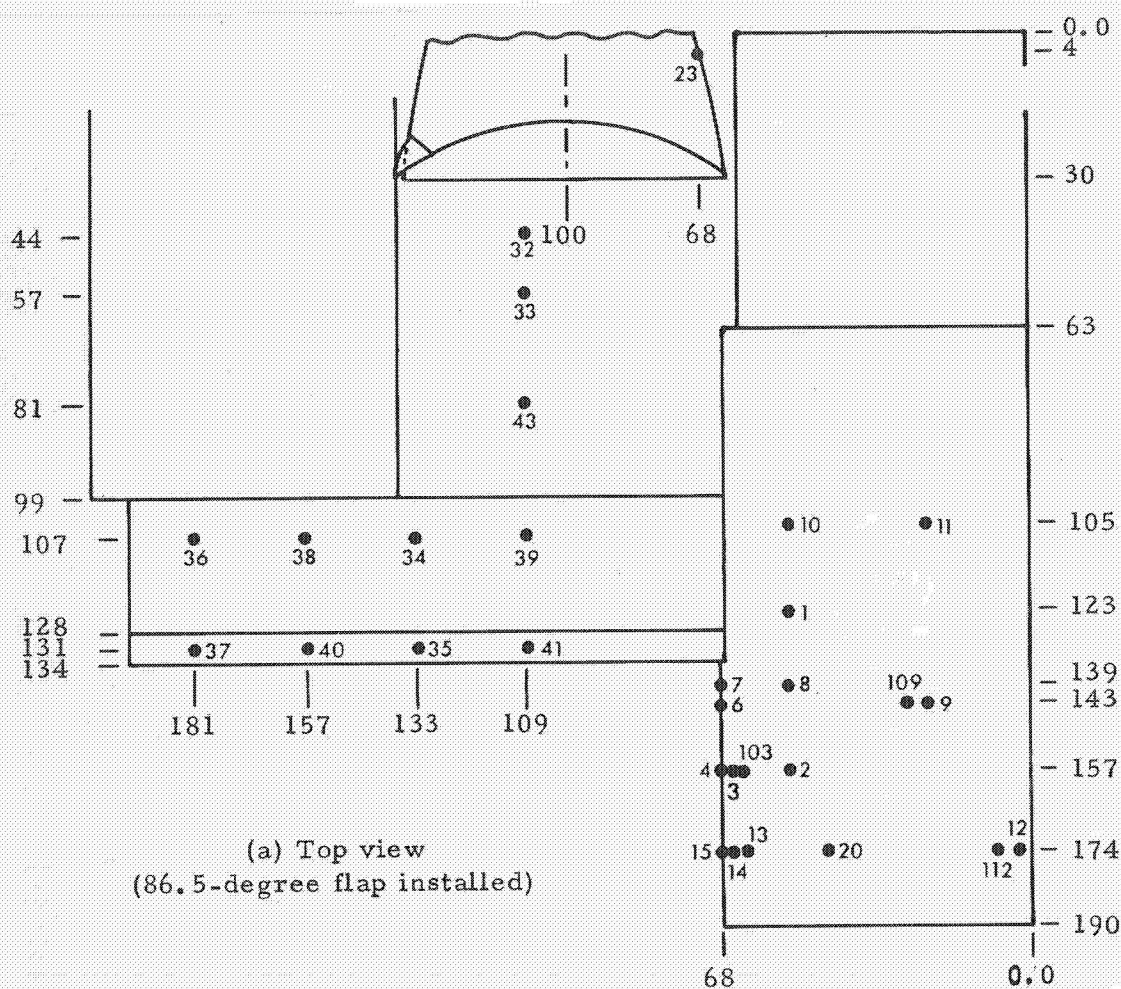
(a) Top view
(86.5-degree flap installed)
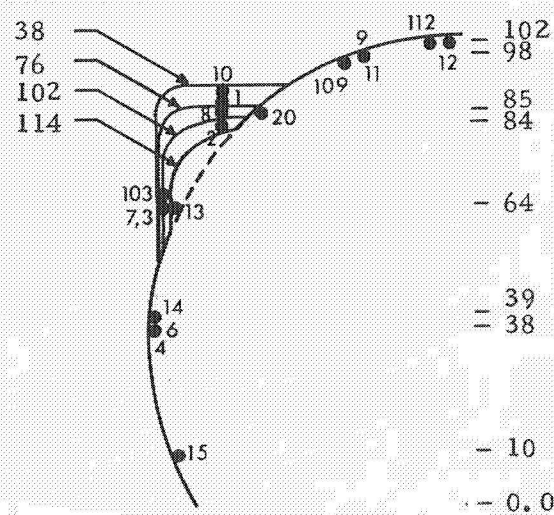
(b) End view of fuselage
and fairing

Fuselage Station

Dimensions are in centimeters

Figure 6. - Locations of measurement positions.

72

Straight-Plug
Design
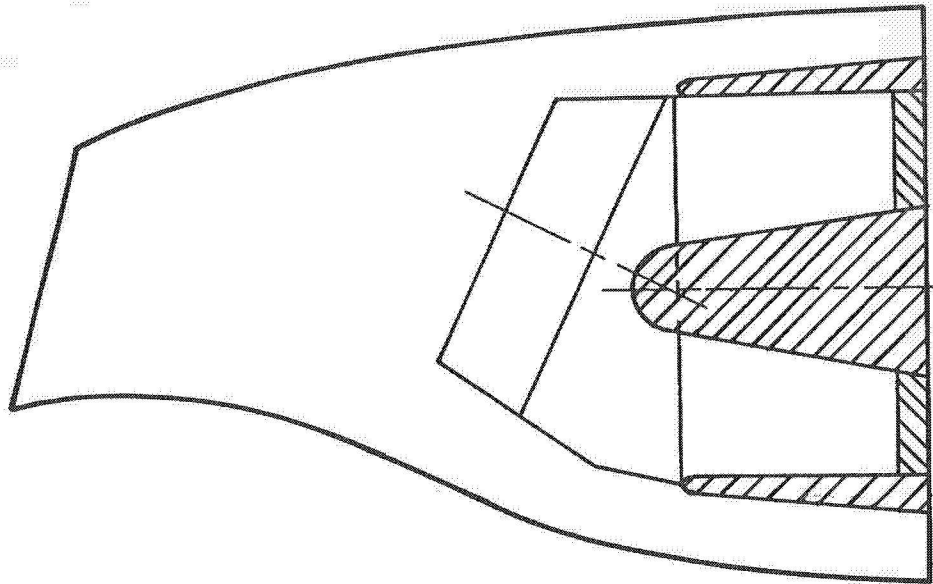
Skewed-Plug
Design
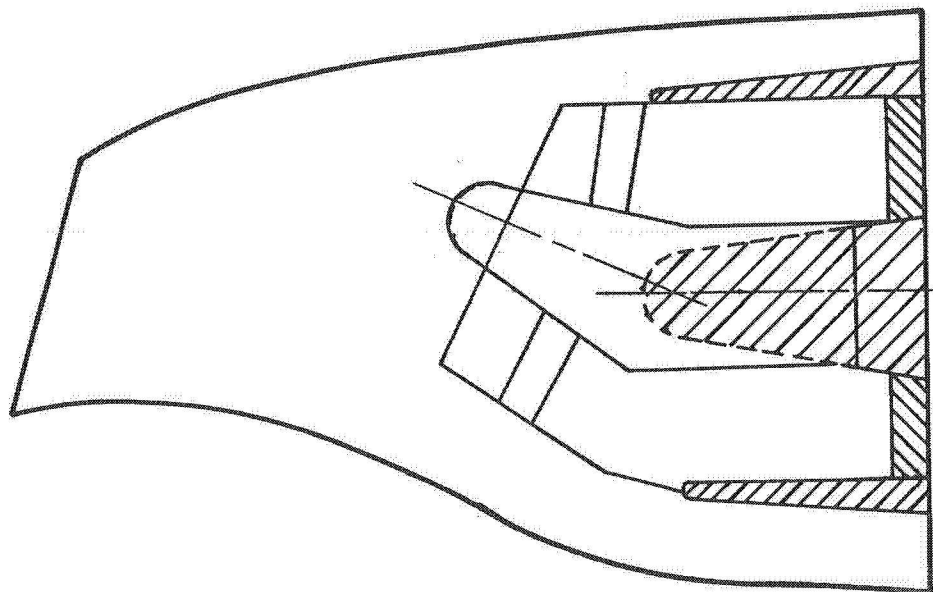
Figure 7. - Geometrics of primary exhaust nozzles.
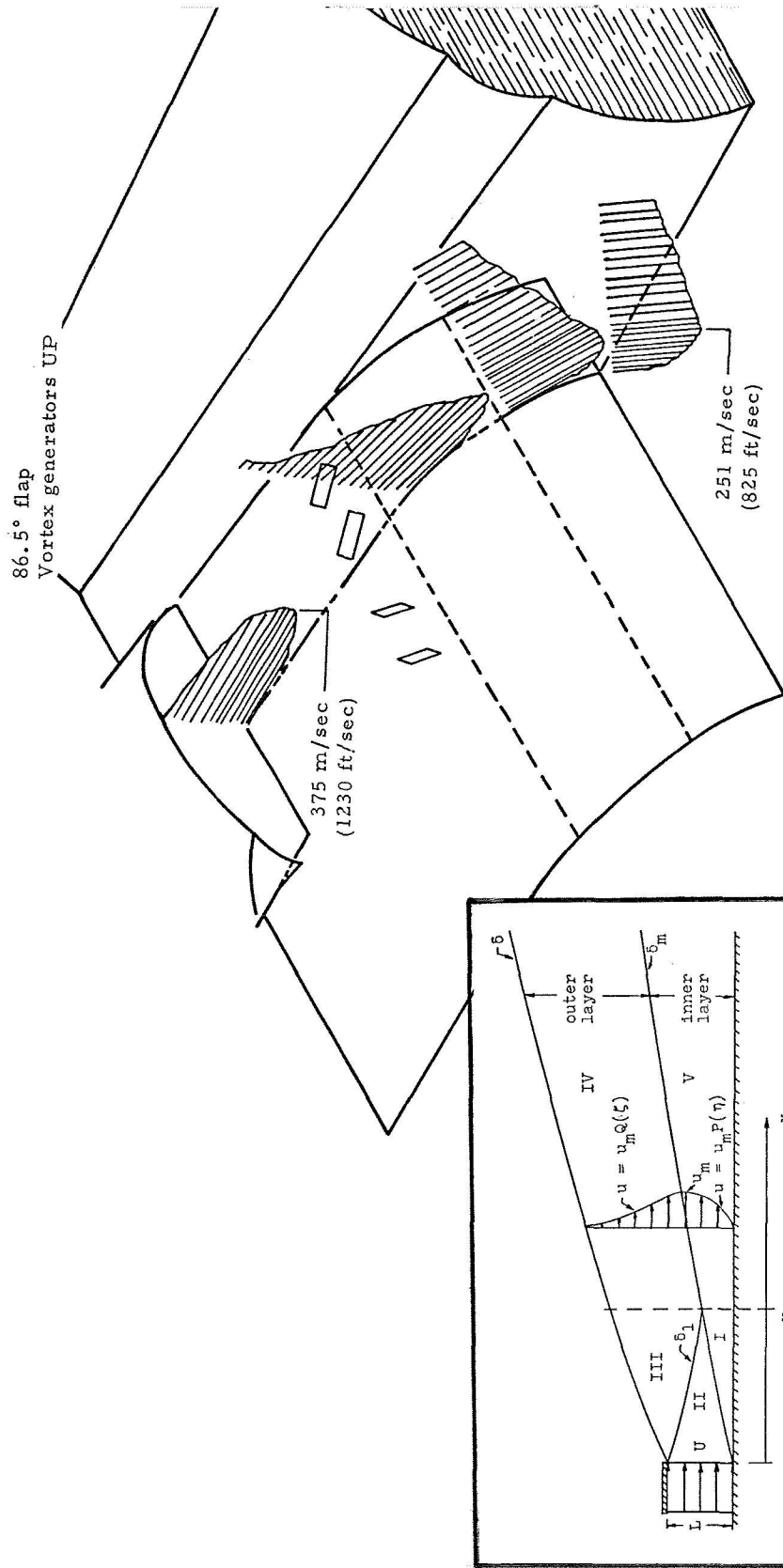
(a) Measurements on YC-14 model.

(b) Wall jet nomenclature.

I, V: Inner or wall layer -- assumed to behave
       like a flat plate boundary layer

II: Uniform core -- region where $u = U$ which
       ends at $x = x_o$

III, IV: Free jet region or outer layer -- assumed to
          behave like free jet mixing

Figure 8. - Velocity profiles at nozzle centerline.
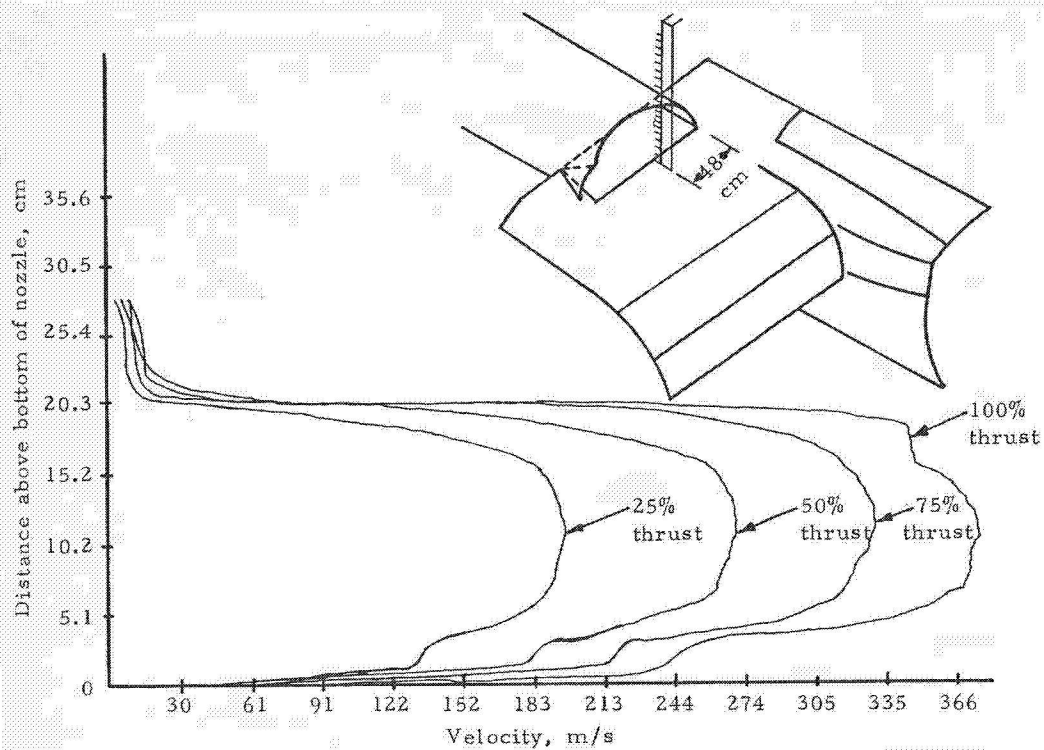
(a) Velocity profiles for four thrust levels
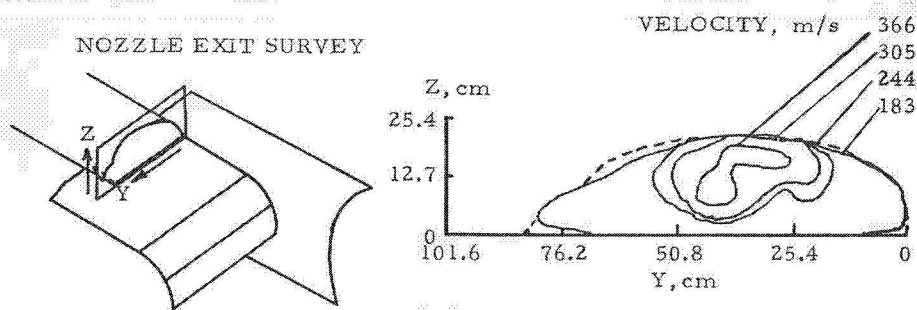
(b) Constant velocity countours (from Ref. 12)

Figure 9. - Velocity surveys at nozzle exit plane.
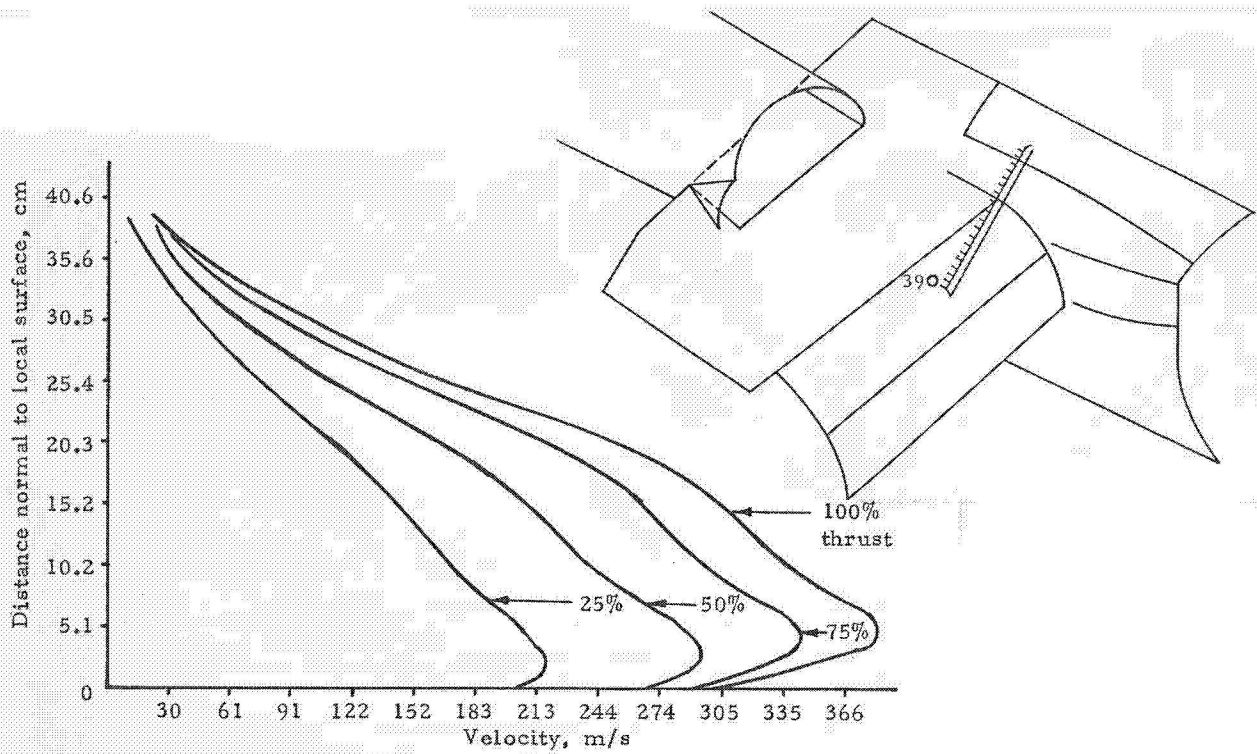
(a) Velocity profiles for four thrust levels
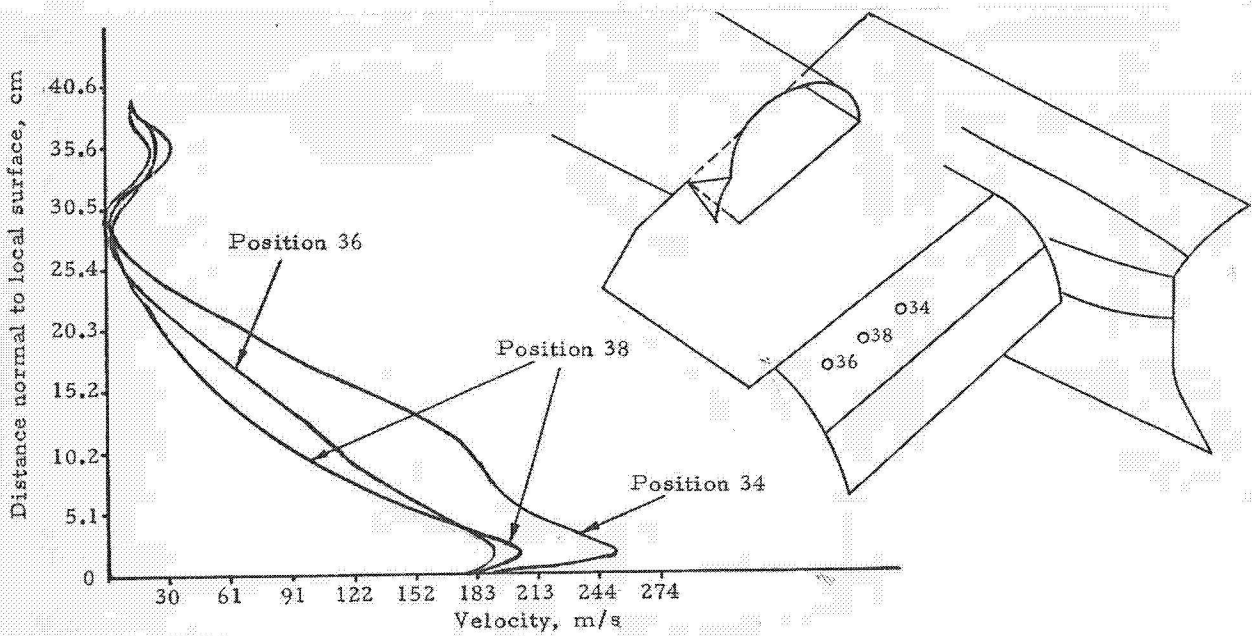
(b) Velocity profiles for three flap positions at 100% thrust

Figure 10. - Velocity profiles above main flap sensors (from Ref. 12).
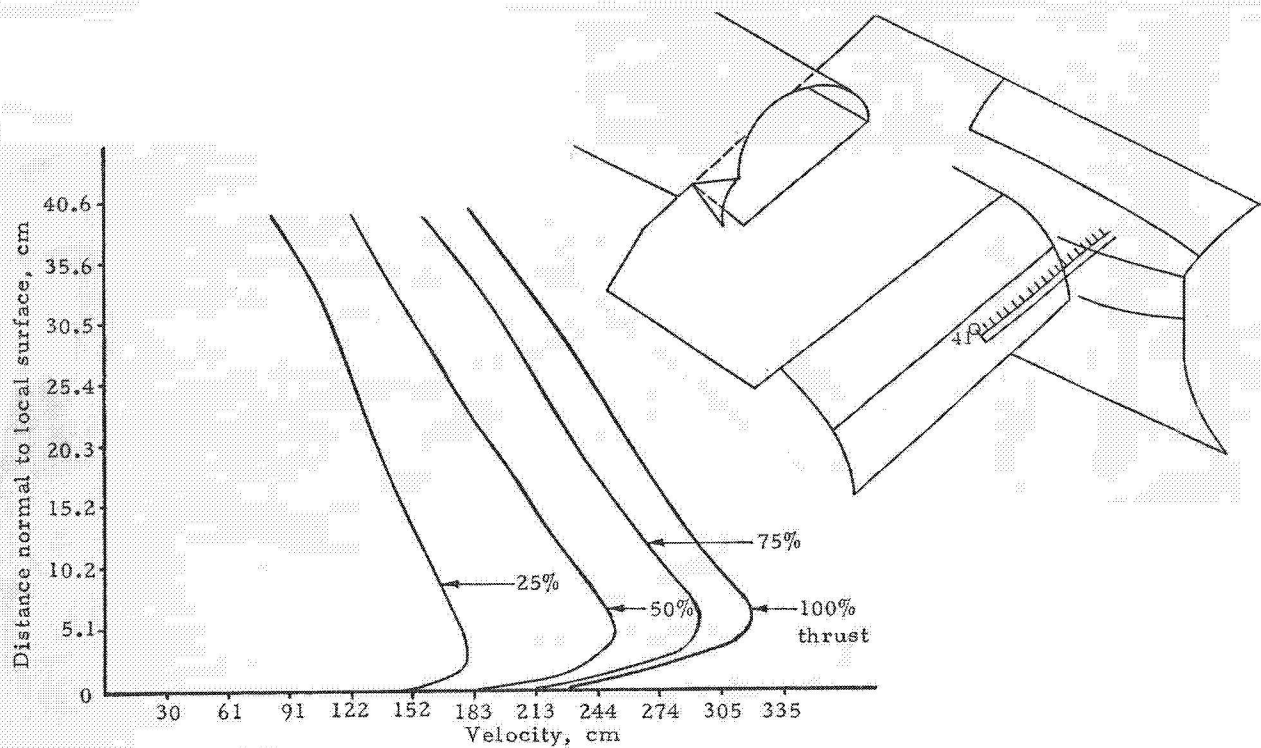
(a) Velocity profiles immediately above transducer no. 41
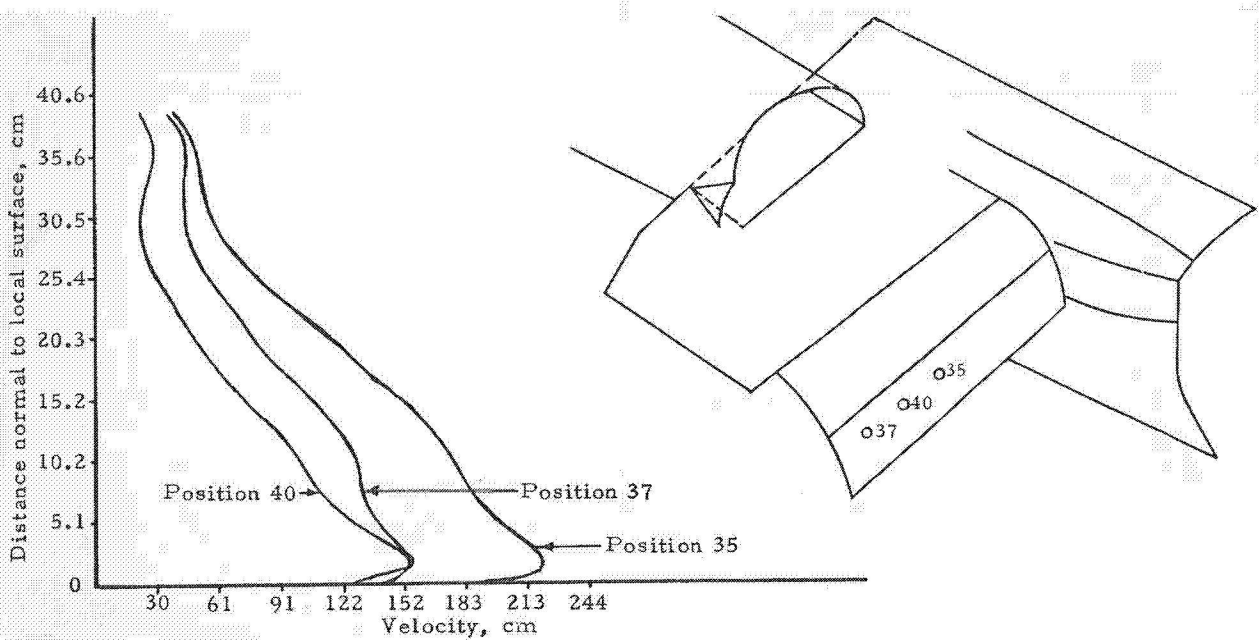
(b) Velocity profiles immediately above transducers at 100% thrust

Figure 11. - Velocity profiles above aft flap sensors (from Ref. 12).
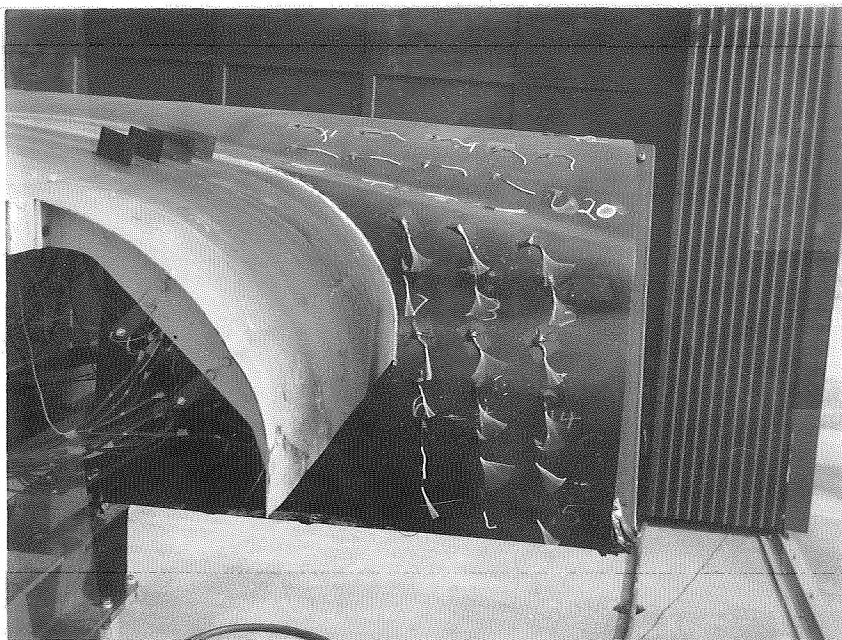
(a) 25% Thrust setting.
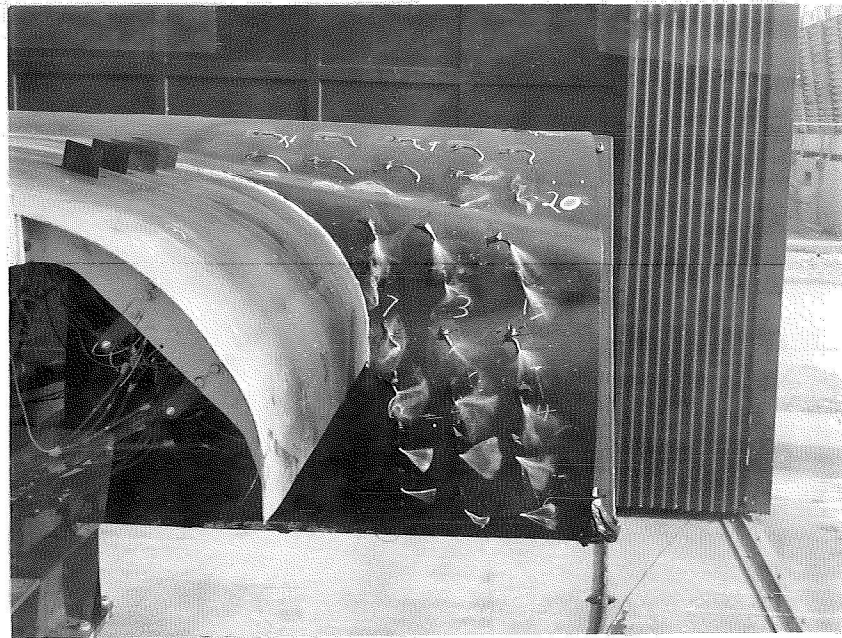
(b) 100% Thrust setting.

Figure 12. – Tuft flow patterns on fuselage.

(a) Vortex generators up (test configuration 1)

(b) Vortex generators down (test configuration 2)
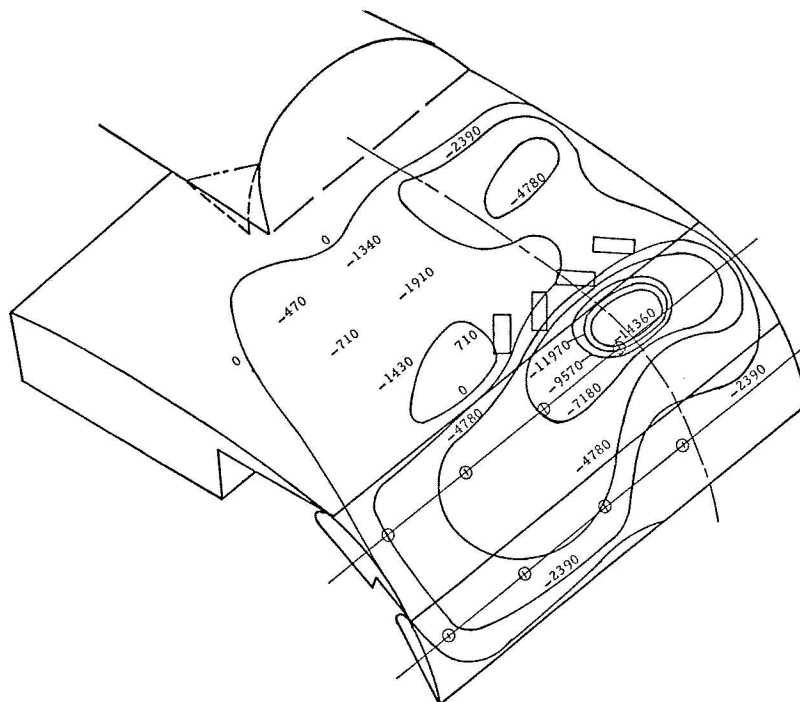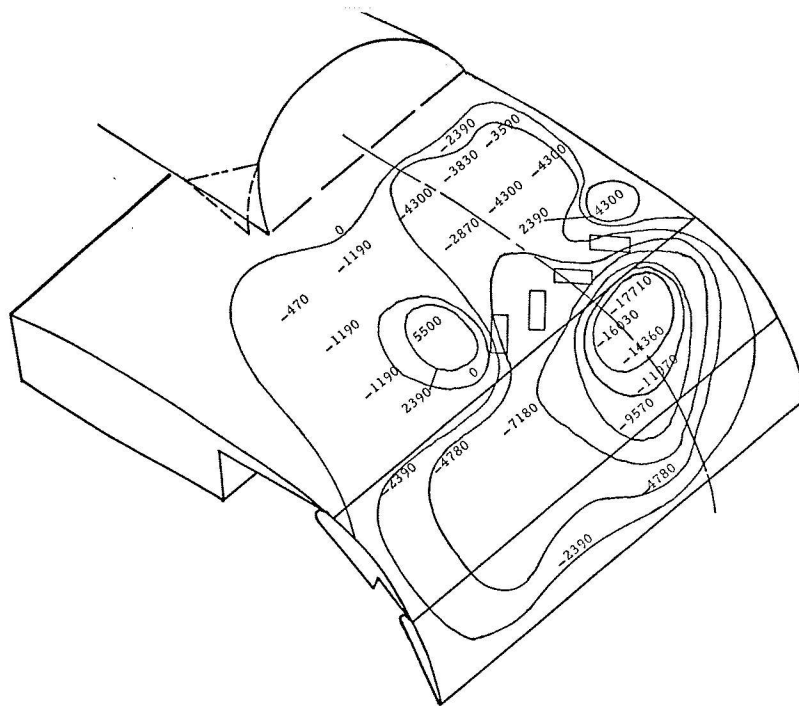
Figure 13. - Static pressure isobars on wing and flap at 100% thrust with straight-plug primary nozzle.
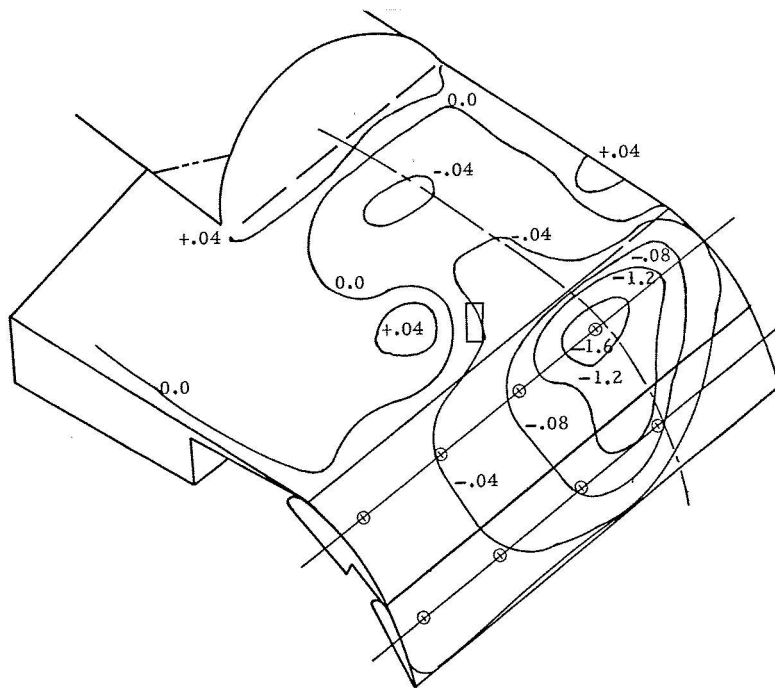
(a) Surface pressure ratio contours (values in P_s/P_{amb}).
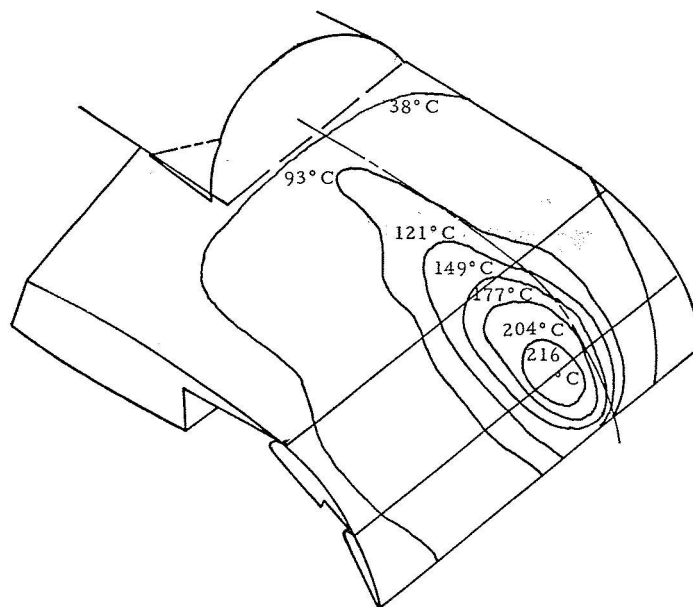
(b) Surface temperature contours, °C.

Figure 14. - Static pressure and temperature isobars on wing and flap at 100% thrust with skewed-plug primary nozzle.

Engine tones (see Table II)

① ② ③ ④ ⑤ ⑥

Idle

Increasing
rpm

100%
Thrust

Frequency (Hz)

0   4000   8000   12 000   16 000   20 000
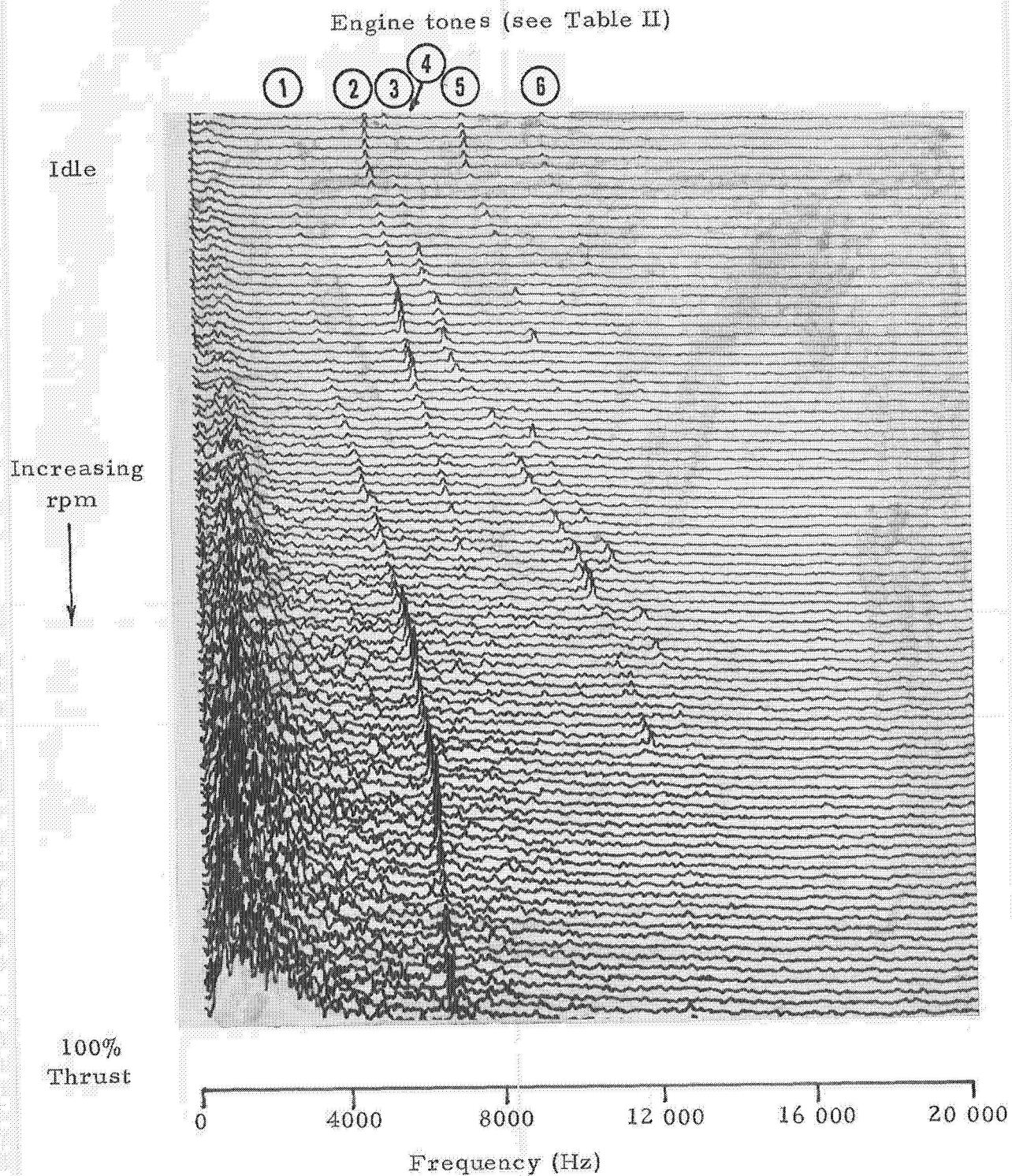
Figure 15. – Successive frequency spectra at wing position 32
during run up of engine from idle to full thrust.
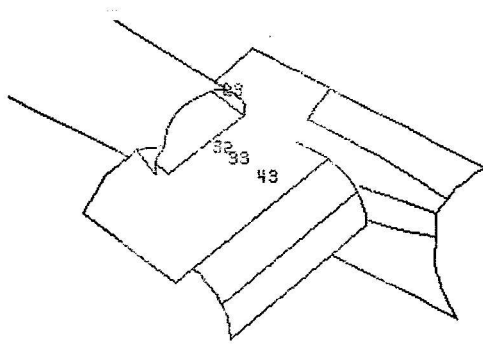
NOZZLE AND WING

* TEST CONFIGURATION 6 *

VORTEX GENERATORS DOWN
86.5-DEGREE FLAP
1.45-METER WING HEIGHT
FLAP/FUSELAGE JUNCTION OPEN
SKEWED-PLUG PRIMARY NOZZLE
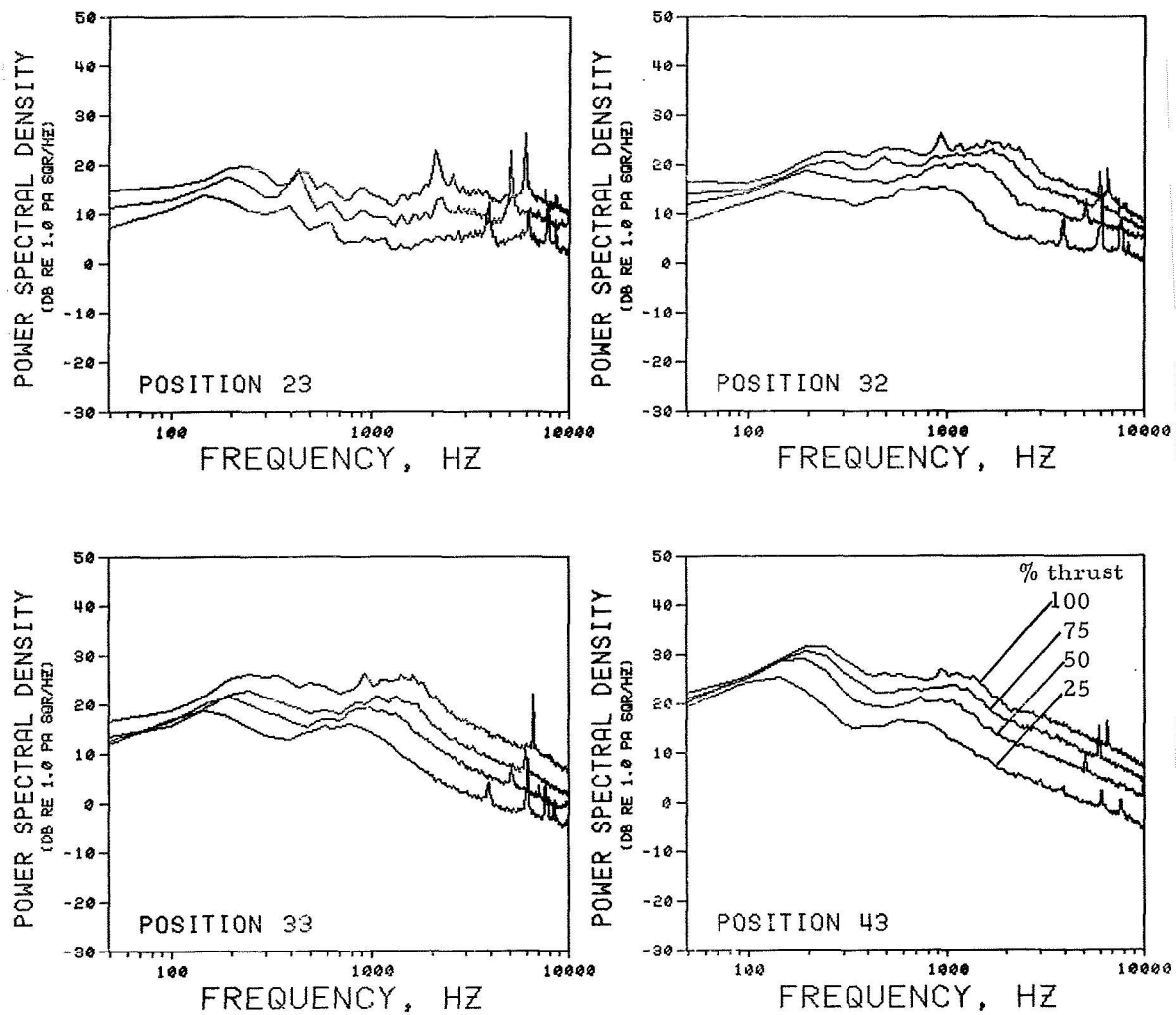
Figure 16. - Effect of thrust setting on surface pressure spectra
at nozzle and wing positions.
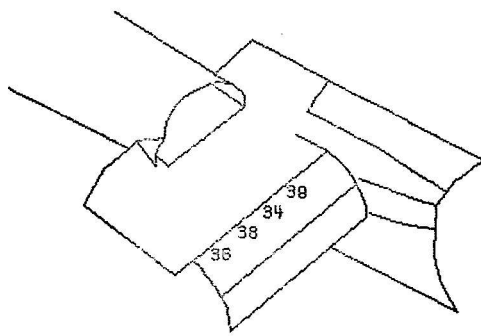
MAIN FLAP

* TEST CONFIGURATION 6 *

VORTEX GENERATORS DOWN
66.5-DEGREE FLAP
1.45-METER WING HEIGHT
FLAP/FUSELAGE JUNCTION OPEN
SKEWED-PLUG PRIMARY NOZZLE
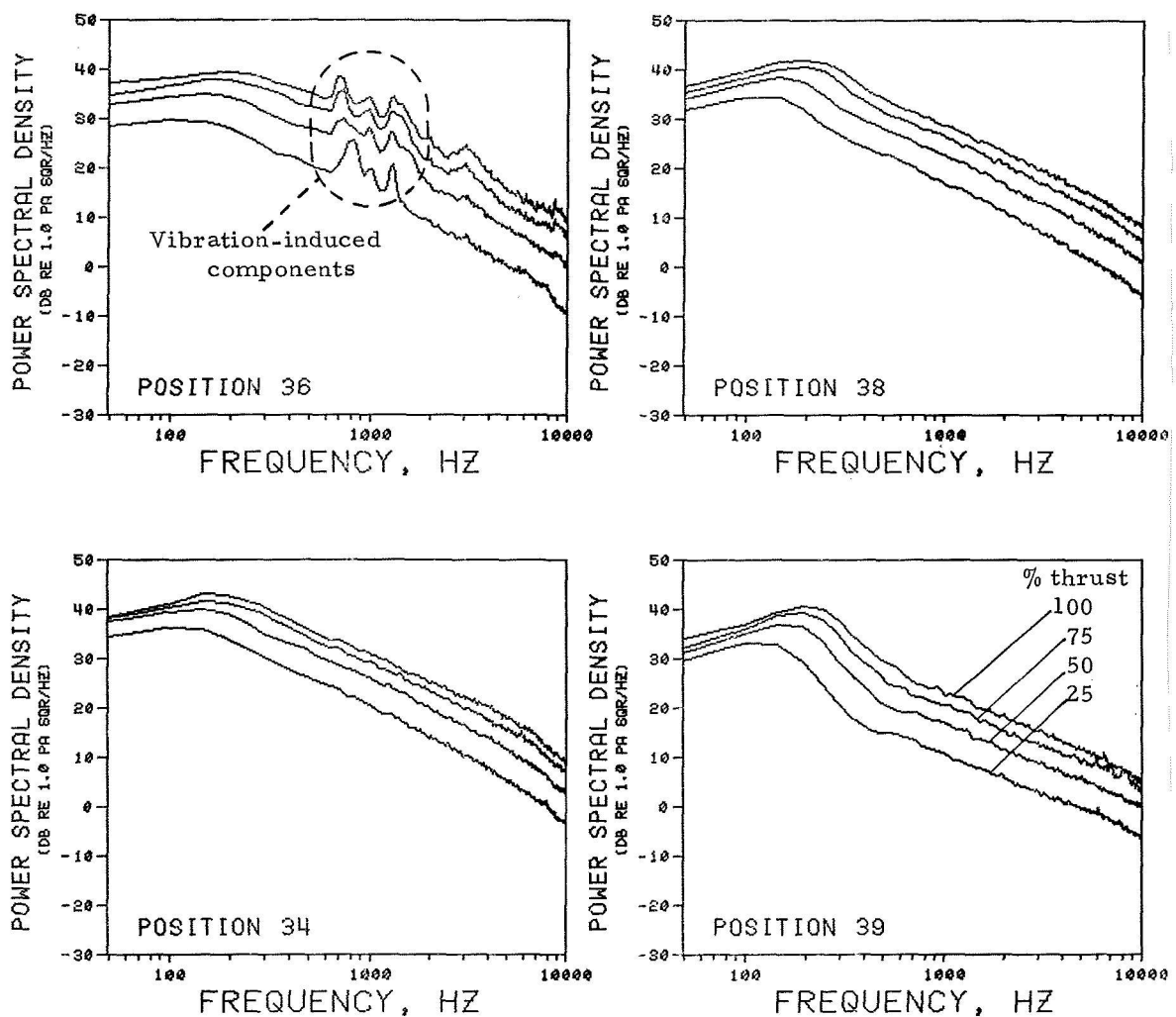
Figure 17. - Effect of thrust setting on surface pressure spectra at main flap positions.
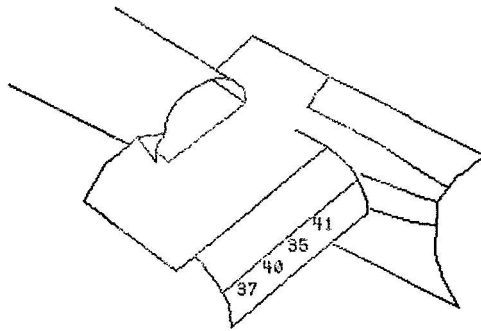
AFT FLAP

* TEST CONFIGURATION 6 *

VORTEX GENERATORS DOWN
86.5-DEGREE FLAP
1.45-METER WING HEIGHT
FLAP/FUSELAGE JUNCTION OPEN
SKEWED-PLUG PRIMARY NOZZLE
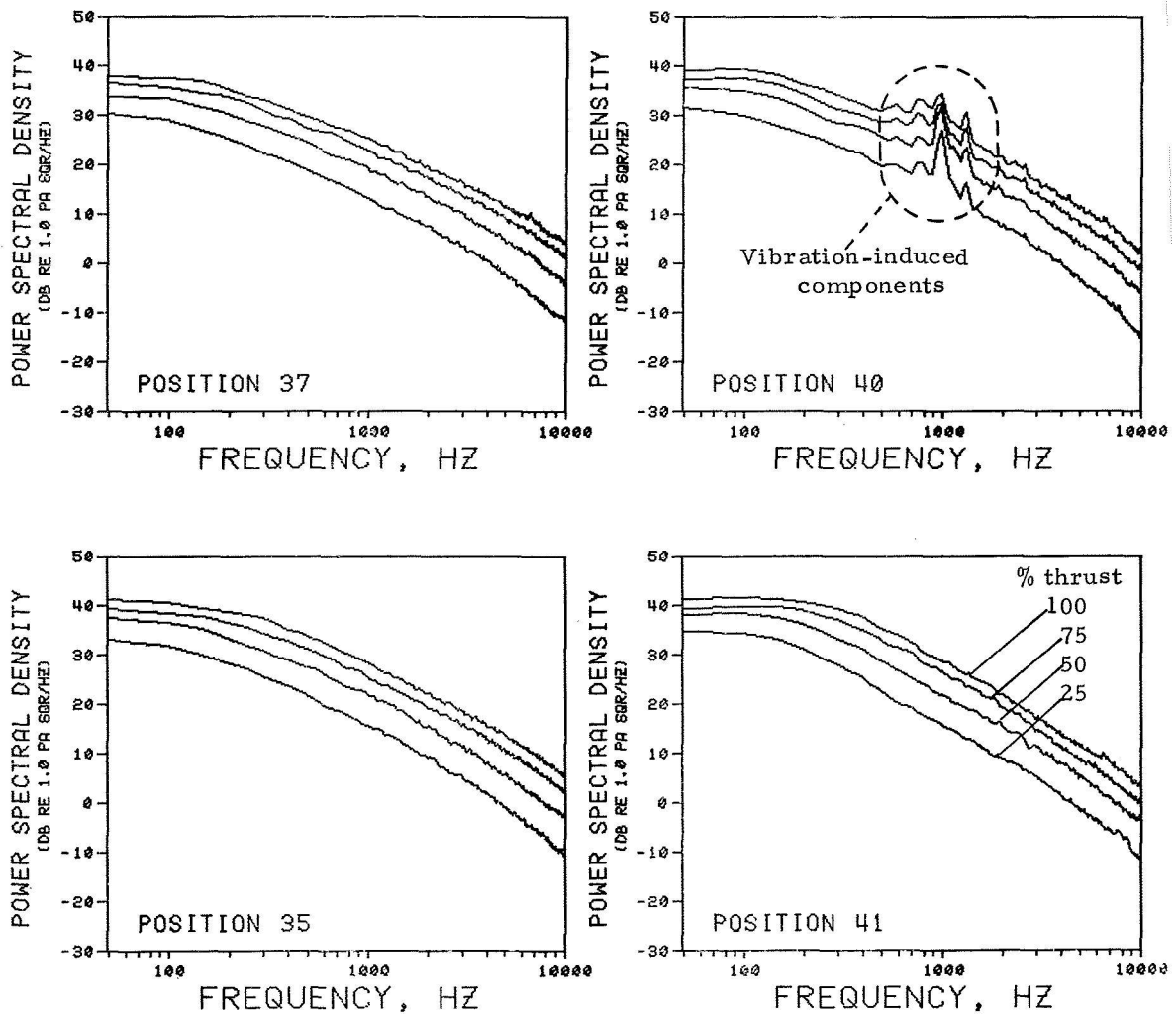
Figure 18. - Effect of thrust setting on surface pressure spectra at aft flap positions.
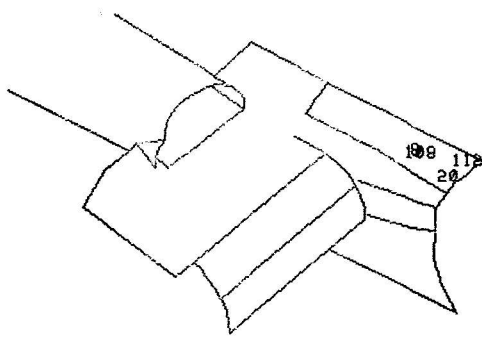
UPPER FUSELAGE

* TEST CONFIGURATION 6 *

VORTEX GENERATORS DOWN
86.5-DEGREE FLAP
1.45-METER WING HEIGHT
FLAP/FUSELAGE JUNCTION OPEN
SKEWED-PLUG PRIMARY NOZZLE
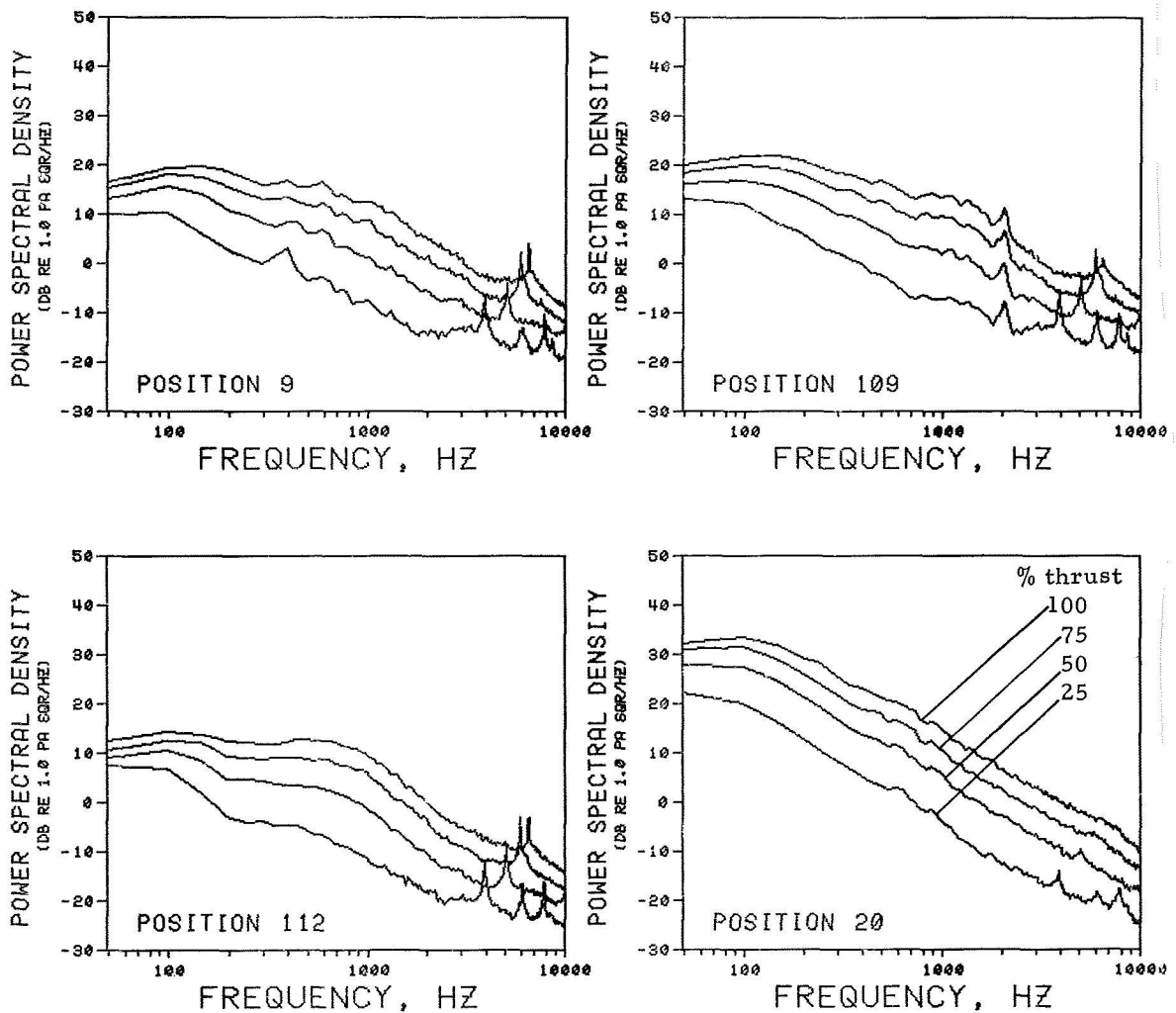
Figure 19. - Effect of thrust setting on surface pressure spectra
at upper fuselage positions.
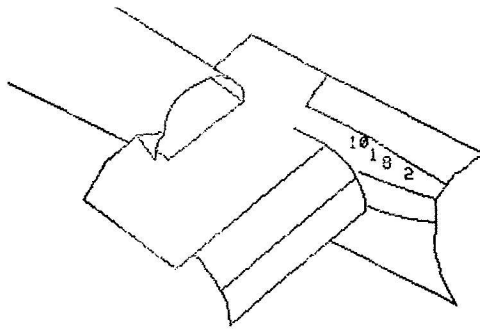
FAIRING TOP

* TEST CONFIGURATION 6 *

VORTEX GENERATORS DOWN
86.5-DEGREE FLAP
1.45-METER WING HEIGHT
FLAP/FUSELAGE JUNCTION OPEN
SKEWED-PLUG PRIMARY NOZZLE
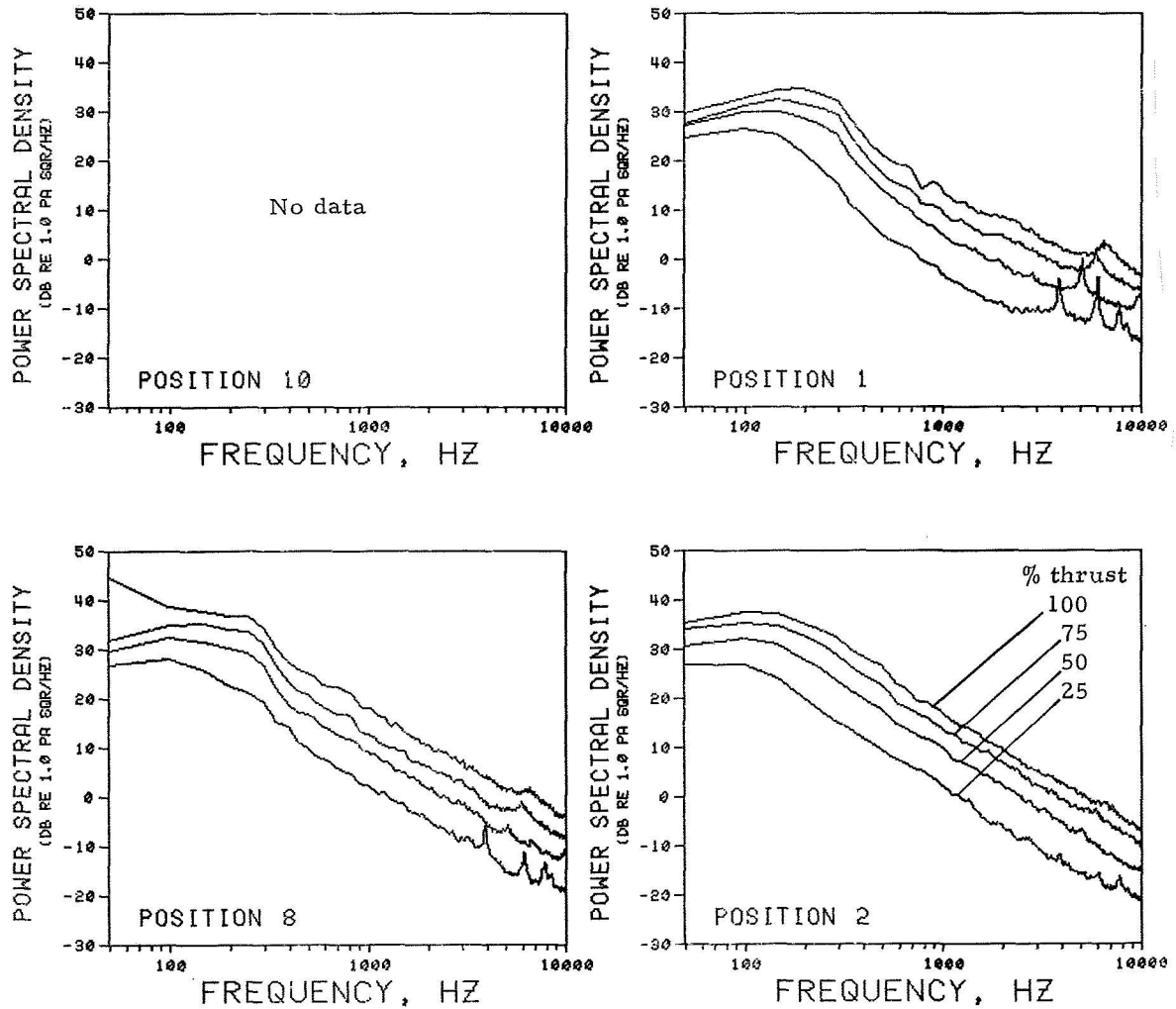
Figure 20. - Effect of thrust setting on surface pressure spectra
at fairing top positions.
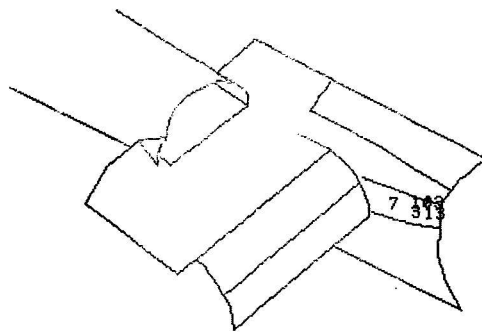
FAIRING SIDE

* TEST CONFIGURATION 6 *

VORTEX GENERATORS DOWN
86.5-DEGREE FLAP
1.45-METER WING HEIGHT
FLAP/FUSELAGE JUNCTION OPEN
SKEWED-PLUG PRIMARY NOZZLE
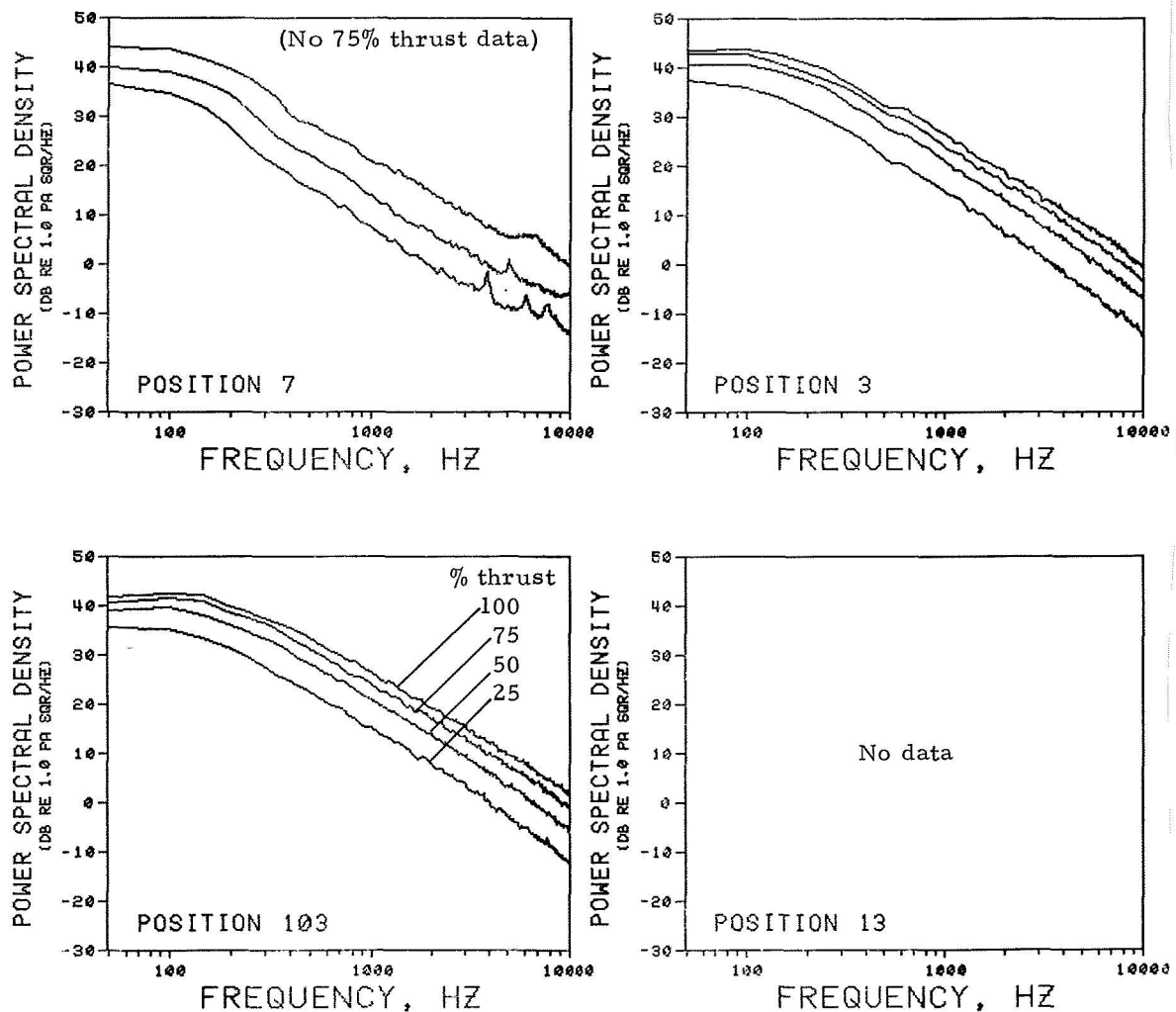
Figure 21. - Effect of thrust setting on surface pressure spectra
at fairing side positions.
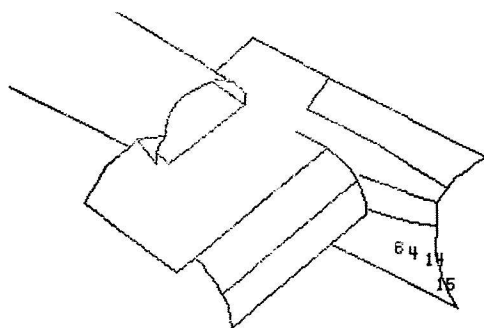
LOWER FUSELAGE

* TEST CONFIGURATION 6 *

VORTEX GENERATORS DOWN
96.5-DEGREE FLAP
1.45-METER WING HEIGHT
FLAP/FUSELAGE JUNCTION OPEN
SKEWED-PLUG PRIMARY NOZZLE
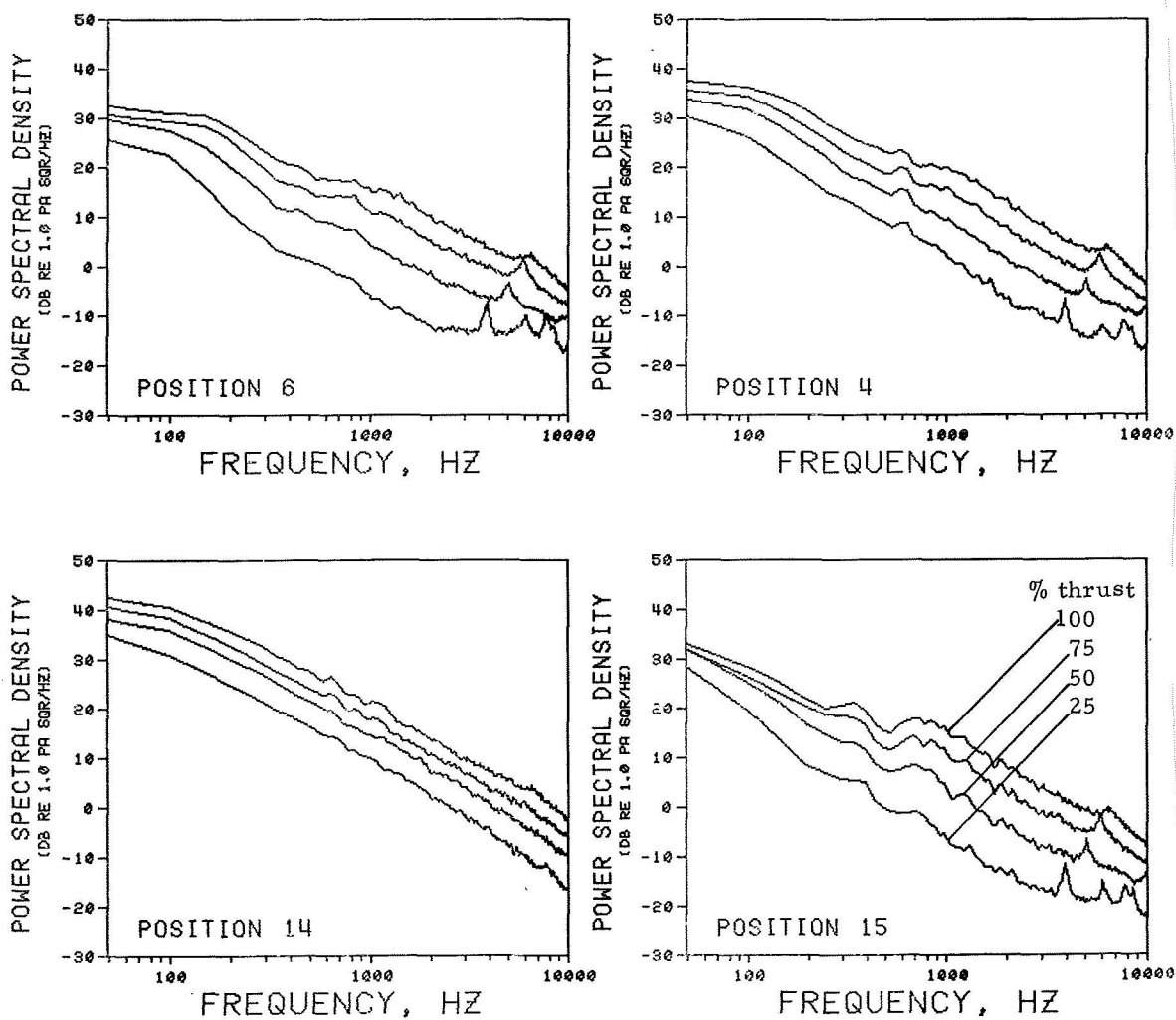
Figure 22. - Effect of thrust setting on surface pressure spectra
at lower fuselage positions.

88

NOZZLE AND WING
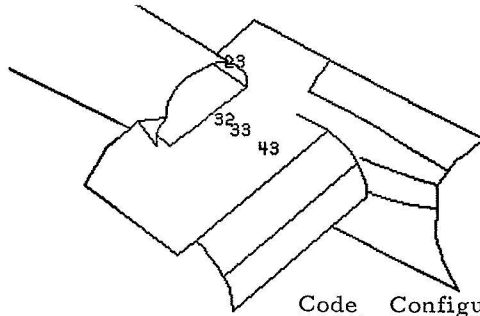
Code	Configuration description
①	Vortex generators up
②	Vortex generators down
③	Modified vortex generators up
④	Straight-plug primary nozzle
⑤	VGs down (skewed-plug), VGs up (straight-plug)
⑥	VGs down (straight-plug
⑦	Test configuration 6
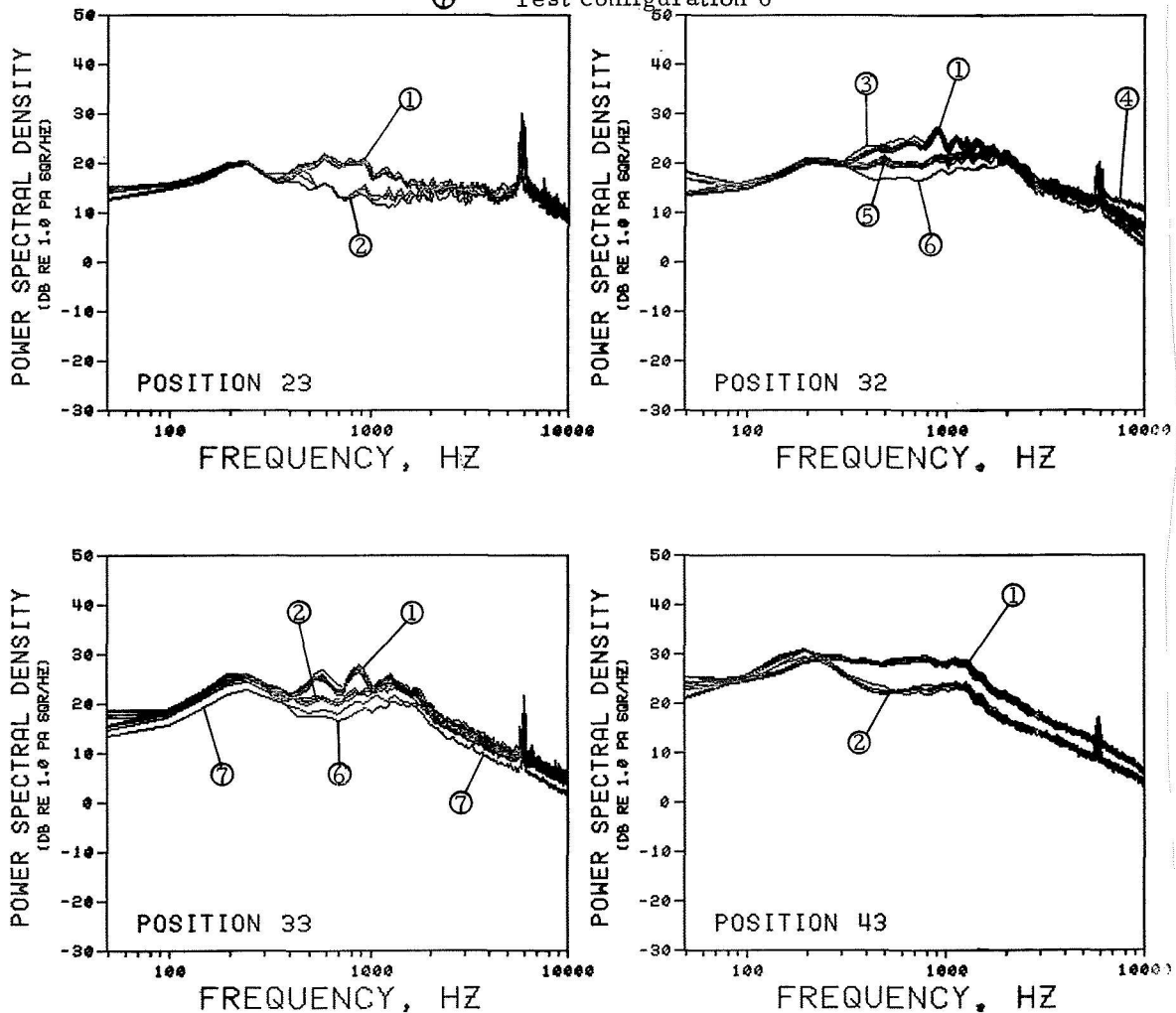
Figure 23. - Comparison of surface pressure PSDs at nozzle and
wing positions for runs at 75% thrust setting.
(See Table III for listing of data presented)

MAIN FLAP

Code	Configuration description
⑤	Skewed-plug, 86.5° flap
⑥	Stright-plug, 86.5° flap & skewed-plug, 70° flap
⑦	Modified VGs up (Config. 16)
⑧	VGs up, 70° flap
⑨	VGs up
⑩	VGs up, straight-plug nozzle
⑪	VGs down, 70° flap
⑫	VGs down
⑬	VGs down, straight-plug nozzle

Code	Configuration description
①	1.45m height, 86.5° flap
②	2.29m height, 86.5° flap & 1.45m heights, 70° & 16° flaps
③	Configs. 14-16 (PCB sensor replaced by Kulite sensor)
④	Vibration-induced components

Figure 24. - Comparison of surface pressure PSDs at main flap
positions for runs at 75% thrust setting.
(See Table III for listing of data presented)

AFT FLAP

Code	Configuration description
⑤	Vibration-induced components
⑥	70° flap (VGs down(lowest of 3 curves))
⑦	VGs up, skewed-plug nozzle, 86.5° flap
	& VGs up & down, straight plug
⑧	VGs down, skewed plug, 86.5° flap
⑨	Same as ⑧ &configuration 16
⑩	VGs up
⑪	VGs down
⑫	Modified VGs up (config. 16)
⑬	VGs up, straight-plug nozzle

Code	Configuration description
①	Test configurations 3 - 6
②	VGs gown, 86.5° flap
③	VGs up, 86.5° flap & VGs down, straight-plug nozzle, 70° flap
④	Configs. 1 & 2 (Kulite sensor installed)

Figure 25. - Comparison of surface pressure PSDs at aft flap positions for runs at 75% thrust setting. (See Table III for listing of data presented)

91
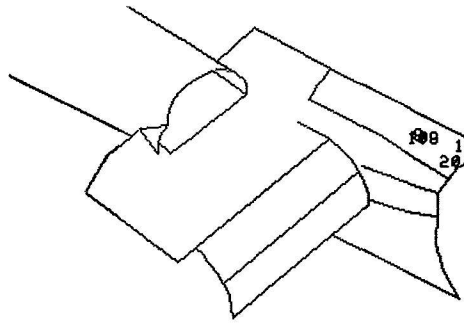
UPPER FUSELAGE

Code	Configuration description
①	Vortex generators up
②	VGs down
③	VGs up, 16° flap
④	Modified VGs up (Config. 16)
⑤	VGs up & down, 16° flap
⑥	VGs down, 16° flap
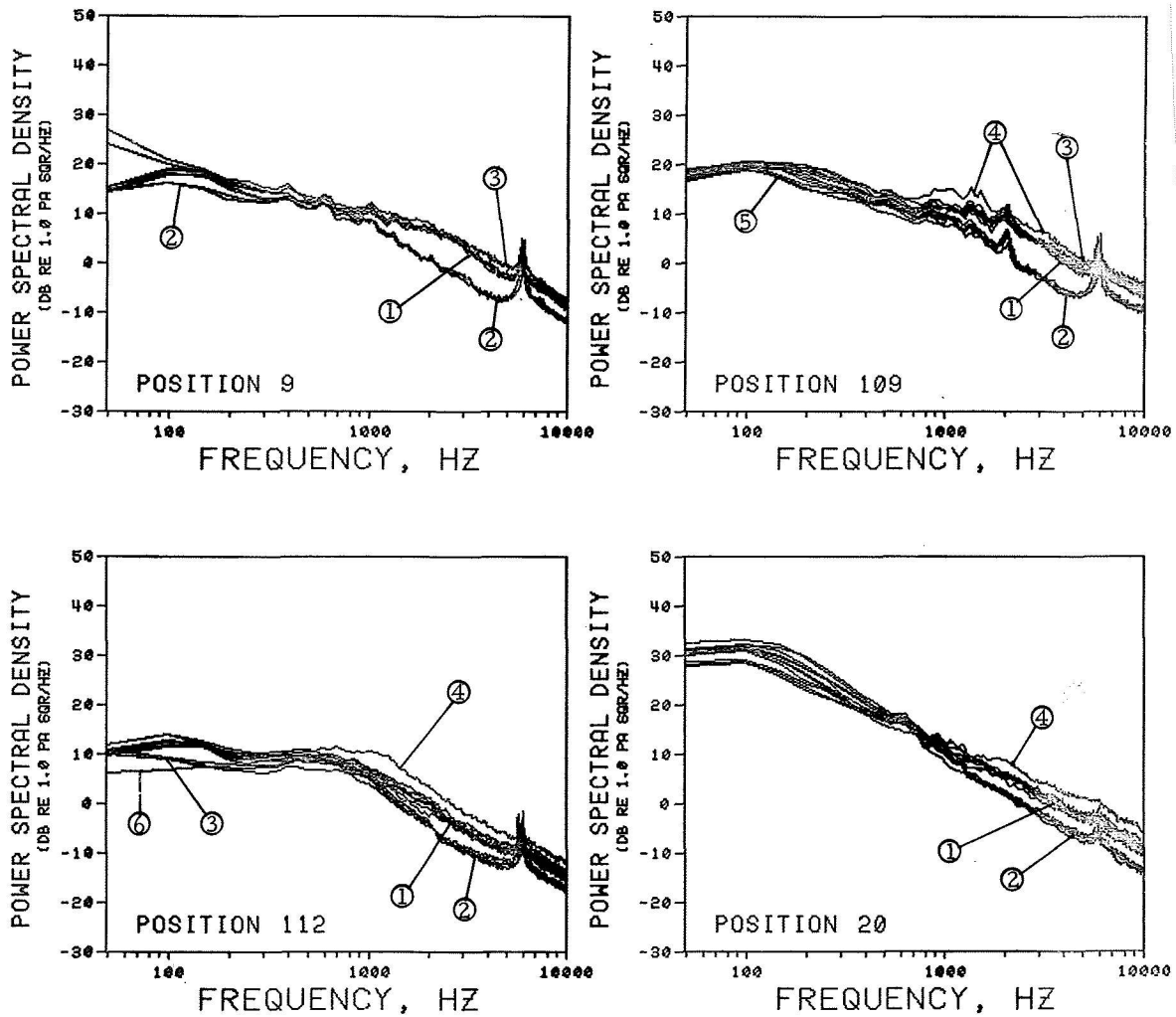
Figure 26. – Comparison of surface pressure PSDs at upper
fuselage positions for runs at 75% thrust setting.
(See Table III for listing of data presented)

FAIRING TOP

Code	Configuration description
⑥	VGs down, 16° flap
⑦	Configuration 7
⑧	Top line; configuration 7
	2nd line; config. 16(mod. VGs up)
⑨	VGs down, 70° flap
⑩	VGs down, 16° flap

Code	Configuration description
①	Configuration 12
②	Configuration 4
③	Modified VGs up (Config. 16)
④	VGs up
⑤	VGs down
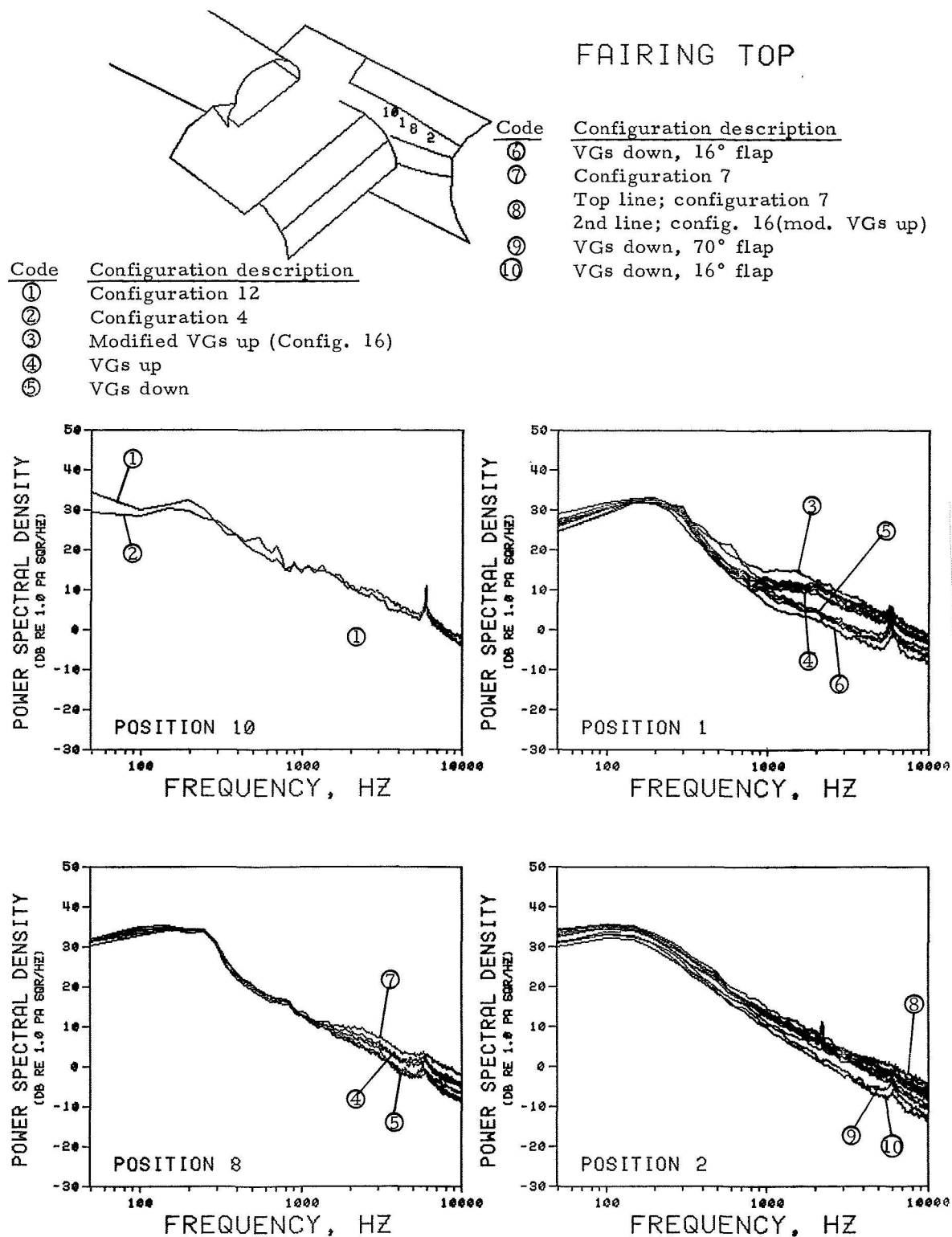
Figure 27. - Comparison of surface pressure PSDs at fairing top
positions for runs at 75% thrust setting.
(See Table III for listing of data presented)

93
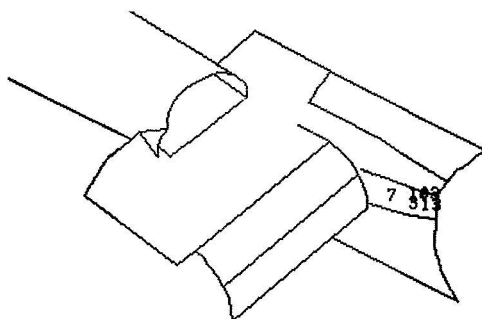
FAIRING SIDE

Code	Configuration description
⑥	VGs down, 1.45m height, config. 3
⑦	VGs cown, 2.29m height, config. 9
⑧	Vibration-induced components

Code	Configuration description
①	Modified VGs up (config. 16)
②	VGs up, 16° flap
③	VGs down, 16° flap
④	VGs up (config. 4)
⑤	Configurations 5 & 6
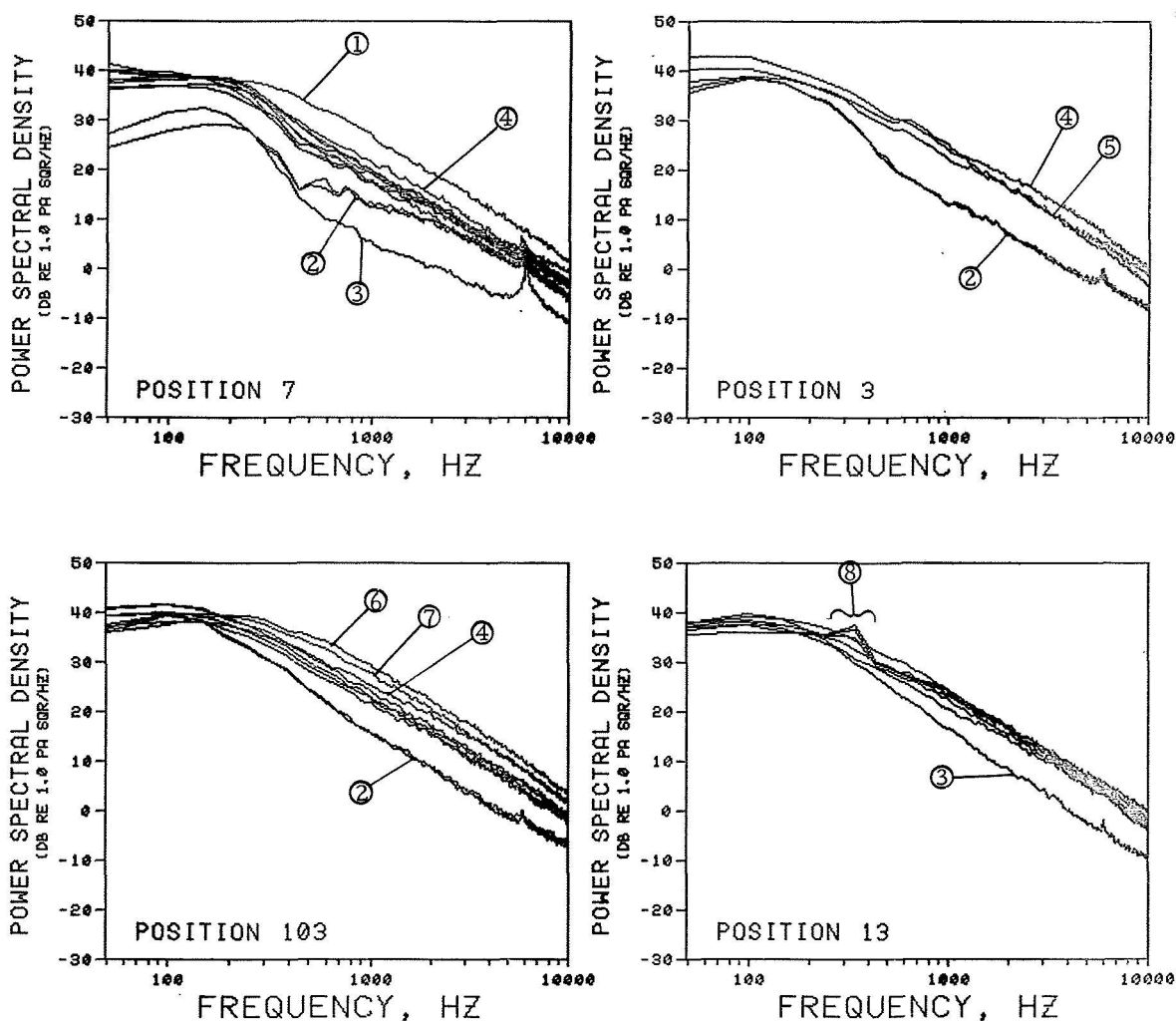
Figure 28. - Comparison of surface pressure PSDs at fairing side positions for runs at 75% thrust setting. (See Table III for listing of data presented)
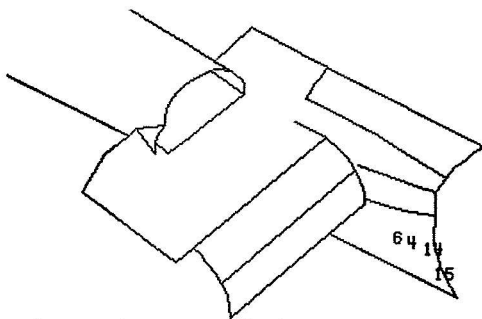
LOWER FUSELAGE

Code	Configuration Description
①	Modified VGs up(config. 16)
②	VGs up & config. 9
③	VGs down, 86.5° & 70° flaps
④	VGs down, 16° flap
⑤	VGs up, 16° flap

Code	Configuration description
⑥	Configurations 4 & 9
⑦	Vibration-induced components
⑧	VGs down, 86.5° flap
⑨	VGs up, 86.5° flap
⑩	Configuration 9
⑪	VGs up
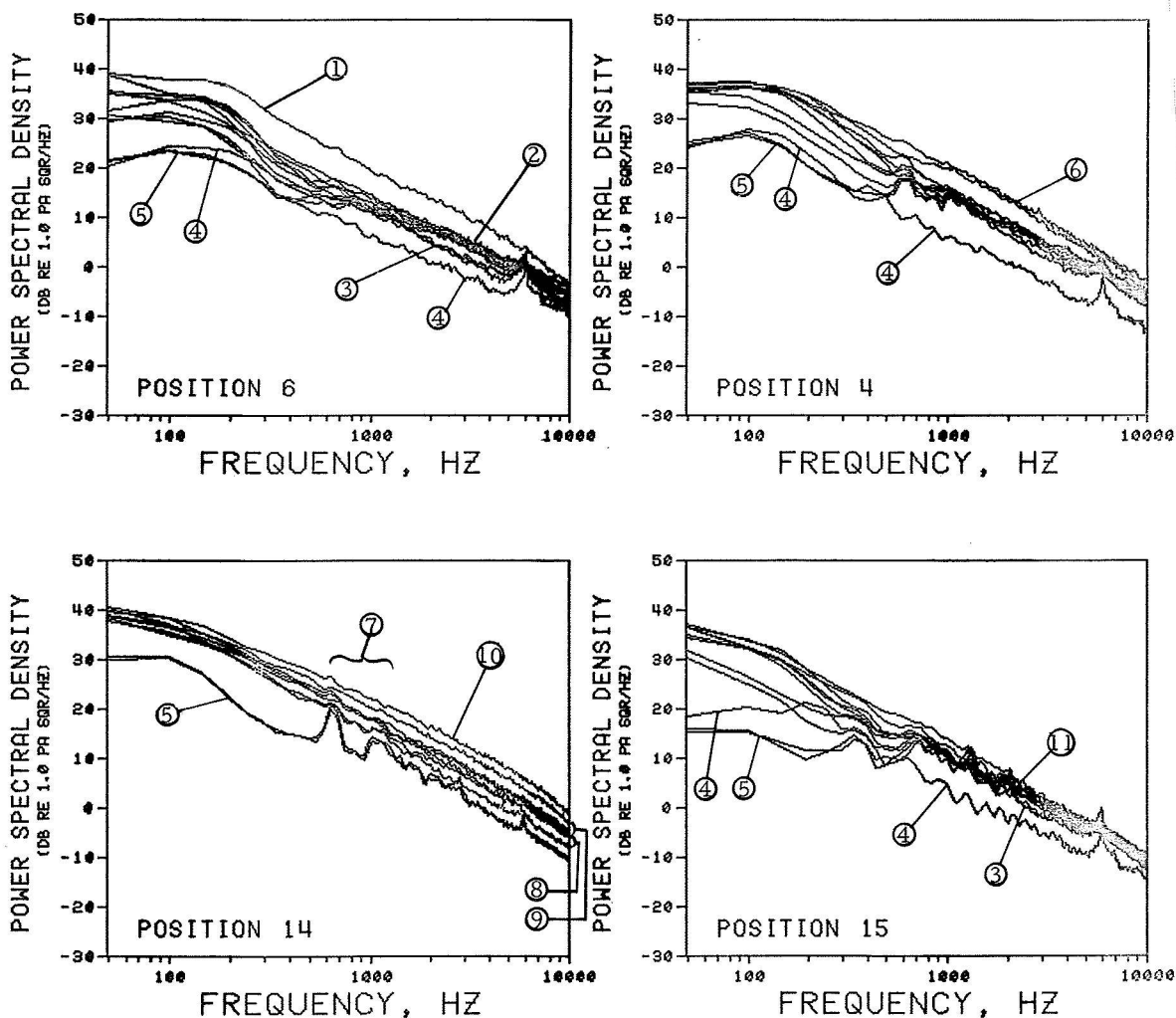
Figure 29. - Comparison of surface pressure PSDs at lower
fuselage positions for runs at 75% thrust setting.
(See Table III for listing of data presented)

95

(a) Vortex generators up

(b) Vortex generators down
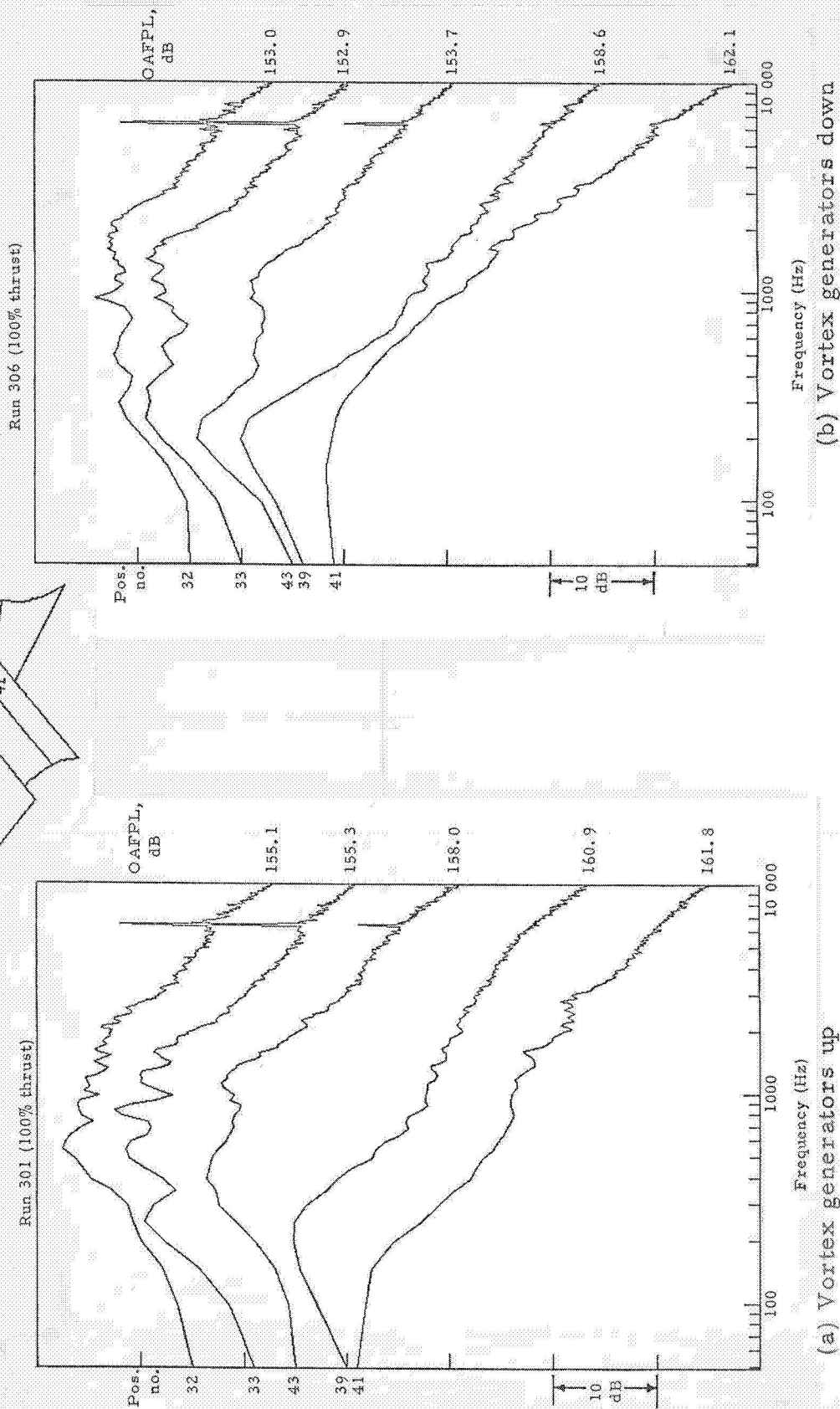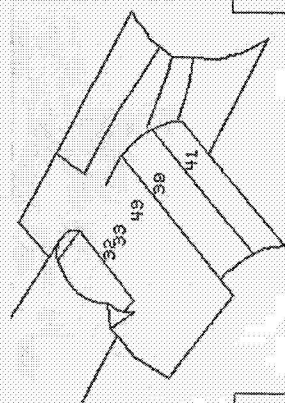
Figure 30. – Comparison of surface pressure spectral shapes at wing and flap positions along nozzle centerline.

96

(a) Figure 6 from reference 23
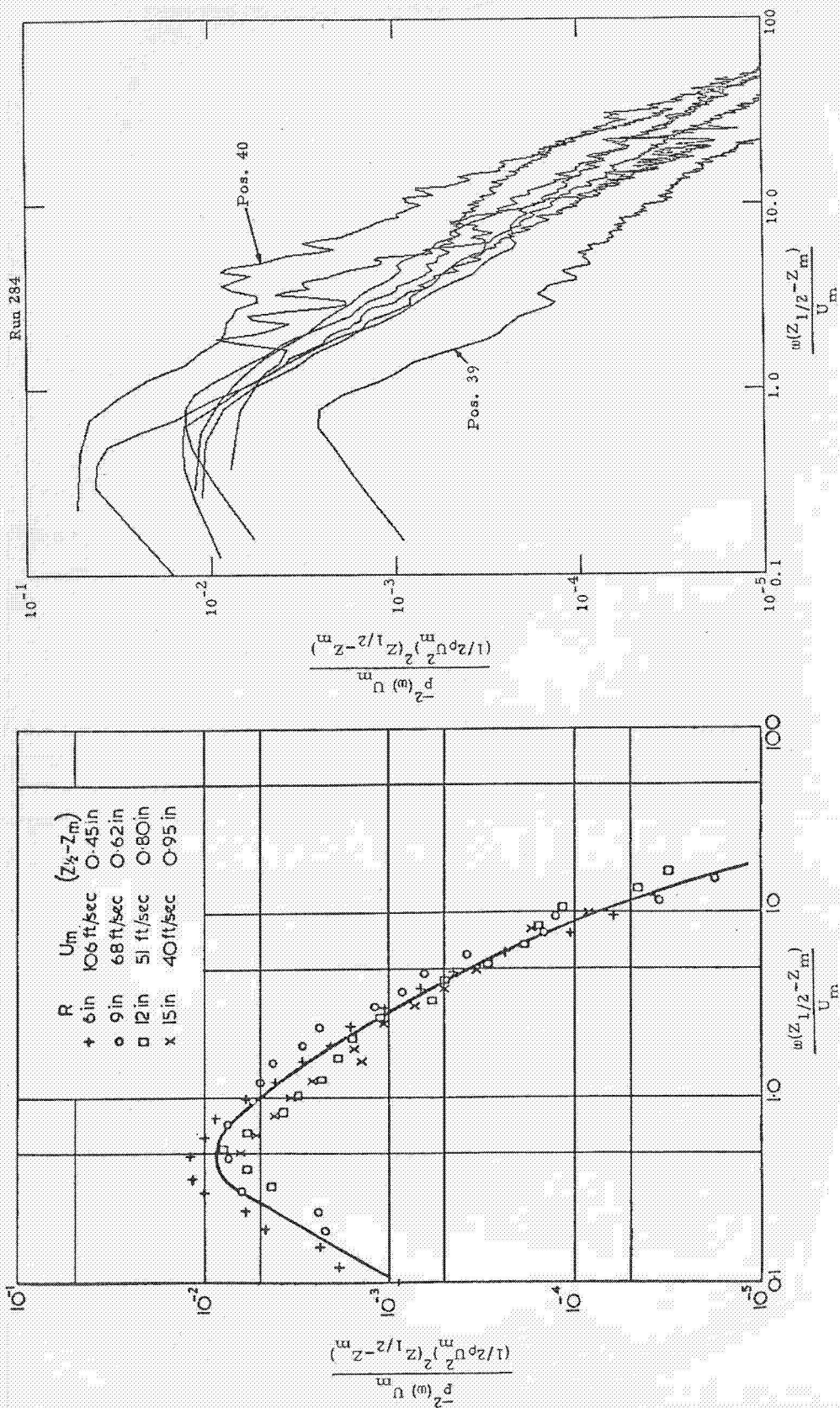
(b) Flap surface pressure spectra normalized by technique of reference 23. (See Table IV for data)

Figure 31. - Flap pressure spectra along nozzle centerline normalized by method of reference 23.

97

(a) Position 39 (b) Position 41

Figure 32. - Effect of thrust setting on normalization of flap pressure spectra along nozzle centerline normalized by method of reference 23. (See Table IV for data)
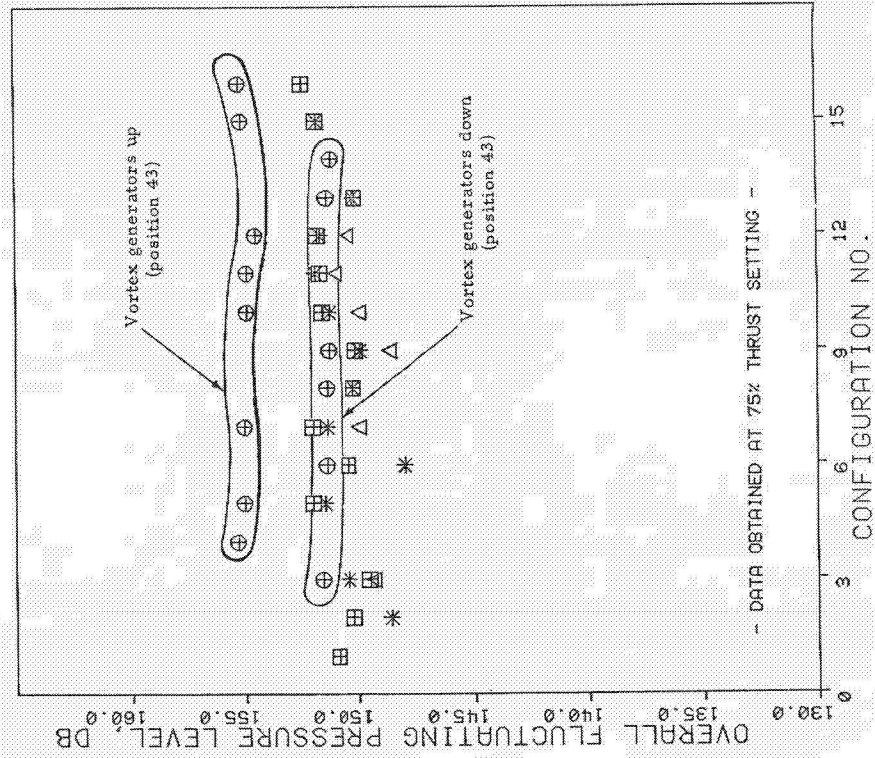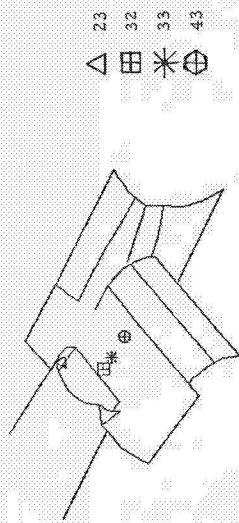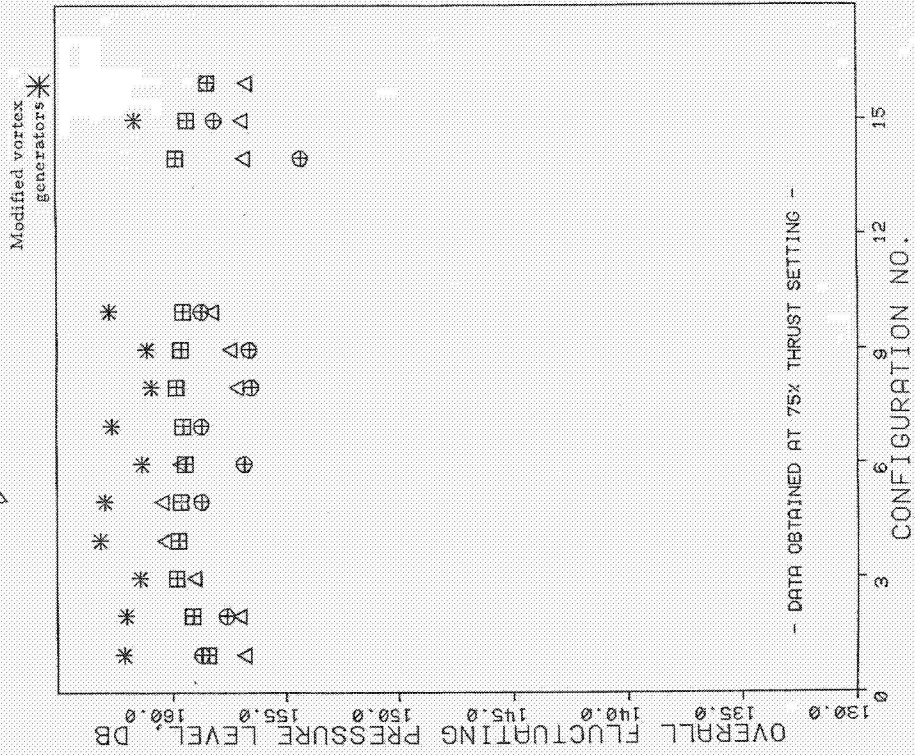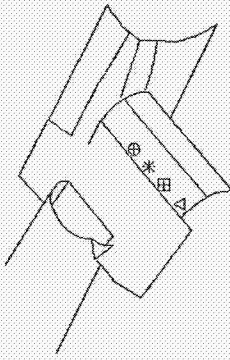
Figure 33. – Variation of overall fluctuating pressure levels (OAFPL) with test configuration.

(a) Nozzle and wing

(b) Main flap

99

Figure 33. – Continued

(c) Aft flap

(d) Upper fuselage

OVERALL FLUCTUATING PRESSURE LEVEL, DB

160.0 155.0 150.0 145.0 140.0 135.0 130.0

7 3 103 13

16° flap installed

3   6   9   12   15
CONFIGURATION NO.

- DATA OBTAINED AT 75% THRUST SETTING -

(f) Fairing side

OVERALL FLUCTUATING PRESSURE LEVEL, DB

160.0 155.0 150.0 145.0 140.0 135.0 130.0

10 1 8 2

3   6   9   12   15
CONFIGURATION NO.

- DATA OBTAINED AT 75% THRUST SETTING -
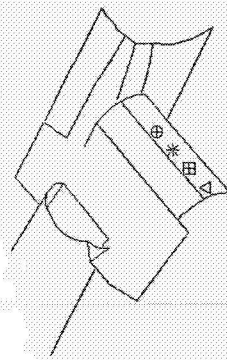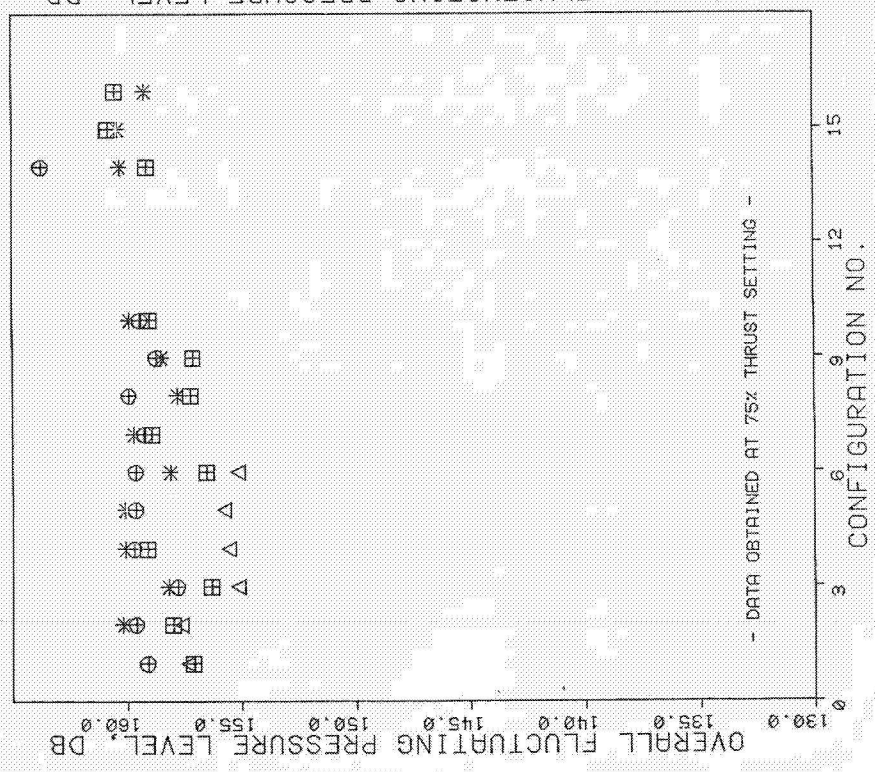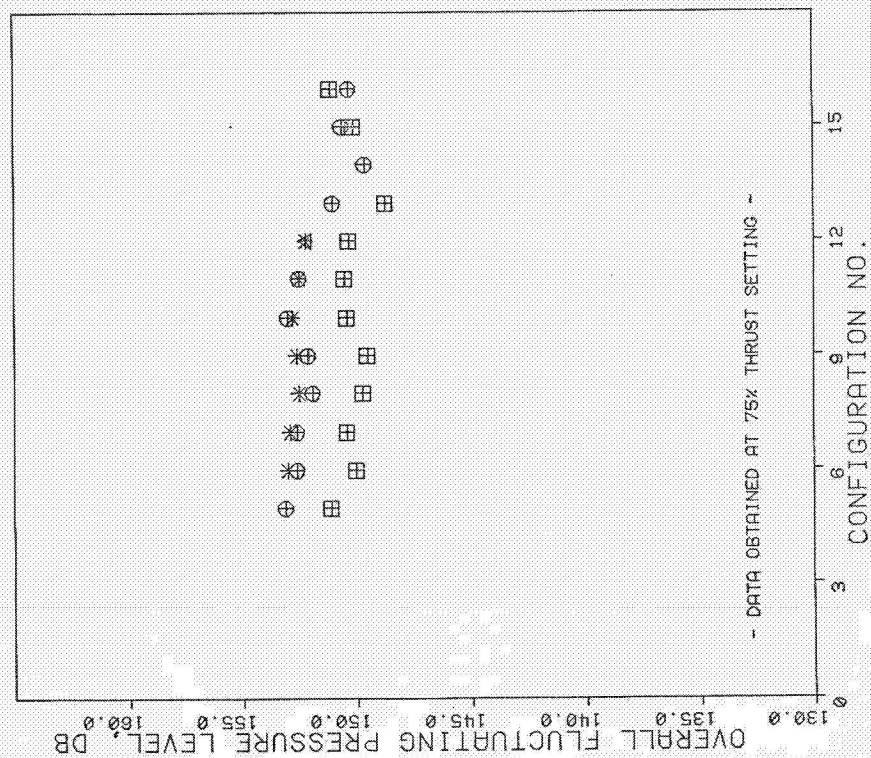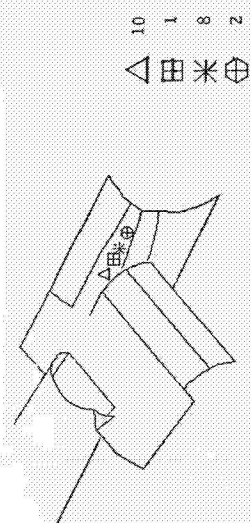
(e) Fairing top
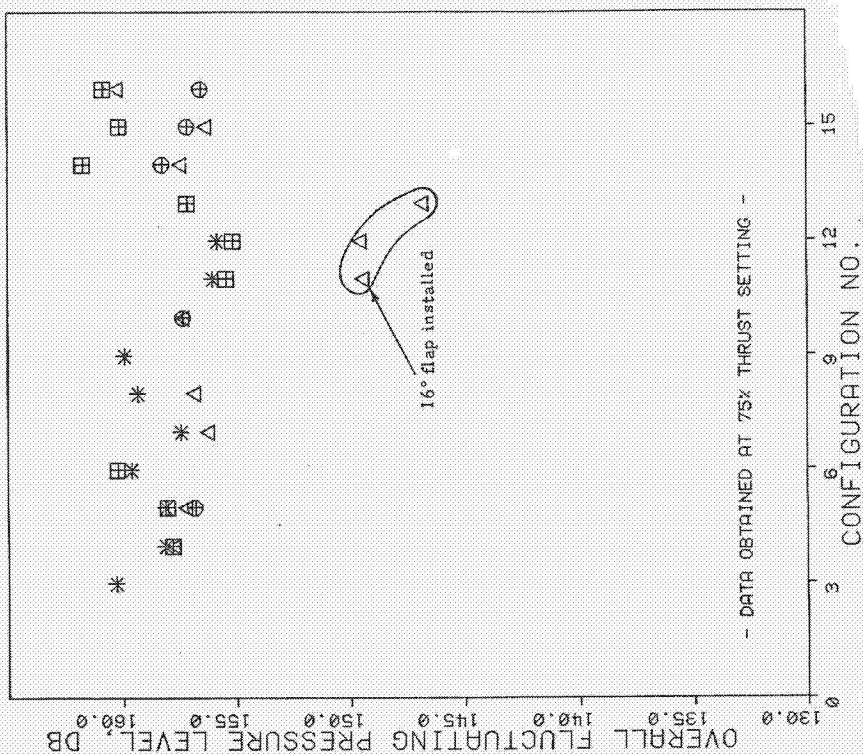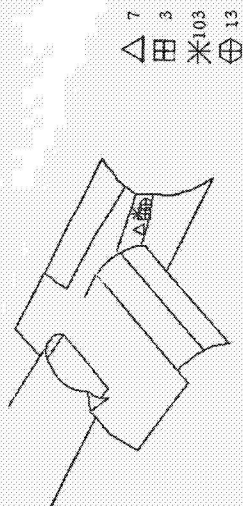
Figure 33. - Continued.
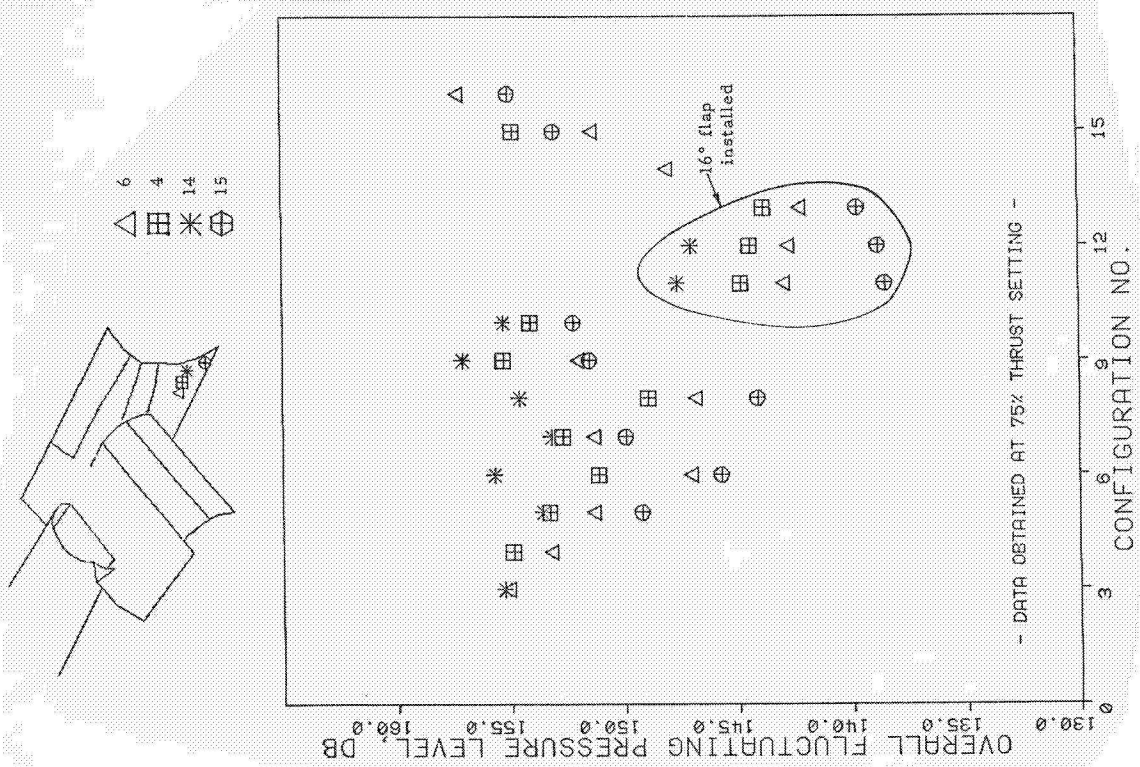
(g) Lower fuselage

Figure 33. – Concluded.

* TEST CONFIGURATION 5 *

86.5-DEGREE FLAP
1.45-METER WING HEIGHT
FLAP/FUSELAGE JUNCTION OPEN
SKEWED-PLUG PRIMARY NOZZLE

RUN 284
100% THRUST

OVERALL FLUCTUATING PRESSURE LEVELS

OVERALL FLUCTUATING PRESSURE LEVELS

165.0 162.0

(dB Re 2 x 10^{-5} Pa)

39
41
35
34
40
38
37
36
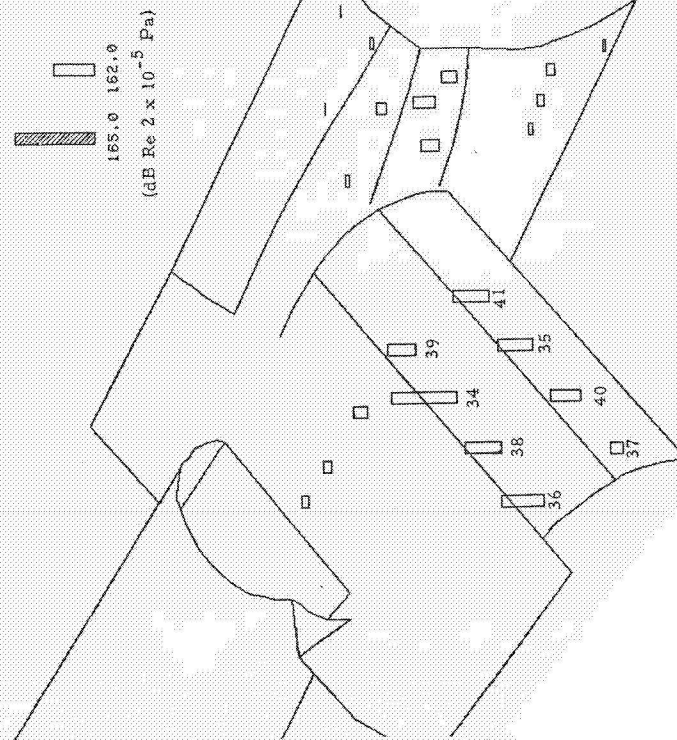
(a) Vortex generators up

* TEST CONFIGURATION 6 *

86.5-DEGREE FLAP
1.45-METER WING HEIGHT
FLAP/FUSELAGE JUNCTION OPEN
SKEWED-PLUG PRIMARY NOZZLE

RUN 289
100% THRUST

OVERALL FLUCTUATING PRESSURE LEVELS

OVERALL FLUCTUATING PRESSURE LEVELS

165.0 162.0

(dB Re 2 x 10^{-5} Pa)
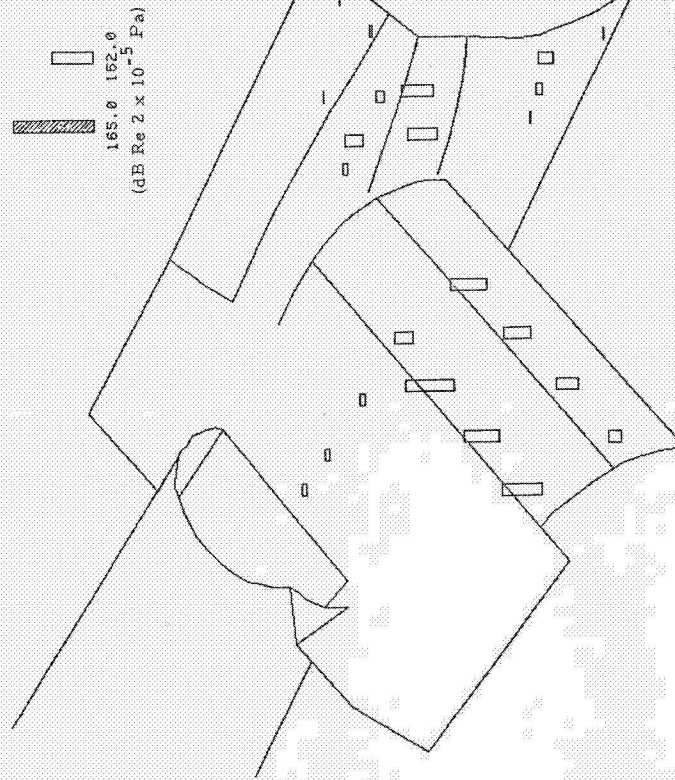
(b) Vortex generators down

Figure 34. - Spatial variation of OAFPL on surface of model at 100%
thrust settings for test configurations 5 and 6.

103
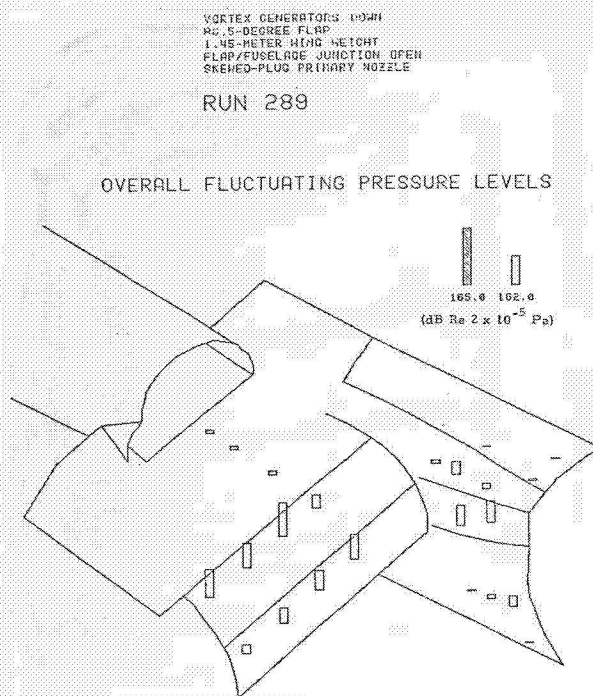
(a) 100% thrust
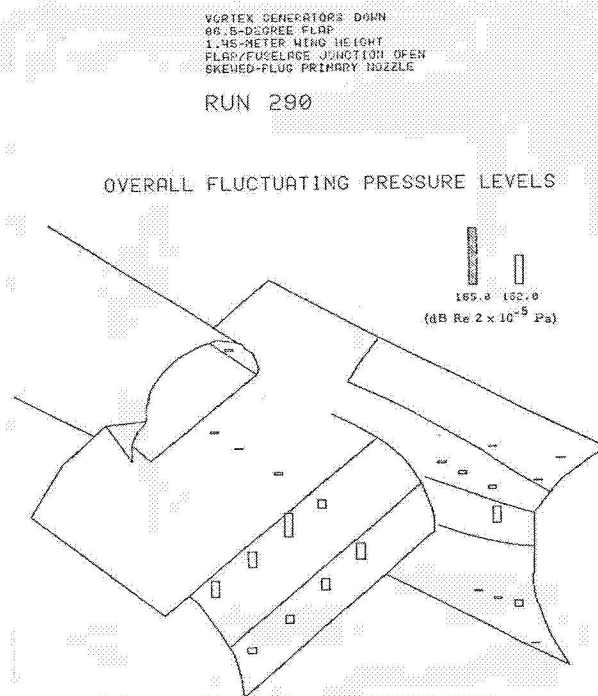
(b) 75% thrust
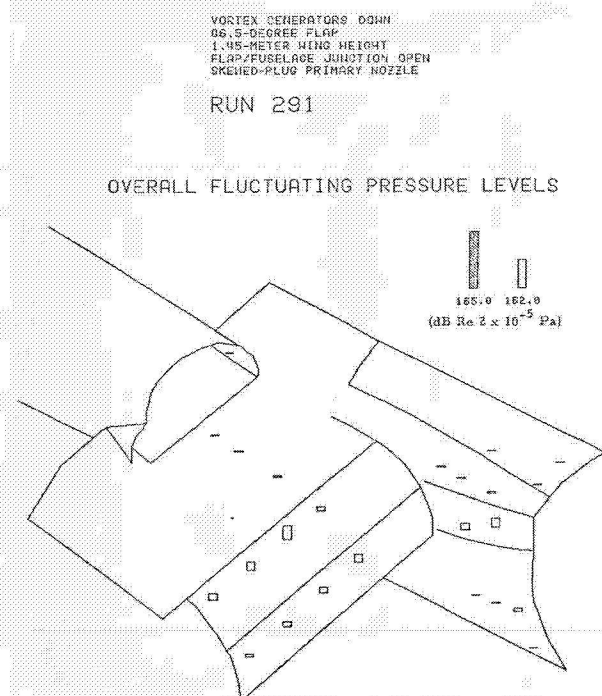
(c) 50% thrust
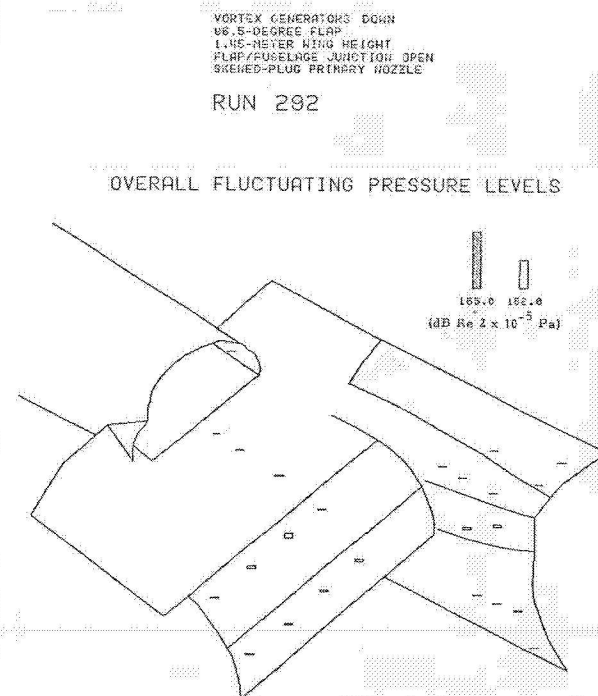
(d) 25% thrust

Figure 35. - Effect of thrust setting on spatial variation of OAFPL
on surface of model. Test configuration 6.

(SLOPE)
△ 23 (3.69)
⊞ 32 (4.62)
✳ 33 (4.69)
⊕ 43 (4.54)

OVERALL FLUCTUATING PRESSURE LEVEL, DB

160.0 153.0 146.0 139.0 132.0 125.0 118.0

RUNS 331 - 334

MAX. NOZZLE CENTERLINE EXIT VELOCITY, M/SEC

(b) Vortex generators up

(SLOPE)
△ 23 (3.33)
⊞ 32 (4.13)
✳ 33 (4.12)
⊕ 43 (3.56)

RUNS 326 - 329

MAX. NOZZLE CENTERLINE EXIT VELOCITY, M/SEC
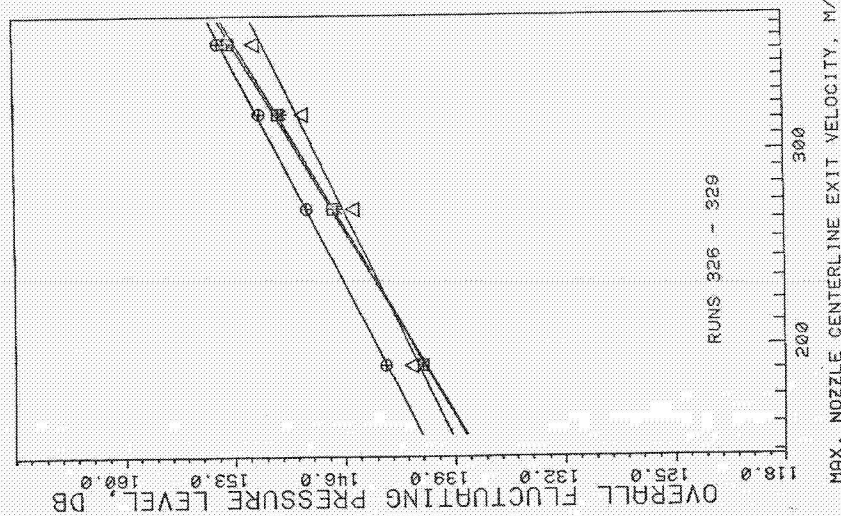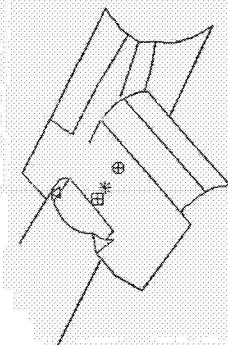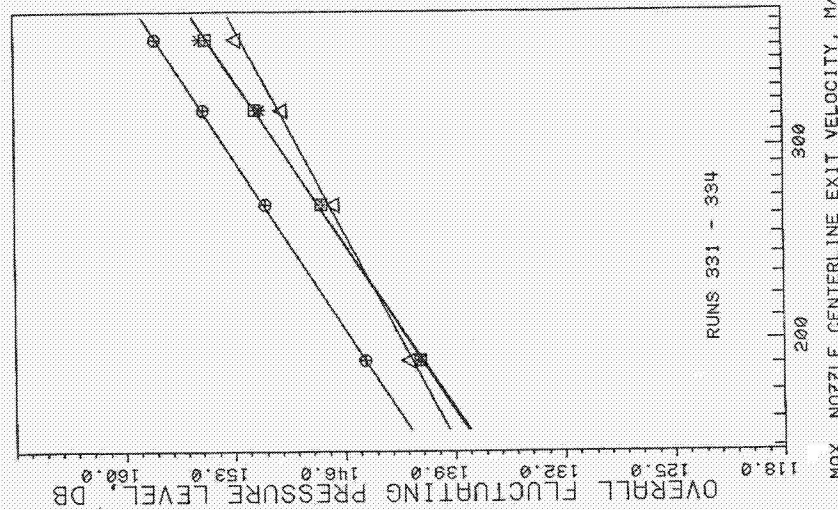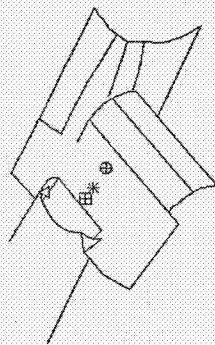
(a) Vortex generators down

Figure 36. – Variations of OAFPL with jet exit velocity at nozzle and wing positions.

105
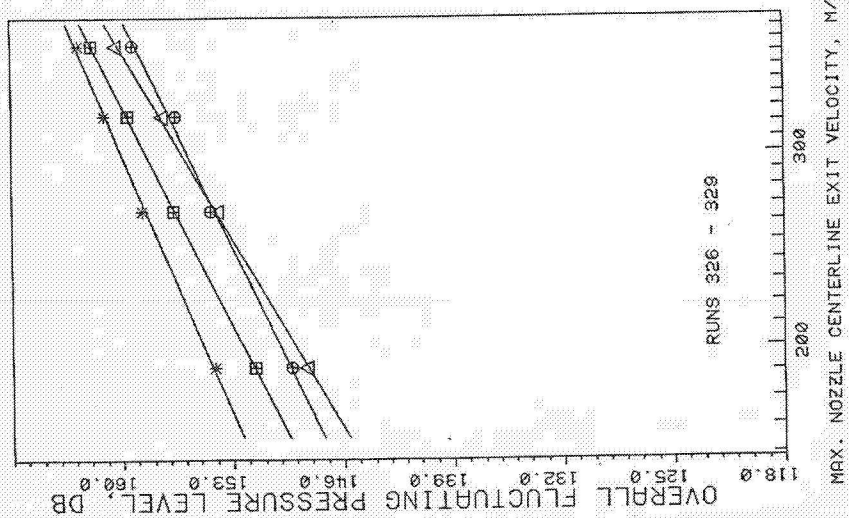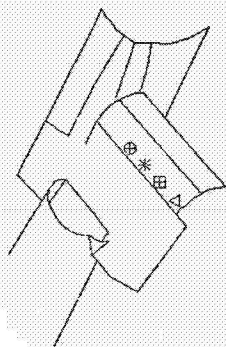
(a) Vortex generators down

(b) Vortex generators up

Figure 37. – Variations of OAFPL with jet exit velocity at main flap positions.

(SLOPE)
⊞ 40 (3.42)
＊ 35 (3.28)
⊕ 41 (3.34)

(SLOPE)
⊞ 40 (3.41)
＊ 35 (3.64)
⊕ 41 (3.64)

(b) Vortex generators up

(a) Vortex generators down

Figure 38. – Variations of OAFPL with jet exit velocity at aft flap positions.

107
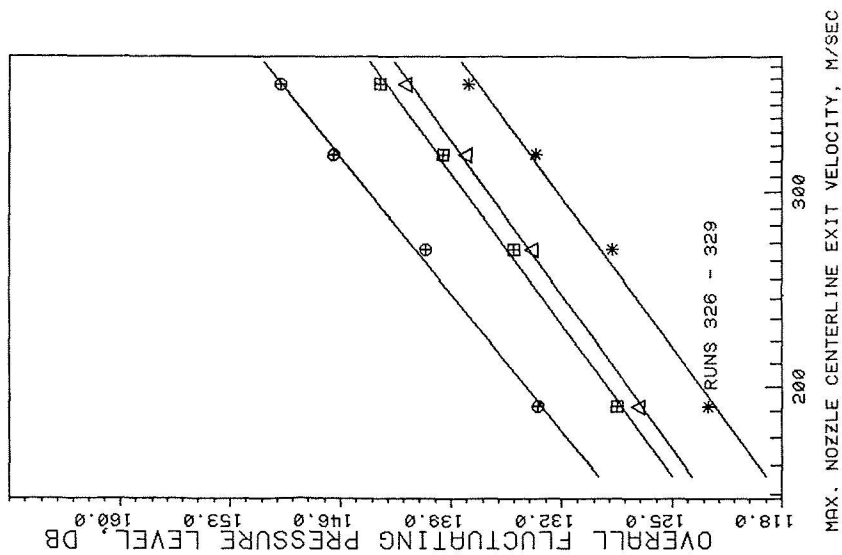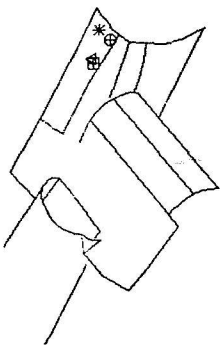
(a) Vortex generators down

(b) Vortex generators up

Figure 39. – Variations of OAFPL with jet exit velocity at upper fuselage positions

108
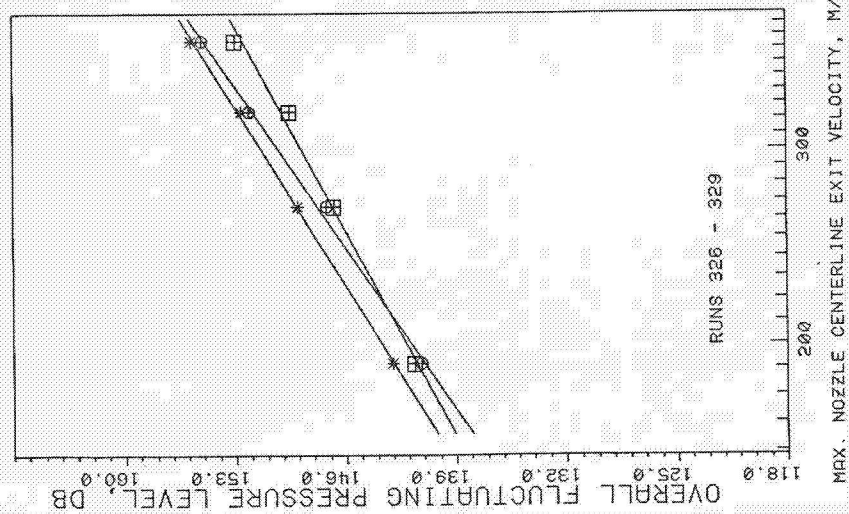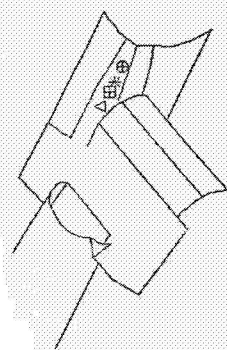
(a) Vortex generators down

(b) Vortex generators up

Figure 40. – Variations of OAFPL with jet exit velocity at fairing top positions.
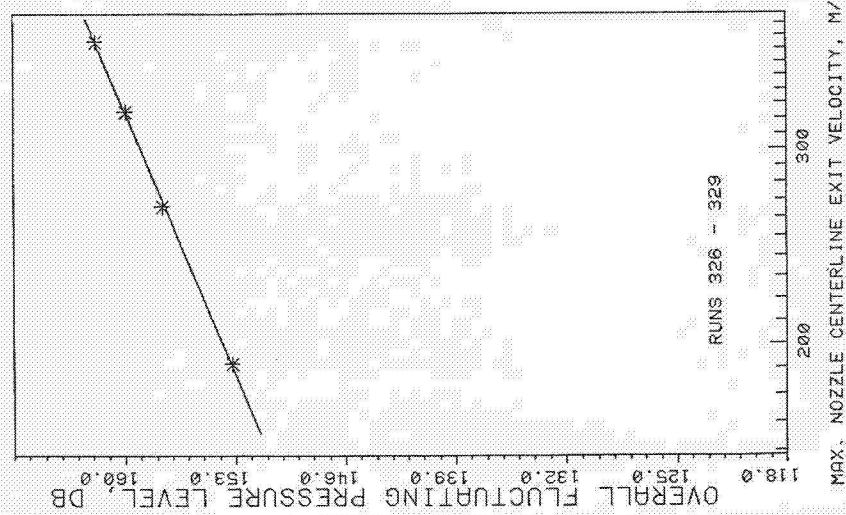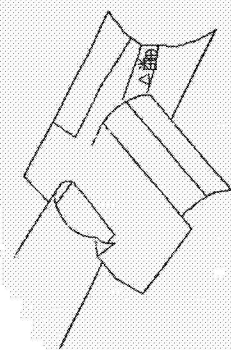
(a) Vortex generators down
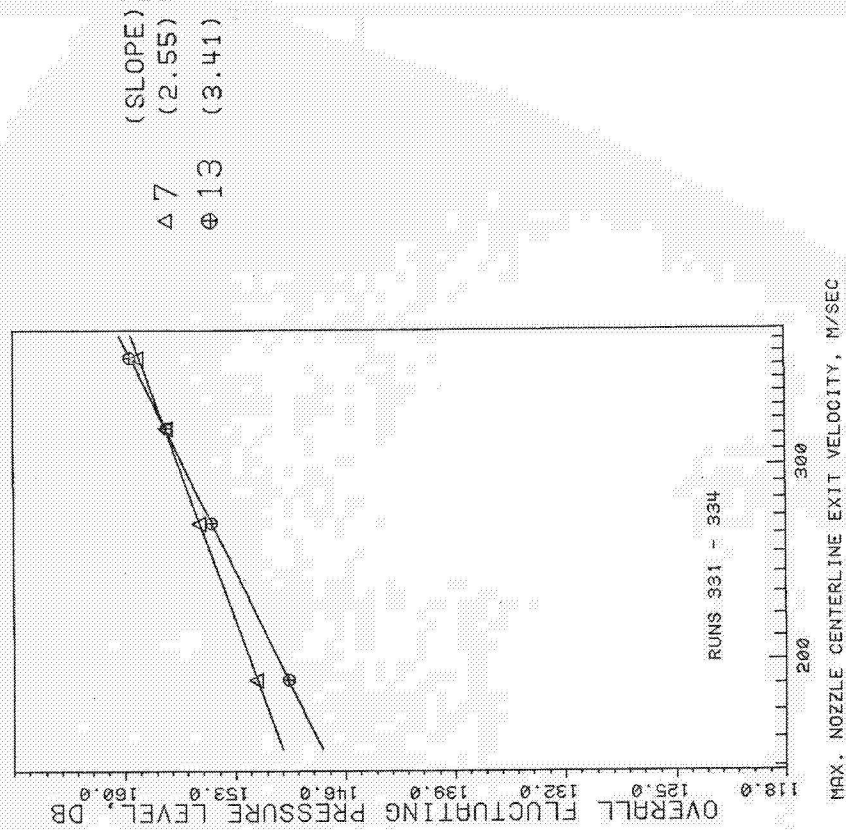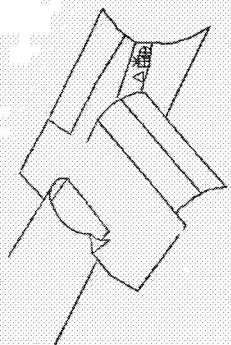
(b) Vortex generators up

Figure 41. – Variation of OAFPL with jet exit velocity at fairing side positions.

110
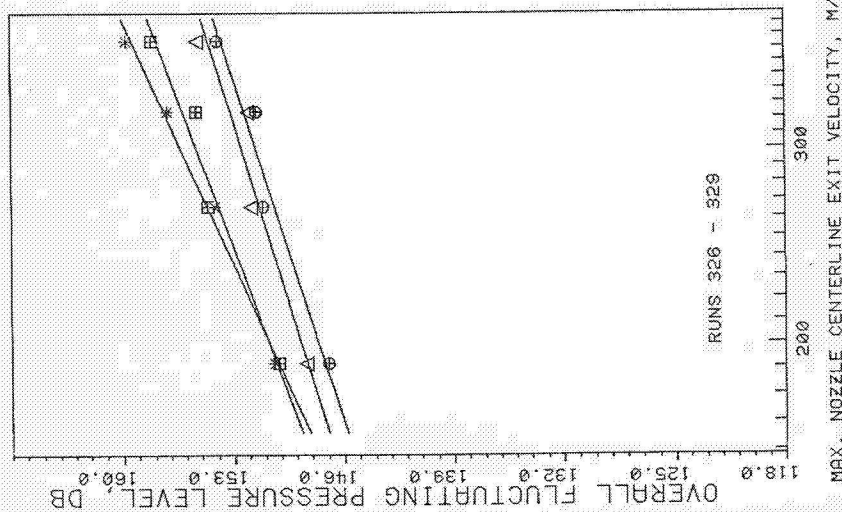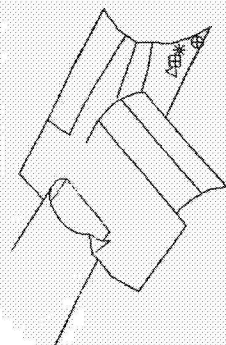
(a) Vortex generators down
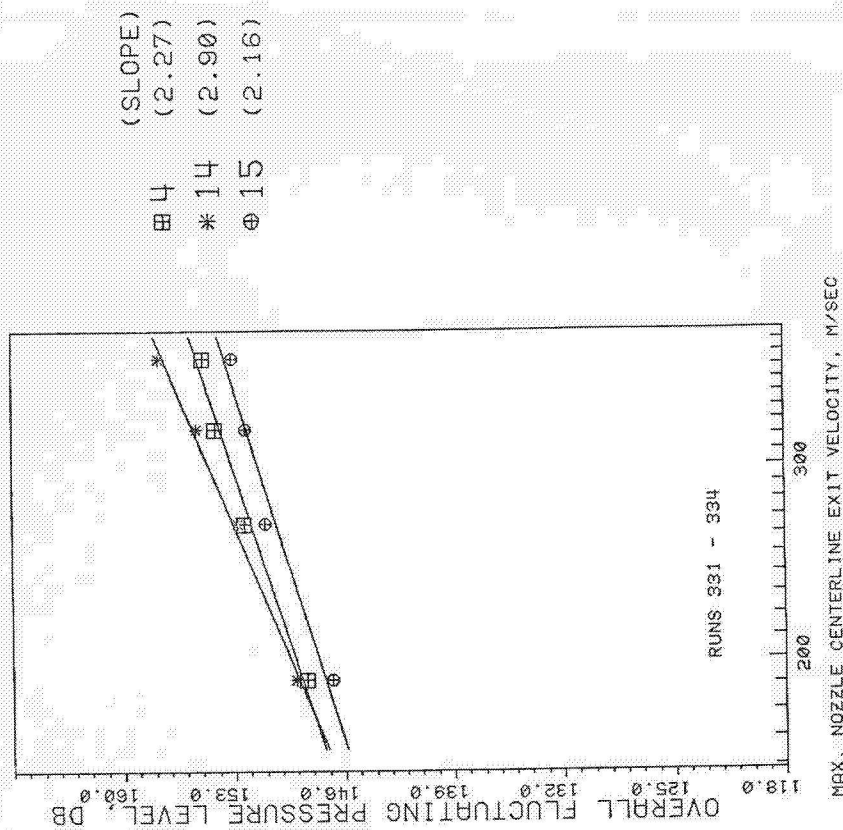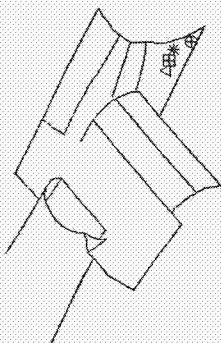
(b) Vortex generators up

Figure 42. – Variation of OAFPL with jet exit velocity at lower fuselage positions.

111
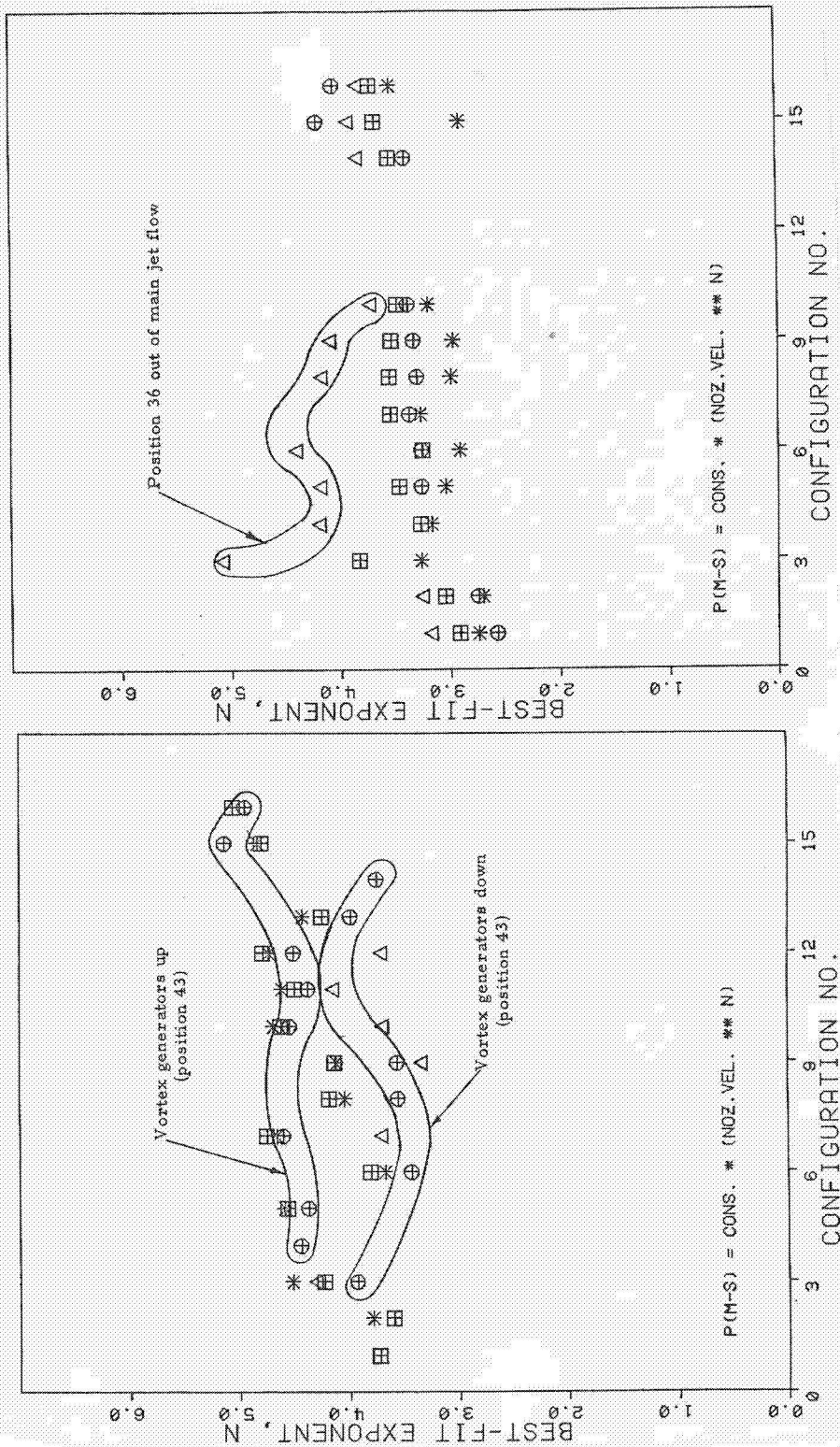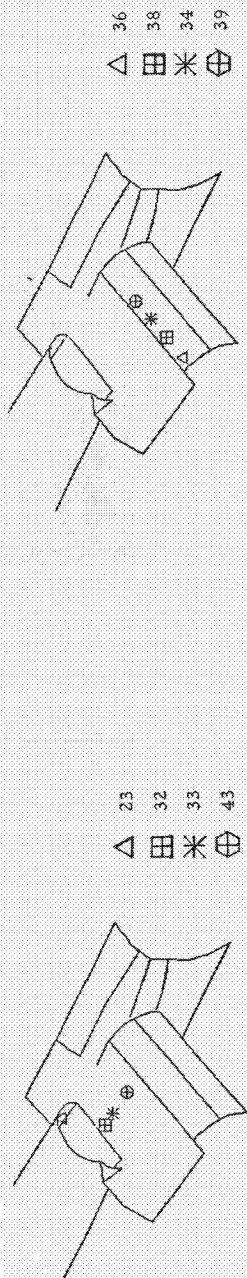
Figure 43. – Best-fit rates of increase (slopes) of mean-square fluctuating pressure with jet exit velocity.

(a) Nozzle and wing

(b) Main flap
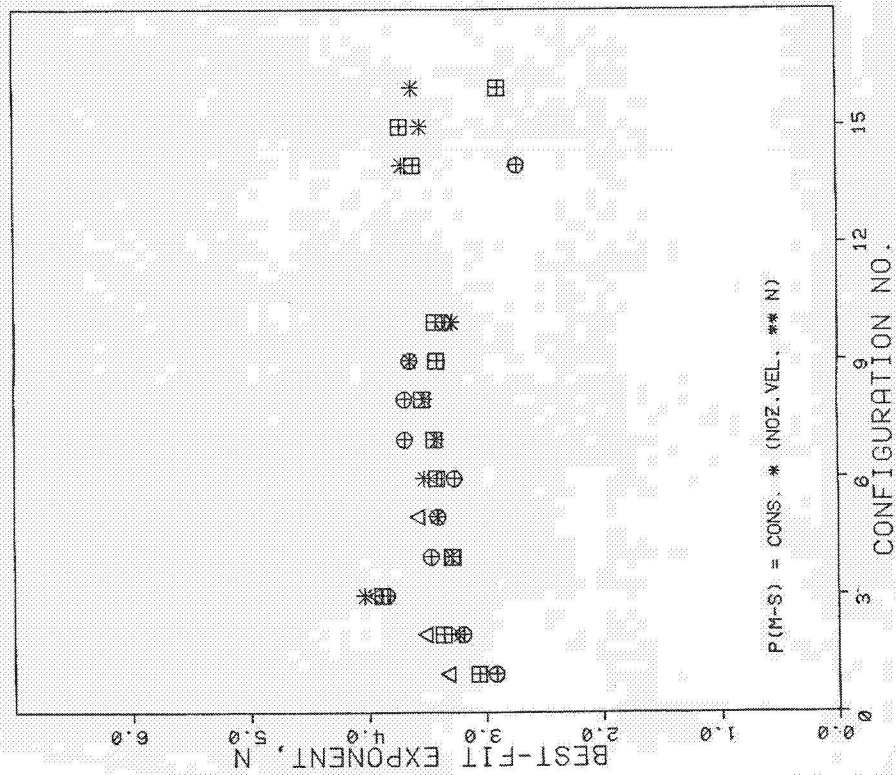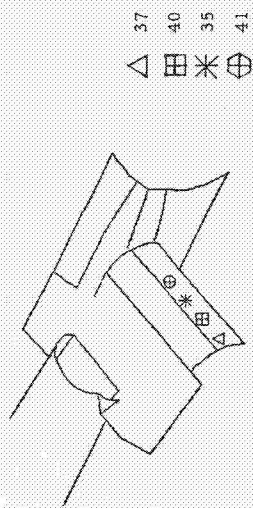
(c) Aft flap
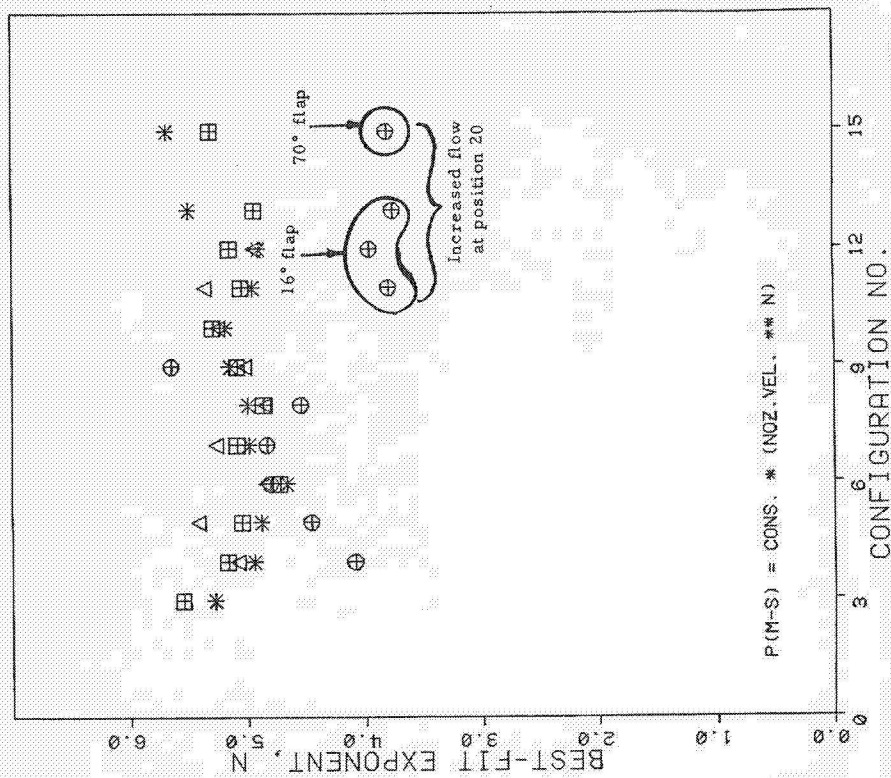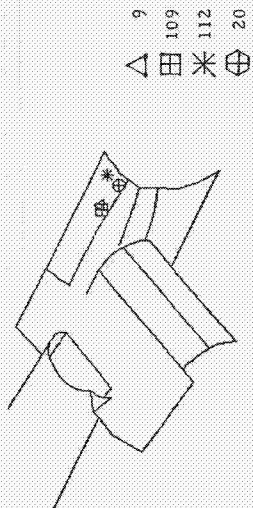
(d) Upper fuselage

Figure 43. – Continued.

113
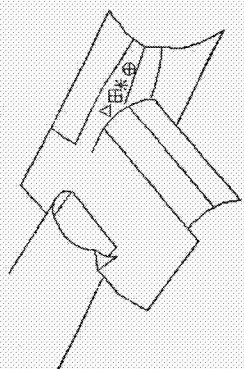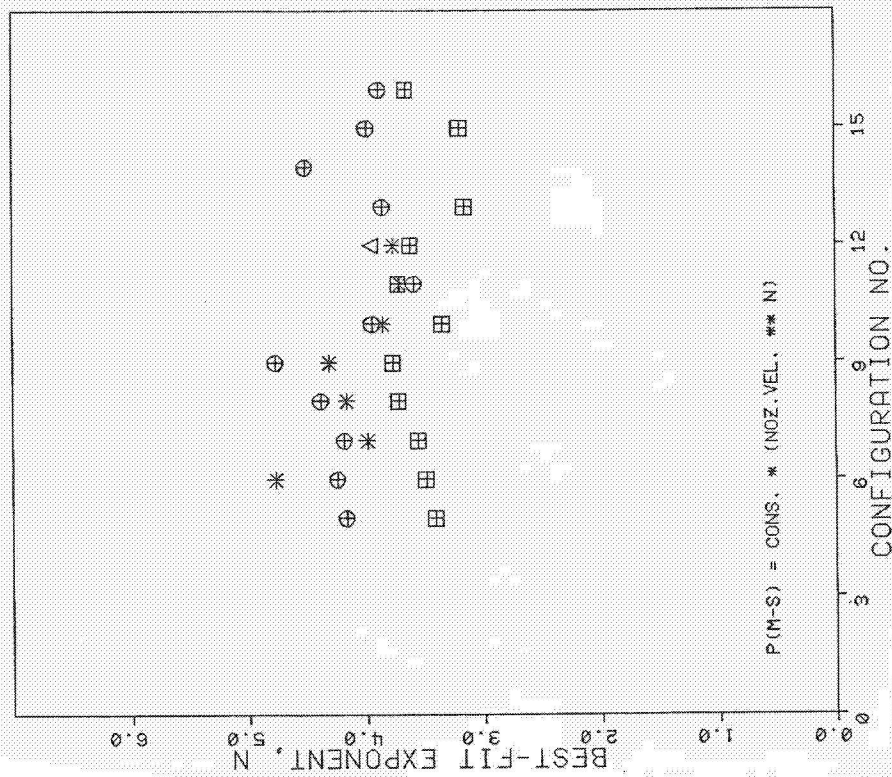
(e) Fairing top
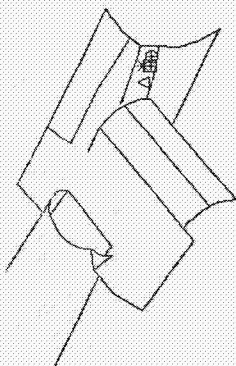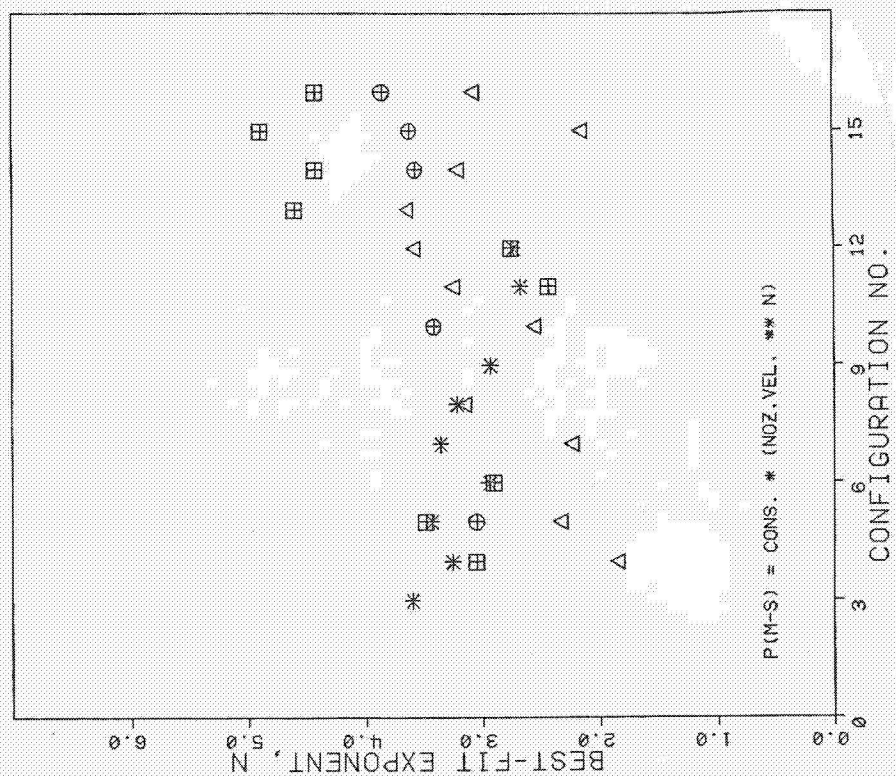
(f) Fairing side

Figure 43. - Continued.
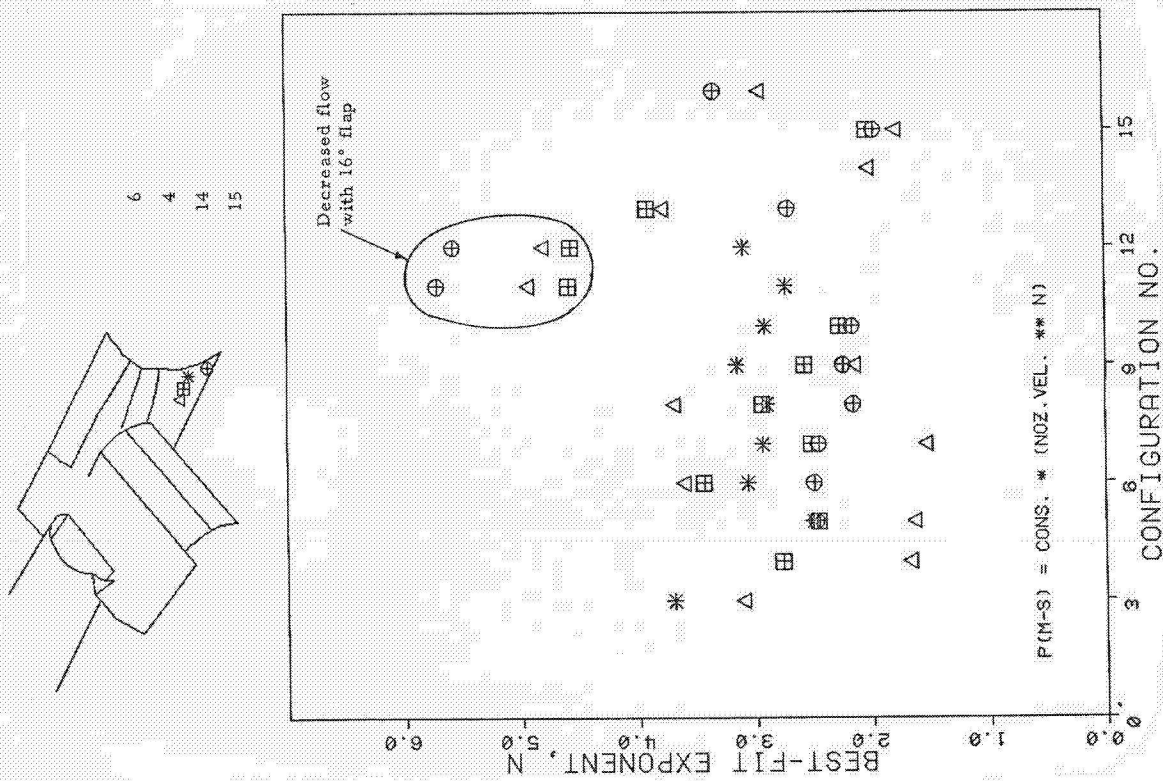
(g) Lower fuselage

Figure 43. - Concluded.
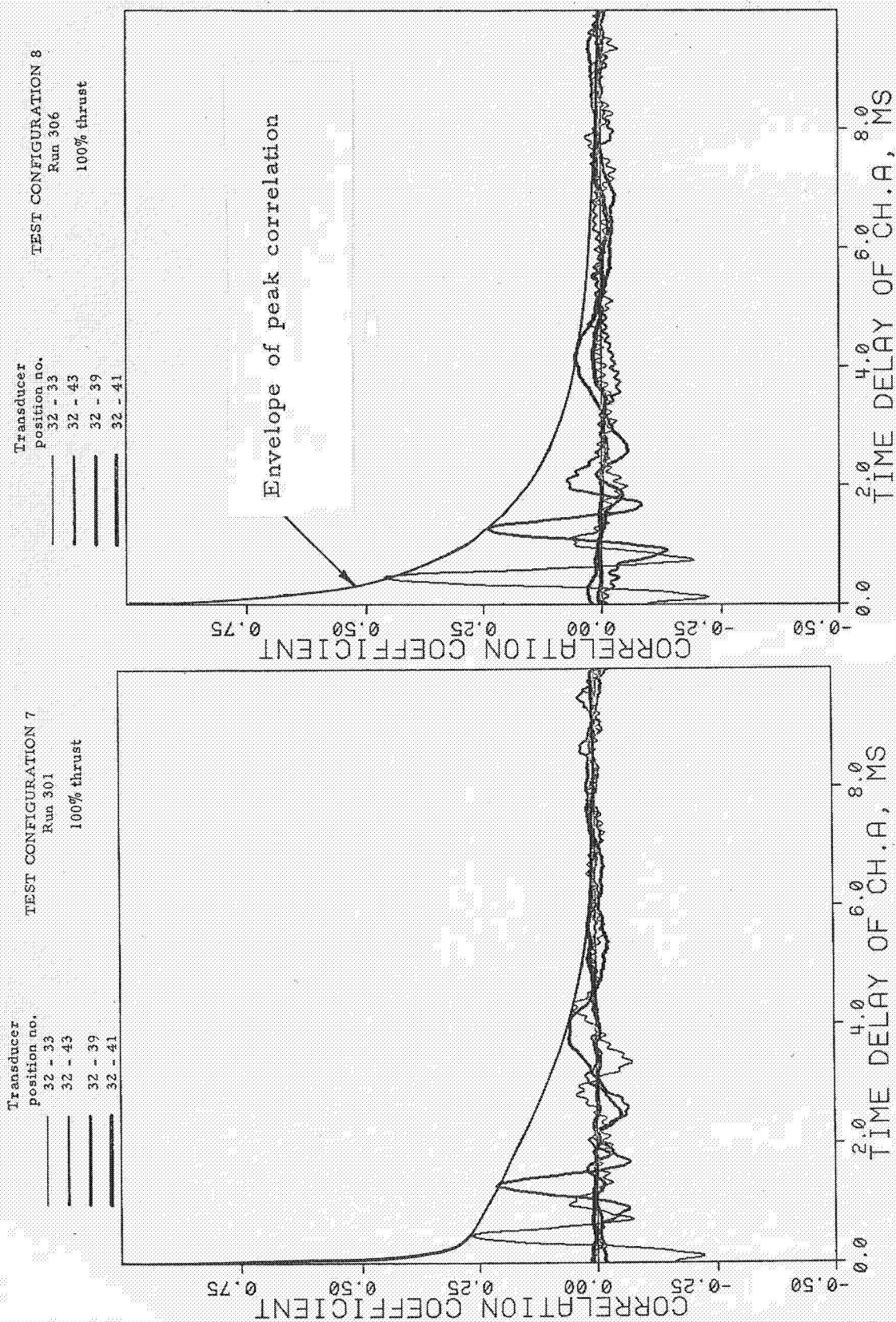
Figure 44. - Space-time broadband correlation of surface fluctuating pressure in longitudinal direction along nozzle centerline.
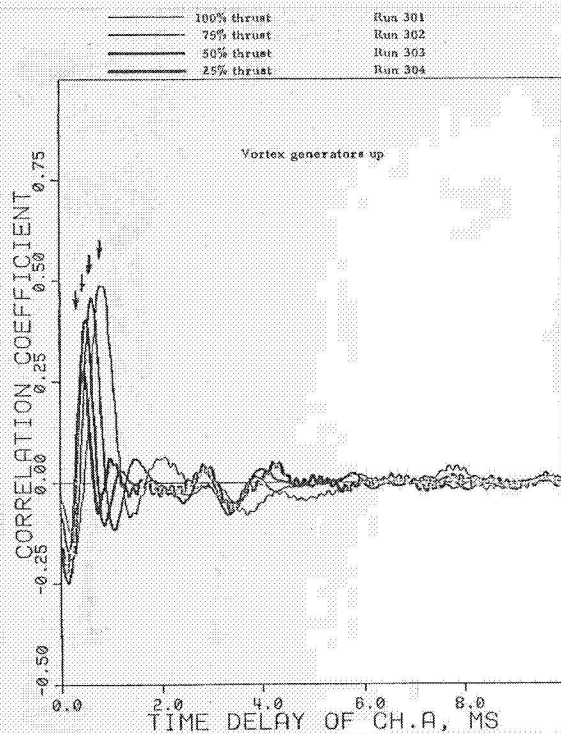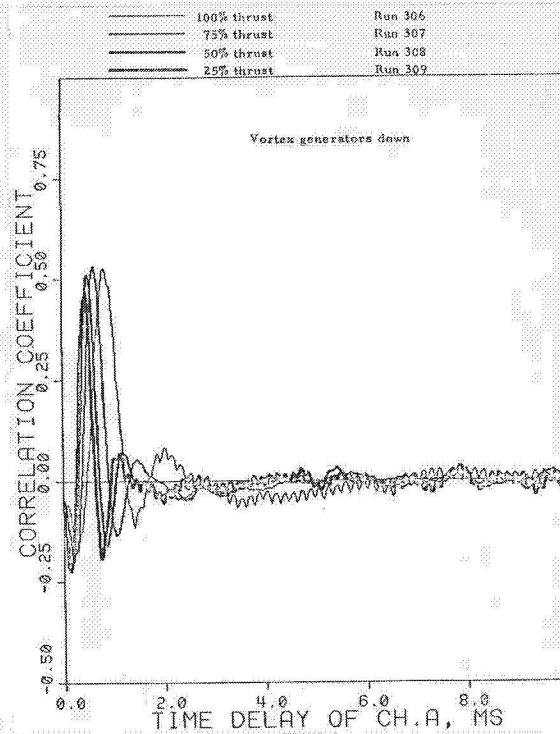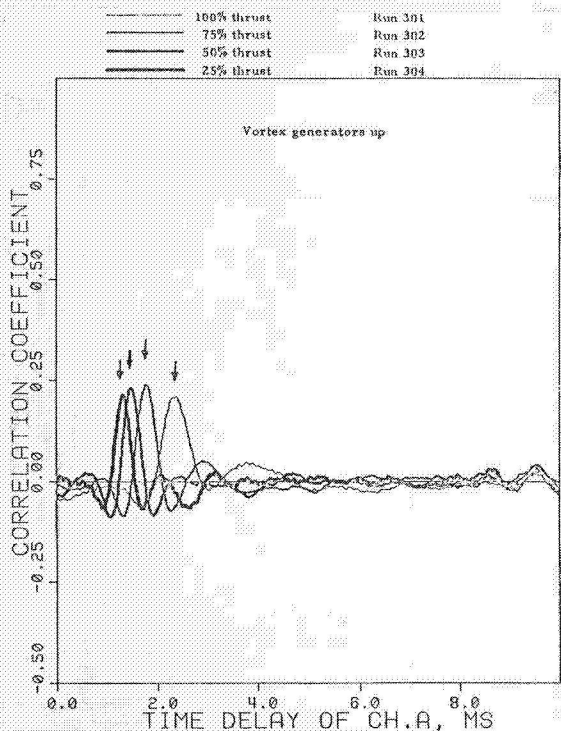
(a) Vortex generators up
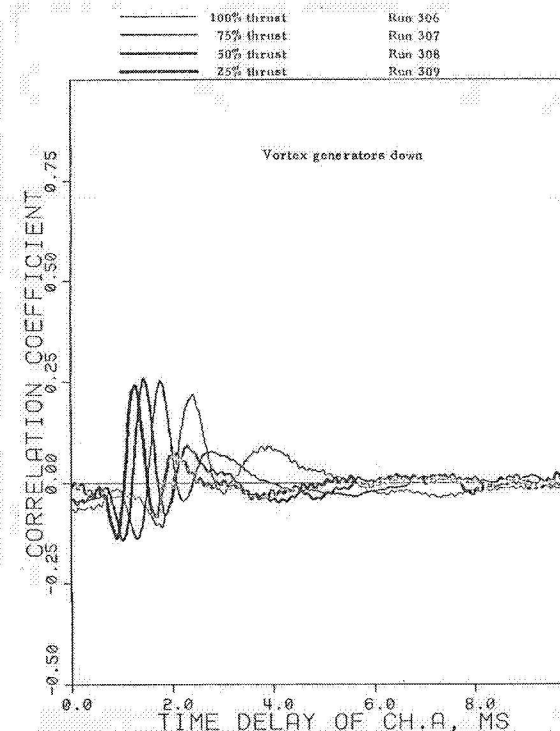
(b) Vortex generators down

Figure 45. - Effects of thrust setting and deployment of vortex generators on broadband correlation functions in longitudinal direction on wing.
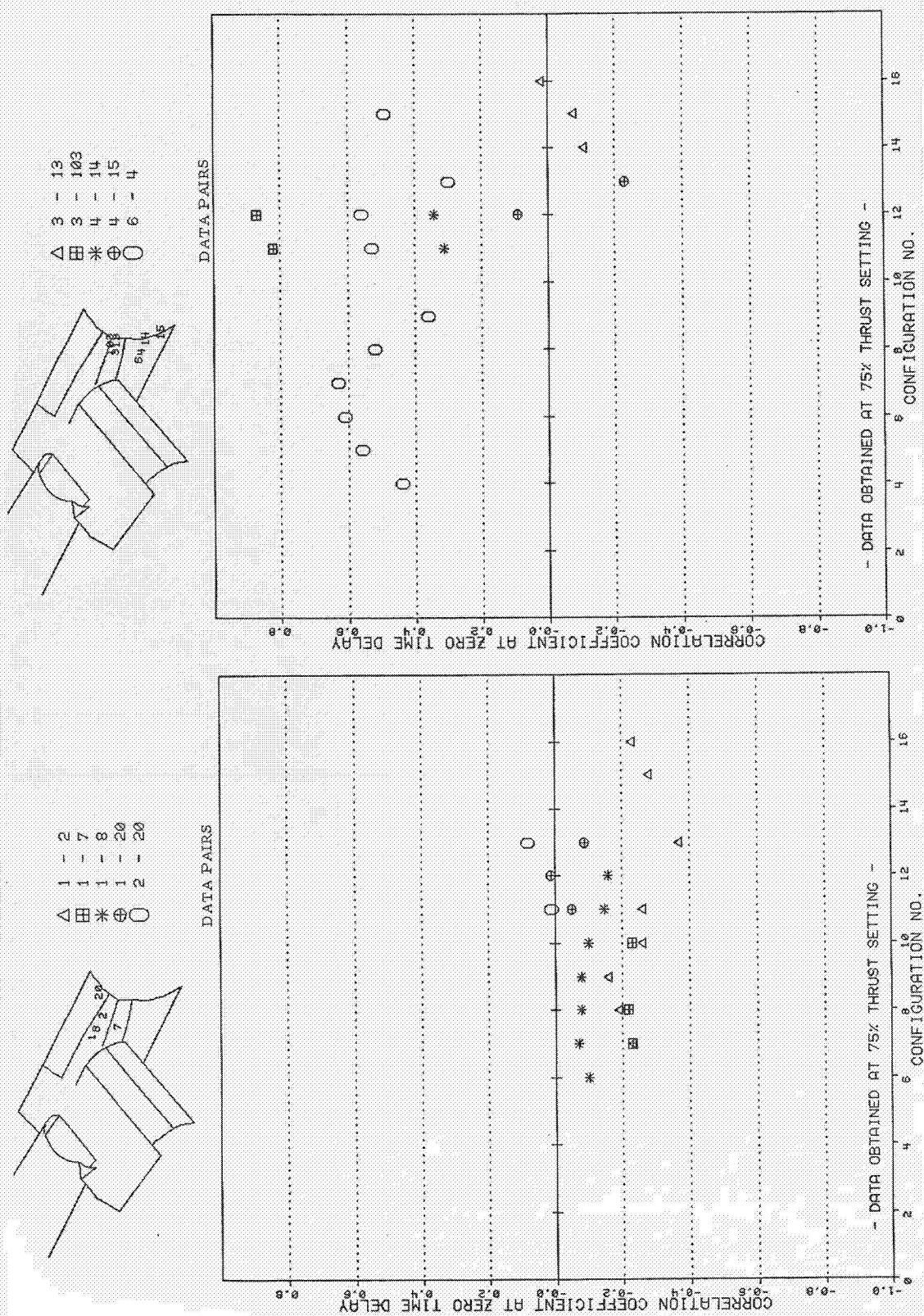
(a) Position nos. 1 and 2

(b) Position nos. 3 - 6

Figure 46. - Variation of correlation coefficient of zero time delay
with test configuration.

DATA PAIRS

△ 8 - 2
⊞ 8 - 20
✳ 9 - 2
⊕ 9 - 12
○ 10 - 1

CORRELATION COEFFICIENT AT ZERO TIME DELAY

CONFIGURATION NO.

- DATA OBTAINED AT 75% THRUST SETTING -
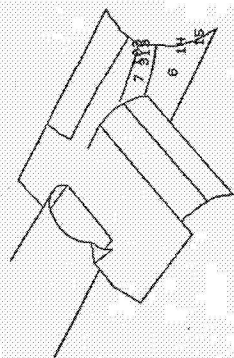
(d) Position nos. 8 - 10

DATA PAIRS

△ 6 - 14
⊞ 6 - 15
✳ 7 - 3
⊕ 7 - 13
○ 7 - 103

CORRELATION COEFFICIENT AT ZERO TIME DELAY

CONFIGURATION NO.

- DATA OBTAINED AT 75% THRUST SETTING -

(c) Position nos. 6 and 7
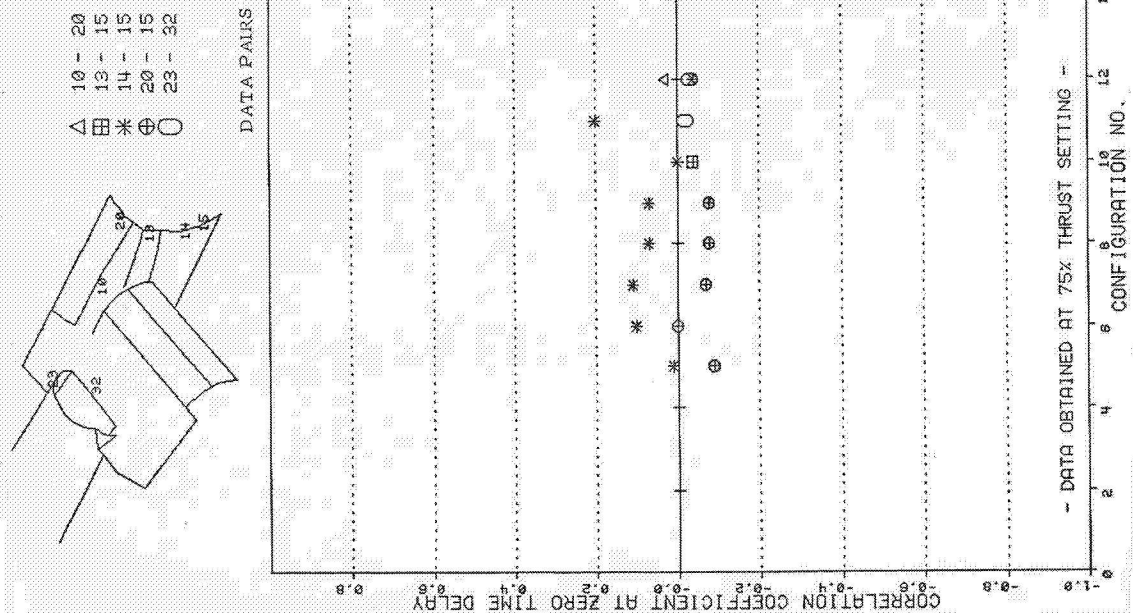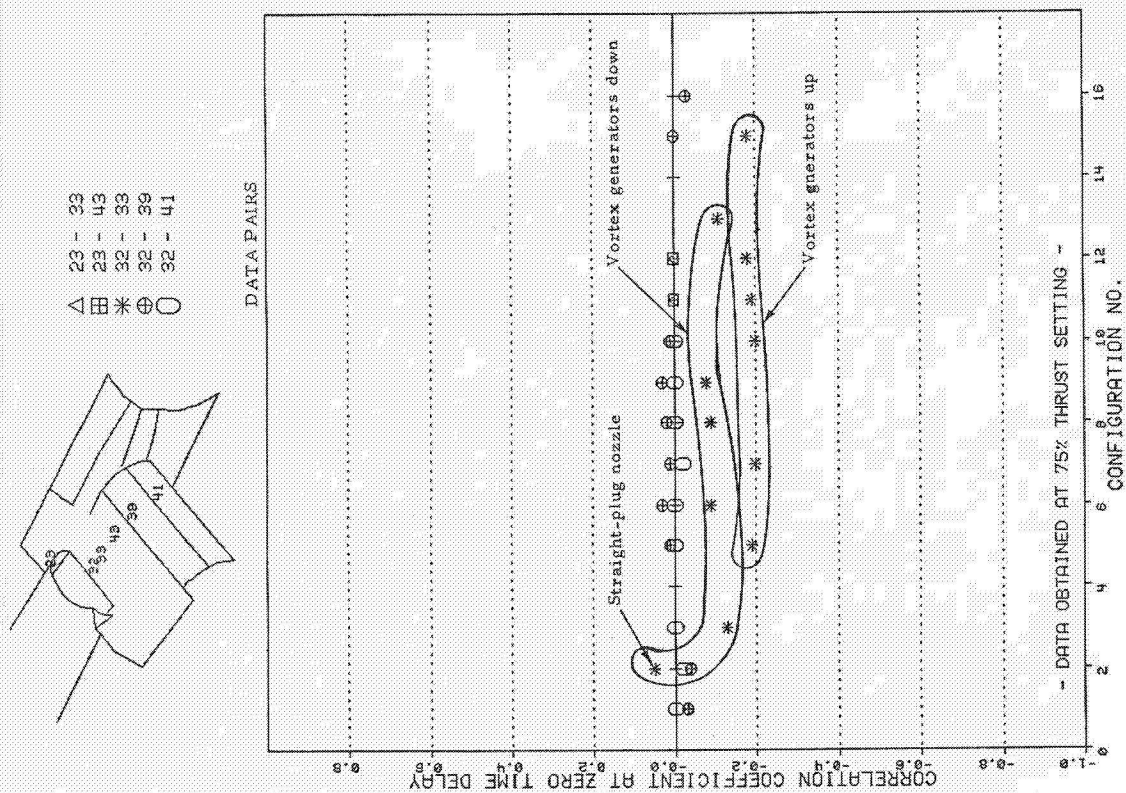
Figure 46. - Continued.

DATA PAIRS

△ 23 - 33
⊞ 23 - 43
✳ 32 - 33
⊕ 32 - 39
○ 32 - 41

Vortex generators down

Vortex generators up

Straight-plug nozzle

CORRELATION COEFFICIENT AT ZERO TIME DELAY

— DATA OBTAINED AT 75% THRUST SETTING —

CONFIGURATION NO.

(f) Position nos. 23 and 32

DATA PAIRS

△ 10 - 20
⊞ 13 - 15
✳ 14 - 15
⊕ 20 - 15
○ 23 - 32

CORRELATION COEFFICIENT AT ZERO TIME DELAY

— DATA OBTAINED AT 75% THRUST SETTING —

CONFIGURATION NO.

(e) Position nos. 10 - 23
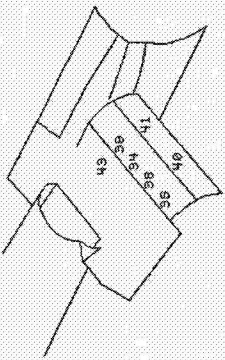
Figure 46. - Continued.
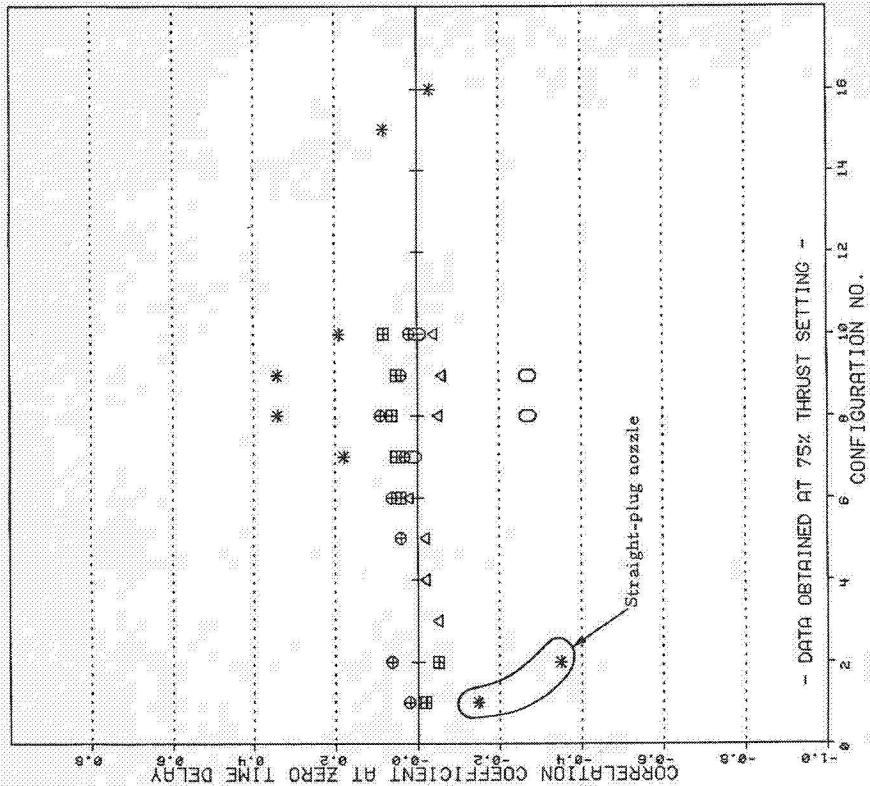
(h) Position nos. 38 - 43

(g) Position nos. 32 - 35

Figure 46. - Continued.
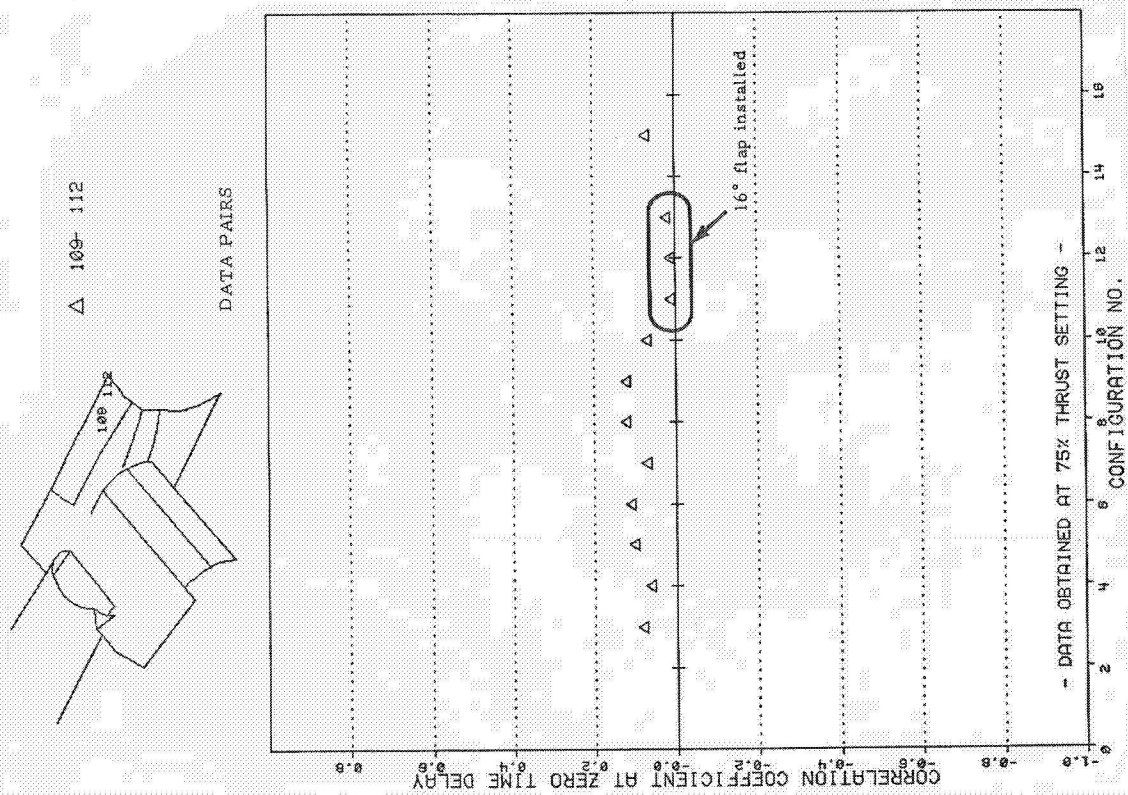
(i) Position 109

Figure 46. - Concluded.
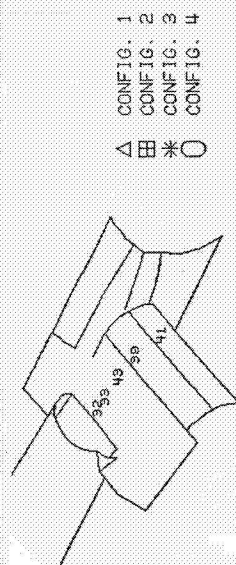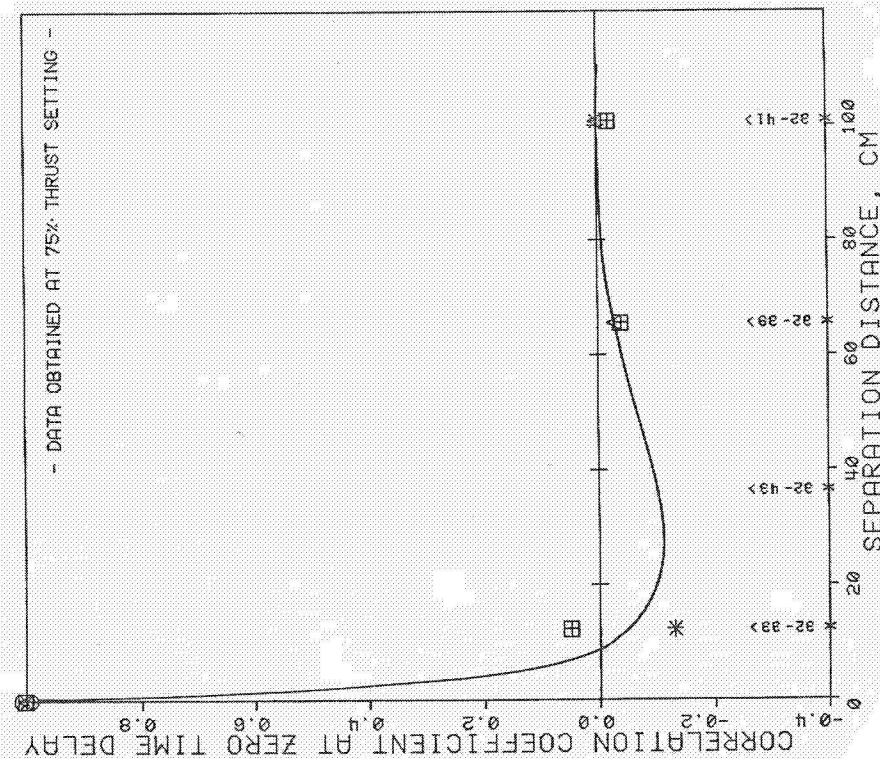
122
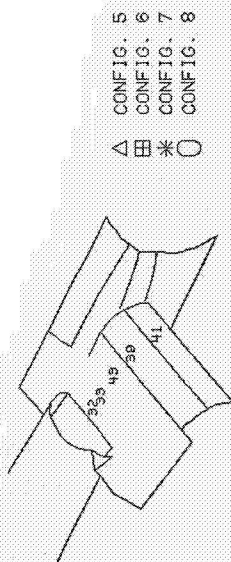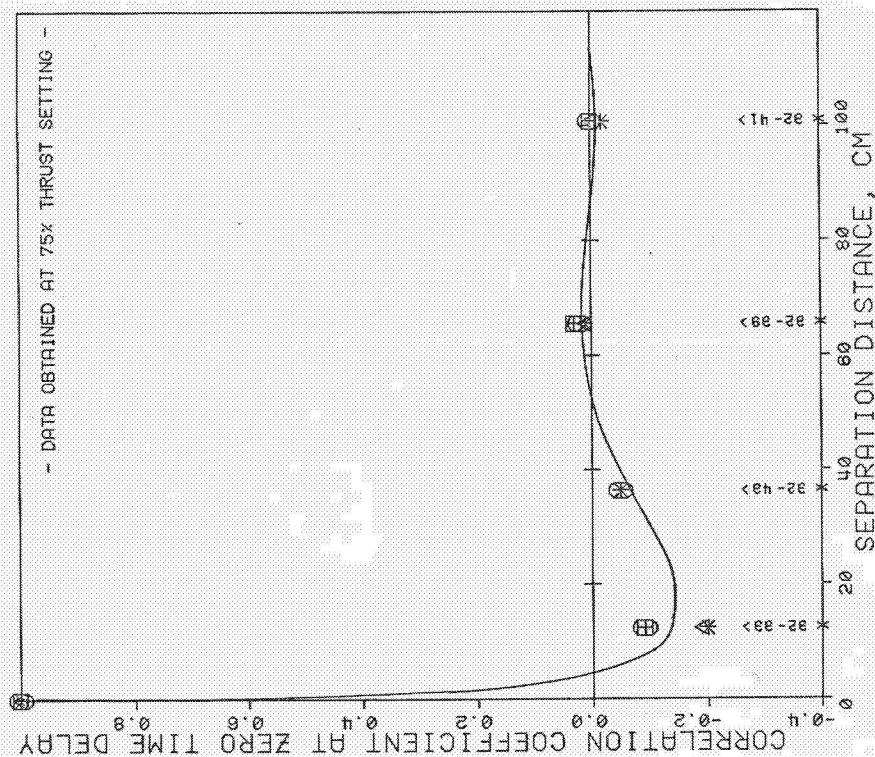
Figure 47. – Space correlation of surface fluctuating pressure in longitudinal direction along nozzle centerline.

123

(d) Configurations 13 – 16

(c) Configurations 9 – 12

Figure 47. – Concluded.
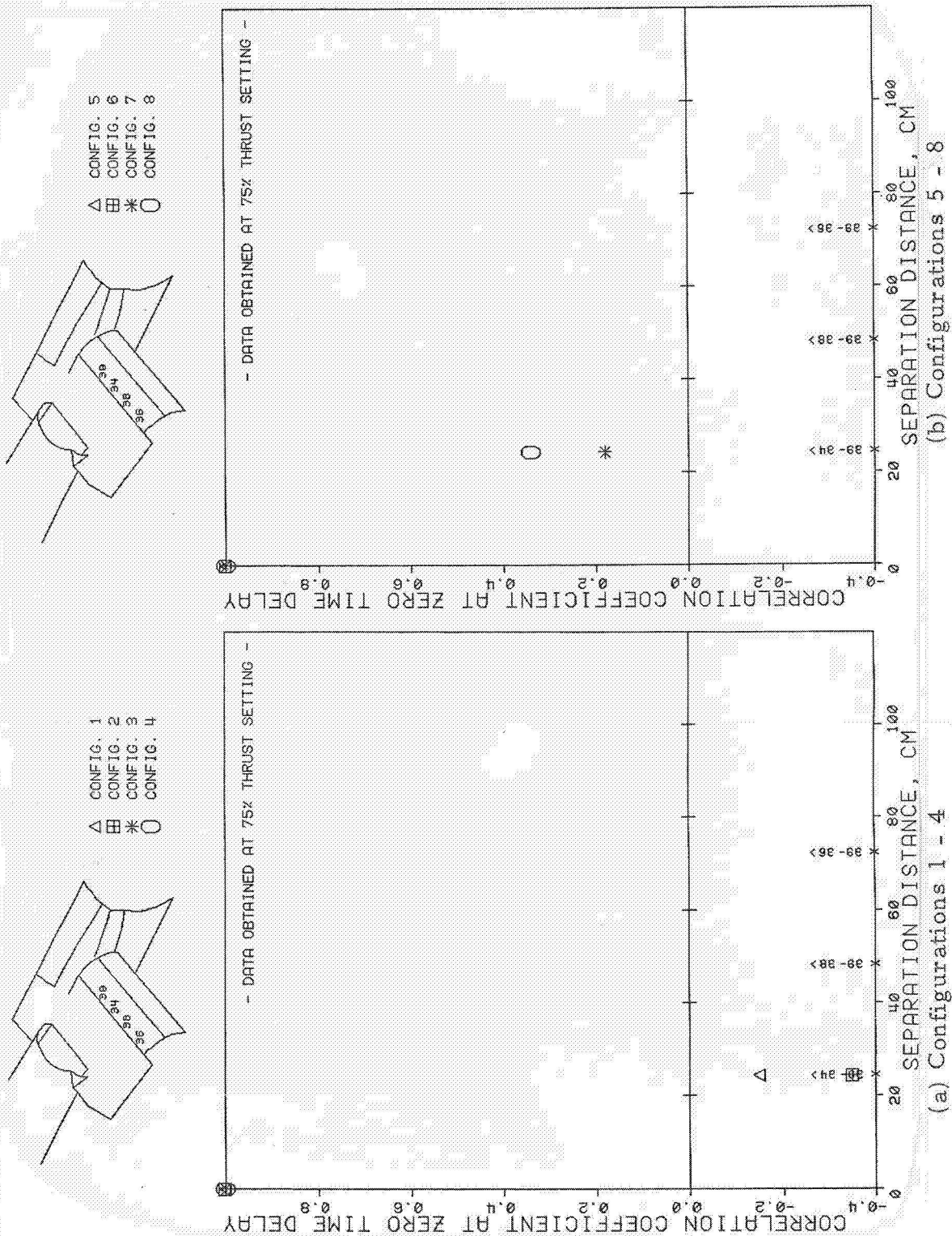
Figure 48. - Space correlation of surface fluctuating pressure in lateral direction along main flap.
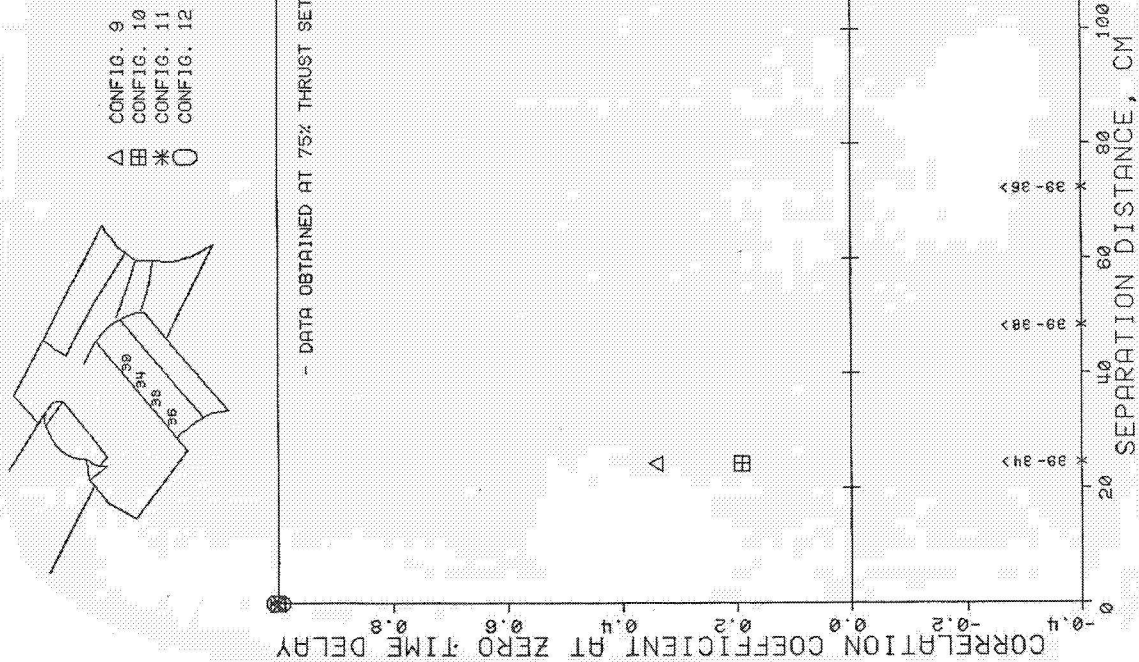
(c) Configurations 9 - 12
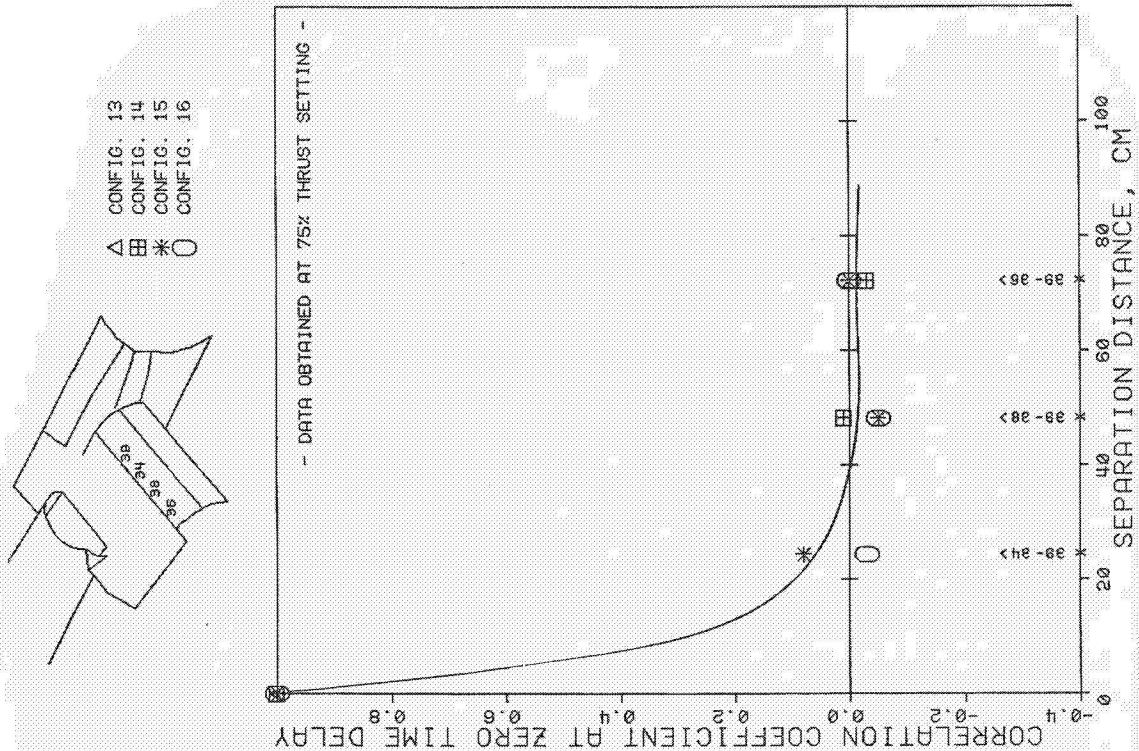
(d) Configurations 13 - 16

Figure 48. - Concluded.
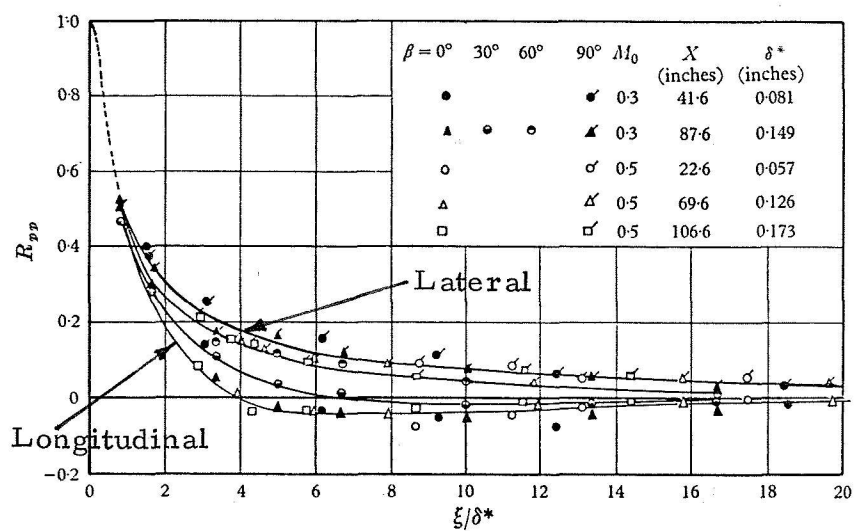
Space correlation of the wall-pressure field, $R_{pp}(\xi\cos\beta, \xi\sin\beta, 0)$ at various angles to the flow direction.

Figure 49. - Measurements by Bull (Fig. 8, Ref. 24) of space correlation of surface fluctuating pressure of various angles to the flow direction.
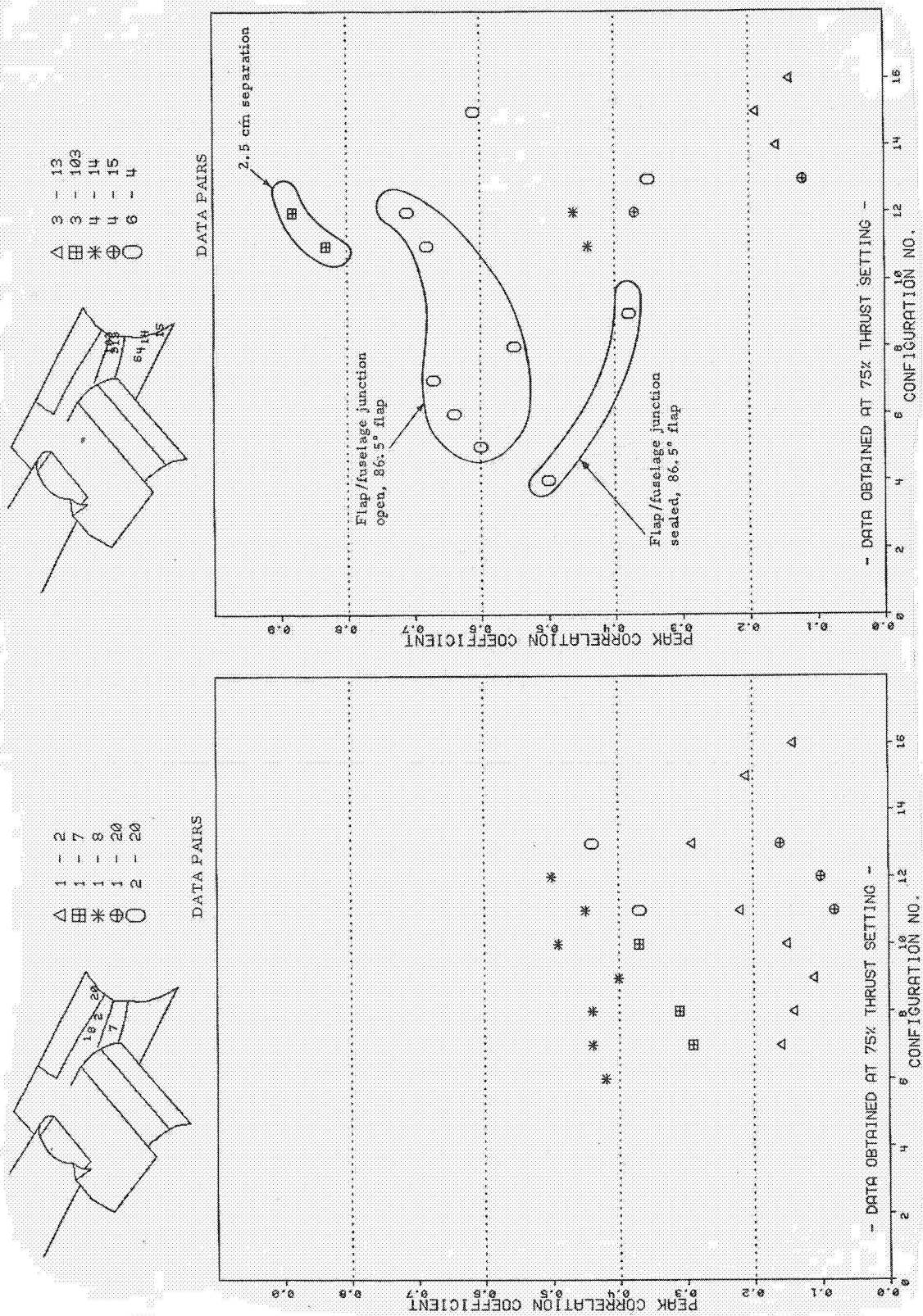
(a) Position nos. 1 and 2

(b) Position nos. 3 – 6

Figure 50. – Variation of peak correlation coefficient with test configuration.

(c) Position nos. 6 and 7

(d) Position nos. 8 – 10

Figure 50. – Continued.
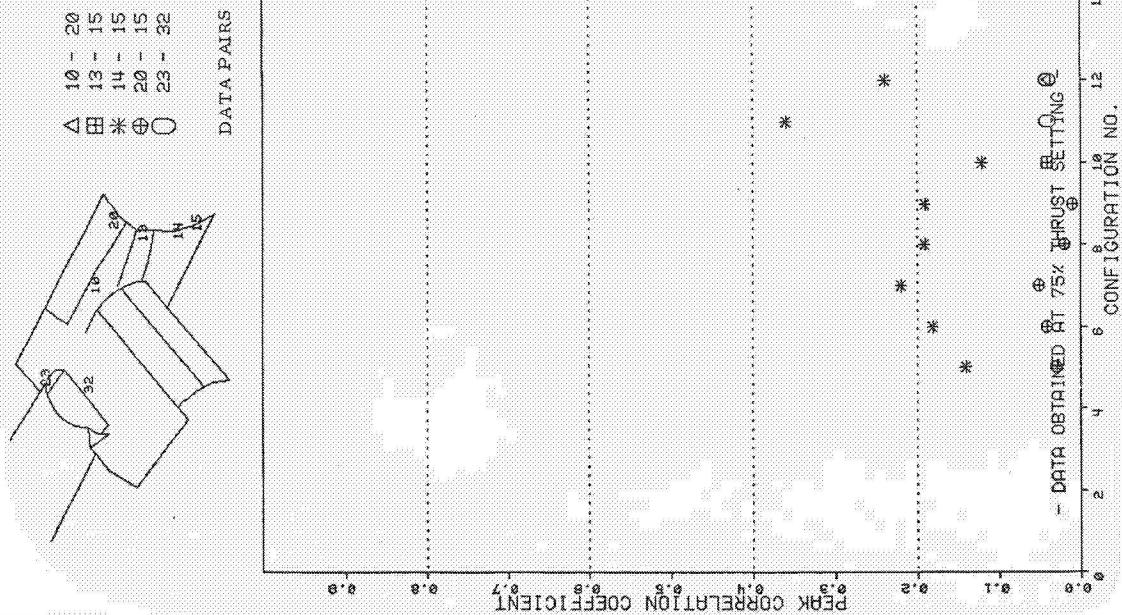
(e) Position nos. 10 - 22
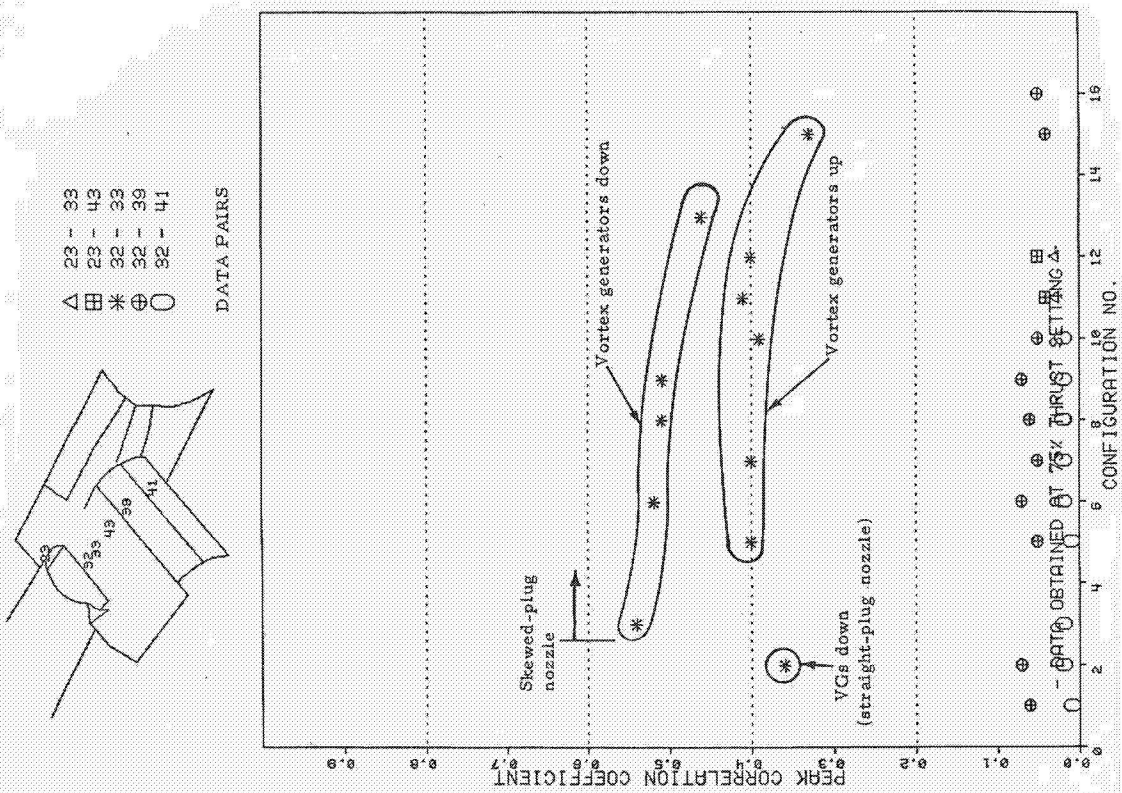
(f) Position nos. 23 - 32

Figure 50. – Continued.
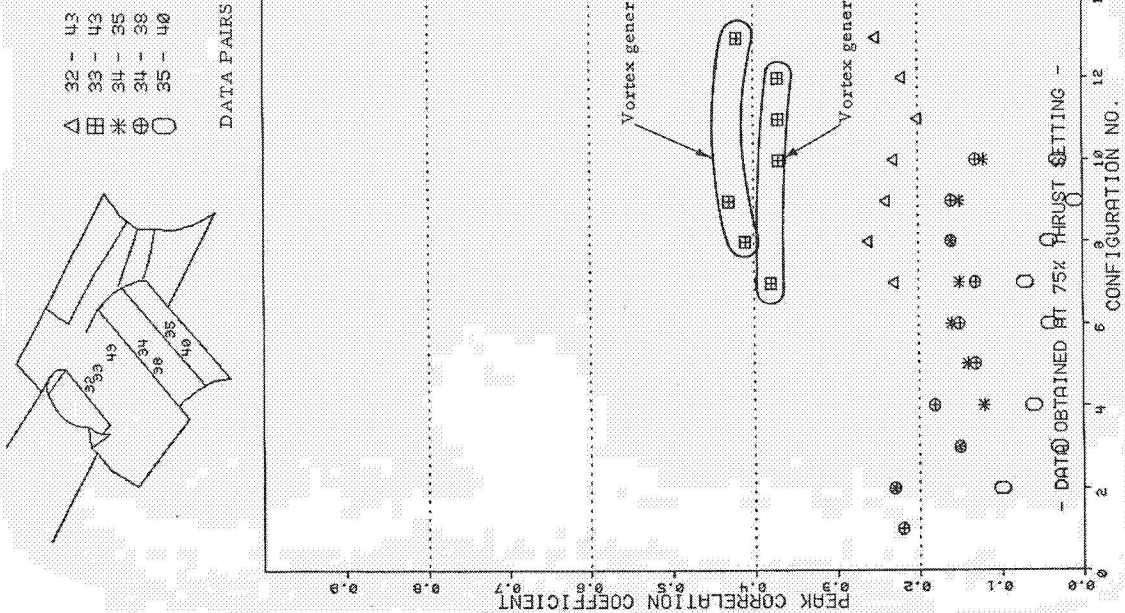
(h) Position nos. 38 – 43

(g) Position nos. 32 – 35

Figure 50. – Continued.

(i) Position no. 109

Figure 50. - Concluded.
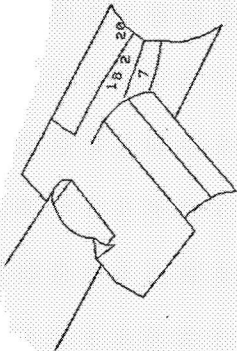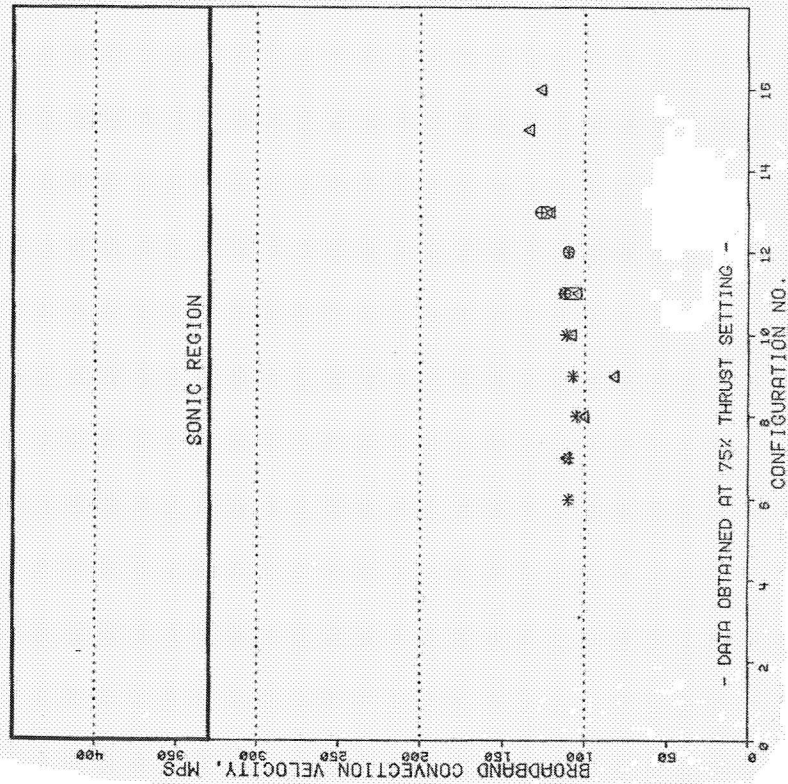
(a) Position nos. 1 and 2
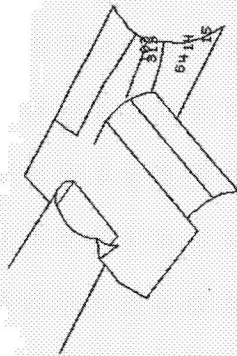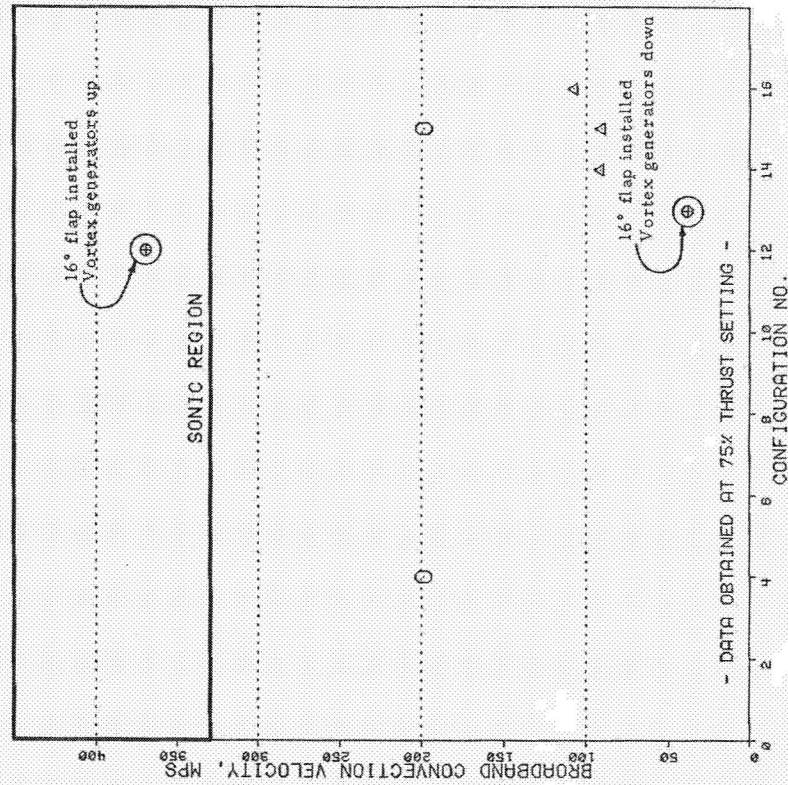
(b) Position nos. 3 - 6

Figure 51. – Variation of broadband convection velocity with test configuration.
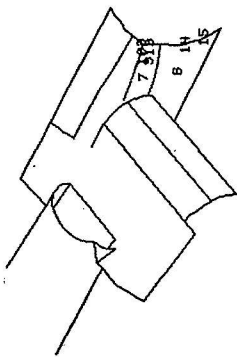
133
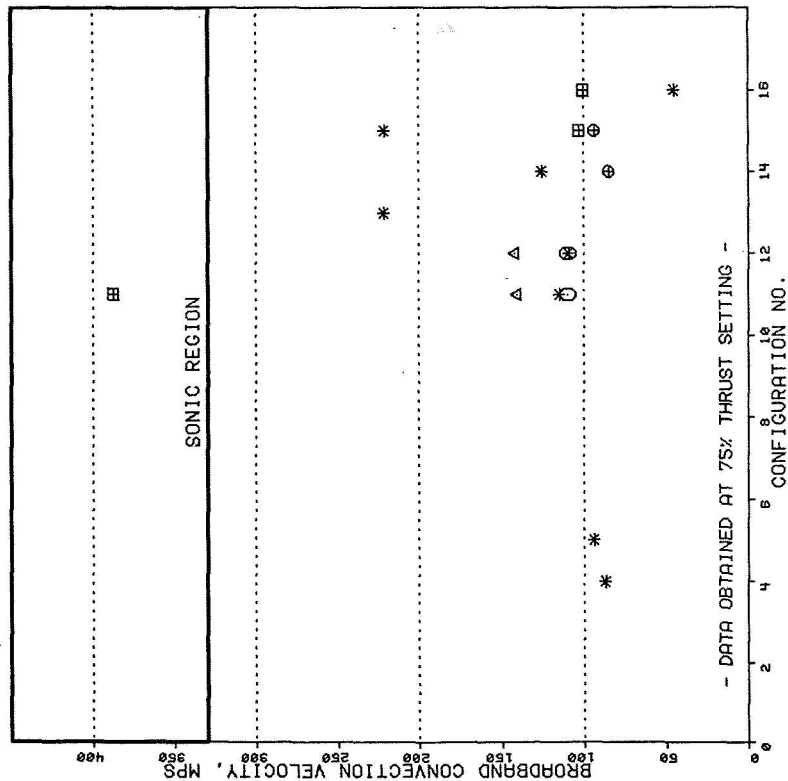
(c) Position nos. 6 and 7

(d) Position nos. 8 – 10

Figure 51. – Continued.

134

DATA PAIRS

△ 32 – 43
⊞ 33 – 43
✳ 34 – 35
⊕ 34 – 38
◯ 35 – 40

SONIC REGION

BROADBAND CONVECTION VELOCITY, MPS

CONFIGURATION NO.

Vortex generators down

Vortex generators up

– DATA OBTAINED AT 75% THRUST SETTING –

(f) Position nos. 32 – 35

DATA PAIRS

△ 23 – 33
⊞ 23 – 43
✳ 32 – 33
⊕ 32 – 39
◯ 32 – 41

SONIC REGION

BROADBAND CONVECTION VELOCITY, MPS

CONFIGURATION NO.

Modified vortex generators (skewed-plug nozzle)

Straight-plug primary nozzle

Skewed-plug primary nozzle

– DATA OBTAINED AT 75% THRUST SETTING –

(e) Position nos. 23 and 32
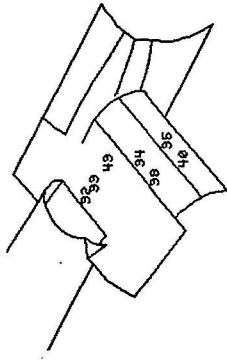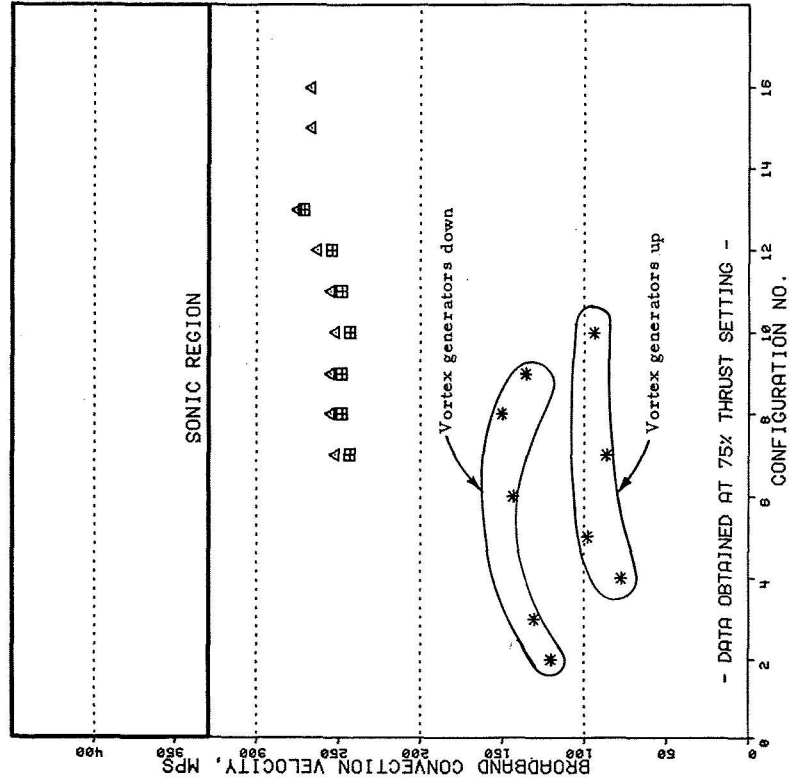
Figure 51. – Continued.
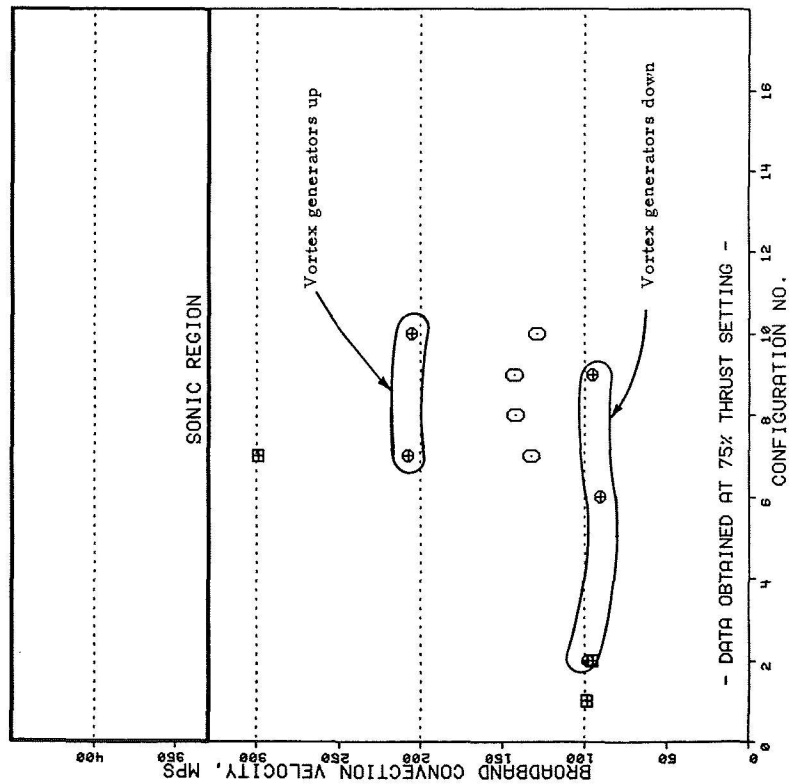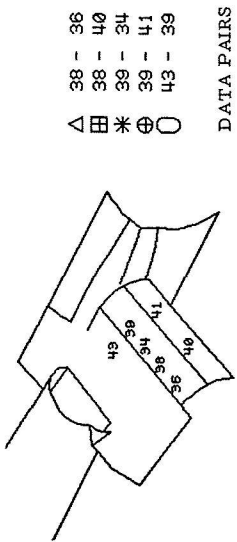
(g) Position nos. 38 – 43
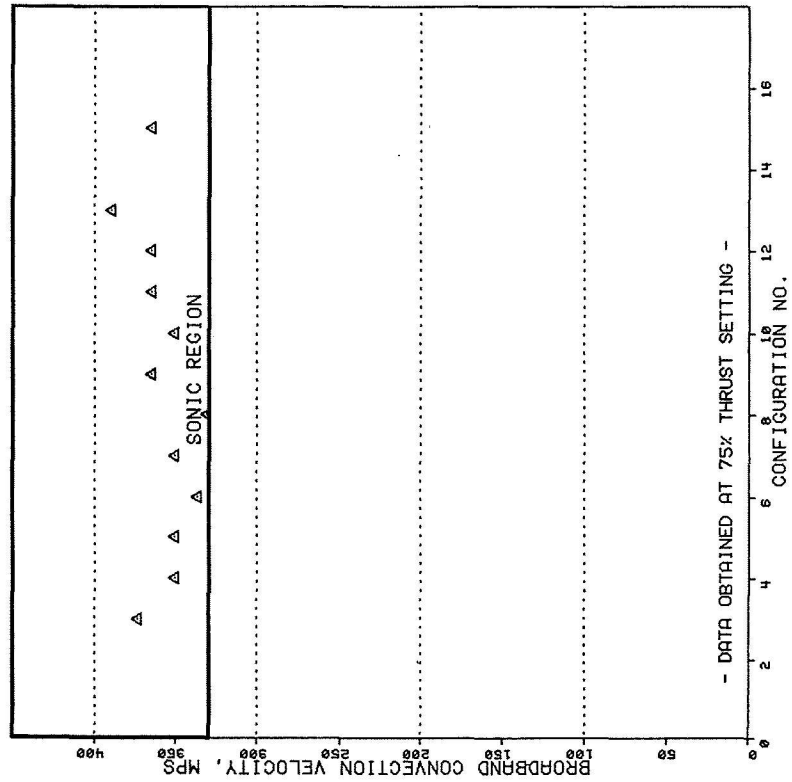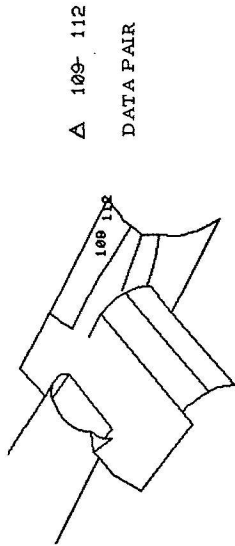
(h) Position no. 109

Figure 51. – Continued.

136

100% thrust (R326)

75% thrust (R327)

50% thrust (R328)

25% thrust (R329)
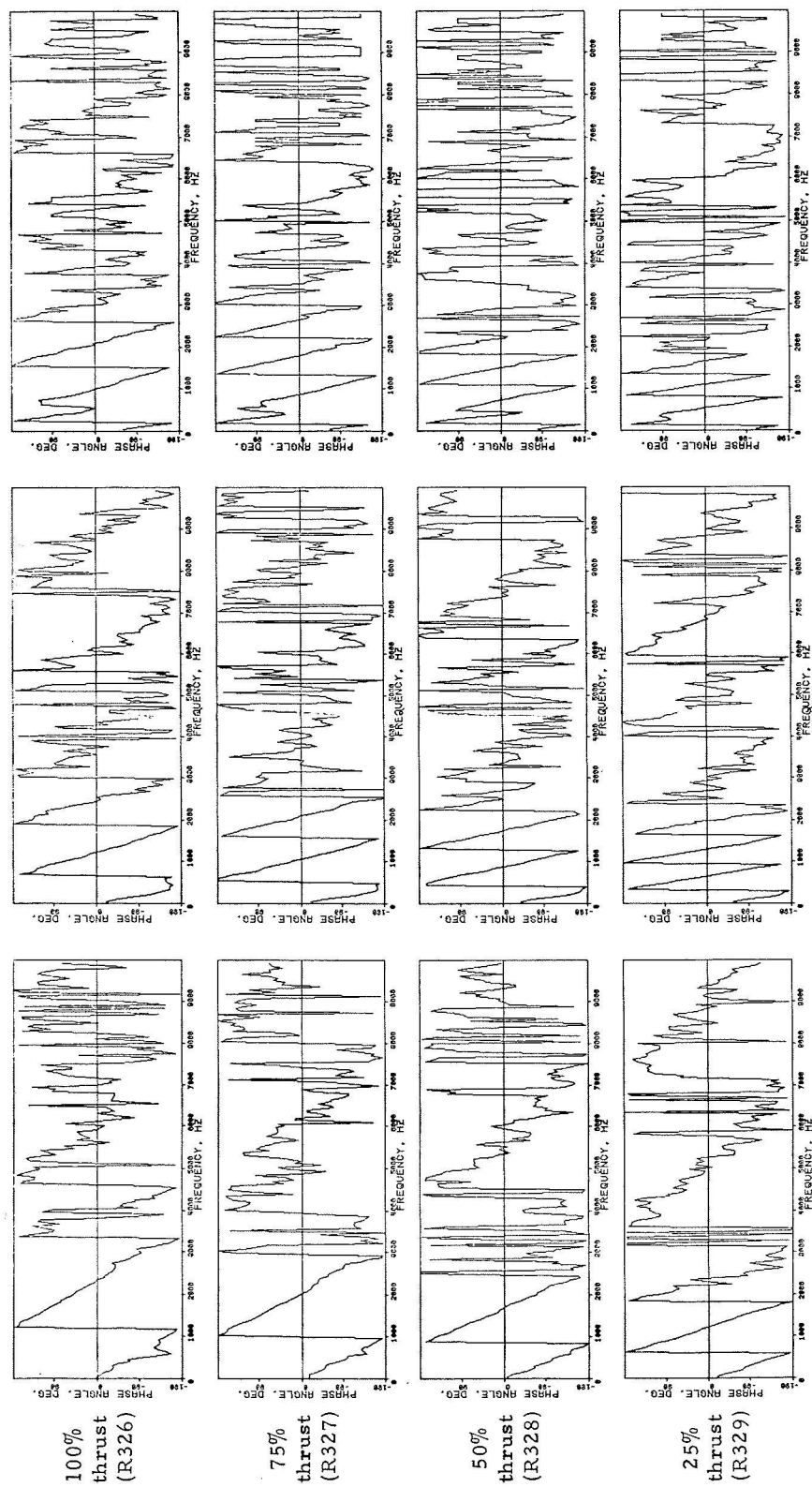
(a) Position nos. 32 -33   (b) Position nos. 33 - 43   (c) Position nos. 43 - 39

Figure 52. - Phase shift of fluctuating pressure components on wing and flap along nozzle centerline with vortex generators down. Test configuration 9.

100%
thrust
(R331)

75%
thrust
(R332)

50%
thrust
(R333)

2.5%
thrust
(R334)

(a) Position nos. 32 – 33   (b) Position nos. 33 – 43   (c) Position nos. 43 – 39
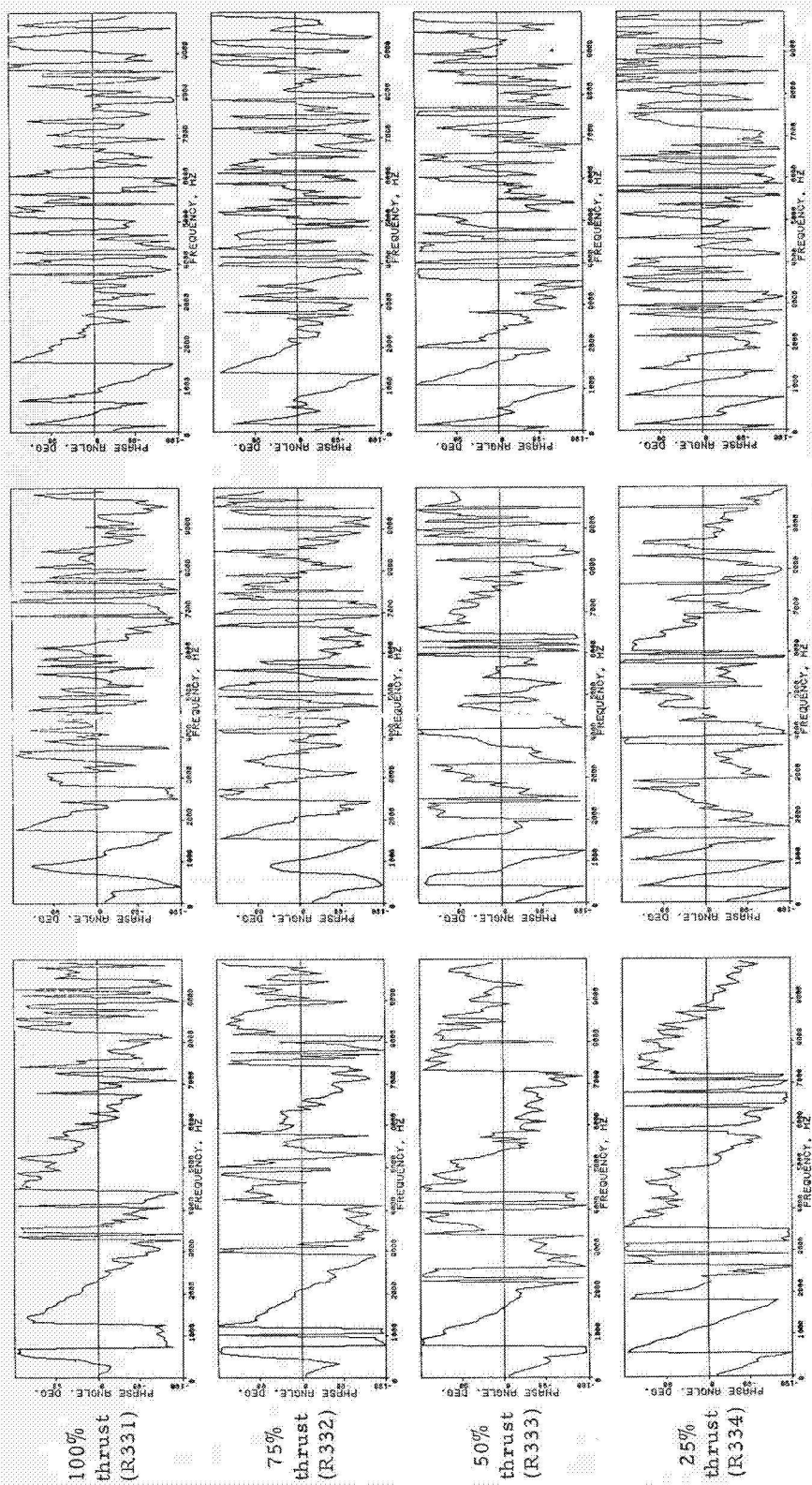
Figure 53. – Phase shift of fluctuating pressure components on wing and flap along nozzle centerline with vortex generators up. Test configuration 10.
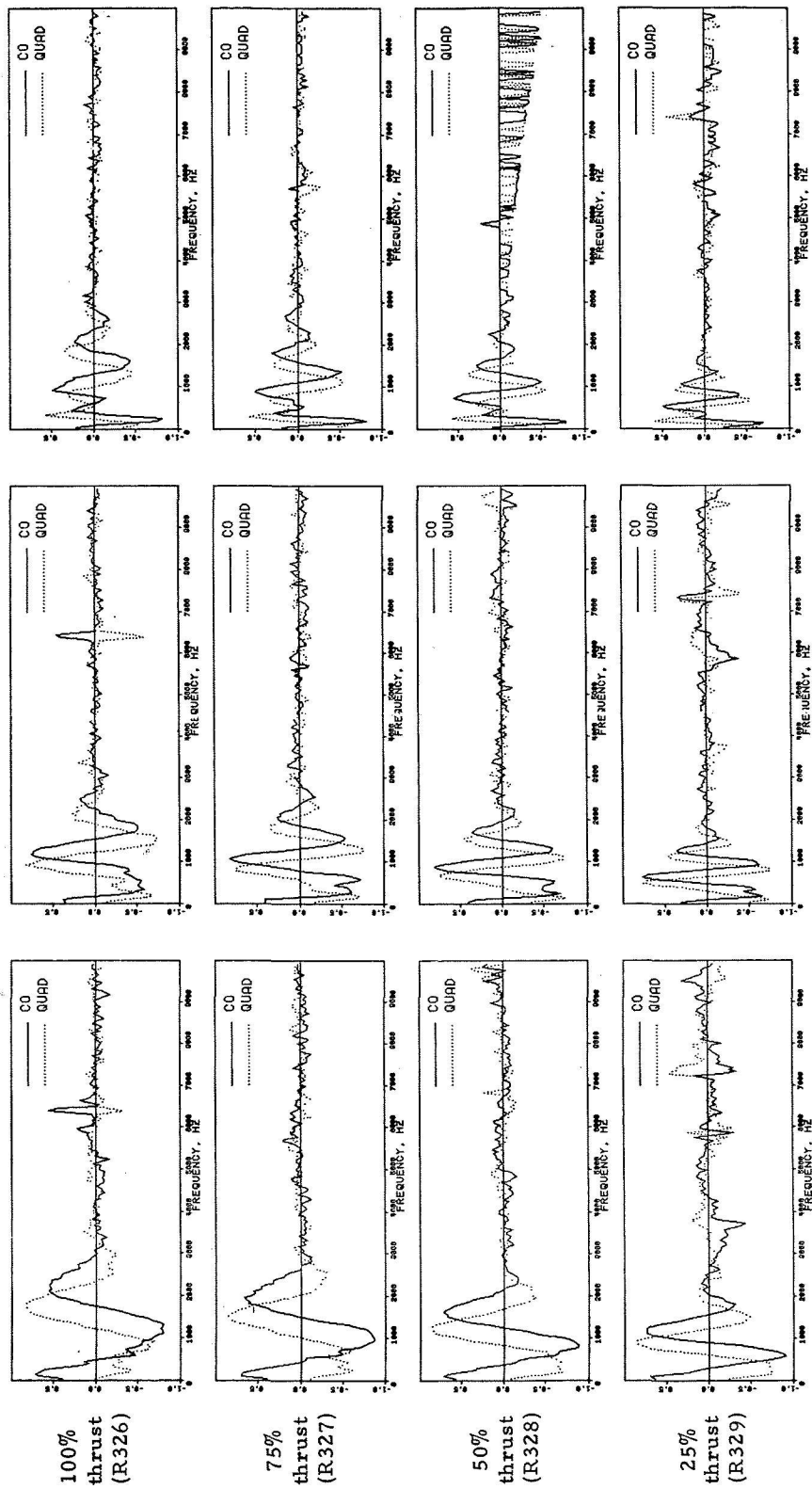
(a) Position nos. 32 - 33   (b) Position nos. 33 - 43   (c) Position nos. 43 - 39

Figure 54. - Co- and quad-spectral functions on wing and flap along nozzle centerline with vortex generators down. Test configuration 9.

100%
thrust
(R331)

75%
thrust
(R332)

50%
thrust
(R333)

25%
thrust
(R334)
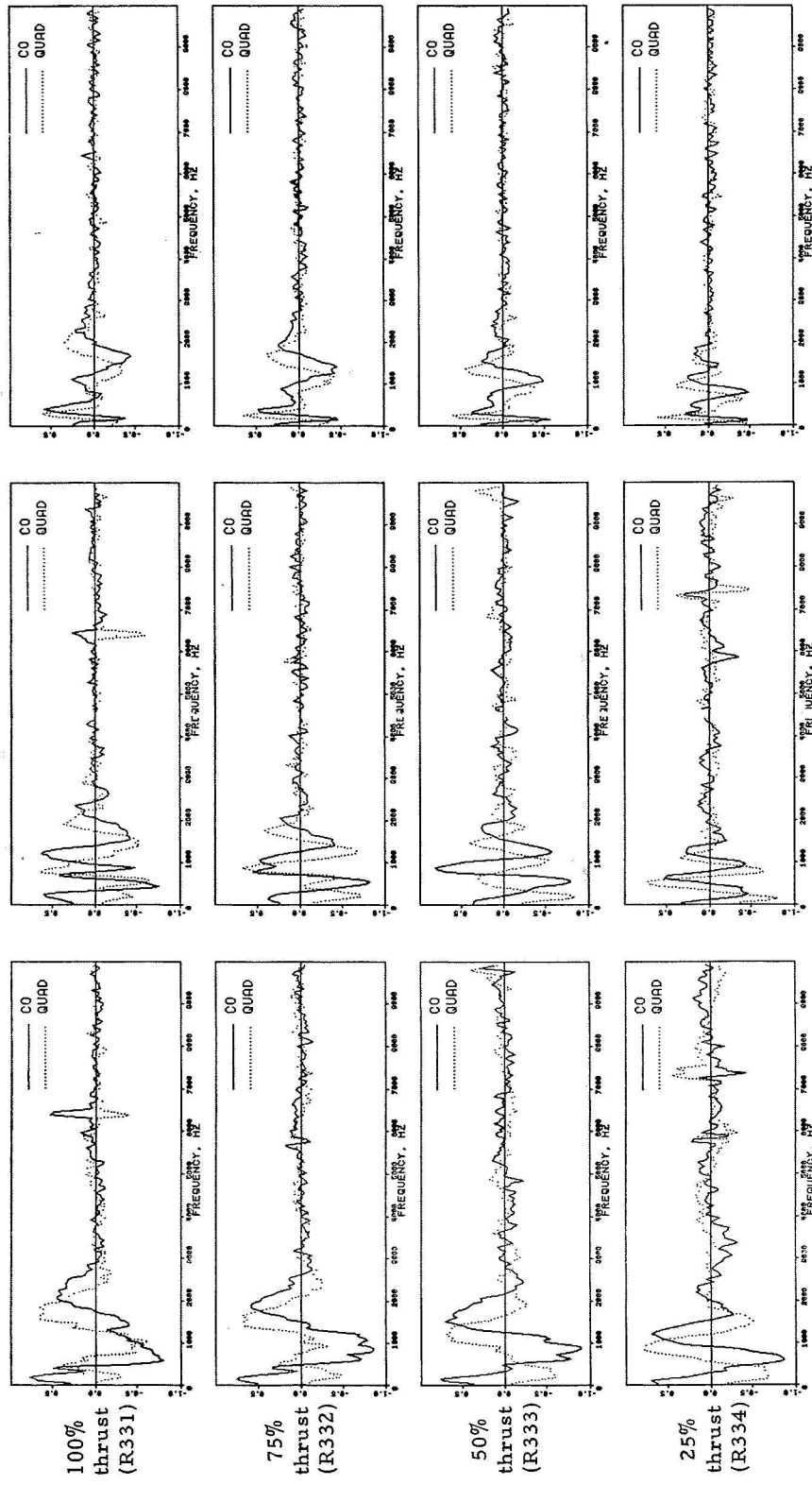
(a) Position nos. 32 - 33   (b) Position nos. 33 - 43   (c) Position nos. 43 39

Figure 55. - Co- and quad-spectral functions on wing and flap along nozzle centerline
with vortex generators up. Test configureation 10.
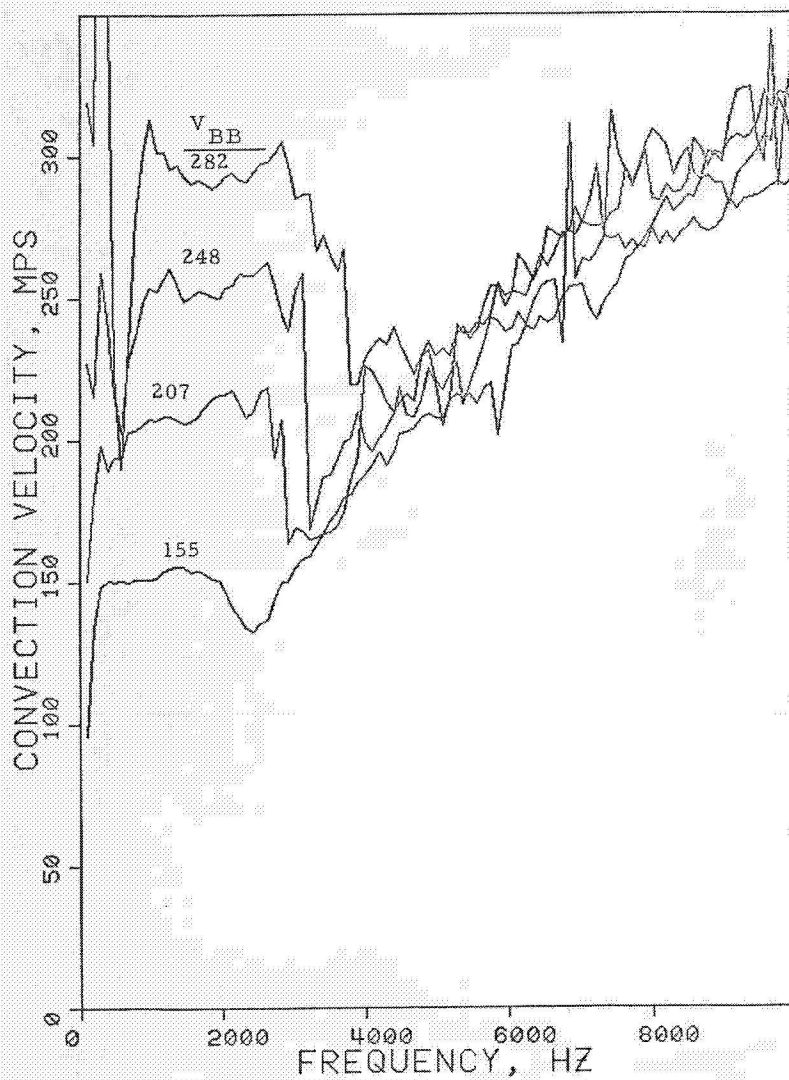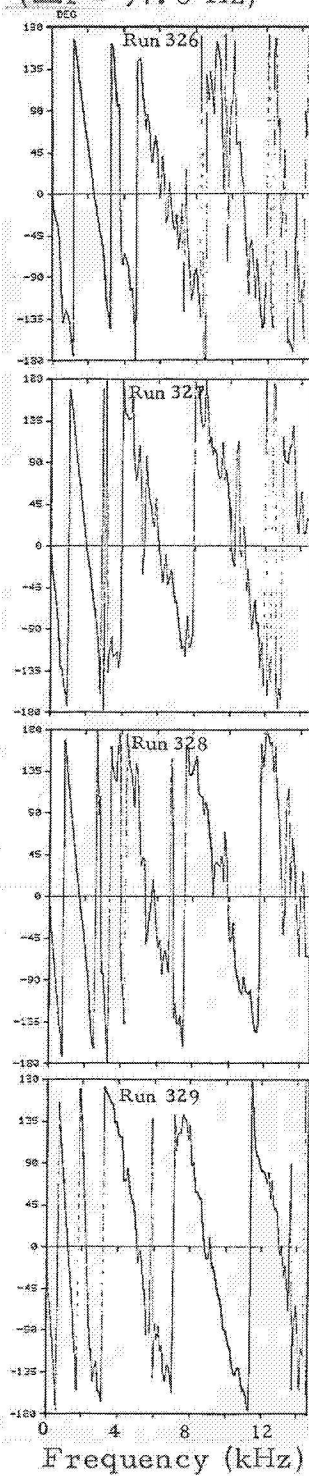
Figure 56. – Convection velocity of fluctuating pressure components
between wing positions 32 and 33 from phase-shift data.
Test configuration 9.

Frequency range
plotted (Hz)
900 – 3800
900 – 3100
100 – 2900
100 – 2300

	Run	Thrust	U_0'(m/s)	δ^*(cm)
△	326	100%	375	3.7
⊕	327	75%	325	3.3
⊞	328	50%	265	2.9
✳	329	25%	190	2.5

	M_O	δ^* (INCHES)	ξ_1/δ^*
●	0.3	0.149	1.66
▶	0.3	0.081	3.07
◀	0.3	0.149	5.00
▦	0.3	0.081	9.24
○	0.5	0.126	7.93
◇	0.5	0.126	11.91
▽	0.5	0.126	15.82
△	0.5	0.126	19.75

MEAN CURVE FOR $\xi_1/\delta^* > 5$

M_O = Mach number

ξ = sensor separation distance

Sensor separation = 12.5 cm
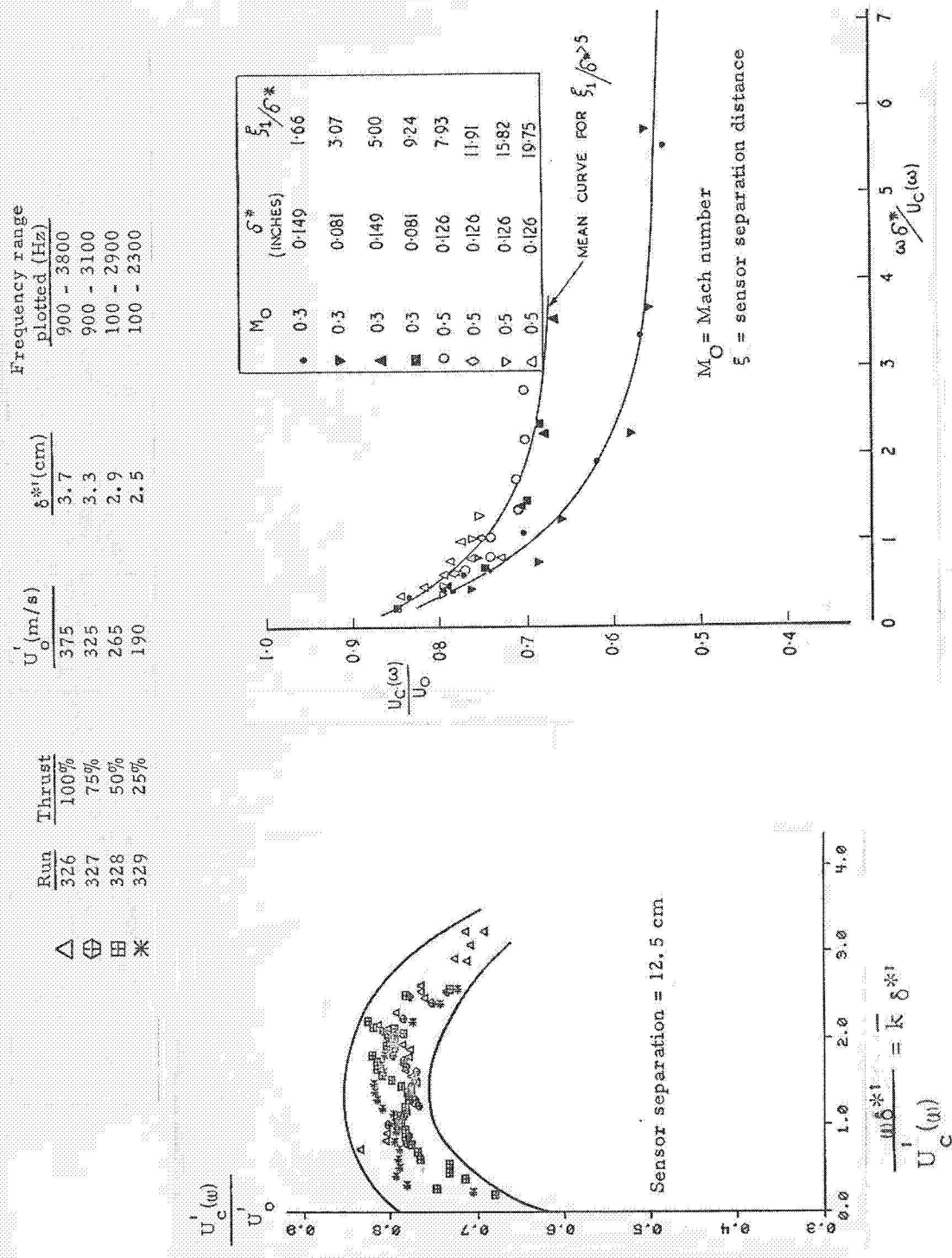
(a) Using data of figure 56,
position nos. 32 – 33

(b) Bull's results (figure 18 of Ref. 25)

Figure 57. – Comparison of normalized narrow-band convection velocities on the YC-14
model wing with boundary-layer results reported by Bull.

142
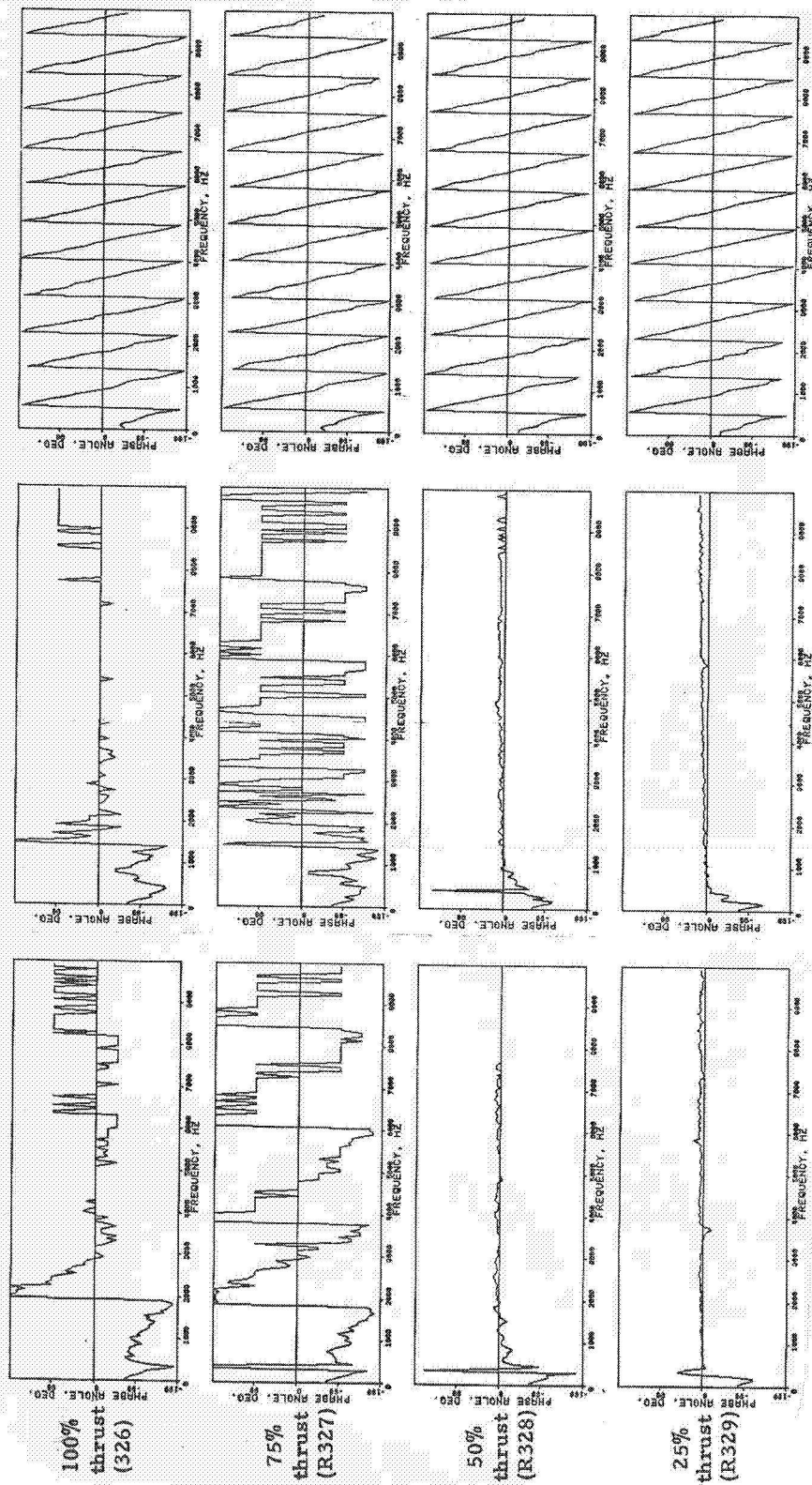
(a) Position nos. 1 – 8   (b) Position nos. 8 – 2   (c) Position nos. 109 – 112

Figure 58. – Phase shift of fluctuating pressure components on upper fuselage
and fairing with vortex generators down. Test configuration 9.

143

100% thrust (R326)

75% thrust (R 327)

50% thrust (R328)

25% thrust (R329)
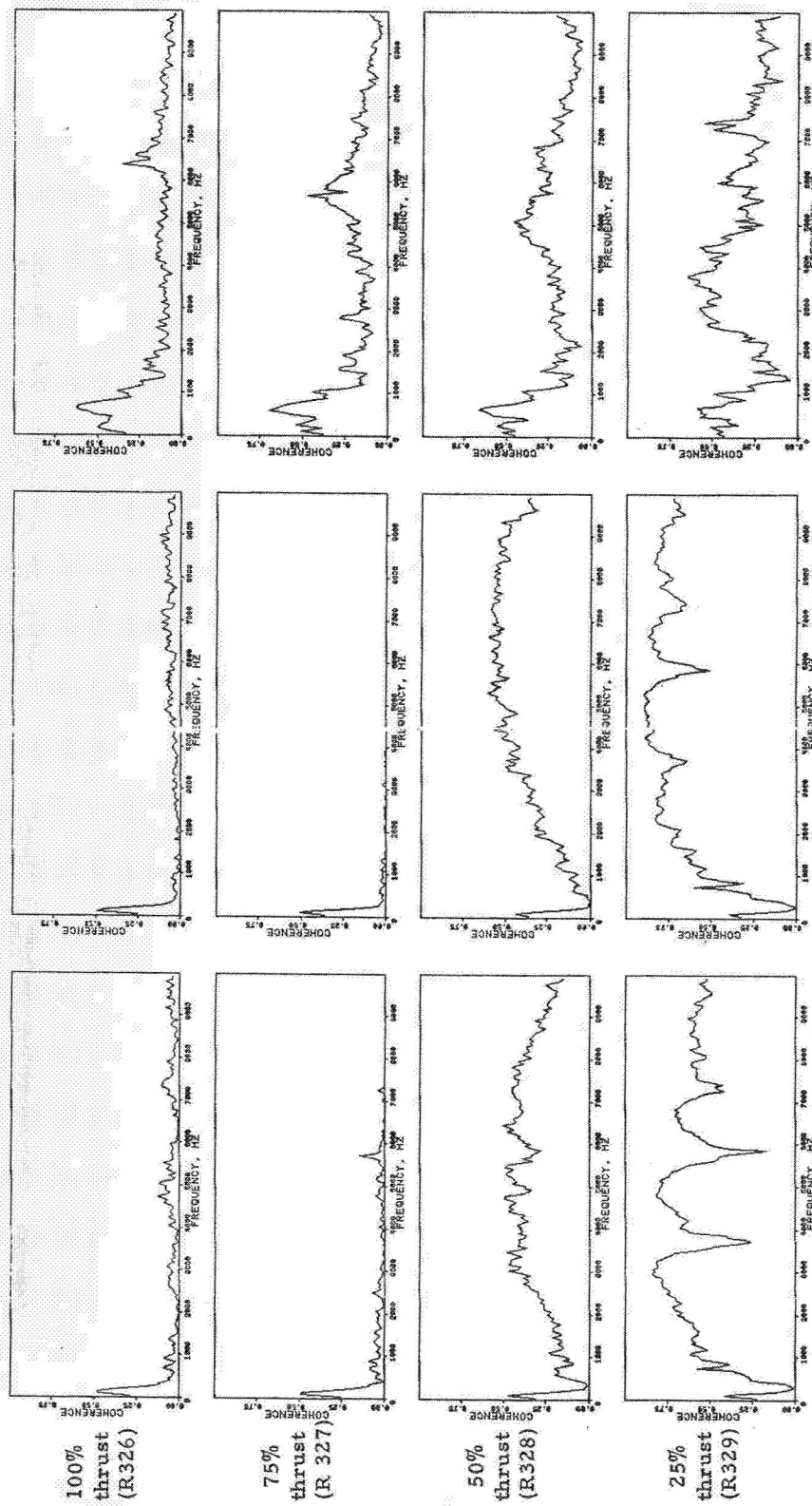
(a) Position nos. 1 - 8   (b) Position nos. 8 - 2   (c) Position nos. 109 - 112

Figure 59. - Corresponding coherence functions of fluctuating pressure for those measurements shown in figure 58. Test configuration 9.
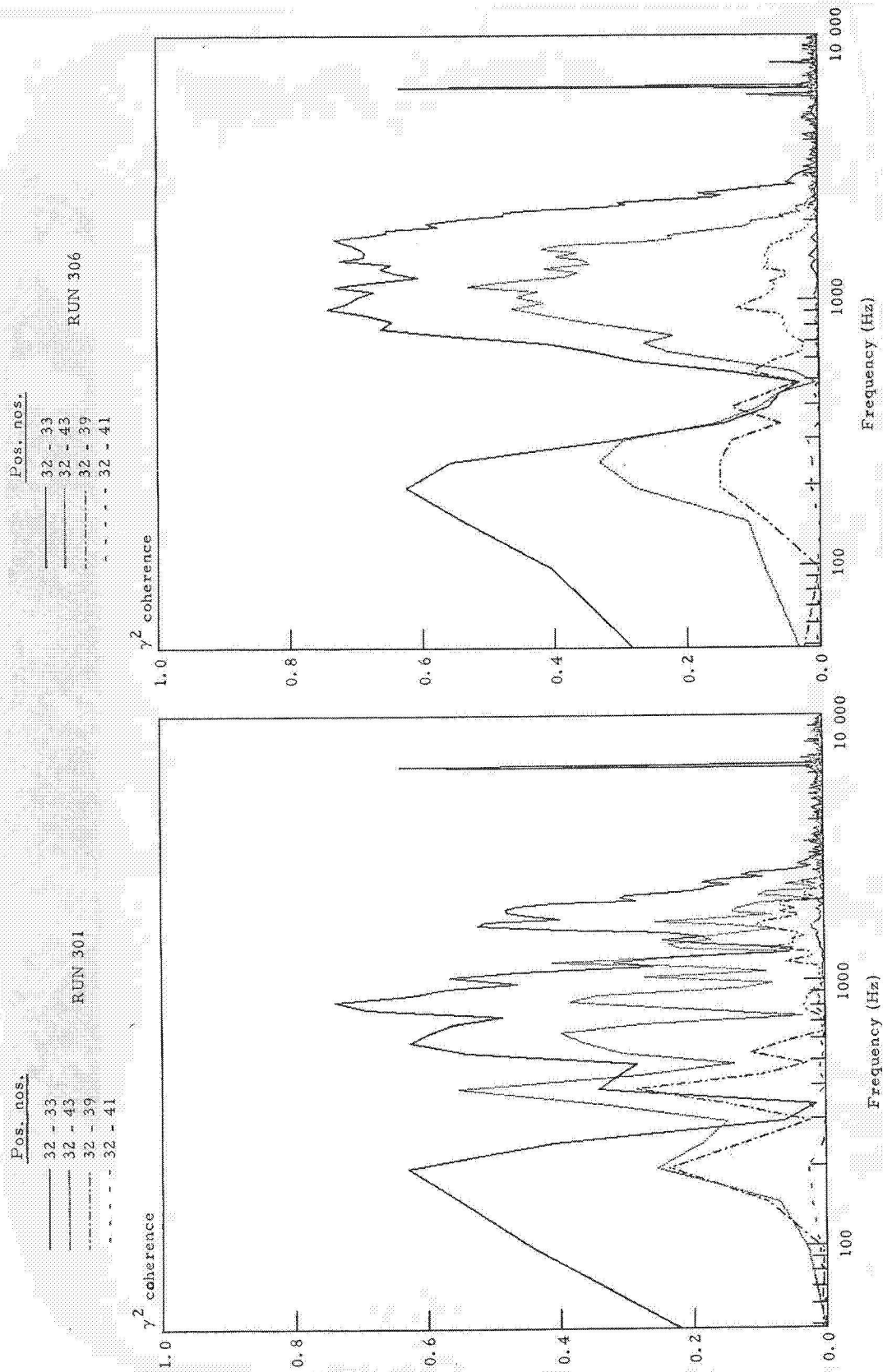
(a) Vortex generators up

(b) Vortex generators down

Figure 60. – Variation of coherence function with separation distance downstream
from wing position 32, showing effect of vortex generator deployment.

Pos. nos.
32 - 33
33 - 43
43 - 39
39 - 41

RUN 301

γ² coherence

Frequency (Hz)

(a) Vortex generators up

Pos. nos.
32 - 33
33 - 43
43 - 39
39 - 41

RUN 306

γ² coherence

Frequency (Hz)
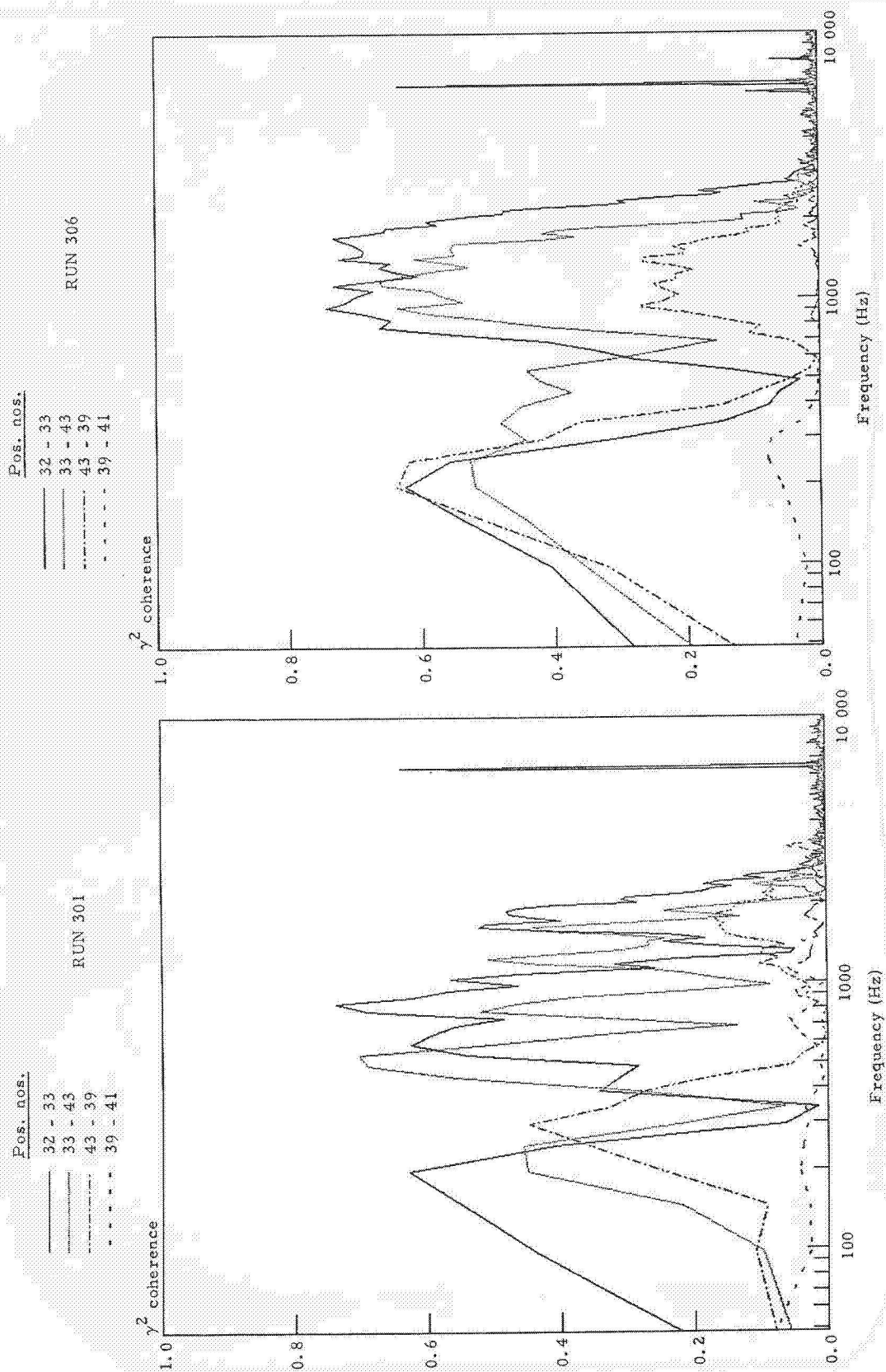
(b) Vortex generators down

Figure 61. – Coherence functions between adjacent measurement position on wing and flap along nozzle centerline, showing effect of vortex generator deployment.

(a) Vortex generators up

(b) Vortex generators down
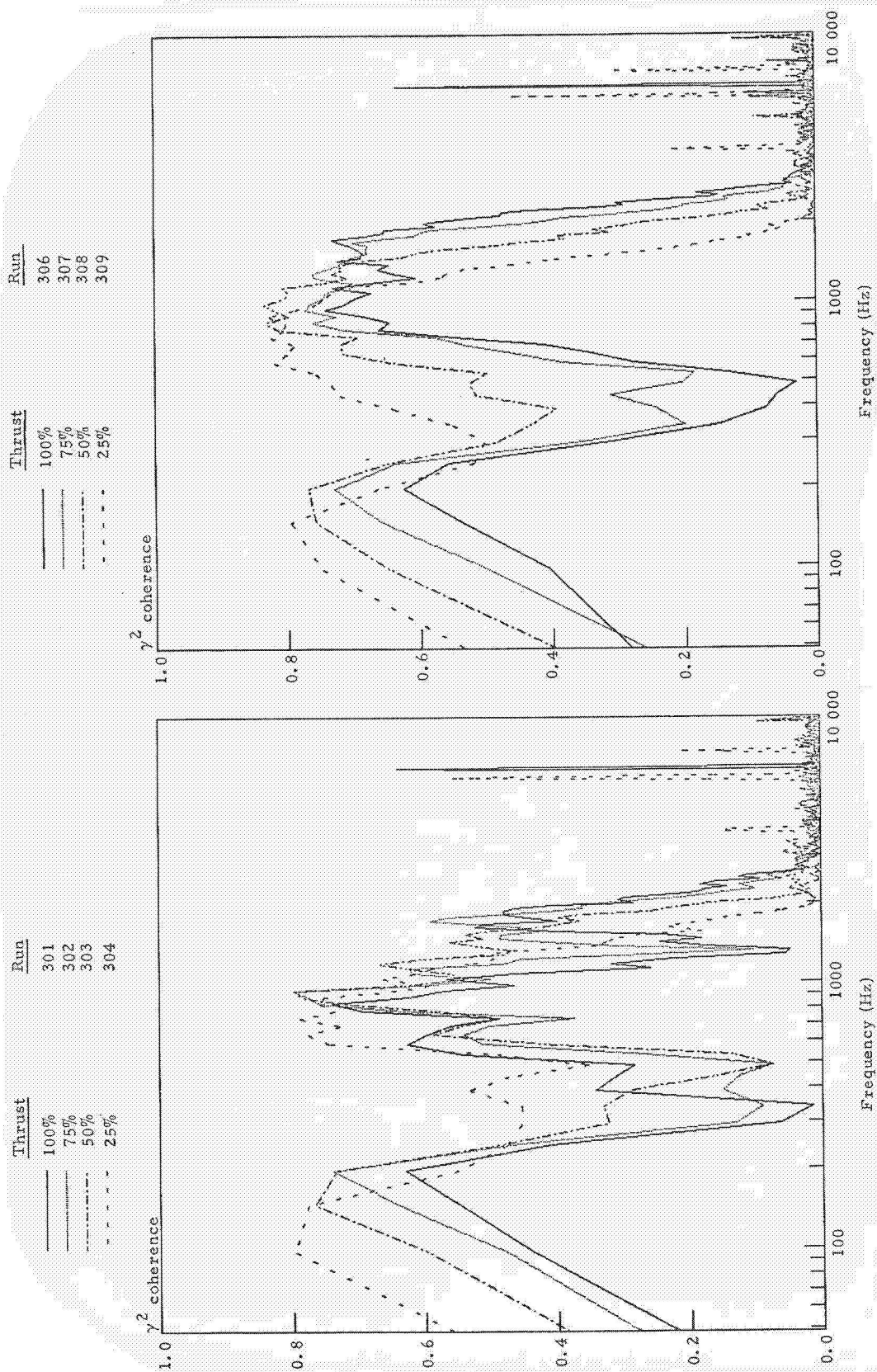
Figure 62. – Effects of thrust setting and vortex generator deployment on coherence function between wing positions 32 and 33.

Thrust	Run
100%	301
75%	302
50%	303
25%	304

(a) Vortex generators up

Thrust	Run
100%	306
75%	307
50%	308
25%	309

(b) Vortex generators down
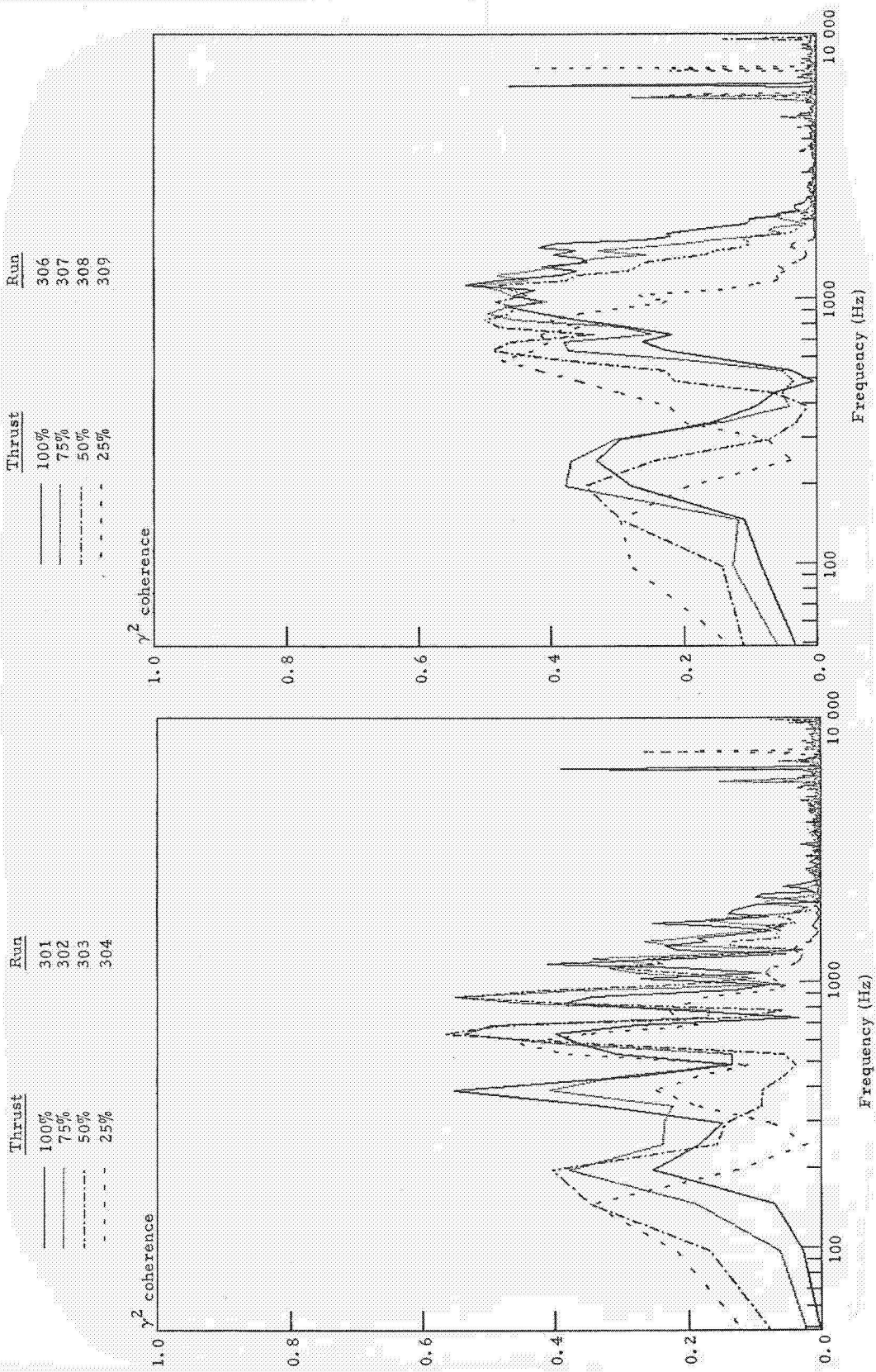
Figure 63. - Effects of thrust setting and vortex generator deployment on coherence function between wing positions 32 and 43.
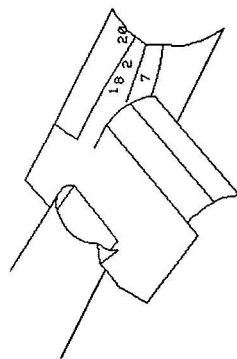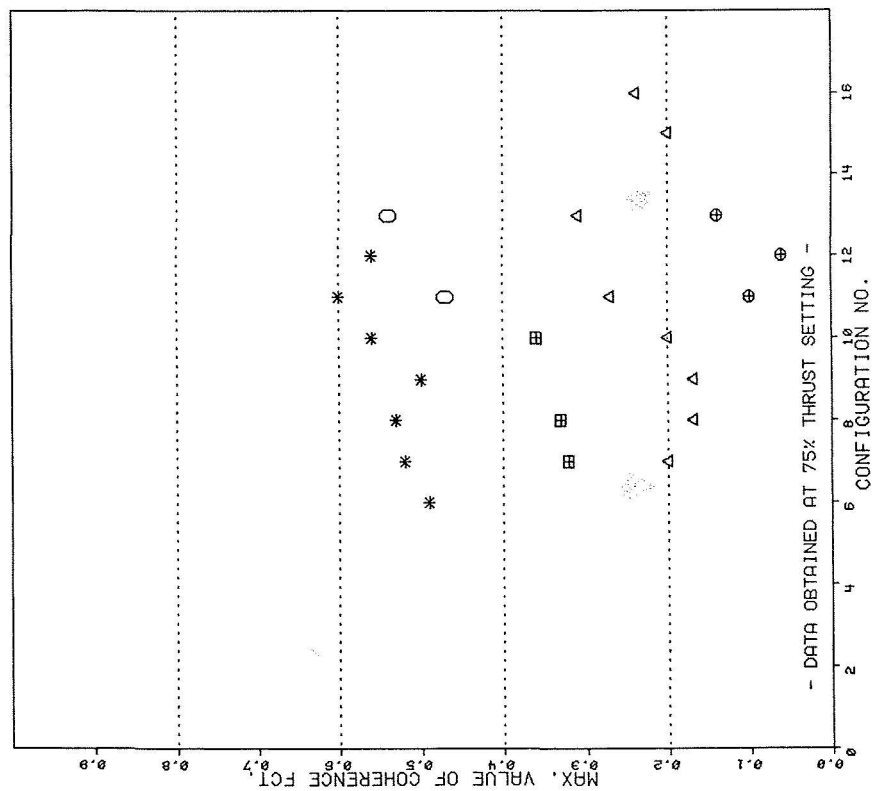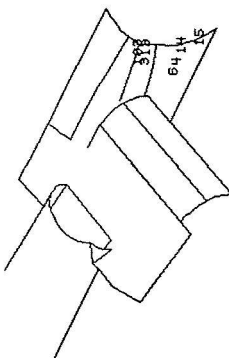
(a) Position nos. 1 and 2
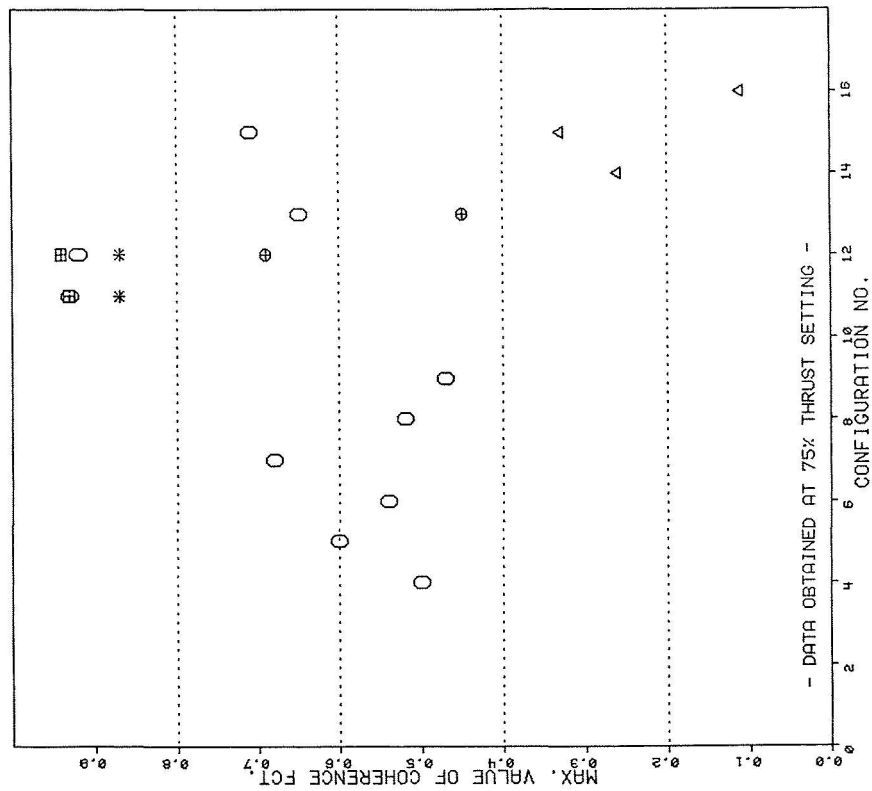
(b) Position nos. 3 - 6

Figure 64. - Comparison of maximum value of coherence function.
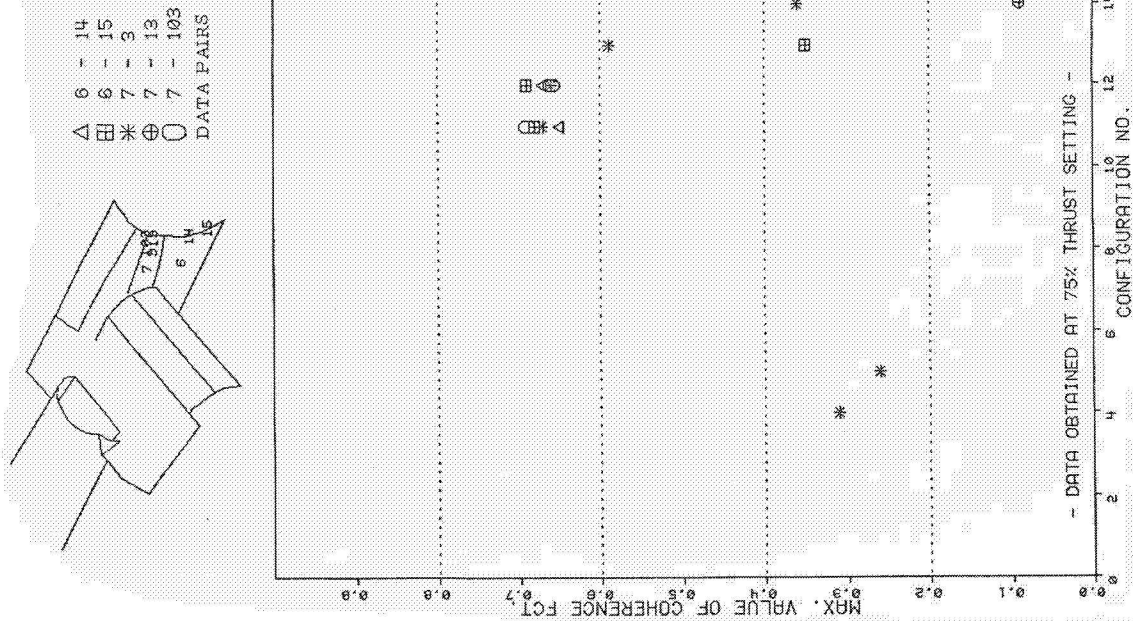
(c) Position nos. 6 and 7
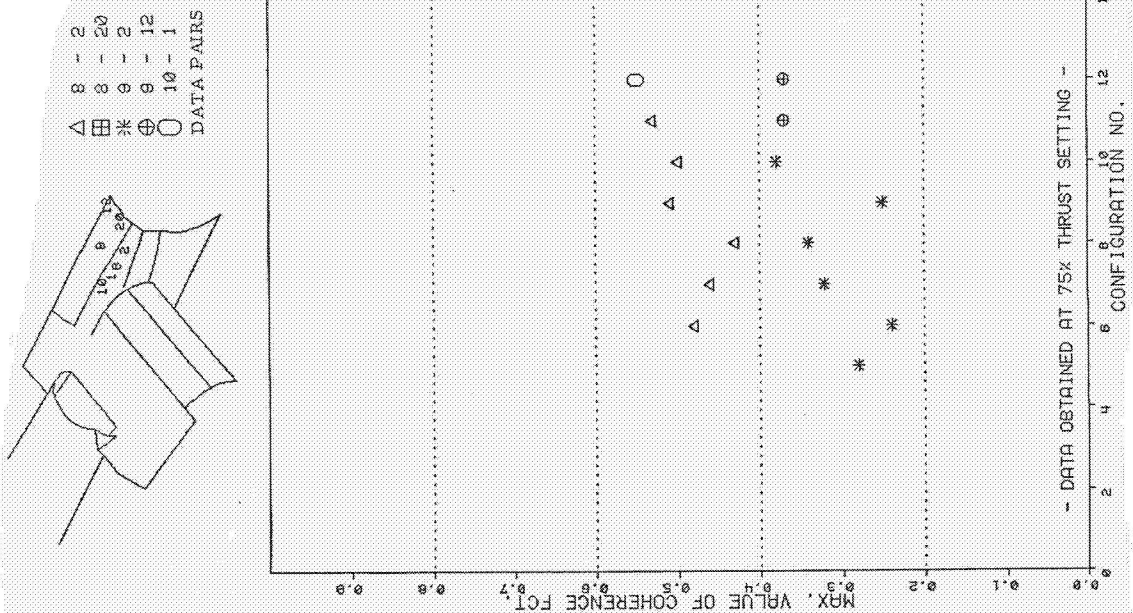
(d) Position nos. 8 - 10

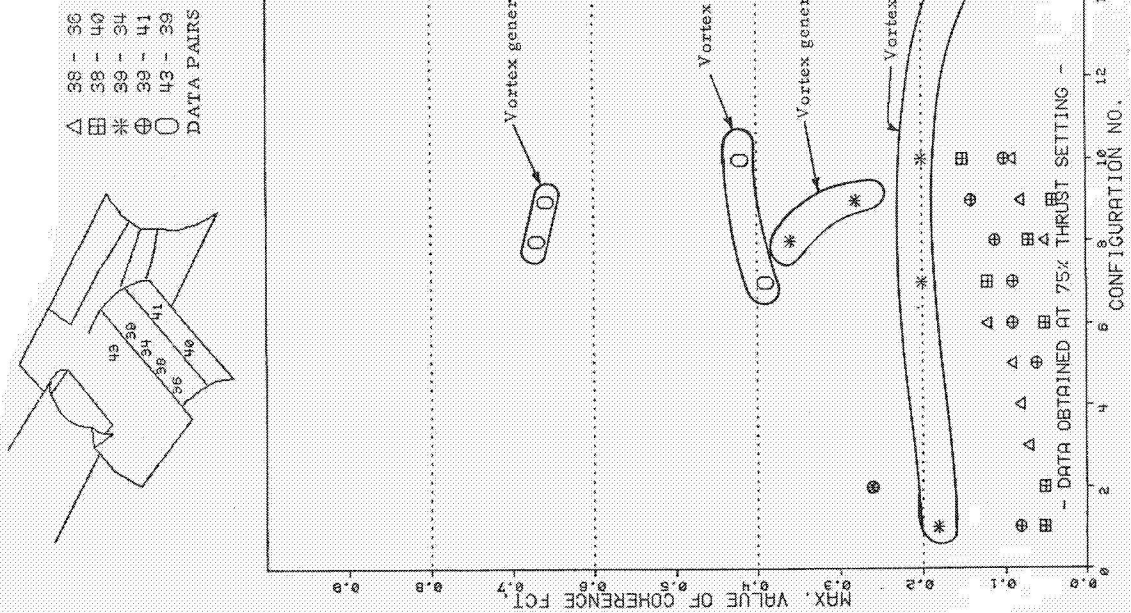Figure 64. - Continued.
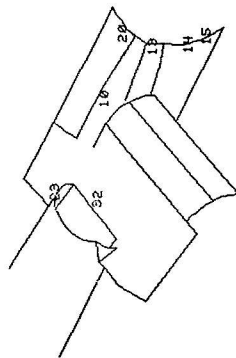
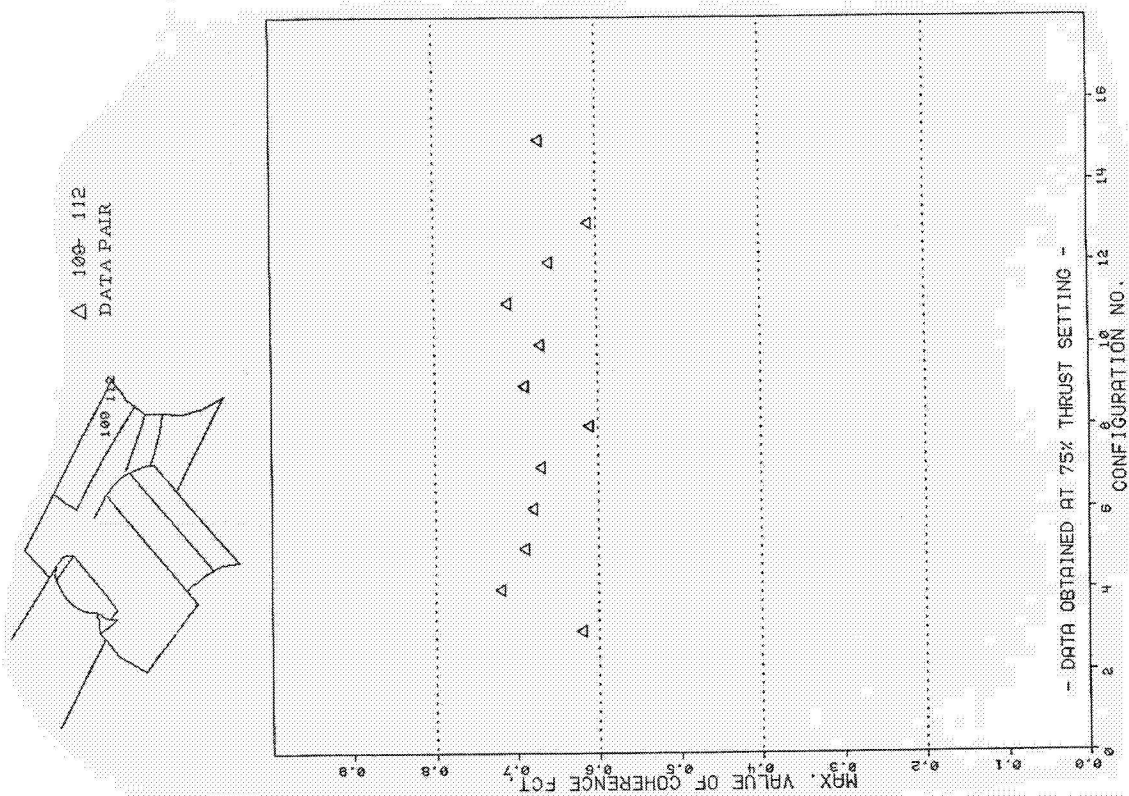(e) Position nos. 10 – 23

(f) Position nos. 23 and 32

Figure 64. – Continued.

151
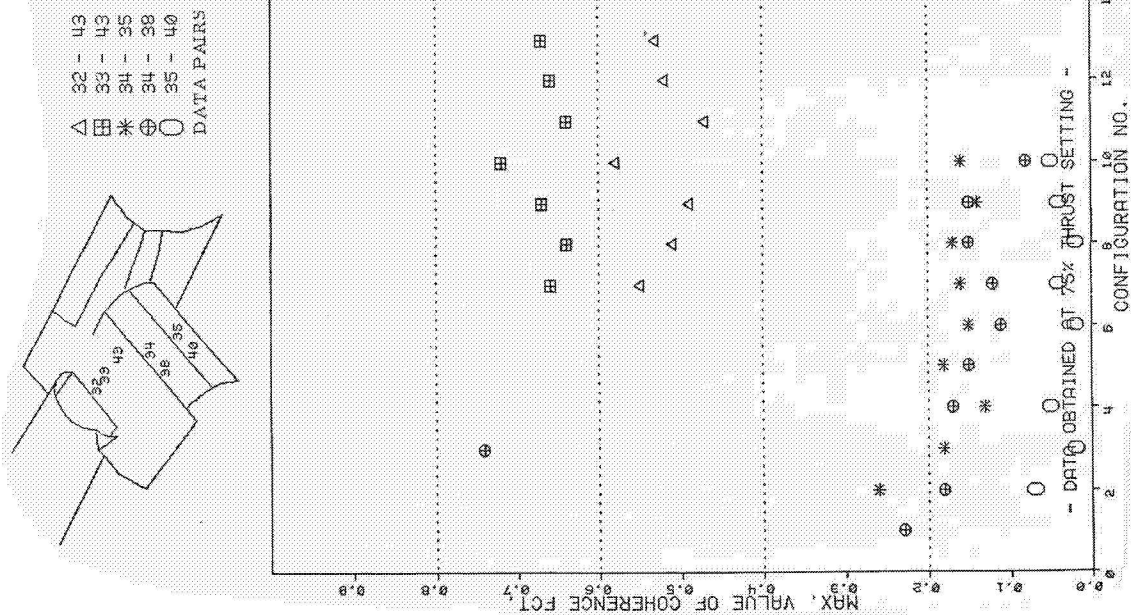
(g) Position nos. 32 – 35

(h) Position nos. 32 – 43

Figure 64. – Continued.

(i) Position no. 109

Figure 64. – Continued

	Position numbers	Separation distance (cm)
——————	32 - 33	12.4
——————	32 - 43	36.3
—·—·—·	32 - 39	65.5
— — — —	32 - 41	100.8

RUN 306
Vortex generators down
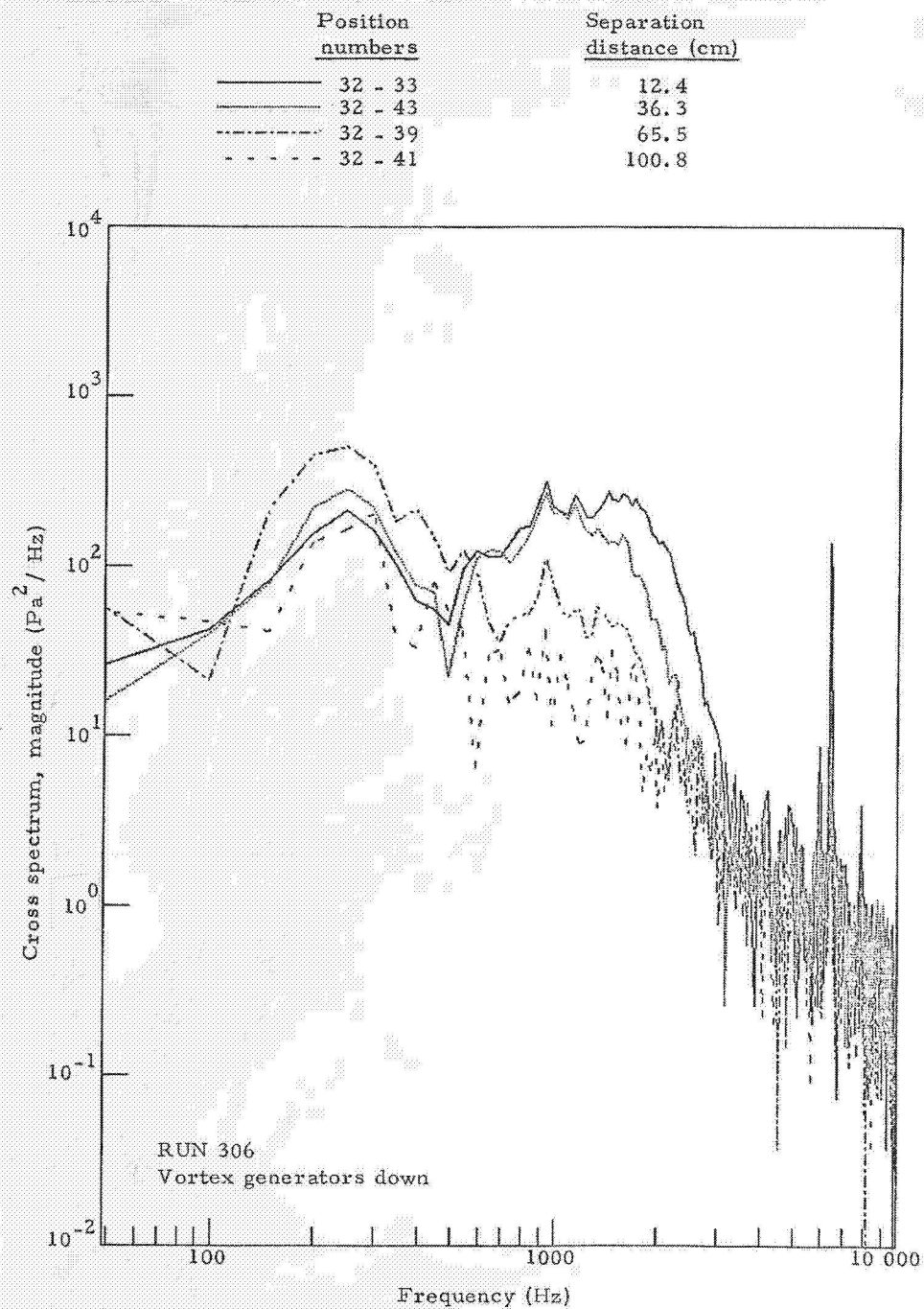
Cross spectrum, magnitude (Pa^2 / Hz)

Frequency (Hz)

Figure 65. - Effect of separation distance on cross spectra
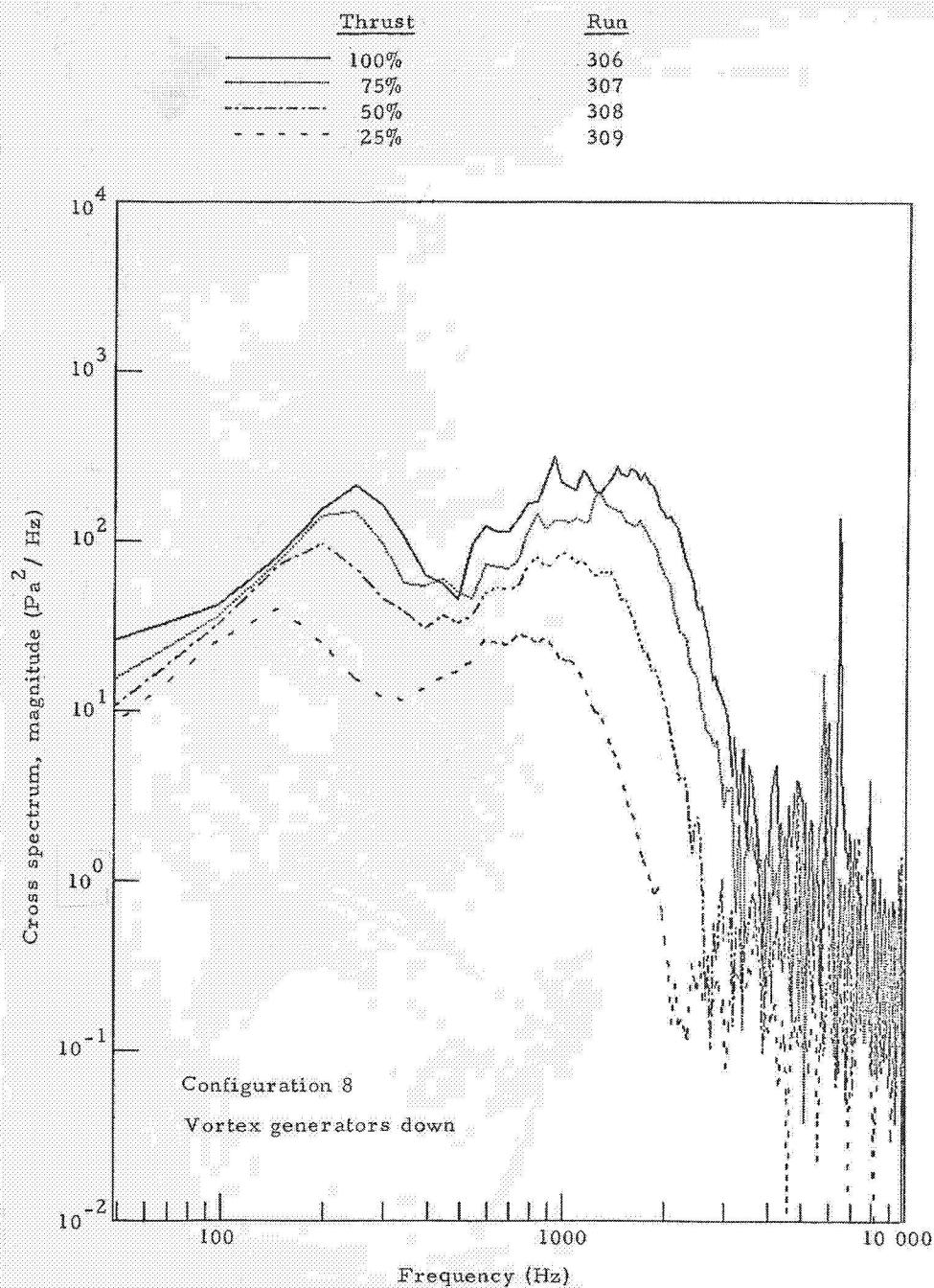along nozzle centerline.

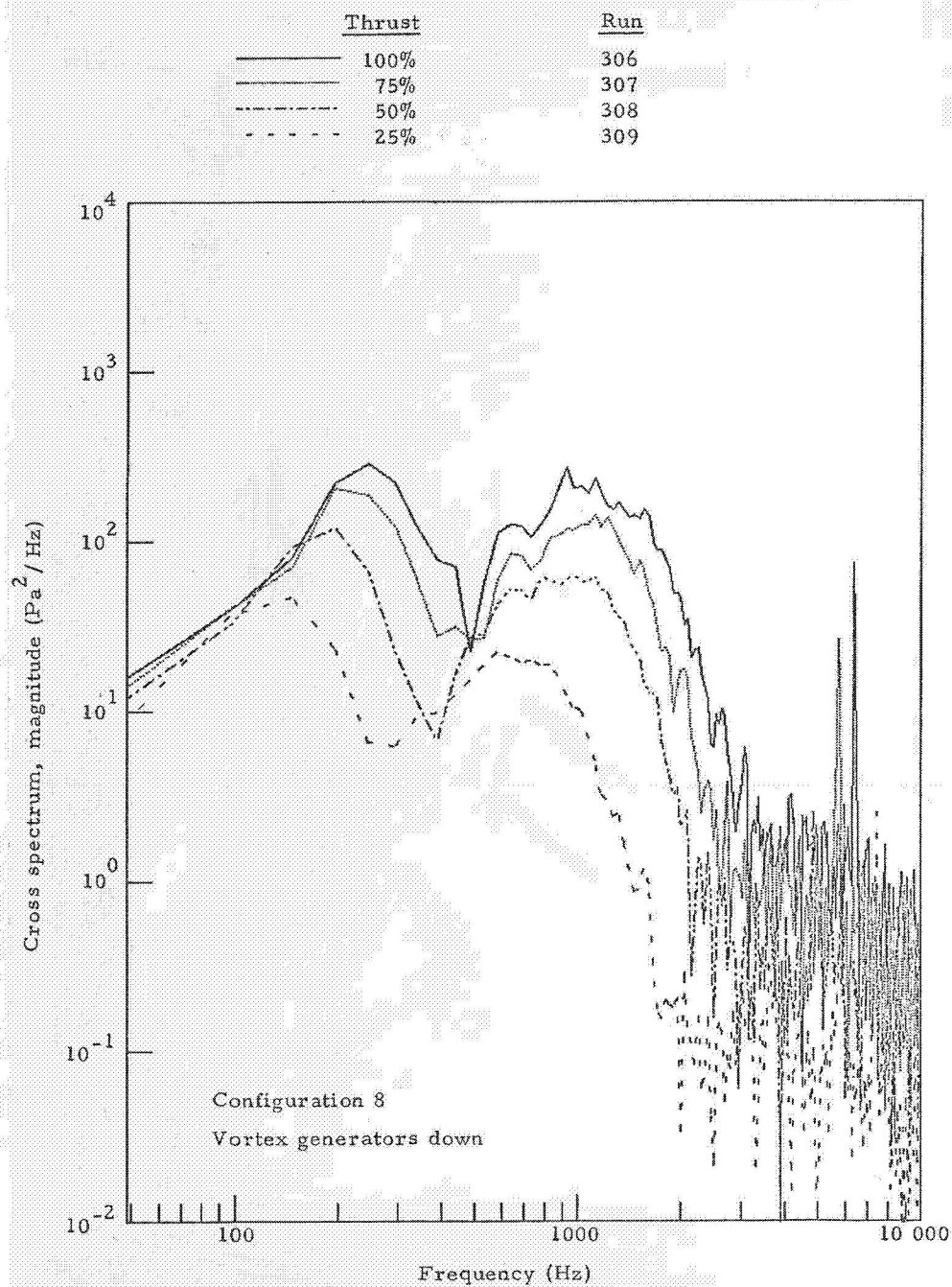Figure 66. – Effects of thrust setting on magnitude of frequency spectrum between wing positions 32 and 33.

Figure 67. - Effects of thrust setting on magnitude of frequency
spectrum between wing positions 32 and 43.

1. Report No. NASA CR-158941	2. Government Accession No.	3. Recipient's Catalog No.
4. Title and Subtitle INVESTIGATION OF SURFACE FLUCTUATING PRESSURES ON A 1/4-SCALE YC-14 UPPER SURFACE BLOWN FLAP MODEL		5. Report Date January 1979
		6. Performing Organization Code
7. Author(s) Richard S. Pappa		8. Performing Organization Report No. 50900
9. Performing Organization Name and Address Wyle Laboratories 3200 Magruder Boulevard Hampton, Virginia 23666		10. Work Unit No.
		11. Contract or Grant No. NAS1-14740
12. Sponsoring Agency Name and Address National Aeronautics and Space Administration Washington, D.C. 20546		13. Type of Report and Period Covered Contractor Report
		14. Sponsoring Agency Code

15. Supplementary Notes

Portions of this work were presented at the AIAA/NASA Ames V/STOL Conference in June 1977 and appear in AIAA paper 77-592.

16. Abstract

Results are reported for an experimental investigation of the fluctuating pressure field on the surfaces of a 1/4-scale YC-14 upper surface blown (USB) flap wing and fuselage section during static ground tests. This USB scale-model study using a JT-15D jet engine, is one phase of a NASA research program to investigate the dynamic loads imposed on powered-lift STOL aircraft configurations by impingement of the jet exhaust flow. The characteristics of the pressure field are described in terms of overall fluctuating pressure levels, auto- and cross-spectral densities, space-time correlations, coherence functions, and both broadband and narrowband convection velocities. The effects of changes in the mean flow conditions over the model on the surface pressure field are discussed, and several comparisons with similar work of previous investigators are provided.

17. Key Words (Suggested by Author(s)) Acoustic loads Jet impingement Random pressures Surface fluctuating pressures USB aircraft	18. Distribution Statement Unclassified - Unlimited STAR Category 71		
19. Security Classif. (of this report) Unclassified	20. Security Classif. (of this page) Unclassified	21. No. of Pages 156	22. Price*